

**UCSF**

**UC San Francisco Electronic Theses and Dissertations**

**Title**

Analysis of microtubule dynamics and chromosome movement in vitro

**Permalink**

<https://escholarship.org/uc/item/9sm3d3n7>

**Author**

Desai, Arshad,

**Publication Date**

1998

Peer reviewed|Thesis/dissertation

Analysis of Microtubule Dynamics and Chromosome  
Movement in vitro

by

Arshad Desai

**DISSERTATION**

**Submitted in partial satisfaction of the requirements for the degree of**

**DOCTOR OF PHILOSOPHY**

in

Biochemistry

in the

**GRADUATE DIVISION**

of the

**UNIVERSITY OF CALIFORNIA**

**San Francisco**



**I dedicate this thesis  
to my parents, for giving me the opportunity to pursue my dreams  
to the van Groenous, for giving me a home and much more  
and to Karen Oegema, for her friendship**

## Acknowledgments

I would like to thank Tim Mitchison for giving me the best support and guidance possible, for sharing his deep love for science and for constantly challenging me to take the road less taken. His fearless pursuit of varied problems in cell biology using diverse approaches, insistence on pursuing non-traditional approaches that often uniquely mark his contributions, and total delight at creative hands-on experimentation have strongly influenced me and will shape my future scientific endeavors.

I would like to thank Andrew Murray for his constant support and friendship throughout graduate school, for turning around my graduate school tenure by inviting me to spend a summer at Woods Hole, and for always willing to give me a (lab) home whenever I faced abandonment. His deep intellect, constant creativity and total willingness to pursue a line of thought to its utmost limit will always inspire me.

I would like to thank Ted Salmon for being my "third PI". I met Ted at Woods Hole and have had the pleasure of working with him on two projects during graduate school. Being around Ted always reminds me of the joy of science that first drives young students into the halls of academia -- in Ted that joy has never faded. His boundless enthusiasm, amazing technical creativity, insistence on quantitative approaches to complex biological problems, and encyclopedic knowledge of the physical mechanisms of cell division make conversations with Ted truly enlightening.

I would also like to thank the Mitchison and Alberts labs, past and present. I feel extremely lucky to have been in such great company during graduate school. In the early days, interactions with David Drechsel and Elly Tanaka were central in stimulating my interest in the cytoskeleton. David

Drechsel imparted to me much of the technical lore on working with tubulin and his insightful views on the mechanism of microtubule dynamic instability. Tatsuya Hirano, Lisa Belmont, Linda Wordeman, Ken Sawin and Louise Cramer helped me in many ways during my early, exploratory phase in the Mitchison lab.

In the later years, I especially thank Claire Walczak, with whom I have enjoyed a wonderful collaboration, and Jody Rosenblatt, for her unwavering support and friendship. Suzie Verma, in addition to keeping the Mitchison lab functional through changing times, was responsible for making my final project possible and I consider it a privilege to have worked with her. Also a privilege has been working with Peg Coughlin, an enthusiastic partner in my electron microscopy forays. Aneil Mallavarapu was a most excellent early baymate and I thank him, not only for being himself, but also for trying to communicate the beauty of electronics to us biologist heathens, for his zen-like incantations in C++, and for fostering the digital imaging revolution in our lab. Chris Field, Matt Welch, Jason Swedlow, Heather Deacon, Jennifer Frazier, Ann Yonetani, Sarita Jain, Michelle Moritz, Yixian Zheng, Raffi Aroian, Jack Barry and Mimi Shirasu all made the Mitchison/Alberts labs a very stimulating environment for doing science. A special note of thanks goes to Jason Swedlow, Inke Näthke, Jack Taunton, Justin Yarrow, Aneil Mallavarapu, Peg Coughlin, Chris Field and especially Mimi Shirasu for their collective role in easing the wrenching transition from the womb (UCSF) to the harsh light of the real world (Harvard).

I also had the good fortune of spending time with the Salmon lab both in Woods Hole and in North Carolina. Paul Maddox has been a wonderful friend and collaborator and Nancy Salmon, Jennifer Waters, Phong Tran,

Clare Waterman-Storer and Julie Canman all made me feel at home in their domain. I will always remember the times spent with the Salmon lab fondly.

Throughout graduate school I had the pleasure and privilege of interacting with wonderful peers. I especially want to thank Paul Peluso for his friendship, late night conversations, junk food forays, sushi excursions and for consistently falling asleep on our living room floor in the middle of movies, regardless of their content. Ramon Tabtiang, Andy Shiau, Kayvan Roayaie, Michael Galko, Jim Wilhelm, Wallace Marshall, and Cara Coburn all contributed to making the journey through graduate school a fondly memorable one.

Finally, I would like to thank my parents, for letting me go halfway across the world in my teens and for supporting me during my endless academic pursuits, and the van Groenous for always giving me a place to come home to in a foreign land and for showing me the right path in life.

And lastly, Karen Oegema, for being the best discovery I made at UCSF, for her combative criticism, insightful analysis, tutelage in biochemistry, constant editing of my verbose outpourings, and most of all for her friendship.

# Analysis of Microtubule Dynamics and Chromosome Movement *in vitro*

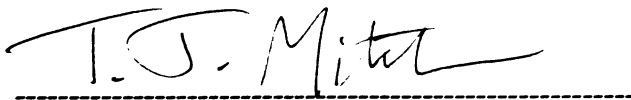
Arshad Desai

## Abstract

Mitosis is a complex process where the concerted action of several hundred proteins orchestrates the accurate segregation of duplicated genetic material to daughter cells. We have approached this complex process using *in vitro* biochemistry, with an emphasis on the polymerization dynamics of microtubules -- polymers of tubulin essential for mitosis in all eukaryotes. In the first project, we used clarified *Xenopus* egg extracts and demembrated *Xenopus* sperm nuclei to develop an *in vitro* reaction for the assembly of kinetochores -- nucleoprotein structures assembled at the centromere that generate a dynamic interface between chromosomes and spindle microtubules. We have demonstrated that this reaction can be used to analyze protein-protein interactions at the kinetochore by depleting a specific kinetochore component from the extract and assaying the effect on targeting of other components.

In the second project, we have used local fluorescence photoactivation to show that the bulk of microtubule disassembly occurs near the spindle poles during anaphase A in *Xenopus* extract spindles. This is in contrast to vertebrate somatic cells, where the majority of microtubule disassembly occurs near the kinetochore. This result highlights the importance of considering non-kinetochore mechanisms for anaphase chromosome movement in systems other than vertebrate somatic cells.

In the final project, we have identified a novel activity for internal catalytic domain kinesins, a specific subclass of the kinesin superfamily. We found that XKCM1, a member of this subclass, acts as a microtubule destabilizing factor in *Xenopus* extracts. Purified XKCM1 and XKIF2, a neuronal kinesin related to XKCM1, destabilize microtubules assembled from pure tubulin *in vitro*. We have analyzed the mechanism of microtubule destabilization by XKCM1 and XKIF2, and have found that these proteins directly target to the ends of microtubules where they cause a destabilizing conformational change. We have also characterized the role of ATP hydrolysis by the catalytic domain of these proteins in this process. In addition to being the first detailed characterization of microtubule-destabilizing proteins, this work provides clear evidence for a non-motor function for a certain subclass of kinesins.

A handwritten signature in black ink, reading "T.S. Mitchison". The signature is written in a cursive style with a long horizontal stroke at the end. Below the signature is a dashed horizontal line.

Timothy Mitchison, Ph.D.

Committee Chair



# Analysis of Microtubule Dynamics and Chromosome Movement *in vitro*

## Table of Contents

### Chapter 1:

Introduction.....	1
-------------------	---

### Chapter 2:

Vertebrate Kinetochores Assembly <i>in vitro</i> .....	13
--	----

### Chapter 3:

Mechanism of Anaphase A in <i>Xenopus</i> Extract Spindles.....	20
---	----

### Chapter 4:

XKCM1: A Microtubule-Destabilizing Kinesin.....	63
---	----

### Chapter 5:

Mechanism of Microtubule Destabilization by XKCM1 and XKIF2 -- Two Internal Catalytic Domain Subfamily Kinesins.....	75
---	----

### Appendix I:

Real Time Observation of Anaphase <i>in vitro</i> .....	103
---	-----

### Appendix II:

Xenopus Extract Methodology.....	110
----------------------------------	-----

**Appendix III:**

A Compendium of Microtubule Methodology.....159

**References**.....202

## List of Tables

### Appendix I:

Table 1:

The effect of cyclin-B  $\Delta 90$  on anaphase movements.....106

### Appendix III:

Table 1:

Properties of commonly used fluorophores.....179

## List of Figures

### Chapter 1

Figure 1:

Microtubule structure and tubulin GTP hydrolysis.....10

Figure 2:

Microtubule dynamic instability.....11

Figure 3:

Microtubule distributions in interphase versus mitosis.....12

### Chapter 2

Figure 1:

Reagents for following kinetochore assembly in *Xenopus* egg extracts.....16

Figure 2:

Schematic of two-step kinetochore assembly reaction in clarified *Xenopus* egg extracts.....16

Figure 3:

Characterization of *in vitro* kinetochore assembly.....17

Figure 4:

Analysis of *in vitro* assembled kinetochores using immunoelectron microscopy.....17

## Figure 5:

Effect of XKCM1 depletion on targeting of CENP-E  
and cytoplasmic dynein.....18

## Figure 6:

Tubulin binding by *in vitro* assembled kinetochores.....18

### Chapter 3

## Figure 1:

Two models for anaphase A.....56

## Figure 2:

Kinetochores lead chromosomes poleward during anaphase *in vitro*.....57

## Figure 3:

Simultaneous analysis of flux and chromosome movement  
during anaphase *in vitro*.....58

## Figure 4:

Pharmacological analysis of chromosome movement and poleward  
microtubule flux in *Xenopus* extract spindles.....59

## Figure 5:

Anaphase kinetics of chromosome separation and spindle elongation.....60

Figure 6:	
Summary of analysis of chromosome movement and poleward flux.....	61

Figure 7:	
Poleward forces act on kinetochores during metaphase in <i>Xenopus</i> extract spindles.....	62

## Chapter 4

Figure 1:	
XKCM1 is a kinesin.....	65

Figure 2:	
Immunolocalization of XKCM1.....	66

Figure 3:	
Biochemical analysis of XKCM1.....	67

Figure 4:	
XKCM1 is required for mitotic spindle assembly.....	68

Figure 5:	
Quantitation of XKCM1 immunodepletion and rescue.....	69

Figure 6:	
Analysis of microtubule dynamics after XKCM1 depletion.....	69

Figure 7:	
Model for XKCM1 destabilization of microtubules.....	71

## Chapter 5

Figure 1:	
Expression and Purification of XKCM1 and XKIF2.....	94

Figure 2:	
XKCM1/XKIF2 is an ATP-dependent inhibitor of microtubule polymerization.....	95

Figure 3:	
XKCM1/XKIF2 depolymerizes GMPCPP microtubules.....	96

Figure 4:	
XKCM1/XKIF2 depolymerizes GMPCPP microtubules equivalently from both ends.....	97

Figure 5:	
XKCM1 depolymerizes GMPCPP microtubules without inducing GMPCPP hydrolysis.....	98

Figure 6:	
XKCM1/XKIF2 induces protofilament peeling at GMPCPP microtubule ends.....	99

Figure 7:	
XKCM1 targets to microtubule ends in AMPPNP.....	100

Figure 8:	
XKCM1/XKIF2 induces protofilament peeling in AMPPNP.....	101

Figure 9:	
A model for microtubule destabilization by XKCM1 and XKIF2.....	102

## **Appendix I:**

Figure 1:	
Anaphase chromosome movement and spindle dynamics <i>in vitro</i> .....	105

Figure 2:	
Astral ejection during anaphase <i>in vitro</i> .....	106

Figure 3:	
Anaphase kinetics of chromosome separation, spindle elongation and spindle microtubule density.....	106

Figure 4:	
Telophase chromosome movements.....	107

Figure 5:	
The role of chromosomes in maintaining spindle integrity.....	107



**Appendix II:**

Figure 1:

*In vitro* spindle assembly pathways.....155

Figure 2:

CSF spindle assembly intermediates.....156

Figure 3:

Optimal spindle fixation.....157

Figure 4:

Anaphase chromosome movement.....158

Harvard Medical School  
DEPARTMENT OF CELL BIOLOGY



240 Longwood Avenue  
Boston, Massachusetts 02115

Arshad Desai  
Phone: (617) 432-2688  
fax: (617) 492-6702  
email: adesai@hms.harvard.edu

February 19, 1998

To: **Permissions Editor**, *Proceedings of the National Academy of Sciences*

From: **Arshad Desai**

I am writing to request permission to reprint the following two papers as part of my Ph.D. thesis at the University of California, San Francisco.

a) Murray AW; Desai AB; Salmon ED.

Real time observation of anaphase in vitro.

Proceedings of the National Academy of Sciences, 1996 Oct 29, 93(22):12327-32.

b) Desai A, Deacon HW; Walczak CB; Mitchison TJ.

A method that allows the assembly of kinetochore components onto chromosomes condensed in clarified *Xenopus* egg extracts.

Proceedings of the National Academy of Sciences, 1997 Nov 11, 94(23):12378-83.

Sincerely,

Arshad Desai  
240 Longwood Ave., Bldg. C-517  
Dept. of Cell Biology  
Harvard Medical School  
Boston, MA 02115  
Phone: (617)-432-2688  
Fax: (617)-432-3702  
EMail: Arshad\_Desai@hms.harvard.edu

---

Permission granted. Please cite full  
journal reference and "Copyright (year)  
National Academy of Sciences, U.S.A."

Diane M. Sullenberger, Managing Editor  
BAB for DMS 2/27/98

Harvard Medical School  
DEPARTMENT OF CELL BIOLOGY



240 Longwood Avenue  
Boston, Massachusetts 02115

Arshad Desai  
Phone: (617) 432-2688  
fax: (617) 432-3702  
email: adesai@hms.harvard.edu

February 19, 1998

*To:* Cell  
*FROM*  
*From:* Arshad Desai  
*TO:*

I am writing to request permission to reprint the following paper as part of my Ph.D. thesis at the University of California, San Francisco.

Walczak CE; Mitchison TJ; Desai A.

XKCM1: a *Xenopus* kinesin-related protein that regulates microtubule dynamics during mitotic spindle assembly.

Cell, 1996 Jan 12, 84(1):37-47.

Sincerely,

Arshad Desai  
240 Longwood Ave., Bldg. C-517  
Dept. of Cell Biology  
Harvard Medical School  
Boston, MA 02115  
Phone: (617)-432-2688  
Fax: (617)-432-3702  
EMail: Arshad\_Desai@hms.harvard.edu

Permission granted subject to citation of the original manuscript, and noting that copyright is held by Cell Press. (Our permission is contingent on permission of the author.)

*Elm J. D. Dwyer*  
2/24/98

**FXED**  
2/24

# Introduction

Since the pioneering observations of late 19th century cell biologists (summarized in Wilson, 1928), deciphering the mechanisms of cell division has been a major focus in cell biology. In the past two decades, tremendous insight has been gained into the mechanisms that transform cytoplasmic state from interphase to mitotic (Murray and Hunt, 1993). How this transformation in cytoplasmic state dictates the execution of downstream processes resulting in the morphological and functional transformation of an interphase cell to a mitotic cell remains largely unexplained. These downstream mitotic processes are the focus of our work, with specific emphasis on the polymerization dynamics of microtubules (MTs), noncovalent polymers of tubulin that are essential for cell division in all eukaryotes (Desai and Mitchison, 1997; Hyams and Lloyd, 1994).

MTs are physically robust polymers, with an intrinsic resistance to bending and compression (Mickey and Howard, 1995; Venier et al., 1994), that organize the cytoplasm of eukaryotes and serve as tracks for intracellular trafficking. The ensemble of actin filaments, intermediate filaments and MTs comprises the cytoskeleton of eukaryotic cells. The term "cytoskeleton" is misleading, however, in the sense that it suggests a static structure. Cytoskeletal polymers are highly dynamic, capable of polymerizing, depolymerizing and moving within the cytoplasm on a time scale of seconds to minutes. The evolutionary conservation of energetically expensive cytoskeletal polymer dynamics suggests important biological roles. MT polymerization dynamics are thought to be important in many cellular processes including cell division (Inoué and Salmon, 1995), cell motility (Gundersen and Bulinski, 1988; Tanaka et al., 1995; Waterman-Storer and Salmon, 1997), and cellular morphogenesis/differentiation (Bre et al., 1990; Bulinski and Gundersen, 1991).

The subunit of a MT is a heterodimer of  $\alpha$ - and  $\beta$ -tubulin.  $\alpha$ - and  $\beta$ -tubulin monomers are ~50% identical at the amino acid level and each have a molecular mass of about 50,000 daltons (Burns, 1991). Within a MT,  $\alpha\beta$  tubulin dimers associate head-to-tail to form linear protofilaments, and 12-15 parallel protofilaments associate laterally to form the 25 nm-diameter polar, hollow, cylindrical polymer (Figure 1A; Amos and Klug, 1974). The different polymerization rates of the two ends of a MT are a consequence of its polarity; the faster growing end is referred to as the plus end and the slower growing end as the minus end (Allen and Borisy, 1974). The polarity of the MT lattice is central to the function of MT motor proteins of the kinesin (Vale and Fletterick, 1997) and dynein (see Hyams & Lloyd, 1994) families, that utilize the energy of ATP hydrolysis to move unidirectionally along the MT. Within each protofilament,  $\alpha\beta$  heterodimers are oriented with  $\beta$ -tubulin pointing towards the plus end of the MT. This arrangement results in  $\beta$ -tubulin being exposed at the plus end and  $\alpha$ -tubulin being exposed at the minus end of the MT (Figure 1).

Tubulin heterodimers copurify with two moles of guanine nucleotide per mole  $\alpha\beta$  dimer (Weisenberg et al., 1968). During polymerization, GTP bound to  $\beta$ -tubulin (at the exchangeable or E-site) is hydrolyzed (David-Pfeuty et al., 1977; MacNeal and Purich, 1978); the resulting E-site GDP does not exchange while  $\beta$ -tubulin remains in the polymer (Figure 1B). Upon depolymerization, the released tubulin subunits can exchange E-site GDP for GTP and undergo another round of polymerization.  $\alpha$ -tubulin also binds GTP but this GTP is bound in a non-exchangeable manner (at the N-site) and does not get hydrolyzed during polymerization (Figure 1B; Spiegelman et al., 1977). MTs are nucleation-condensation polymers with a kinetically unfavorable nucleation phase prior to a favorable elongation phase (Oosawa

and Asakura, 1975). This kinetic barrier to spontaneous nucleation is exploited by MT-nucleating sites, such as centrosomes, to control the spatial organization of MTs *in vivo* (Kellogg et al., 1994).

MTs utilize polymerization-triggered GTP hydrolysis on  $\beta$ -tubulin to destabilize the MT lattice, thereby generating dynamic instability -- a special polymerization behavior where both polymerizing and depolymerizing MTs coexist in the same population and infrequently interconvert between these two states (Figure 2; Mitchison and Kirschner, 1984a; 1984b). A popular hypothesis for the mechanism of dynamic instability postulates a heterogeneity in nucleotide content at MT ends combined with the difference in the lattice stability of GTP- versus GDP-tubulin (Mitchison and Kirschner, 1984a). Polymerizing ends are thought to maintain a stabilizing cap of GTP/GDP.P<sub>i</sub>, the loss of which results in exposure of an unstable GDP-tubulin core and subsequent rapid depolymerization (Figure 2). GTP-hydrolysis driven destabilization of the MT lattice is supported by many different studies. Kinetically, hydrolysis results in a GDP-tubulin lattice that has >1000-fold higher subunit off rate than GTP-tubulin from a MT end (Caplow et al., 1994; Walker et al., 1988). Structurally, GDP-tubulin protofilaments generated after hydrolysis are thought to prefer a conformation with increased outward protofilament curvature (Mandelkow et al., 1991; Melki et al., 1989). In a MT, a GDP-tubulin protofilament is constrained to being straight, presumably by lattice interactions, but during depolymerization it can relax into the preferred curved conformation (Figure 1B). The free energy released during this relaxation is thought to drive the rapid depolymerization phase of dynamic instability. Thus, the energy of GTP hydrolysis accompanying MT polymerization is stored as mechanical strain in the lattice that is subsequently released upon depolymerization. The coupling of GTP

hydrolysis to MT dynamics also endows both MT polymerization and depolymerization with the potential to perform mechanical work -- a property probably important in the intracellular functions of MT dynamics (e.g. see Inoué and Salmon, 1995).

The biological importance of MT polymerization dynamics is most dramatically highlighted during cell division by the striking rearrangements of cytoplasmic MTs during the transition from interphase to mitosis (Figure 3; McNally, 1996) and by the intricate dance of the chromosomes that is tightly coupled to the dynamics of their bound MTs (Inoué and Salmon, 1995; Mitchison, 1988; Salmon, 1989). Both mitotic and meiotic cells assemble a bipolar, microtubule (MT)-based spindle (Figure 3 *lower panel*) to execute chromosome segregation. Chromosomes connect to the spindle MTs via their kinetochores -- specialized nucleoprotein structures assembled at the centromere of mitotic chromosomes (red dots in Figure 3 *lower panel*). Sister kinetochores of replicated chromosomes capture the plus ends of dynamically unstable MTs associated with opposite spindle poles, and become tethered to the poles by forming a stable bundle of kinetochore MTs. After all the chromosomes are properly attached, the connections holding the sister chromatids (mitosis, meiosis II) or homologous chromosomes (meiosis I) are dissolved and the separated chromosomes move toward opposite spindle poles. Segregation of sisters to daughter cells involves both chromosome-to-pole movement (anaphase A), coupled to depolymerization of the kinetochore MTs, and spindle pole-to-pole elongation (anaphase B). The exit from mitosis is also accompanied by dramatic changes in MT organization and dynamics that initially direct the proper assembly of the cleavage furrow and eventually reestablish the interphase configuration of the cellular MT distribution.



Within the mitotic spindle, the large majority of MTs turn over very rapidly with a half-life of 30 sec - 1 minute (Salmon et al., 1984). However, the small fraction of spindle MTs bound to the kinetochore are approximately an order of magnitude more stable than the rest of the spindle MTs (half-life of ~5-10 minutes; Zhai et al., 1995). Although kinetochore MTs turn over slower than other spindle MTs, the interface of the kinetochore with the plus ends of the attached MTs is very dynamic. In vertebrate somatic cells, where this interaction has been analyzed in the greatest detail, the kinetochore couples continuous poleward and anti-poleward movement of chromosomes to the polymerization and depolymerization of the attached MTs (Rieder and Salmon, 1998). Deciphering the mechanisms that generate and modulate this dynamic interface remains one of the most interesting and challenging problems in the study of MT dynamics.

A mechanistic analysis of the kinetochore-MT interface has been limited primarily by the functional complexity and small size of the kinetochore. The kinetochore is a minute fraction of the chromosome in terms of size and protein content, but possesses many complex activities including MT capture, MT motility, coupling to MT dynamics, and monitoring MT attachment to ensure accuracy of chromosome segregation (Rieder and Salmon, 1998). To date, the best progress toward a molecular dissection of kinetochores has been in budding yeast, primarily because their simple centromere structure has enabled extensive genetic and biochemical analysis (Hyman and Sorger, 1995). However, the much greater complexity of centromere structure in other eukaryotes (Bloom, 1993), including fission yeast, indicate the necessity of an experimentally amenable system for dissecting kinetochores formed on these complex centromeres. In Chapter 2

we describe our attempt to accomplish this using *Xenopus* egg extracts to assemble vertebrate kinetochores *in vitro*.

In the last decade, much emphasis has been placed on the kinetochore-MT interface as the predominant site of changes in the polymerization/depolymerization of chromosome-attached MTs. One factor contributing to this emphasis has been the finding that MT minus ends, while exhibiting dynamic instability in MTs assembled with pure tubulin *in vitro*, appear to be inertly buried in the matrix of a nucleating structure *in vivo* (e.g. the pericentriolar material of animal cell centrosomes; Kellogg et al., 1994). Evidence for a dynamic MT interface distinct from the kinetochore-MT interface during chromosome movement, as well as for minus end MT dynamics *in vivo*, was first obtained in mitotic spindles of mammalian cells. Fluorescent marks on the kinetochore MT lattice moved poleward during metaphase, with plus end polymerization near the kinetochore being balanced by minus end depolymerization near the spindle poles (Mitchison, 1989). The discovery of this "poleward MT flux" in mitotic spindles rekindled the possibility that chromosome-to-pole movement in anaphase A may occur as a result of poleward translocation of the MT lattice, coupled to minus end depolymerization near the poles, as opposed to kinetochore motility over stationary MTs, coupled to plus end depolymerization near the kinetochore. However, this possibility has been discounted in the decade following the discovery of MT flux, primarily as a result of studies in vertebrate somatic cells showing that the kinetochore is the predominant site of MT depolymerization during chromosome-to-pole movement (Gorbsky et al., 1988; Mitchison and Salmon, 1992; Waters et al., 1996; Zhai et al., 1995). In Chapter 3, we describe studies in *Xenopus* egg extracts that suggest predominance of a poleward flux mechanism for anaphase chromosome

movement in this non-somatic system. This finding indicates the importance of considering MT flux as a relevant alternative mechanism to kinetochore motility for moving chromosomes poleward and also stimulates analysis of the mechanism of spindle MT flux.

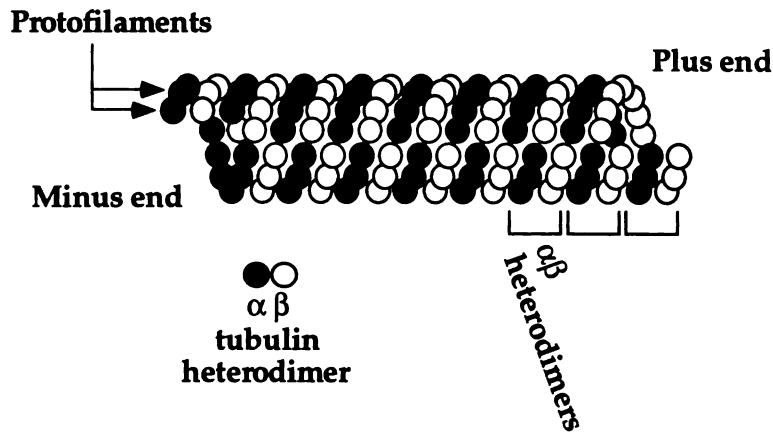
Direct observation of single MT polymerization/depolymerization allows a description of MT dynamic instability by four parameters: the rates of polymerization and depolymerization, and the frequencies of catastrophe (the transition from polymerization to depolymerization) and of rescue (the transition from depolymerization to polymerization) (Figure 2; Walker et al., 1988). Although the precise mechanism by which GTP hydrolysis generates dynamic instability of pure tubulin remains to be elucidated, much is known about MT dynamics inside cells. MTs *in vivo* differ from pure tubulin primarily in their rapid polymerization rates and their high transition frequencies (Cassimeris, 1993). Studies with pure tubulin have shown that increasing the tubulin concentration, and thus the polymerization rate, results in a decrease in the catastrophe frequency (Erickson and O'Brien, 1992; Walker et al., 1988). The polymerization rate of tubulin *in vivo* is about 5 to 10-fold higher than that of a similar concentration of pure tubulin. Despite these rapid polymerization rates, MTs *in vivo* exhibit a high frequency of catastrophe (Belmont et al., 1990; Cassimeris, 1993). If the relationship between polymerization rate and catastrophe frequency for pure tubulin is used as a reference, at the polymerization rates observed *in vivo* one would expect a near-zero frequency of catastrophe. This apparent paradox can be resolved if distinct mechanisms exist to promote polymerization and to induce catastrophes *in vivo*. Particular emphasis has been placed on the mechanisms stimulating catastrophes since computer simulations have shown the exquisite sensitivity of MT distributions to changes in the

catastrophe frequency (Gliksman and Salmon, 1993; Verde et al., 1992) and analyses of MT dynamics in *Xenopus* extracts have implicated increases in the catastrophe frequency as underlying the dramatic reorganization of MT distributions between interphase and mitosis (Figure 3; Belmont et al., 1990; Verde et al., 1992). Furthermore, in addition to their potential importance in regulation of dynamics *in vivo*, analysis of catastrophe factors may help elucidate the mechanism of catastrophe, which is still unclear from pure tubulin work. A major part of this thesis (Chapters 4 and 5) describes two members of a subfamily of kinesins that possess the novel non-motor function of destabilizing MTs by inducing catastrophes, and explores in detail the mechanism of their action.

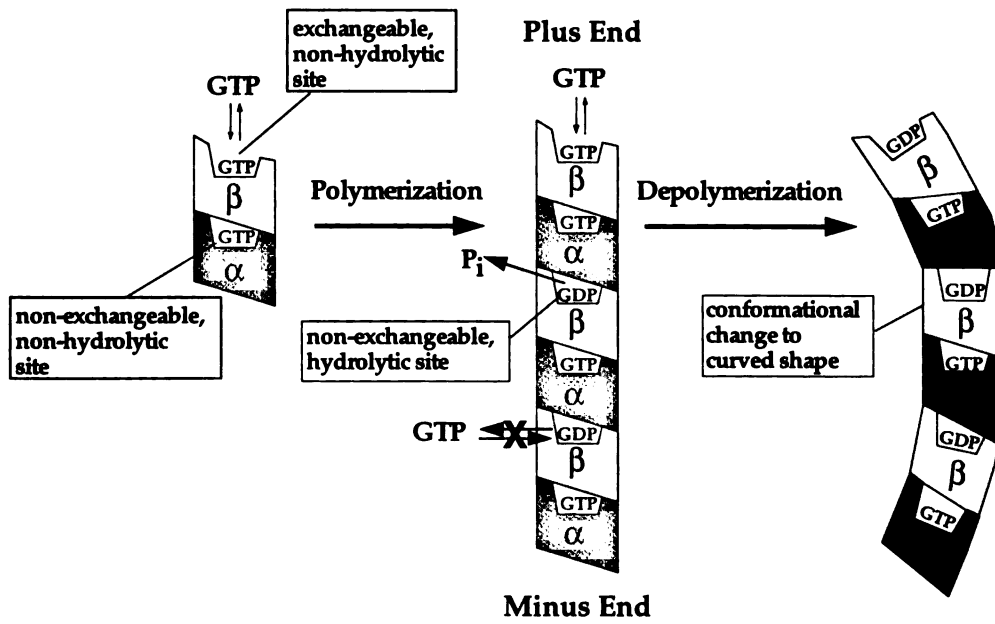
The three projects described in this thesis, although seemingly disparate, have in common an emphasis on the polymerization dynamics of MTs. While kinetochore assembly seems distant from MT dynamics, the long term goal behind the development of a kinetochore assembly assay was to understand how the kinetochore generates a dynamic interface with MTs. The discovery and mechanistic characterization of a new class of MT-destabilizing proteins more directly addresses intracellular regulation of MT dynamics. The demonstration of predominantly poleward flux-driven anaphase chromosome movement stimulates inquiry into the mechanism of this complex dynamic behavior of spindle MTs, particularly the mechanism generating the flux-associated depolymerization of MT minus ends.

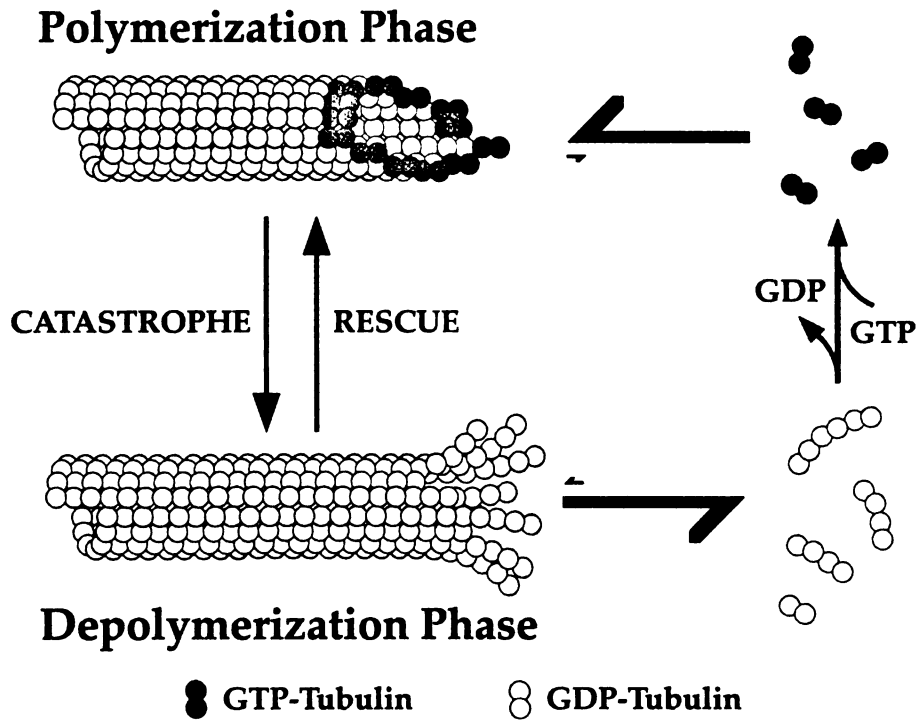
Figure 1

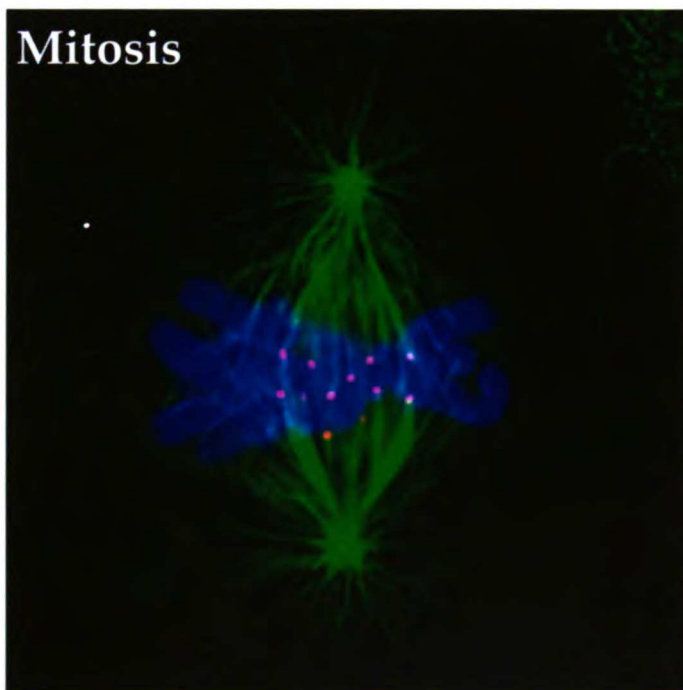
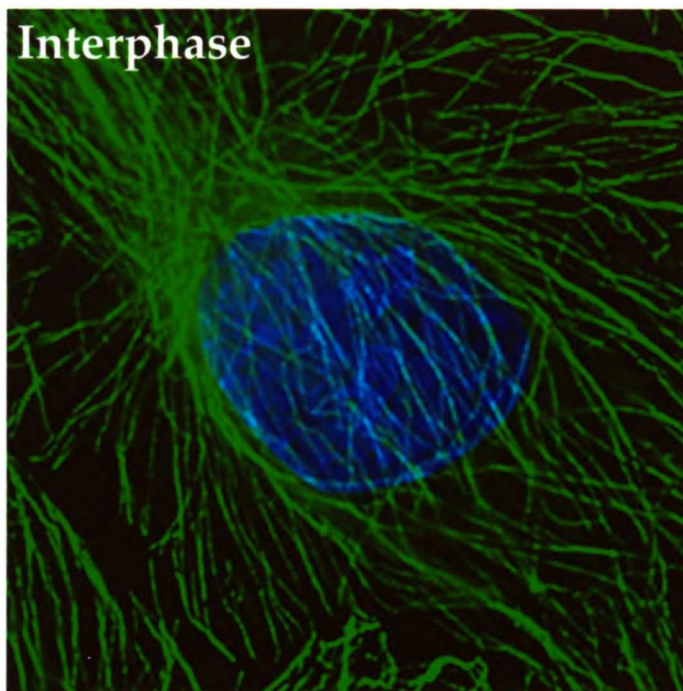
## A. Microtubule Structure



## B. Tubulin GTP Hydrolysis



**Figure 2****Microtubule Dynamic Instability**

**Figure 3**

## Chapter 2

### Vertebrate Kinetochores Assembly *in vitro*

The text of this chapter has been reproduced from the Proceedings of the National Academy of Sciences, 1997, Volume 94 pages 12378-83. Copyright (1997) National Academy of Sciences, U.S.A.

I performed all the experiments in this paper and wrote the paper with the help of comments from the co-authors. H. W. Deacon made an important observation as a rotation student that allowed the development of the assay described in this paper and Dr. C. E. Walczak provided the anti-XKCM1 antibody central to many aspects of this work.



## A method that allows the assembly of kinetochore components onto chromosomes condensed in clarified *Xenopus* egg extracts

(*in vitro*/mitosis/CENP-E/XKCM1/dynein)

ARSHAD DESAI\*†, HEATHER W. DEACON\*, CLAIRE E. WALCZAK‡, AND TIMOTHY J. MITCHISON‡

Departments of \*Biochemistry and Biophysics and †Cellular and Molecular Pharmacology, University of California, San Francisco, CA 94143-0448

Communicated by Bruce Alberts, National Academy of Sciences, Washington, DC, August 29, 1997 (received for review August 18, 1997)

**ABSTRACT** Kinetochore are complex macromolecular structures that link mitotic chromosomes to spindle microtubules. Although a small number of kinetochore components have been identified, including the kinesins CENP-E and XKCM1 as well as cytoplasmic dynein, neither how these and other proteins are organized to produce a kinetochore nor their exact functions within this structure are understood. For this reason, we have developed an assay that allows kinetochore components to assemble onto discrete foci on *in vitro*-condensed chromosomes. The source of the kinetochore components is a clarified cell extract from *Xenopus* eggs that can be fractionated or immunodepleted of individual proteins. Kinetochore assembly in these clarified extracts requires preincubating the substrate sperm nuclei in an extract under low ATP conditions. Immunodepletion of XKCM1 from the extracts prevents the localization of kinetochore-associated XKCM1 without affecting the targeting of CENP-E and cytoplasmic dynein or the binding of monomeric tubulin to the kinetochore. Extension of this assay for the analysis of other components should help to dissect the protein–protein interactions involved in kinetochore assembly and function.

A key event during mitosis is the segregation of replicated chromosomes to daughter cells. During chromosome segregation, kinetochores play a central role by mediating chromosome–microtubule interactions. In mammalian cells, the kinetochore is a complex trilaminar structure assembled on the centromeric region of mitotic chromosomes (1–3). Molecules that may interact with microtubules are thought to localize to the fibrous corona and the outer plate—the two outermost regions of the kinetochore (3, 4).

Biochemical analysis of kinetochores has been limited by difficulties in purifying kinetochores and by their small size; kinetochore components constitute only a minor fraction of chromosomal proteins. Despite these drawbacks, a number of kinetochore components have been identified in mammals. These components fall into two classes: constitutive components, present at kinetochore regions throughout the cell cycle, and mitosis-specific components, targeted to the kinetochore region specifically during its mitotic maturation (1, 2).

The three known constitutive components, CENP-A, CENP-B, and CENP-C were identified in studies using autoimmune sera directed against human centromeres (5–7). Several mitosis-specific kinetochore components have also been identified. Included in this second group are three microtubule motor proteins: cytoplasmic dynein, CENP-E, and XKCM1. Cytoplasmic dynein, a minus end-directed microtubule motor, localizes to the corona which is the outer-most region of the kinetochore (4). CENP-E, a kinesin identified as a salt-

resistant chromosomal scaffold component of mammalian tissue culture cell chromosomes, localizes to the kinetochore region of mitotic chromosomes (8). XKCM1 is a kinesin isolated from *Xenopus* that localizes to the centromeric region of mitotic chromosomes by light microscopy, but has yet to be localized at high resolution using immunoelectron microscopy. It has 55% overall amino acid identity with MCAK, a kinesin identified earlier in mammalian (CHO) cells that is similarly localized (9, 10).

The development of methods to isolate mitotic chromosomes from mammalian tissue culture cells has led to the *in vitro* study of kinetochore structure and function. Kinetochore can bind monomeric tubulin, nucleate microtubule assembly, capture and move microtubules, and remain attached to depolymerizing microtubules (refs. 11–15; reviewed in ref. 16). An alternative approach to the study of kinetochore structure and function has been the use of antibody microinjection into tissue culture cells (17, 18).

To extend the work on mammalian kinetochores to a biochemical level, it will be necessary to correlate specific molecules with specific functions. So far, little progress has been made in this direction. The major barriers to such progress are the difficulty in manipulating kinetochores on chromosomes purified from tissue culture cells and in interpreting the results of microinjection studies. Development of an *in vitro* system for kinetochore assembly would complement existing approaches by allowing the assembly of large numbers of kinetochores under reproducible conditions. In addition, the contribution of individual components could be tested by immunodepletion before assembly. *Xenopus* egg extracts provide an *in vitro* system for studying mitotic processes in which a pseudo-genetic approach is available using antibodies to inhibit or remove specific components (9).

To develop an *in vitro* kinetochore assembly assay, we first needed to establish markers for kinetochores in *Xenopus*. To this end, we demonstrate using antisera to three mitotic kinetochore markers—cytoplasmic dynein, CENP-E, and XKCM1—that *Xenopus* and mammalian kinetochores recruit similar mitosis-specific components. Using these proteins as markers, we have developed an *in vitro* reaction for kinetochore assembly on chromosomes condensed in clarified extracts of *Xenopus* eggs. Ideally, we would like to analyze kinetochore assembly in crude cycled extracts (extracts in which the sperm DNA has been replicated prior to assembling mitotic chromatin), so that the segregation competence of the kinetochores could be directly assayed following assembly. However, to date, it has been impossible to immunodeplete components from crude extracts while maintaining their ability to segregate chromosomes. In addition to ease of immunodepletion, clarified extracts have other advantages over crude extracts. Membranes and cytoskeletal elements do not

The publication costs of this article were defrayed in part by page charge payment. This article must therefore be hereby marked "advertisement" in accordance with 18 U.S.C. §1734 solely to indicate this fact.

© 1997 by The National Academy of Sciences 0027-8424/97/9412378-6\$2.00/0  
PNAS is available online at <http://www.pnas.org>.

†To whom reprint requests should be sent at the present address: Department of Cell Biology, Harvard Medical School, 240 Longwood Avenue, Building C-517, Boston, MA 02115. e-mail: [adesai@hms.harvard.edu](mailto:adesai@hms.harvard.edu).

assemble in clarified extracts facilitating identification of chromosomal components (18, 19), and clarified extracts are also more reproducible, more stable while frozen, and offer the potential for direct biochemical fractionation. Because of these technical advantages we have concentrated our efforts on clarified extracts.

## MATERIALS AND METHODS

**Tissue Culture Cell Chromosome Isolation and Immunofluorescence.** Tissue culture cell chromosomes were purified from CHO cells and *Xenopus* A6 cells as described (4) with minor modifications for A6 cells.

For immunofluorescence, appropriate volumes of CHO and A6 chromosomes were diluted to 10  $\mu$ l with PME buffer (10 mM K-Pipes, pH 7.2/5 mM MgCl<sub>2</sub>/1 mM EGTA) on ice and fixed by addition of 200  $\mu$ l of PME plus 1% formaldehyde at room temperature for 10 min. Fixed chromosomes were layered onto a 5 ml cushion of 30% (vol/vol) glycerol in PME and pelleted onto polylysine-coated coverslips at 10,000 rpm for 15' at 4°C in an HB-4 rotor. Pelleted chromosomes were postfixed in -20°C methanol for 3 min before processing for immunofluorescence.

**In Vitro Kinetochores Assembly.** Clarified cytotostatic factor (CSF)—arrested extracts and demembrated sperm nuclei—were prepared as described (20, 21) with minor modifications. Crude CSF extracts were prepared by crushing dejellied eggs exactly as described (20). The crude extract was supplemented with protease inhibitors, 10  $\mu$ g/ml cytochalasin D, and 1 $\times$  energy regeneration mix (added from a 20 $\times$  stock: 1 $\times$  = 7.5 mM creatine phosphate/1 mM ATP/1 mM MgCl<sub>2</sub>; see ref. 20 for details) then clarified at 50,000 rpm in a TLS55 rotor at 4°C for 2 h. The clarified extracts were recovered using a 20 gauge needle, respun at 55,000 rpm for 30 min in a TLS55 rotor at 4°C, frozen in liquid nitrogen in 50–100  $\mu$ l aliquots, and stored at -80°C. Extracts prepared and stored in this manner retain the ability to reproducibly assemble kinetochores for at least 6 months.

Kinetochores assembly was performed as diagrammed in Fig. 2. A total of 4  $\mu$ l of 3  $\times$  10<sup>7</sup> sperm nuclei/ml was mixed on ice with 8  $\mu$ l of clarified extract and 8  $\mu$ l of XBE5 (10 mM K-Hepes, pH 7.7/50 mM sucrose/100 mM KCl/0.1 mM CaCl<sub>2</sub>/5 mM EGTA/5 mM MgCl<sub>2</sub>) before incubation at 20°C for 2 h (preincubation). On ice, 5  $\mu$ l of the preincubation reaction were mixed with 25  $\mu$ l of XBE5 plus 2 $\times$  energy mix (1 $\times$  = 7.5 mM creatine phosphate/1 mM ATP/1 mM MgCl<sub>2</sub>/50  $\mu$ g/ml creatine kinase) and 20  $\mu$ l of clarified extract containing 10  $\mu$ g/ml nocodazole, then incubated at 20°C for 1.5–2 h (assembly).

**Immunofluorescence Analysis of In Vitro Kinetochores Assembly.** A total of 15  $\mu$ l of the assembly reaction was fixed by pipeting in 300  $\mu$ l of XBE2 (10 mM K-Hepes, pH 7.7/50 mM sucrose/100 mM KCl/0.1 mM CaCl<sub>2</sub>/5 mM EGTA/2 mM MgCl<sub>2</sub>) plus 1% formaldehyde and immediately mixing well with a cutoff pipet tip. After 12 min at room temperature the fixed reaction was pelleted onto polylysine-coated coverslips through an ice-cold 5 ml cushion of 30% (vol/vol) glycerol in XBE2. Coverslips were postfixed in -20°C methanol for 3 min and processed for immunofluorescence. Antibodies were used in the following order: 70.1 anti-dynein intermediate chain monoclonal ascites fluid, Texas Red goat anti-mouse IgM (Jackson ImmunoResearch), 3  $\mu$ g/ml affinity-purified rabbit anti-human CENP-E (HX antibody raised to rod domain of CENP-E (22); gift of B. Schaar and T. Yen), or 0.5  $\mu$ g/ml affinity-purified rabbit anti-XKCM1 (9), and fluorescein isothiocyanate donkey anti-rabbit (Jackson ImmunoResearch). Often, the dynein signal was amplified by use of a Texas Red-labeled tertiary antibody as the penultimate antibody (Texas Red donkey anti-goat, Jackson ImmunoResearch). Coverslips were rinsed with TBST containing 1  $\mu$ g/ml Hoechst

33342 and mounted in 0.5% *p*-phenylenediamine (free base; Sigma) in 20 mM Tris-HCl, pH 9/90% glycerol.

Although both CENP-E and dynein were always detectable using a straight XBE2 plus 1% formaldehyde fixation, we observed some variation between extracts in our ability to detect XKCM1 using this fixation. We could eliminate this variability by diluting the reactions in 10 volumes of PME plus 0.2 M sucrose plus 0.1% Triton X-100 at 0°C for 10 min and then fixing by adding 10 volumes of PME plus 1% formaldehyde for 12 min at room temperature.

**Assaying Tubulin Binding by Kinetochores.** To purify condensed sperm nuclei, 0.1 ml of 66% (wt/wt) sucrose in PME at the bottom of a 0.5 ml Eppendorf tube was overlaid with a 0.4 ml cushion of 30% (wt/vol) sucrose in PME. A total of 50–100  $\mu$ l of the assembly reaction were layered on top of the cushion before spinning in an HB-4 rotor at 10,000 rpm for 15 min at 4°C. The cushion was washed several times while aspirating, and the interface between the cushion and the heavy sucrose pad was collected in the starting reaction volume. In case of salt extraction, the assembly reactions were diluted prior to purification with an equal volume of XBE5 plus 0.5 $\times$  energy mix containing either 0 mM or 200 mM extra NaCl and incubated at room temperature for 10 min.

Tubulin binding assays were performed as described (14) with some modifications. Purified condensed sperm nuclei were diluted at least 10-fold into 50 mM K-Pipes, pH 7.2/1 mM EGTA/5 mM MgCl<sub>2</sub>/1 mM GTP with or without 10  $\mu$ M bovine brain tubulin and incubated at 37°C for 10 min. The reaction mix was diluted with an equal volume of ice-cold PME plus 0.1% Triton X-100 and incubated on ice for 5 min to depolymerize any microtubules before being sedimented unfixed onto polylysine coated coverslips, fixed in PME plus 0.1% Triton X-100 plus 2% formaldehyde at 0°C for 10 min, postfixed in -20°C methanol for 3 min and processed for double label immunofluorescence for tubulin and CENP-E as described above. DM1 $\alpha$  antibody was used to detect  $\alpha$ -tubulin.

**Transmission and Immunoelectron Microscopy.** For immunoelectron microscopy, fixed assembly reactions were sedimented onto Aclar (Ted Pella, Irvine, CA) coverslips as above, omitting methanol postfixation. Coverslips were blocked in EMBlock [PBS (137 mM NaCl/5.4 mM Na<sub>2</sub>HPO<sub>4</sub>/1.8 mM KH<sub>2</sub>PO<sub>4</sub>/2.7 mM KCl, pH 7.2) plus 0.1% Tween-20 plus 1.5% (wt/vol) BSA plus 0.5% (wt/vol) teleost fish gelatin (Sigma)] for 30 min, incubated in 3  $\mu$ g/ml anti-CENP-E antibody diluted in EMBlock for 45 min, rinsed well in EMBlock, and then extensively in PBS plus 0.1% Tween (PBSTw), incubated for 45 min in 1/30 dilution in EMBlock of 6 nm colloidal gold-conjugated goat anti-rabbit secondary (Jackson ImmunoResearch), rinsed well in EMBlock, and extensively in PBSTw, rinsed with PBS, and fixed in 1% glutaraldehyde in 0.1 M Na-cacodylate (pH 7.4) for 30 min at room temperature. Coverslips were then rinsed in cacodylate buffer, osmicated in 1% reduced osmium in 1.6% potassium ferricyanide in 0.1 M Na-cacodylate (pH 7.4) for 15 min on ice, *en bloc* stained overnight at 4°C with 1% uranyl acetate, dehydrated, and embedded in Epon Araldite resin. Sections were cut on a Reichert Ultracut S ultramicrotome and observed with a Philips EM400 electron microscope.

For transmission electron microscopy XL177 *Xenopus* tissue culture cells were plated on polylysine-coated Aclar coverslips, simultaneously permeabilized, and fixed in EMB (80 mM K-Pipes, pH 6.9/3 mM MgCl<sub>2</sub>/5 mM EGTA/0.5% Triton X-100) plus 0.1% glutaraldehyde for 5 min at room temperature, and then fixed in EMB plus 1% glutaraldehyde for 60 min at room temperature. Subsequent processing steps were performed as described above.

## RESULTS AND DISCUSSION

**Reagents for Following Kinetochores Assembly in *Xenopus* Egg Extracts.** To develop an *in vitro* assay for kinetochores

assembly using *Xenopus* egg extracts, we needed reagents directed against *Xenopus* kinetochore components. We analyzed four different human autoimmune sera (CREST sera; ref. 23) that recognize constitutive centromeric components in mammals, but failed to observe any localization of these sera to centromeric regions in *Xenopus* A6 tissue culture cells or on purified A6 chromosomes (not shown). We then tried antibodies to three different mitosis-specific kinetochore components—CENP-E, cytoplasmic dynein (intermediate chain of 78 kDa), and XKCM1—of which only XKCM1 is a *Xenopus*-specific protein. Antibodies to each of these three proteins recognize single bands of the expected sizes on immunoblots of *Xenopus* egg extracts (Fig. 1A) and localize identically to the kinetochore regions of both isolated A6 and CHO cell chromosomes (Fig. 1B), suggesting that *Xenopus* and mammalian kinetochores recruit similar mitosis-specific motor proteins. In addition, electron microscopy revealed that chromosomes in mitotic *Xenopus* tissue culture cells possess the characteristic trilaminar plate structure described for mammalian kinetochores (Fig. 1C).

**Kinetochore Assembly *In Vitro* Using Clarified *Xenopus* Egg Extracts.** To develop an assay for kinetochore assembly *in vitro*, we monitored the targeting of cytoplasmic dynein, CENP-E, and XKCM1 to discrete points on chromosomes condensed in clarified cytosstatic factor-arrested *Xenopus* egg extracts. Using demembrated *Xenopus* sperm nuclei as substrates, we began our studies using the conditions described by Hirano and Mitchison (21), which were optimized for mitotic chromosome condensation. Under these conditions, we failed to detect targeting of any of the three kinetochore markers to discrete regions on the condensed chromosomes.

We found that modification of the chromosome assembly assay into a two-step reaction (diagrammed in Fig. 2) leads to efficient targeting of all three kinetochore markers to discrete dots on the condensed chromosomes. In the first step in this reaction, the "preincubation" phase, sperm nuclei are held for 2 h at 20°C in a 2-fold diluted clarified extract without addition of an energy regeneration system. At the end of this phase, the sperm nuclei are present as tightly clustered thin fibers of

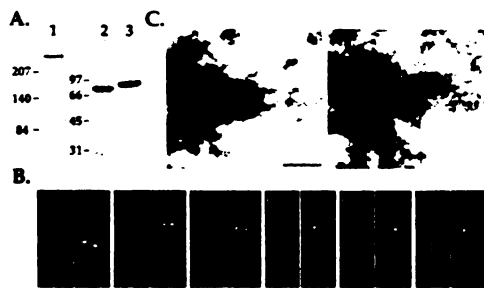


**FIG. 1.** Reagents for following kinetochore assembly in *Xenopus* egg extracts. (A) Immunoblots of *Xenopus* extracts using 1 µg/ml affinity-purified anti-human CENP-E (lane 1), anti-chicken cytoplasmic dynein intermediate chain mAb 70.1 ascites fluid (lane 2), and 0.1 µg/ml affinity-purified anti-XKCM1 (lane 3) antibodies. Extracts were fractionated by 6% SDS/PAGE for CENP-E immunoblots and by 10% SDS/PAGE for dynein and XKCM1 immunoblots. Molecular mass markers (in kDa) are indicated to the left of each set of panels. (B) Comparative immunofluorescence of CHO (a, c, and e) and A6 (b, d, and f) cell chromosomes using antibodies to CENP-E (a and b), cytoplasmic dynein intermediate chain (c and d), and XKCM1 (e and f). Antibody localizations are shown in the right panel of each pair and DNA in the left panel. (Bar = 5 µm.) (C) Analysis of mitotic XL177 cells by electron microscopy demonstrating the presence of a trilaminar plate kinetochore structure at the point of interaction of kinetochore microtubules with the chromosome. Two separate examples are shown. (Bar = 0.2 µm.)

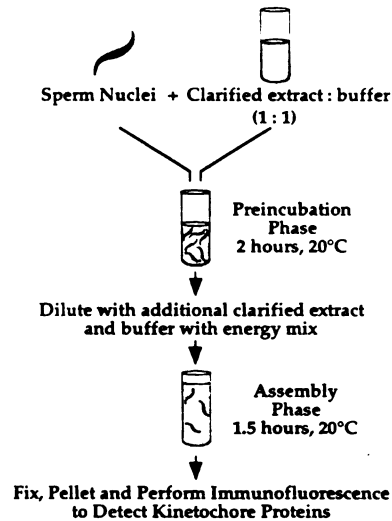


**FIG. 2.** Schematic of the two-step kinetochore assembly reaction in clarified *Xenopus* egg extracts (see text for details).

condensed chromatin, demonstrating maintenance of mitotic state. However, none of the kinetochore markers are detectable by immunofluorescence on the DNA at the end of the preincubation (data not shown). The second step of the reaction, the "assembly" phase, mimics the chromosome condensation reaction of Hirano and Mitchison (21). To initiate this phase of the reaction, additional clarified extract and buffer containing energy mix are added to the preincubation reaction. The assembly reaction is then incubated at 20°C for 1.5 h. Nocodazole is added in the second step of the reaction, but the results are essentially unchanged without it (there is no spindle assembly in these clarified extracts).

An example of the products from this reaction scheme and the inhibitory effect of energy regeneration mix in the preincubation buffer is shown in Fig. 3A: quantitation of this effect is shown in Fig. 3B. The requirement for a preincubation under low ATP conditions is specific to clarified extracts and is not necessary in low speed crude *Xenopus* extracts. We do not understand the function of the preincubation phase: it could be necessary to overcome an imbalance in cell cycle state regulators generated by centrifugation (24, 25) or for some prerequisite alteration in centromeric chromatin structure. Absence of sperm nuclei in the preincubation phase of the two-step reaction, followed by the addition of sperm nuclei for a brief period prior to the assembly phase, does not result in kinetochore assembly (data not shown), suggesting that the preincubation phase is priming the sperm chromatin for kinetochore assembly.

As shown in Fig. 3C, the structures obtained in our *in vitro* assembly reaction colocalize all three mitotic kinetochore markers to the same discrete foci on the DNA. In addition, the number of dots of kinetochore markers associated with each sperm nucleus is consistent with the number expected. *Xenopus* sperm nuclei have 18 chromosomes (26) and, because there is no DNA replication in clarified extracts, we expect one kinetochore per chromosome at the end of the assembly reaction. Counting the number of dots of kinetochore marker proteins associated with each condensed chromosomal cluster, we find on average 16 dots (Fig. 3B), close to the expected number of 18. Unlike the reaction conditions used by Hirano and Mitchison (21), our assay conditions do not result in

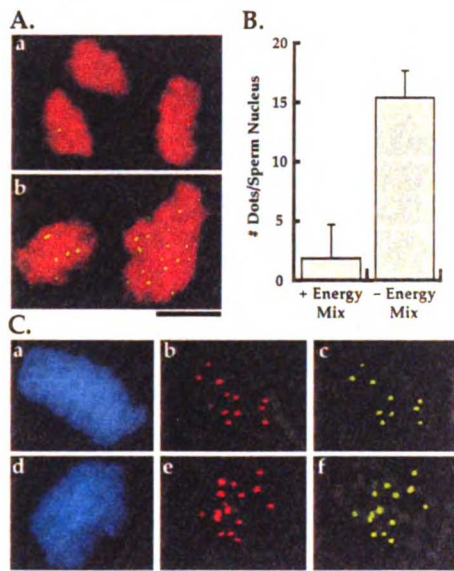


**FIG. 3.** Characterization of *in vitro* kinetochore assembly. (*A*) Effect of presence (*a*) or absence (*b*) of energy mix in preincubation buffer on kinetochore assembly. DNA is in red and CENP-E is in green. The same result is obtained with anti-dynein and anti-XKCM1 antibodies. There is no striking difference in the morphology of the condensed DNA at the end of the assembly reaction between the two conditions. (*B*) Quantitation of kinetochore assembly and effect of energy mix in preincubation buffer. The bars represent the mean number of dots of kinetochore marker proteins per sperm nucleus  $\pm$  1 SD. For the left column (+ Energy Mix in preincubation buffer)  $n = 103$  sperm nuclei from two experiments on two different extract preparations. For the right column (- Energy Mix in preincubation buffer; standard kinetochore assembly reaction)  $n = 303$  sperm nuclei from four experiments on three different extract preparations. The absence of energy mix in the preincubation buffer results in >90% of the sperm nuclei demonstrating colocalization of all three markers at the reported density. The residual sperm nuclei show no localization of any of the three markers. (Bars = 10  $\mu$ m.) (*C*) Double label immunofluorescence of *in vitro* assembled kinetochores demonstrating colocalization of all three mitotic markers to discrete foci on the DNA. Panels show 4',6'-diamidino-2-phenylindole (DAPI)-labeled sperm nucleus DNA (*a* and *d*) and corresponding double label localization of dynein and CENP-E (*b* and *c*) or dynein and XKCM1 (*e* and *f*). Dots associated with the chromosome clusters are distributed over several focal planes; the images shown are photomicrographs of single focal planes and do not account for all dots present on these chromosomal clusters.

separated single chromosomes; instead, we obtain clusters of tightly intertwined, condensed chromosomes presumably derived from single sperm nuclei.

The targeting of mitosis-specific kinetochore components such as cytoplasmic dynein and CENP-E in our assay suggests that underlying more chromatin-proximal structures may also be present on the *in vitro* assembled kinetochores. Confirming this will require *Xenopus*-specific antibodies to constitutive kinetochore components such as CENP-A and CENP-C.

**Morphology of *In Vitro*-Assembled Kinetochores.** In previous studies, electron microscopy was used on spindles formed in crude *Xenopus* extracts to characterize the structures at the point where spindle microtubules intersect the mitotic chromatin (27, 28). Even though these chromosomes are segregation-competent and were fixed using optimal fixation methods while undergoing anaphase (28), no trilaminar plate-like structures were observed. Because sperm nuclei are converted to large clusters of condensed chromosomes in our assay, with the

domains of interest forming only a minute subset of the total condensed chromatin, we decided to use immunoelectron microscopy to examine the morphology of our *in vitro*-assembled kinetochores. Our fixation conditions were based on those used previously to preserve the trilaminar plate morphology of CHO chromosomes for immunoelectron microscopy (4, 14). Two examples using the anti-CENP-E antibody are shown in Fig. 4. We observe very specific localization of gold particles to small regions of the mitotic chromatin. These regions had on average seven tightly clustered gold particles with a diameter of about 0.2  $\mu$ m (range, 0.1–0.3  $\mu$ m;  $n = 24$  gold clusters) and typically stained more lightly than the surrounding chromatin. The gold clusters were usually, but not exclusively, observed near the edge of the chromatin. The absence of any background gold particles strongly suggests that these clusters represent the dots observed by light microscopy. We did not observe a striking lamellar morphology associated with any of the gold clusters, although we did observe some degree of chromatin differentiation relative to the surrounding chromatin at all of the examined clusters. Although we cannot exclude the possibility that our experimental manipulations damaged existing lamellar kinetochore structure, our results are consistent with the results obtained for segregation-competent chromosomes in crude extracts.

**Analysis of Kinetochore Assembly.** As antibodies to kinetochore components become available, our system can be used to dissect dependency relationships in kinetochore assembly. To demonstrate this potential, we have used our assay to determine if prior assembly of XKCM1 is required for targeting of either CENP-E or cytoplasmic dynein to kinetochores. Immunodepletion of XKCM1 from extracts prior to kinetochore assembly eliminates the observed localization of XKCM1 on chromosomes but has no effect on the targeting of either CENP-E or cytoplasmic dynein (Fig. 5). Therefore, we can conclude that assembly of CENP-E and cytoplasmic dynein onto kinetochores is independent of the assembly of XKCM1. We could not perform the equivalent experiment for CENP-E or dynein because neither the anti-human CENP-E nor the anti-dynein antibody are capable of immunodepleting their *Xenopus* antigens to a sufficient extent to prevent kinetochore targeting (data not shown). UV-vanadate cleavage of dynein heavy chain in extracts also does not affect the targeting of dynein to kinetochores (data not shown).

In addition to a requirement for reagents capable of immunodepleting other kinetochore components from extracts, this type of analysis will also depend on the contribution of pre-established centromere structure present in the substrate sperm chromatin to kinetochore assembly in our assay. The presence of constitutive kinetochore components on mature

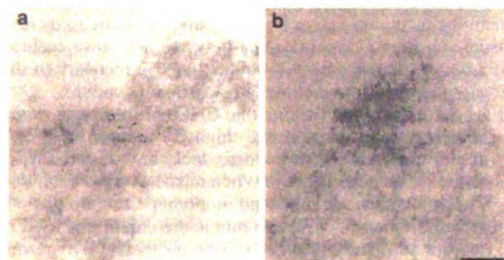


**FIG. 4.** Morphological analysis of *in vitro* assembled kinetochores using immunoelectron microscopy. Anti-CENP-E antibody was used for the immunoelectron microscopy. Two examples of gold clusters (*a* and *b*) show the specificity of labeling, the absence of a striking lamellar morphology and differentiation of the chromatin at the region of labeling. The cluster in *a* appears to show a slight degree of constriction; the cluster in *b* shows clear organization of the underlying chromatin fibers. (Bar = 0.2  $\mu$ m.)

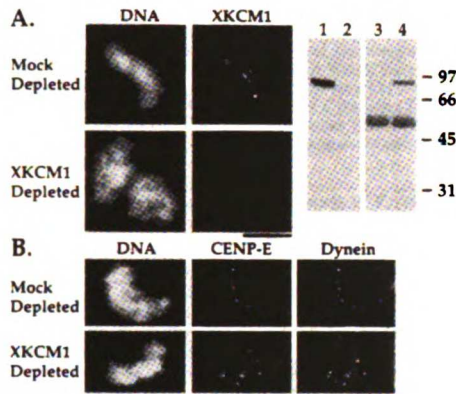


**FIG. 5.** XKCM1 depletion does not affect targeting of dynein and CENP-E to kinetochores. (A) XKCM1 localization to condensed chromosomes is abolished by XKCM1 depletion. Right two panels show an immunoblot (lanes 1 and 2) of equal amounts of mock-depleted (lane 1) and XKCM1-depleted (lane 2) extracts probed with anti-XKCM1 antibody, and a Coomassie-stained gel (lanes 3 and 4) of the corresponding immunoprecipitates: control IgG (lane 3) and anti-XKCM1 (lane 4). (B) XKCM1 depletion does not affect CENP-E and dynein localization. CENP-E and dynein targeting to kinetochores was compared in XKCM1-depleted vs. mock-depleted extracts. Quantitation of number of dots of CENP-E and dynein per sperm nucleus show no difference between mock- and XKCM1-depleted extracts ( $n = 100$  sperm nuclei from two experiments on two different extract preparations). (Bars =  $10 \mu\text{m}$ .)

sperm chromatin in mice and amphibians (29, 30) suggests that the substrate sperm nuclei do possess some amount of pre-established centromere structure. This structure may play an important role in kinetochore assembly in our assay. However, experiments in several organisms have shown that sperm nuclei undergo a dramatic reorganization of their chromatin structure upon entry into eggs (31). This reorganization may include exchange of pre-existing constitutive kinetochore components with components present in the extract, thus making it feasible to assay the role of such components in kinetochore assembly. Defining the role of pre-established centromere structure in our assay will require reagents to follow constitutive kinetochore components in *Xenopus*.

**In Vitro-Assembled Kinetochores Bind Monomeric Tubulin.** Assays testing kinetochore functions require reisolation of the condensed chromosomes after kinetochore assembly. Therefore, we devised a method to purify the end products of our assembly reaction in native form by trapping condensed chromosome clusters at the interface between a sucrose cushion and a heavy sucrose pad. We obtain 20–30% recovery of the starting number of sperm nuclei using this procedure.

Earlier studies demonstrated that CHO chromosomes, when purified from cells arrested with high concentrations of microtubule depolymerizing drugs, lack any kinetochore-associated monomeric tubulin. When mixed with pure tubulin, these purified chromosomes bind monomeric tubulin at their kinetochore region (11, 14). To mimic the conditions used in the isolation of tissue culture cell chromosomes, and to permit direct functional comparisons between our *in vitro* assembled chromosomes and tissue culture cell chromosomes, the assembly phase of our two-step reaction is performed in the presence of nocodazole. Therefore, we predicted that there would be no monomeric tubulin associated with the *in vitro* assembled kinetochores and, as shown in Fig. 6A, we found this to be the case. Furthermore, when purified chromosome clusters were mixed with monomeric tubulin, we detected binding of the

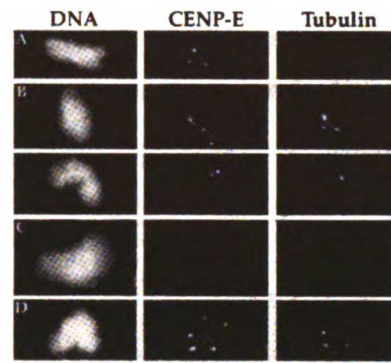


**FIG. 6.** Tubulin binding by *in vitro*-assembled kinetochores. Kinetochores were identified using the anti-CENP-E antibody. (A) Purified condensed chromosome clusters lack associated monomeric tubulin. (B) *In vitro*-assembled kinetochores bind exogenously added monomeric tubulin. Purified condensed chromosome clusters were incubated with  $10 \mu\text{M}$  tubulin and then assayed for binding of monomeric tubulin. As shown here for two separate sperm nuclei, every CENP-E dot was associated with monomeric tubulin (100 sperm nuclei, two experiments). The tubulin also shows faint punctate background staining of the DNA and, occasionally, a few larger dots which do not correspond to CENP-E dots. (C) *In vitro*-assembled kinetochores fail to bind monomeric tubulin after salt extraction. Assembled kinetochores were extracted using 100 mM extra NaCl before being purified and assayed for binding of monomeric tubulin. This extraction removes kinetochore-associated CENP-E, XKCM1, and dynein but does not remove chromosomal histones (data not shown). (D) XKCM1 depletion does not affect tubulin binding by *in vitro*-assembled kinetochores. XKCM1 depletion was assayed in parallel by immunoblots and immunofluorescence as described in Fig. 5. (Bar =  $10 \mu\text{m}$ .)

tubulin to the kinetochore regions (Fig. 6B). Extraction with 0.1 M NaCl after assembly abolishes the tubulin binding (Fig. 6C), but XKCM1 depletion does not affect the tubulin binding of *in vitro*-assembled kinetochores (Fig. 6D). These results suggest that the tubulin binding activity of the kinetochore is due to a salt-sensitive kinetochore component that is not XKCM1.

**Future Directions.** The primary application of our assay will be in the dissection of protein–protein interactions involved in kinetochore assembly. Doing this will require antibodies capable of immunodepleting different kinetochore components from *Xenopus* egg extracts, a task likely to be aided by the current emphasis on genome sequencing. Once such reagents are available, our assay will be useful for a systematic dissection of the dependency relationships in kinetochore assembly.

An interesting avenue for future exploration will be to assay different kinetochore functions following biochemical manipulation of kinetochore assembly. We have shown that kinetochores assembled in our assay will bind exogenously added monomeric tubulin. Tubulin binding is independent of XKCM1 but is dependent on components removed by salt extraction of assembled kinetochores. It may be possible to add back this tubulin binding component by incubating salt-extracted kinetochores with extract, and use this as an assay to identify the component responsible for the tubulin binding activity. Additional functional assays will become possible if the technical problem of separating single chromosomes from the clusters formed in our system can be solved.

Finally, our assay may be of some use in the definition of vertebrate centromeric DNA sequences and in the identification of novel kinetochore components. This will require that pure DNA, as opposed to sperm chromatin, is able to recruit kinetochore components when used in our assay.

We thank Bruce Schaar and Tim Yen for their gift of anti-CENP-E antibody, Peg Siebert for help with electron microscopy, and Linda Wordeman and Tatsuya Hirano for advice and encouragement during the early phases of this work. Sarita Jain, Matt Welch, Karen Oegema, Jody Rosenblatt, and Doug Kellogg provided valuable comments on the manuscript. This work was supported by a National Institutes of Health Grant (to T.J.M.); C.E.W. is a National Institutes of Health postdoctoral fellow; A.D. is a Howard Hughes Medical Institute predoctoral fellow.

1. Brinkley, B. R., Ouspenski, I. & Zinkowski, R. P. (1992) *Trends Cell Biol.* **2**, 15–21.
2. Earnshaw, W. C. & Tomkiel, J. E. (1992) *Curr. Opin. Cell Biol.* **4**, 86–93.
3. Rieder, C. L. (1982) *Int. Rev. Cytol.* **79**, 1–58.
4. Wordeman, L., Steuer, E. R., Sheetz, M. P. & Mitchison, T. (1991) *J. Cell Biol.* **114**, 285–294.
5. Palmer, D. K., O'Day, K., Wener, M. H., Andrews, B. S. & Margolis, R. L. (1987) *J. Cell Biol.* **104**, 805–815.
6. Earnshaw, W. C., Sullivan, K. F., Machlin, P. S., Cooke, C. A., Kaiser, D. A., Pollard, T. D., Rothfield, N. F. & Cleveland, D. W. (1987) *J. Cell Biol.* **104**, 817–829.
7. Saitoh, H., Tomkiel, J., Cooke, C. A., Ratrie, H. D., Maurer, M., Rothfield, N. F. & Earnshaw, W. C. (1992) *Cell* **70**, 115–125.
8. Yen, T. J., Li, G., Schaar, B. T., Szilak, I. & Cleveland, D. W. (1992) *Nature (London)* **359**, 536–539.
9. Walczak, C. E., Mitchison, T. J. & Desai, A. (1996) *Cell* **84**, 37–47.
10. Wordeman, L. & Mitchison, T. J. (1995) *J. Cell Biol.* **128**, 95–104.
11. Balczon, R. D. & Brinkley, B. R. (1987) *J. Cell Biol.* **105**, 855–862.
12. Coue, M., Lombillo, V. A. & McIntosh, J. R. (1991) *J. Cell Biol.* **112**, 1165–1175.
13. Hyman, A. A. & Mitchison, T. J. (1991) *Nature (London)* **351**, 206–211.
14. Mitchison, T. J. & Kirschner, M. W. (1985a) *J. Cell Biol.* **101**, 755–765.
15. Mitchison, T. J. & Kirschner, M. W. (1985b) *J. Cell Biol.* **101**, 766–777.
16. Desai, A. & Mitchison, T. J. (1995) *J. Cell Biol.* **128**, 1–4.
17. Bernat, R. L., Delannoy, M. R., Rothfield, N. F. & Earnshaw, W. C. (1991) *Cell* **66**, 1229–1238.
18. Tomkiel, J., Cooke, C. A., Saitoh, H., Bernat, R. L. & Earnshaw, W. C. (1994) *J. Cell Biol.* **125**, 531–545.
19. Hirano, T. & Mitchison, T. J. (1994) *Cell* **79**, 449–458.
20. Murray, A. W. (1991) *Methods Cell Biol.* **36**, 581–605.
21. Hirano, T. & Mitchison, T. J. (1993) *J. Cell Biol.* **120**, 601–612.
22. Lombillo, V. A., Nislow, C., Yen, T. J., Gelfand, V. I. & McIntosh, J. R. (1995) *J. Cell Biol.* **128**, 107–115.
23. Earnshaw, W. C. & Rothfield, N. (1985) *Chromosoma* **91**, 313–321.
24. Felix, M. A., Pines, J., Hunt, T. & Karsenti, E. (1989) *EMBO J.* **8**, 3059–3069.
25. Leiss, D., Felix, M. A. & Karsenti, E. (1992) *J. Cell Sci.* **102**, 285–297.
26. Graf, J. D. & Kobel, H. R. (1991) *Methods Cell Biol.* **36**, 19–34.
27. Sawin, K. E. & Mitchison, T. J. (1991) *J. Cell Biol.* **112**, 925–940.
28. Shamu, C. E. & Murray, A. W. (1992) *J. Cell Biol.* **117**, 921–934.
29. Brinkley, B. R., Brenner, S. L., Hall, J. M., Tousson, A., Balczon, R. D. & Valdivia, M. M. (1986) *Chromosoma* **94**, 309–317.
30. Haaf, T., Grunenberg, H. & Schmid, M. (1990) *Exp. Cell Res.* **187**, 157–161.
31. Poccia, D. (1989) in *The Molecular Biology of Fertilization*, eds. Schatten H. & Schatten G. (Academic, San Diego), pp. 115–135.

## Chapter 3

# Mechanism of Anaphase A in *Xenopus* Extract Spindles

This chapter presents work done in collaboration with Dr. E. D. Salmon, Professor of Biology at the University of North Carolina, Chapel Hill. I performed all the experiments described in this paper (submitted for publication in the *Journal of Cell Biology*) and wrote the paper with the help of Dr. Salmon and with comments from Dr. Mitchison. Paul Maddox, a student in Dr. Salmon's lab, helped with the experiments described in Figure 4 and performed the analysis described in Figure 5 and Figure 6.

**Anaphase A Chromosome Movement and Poleward Spindle Microtubule  
Flux Occur At Similar Rates in *Xenopus* Extract Spindles**

Arshad Desai\*, Paul S. Maddox#, Timothy J. Mitchison\$ and E. D. Salmon#

Marine Biological Laboratory, Woods Hole

and

\*Department of Biochemistry and Biophysics, University of California, San  
Francisco

#Department of Biology, University of North Carolina, Chapel Hill

\$Department of Cell Biology, Harvard Medical School

\*To whom all correspondence should be addressed at:

240 Longwood Ave., Bldg. C-517

Dept. of Cell Biology, Harvard Medical School

Boston, MA 02115

Phone: (617)-432-2688

(617)-432-3804

Fax: (617)-975-0527

(617)-432-3702

email: Arshad\_Desai@hms.harvard.edu

**Running Title:** Poleward Flux and Chromosome Movement

**Keywords:** mitosis, anaphase, microtubule, flux, kinetochore



## Abstract

We have used local fluorescence photoactivation to mark the lattice of spindle microtubules during anaphase A in *Xenopus* extract spindles. We find that both poleward spindle microtubule flux and anaphase A chromosome movement occur at similar rates ( $\sim 2 \mu\text{m}/\text{min}$ ). This result suggests that poleward microtubule flux, coupled to microtubule depolymerization near the spindle poles, is the predominant mechanism for anaphase A in *Xenopus* egg extracts. In contrast, in vertebrate somatic cells a "Pacman" kinetochore mechanism, coupled to microtubule depolymerization near the kinetochore, predominates during anaphase A. Consistent with the conclusion from fluorescence photoactivation analysis, both anaphase A chromosome movement and poleward spindle microtubule flux respond similarly to pharmacological perturbations in *Xenopus* extracts. Furthermore, the pharmacological profile of anaphase A in *Xenopus* extracts differs from the previously established profile for anaphase A in vertebrate somatic cells. The difference between these profiles is consistent with poleward microtubule flux playing the predominant role in anaphase chromosome movement in *Xenopus* extracts, but not in vertebrate somatic cells. We discuss the possible biological implications of the existence of two distinct anaphase A mechanisms and their differential contributions to poleward chromosome movement in different cell types.

## Introduction

A major focus in the study of cell division is to define the physical mechanisms that segregate replicated chromosomes to daughter cells. Both mitotic and meiotic cells assemble a bipolar, microtubule (MT)<sup>1</sup>-based spindle

to execute chromosome segregation. The primary site for attachment of chromosomes to the spindle MTs is the kinetochore -- a nucleoprotein structure formed at the primary constriction of mitotic chromosomes (Rieder and Salmon, 1998). During spindle assembly, kinetochores capture the plus ends of dynamically unstable MTs associated with opposite spindle poles, and become tethered to the poles by forming a stable bundle of kinetochore MTs (kMTs). After all the chromosomes are properly attached, the connections holding the sister chromatids (mitosis, meiosis II) or homologous chromosomes (meiosis I) are dissolved and the separated chromosomes move toward opposite spindle poles. Segregation of sisters to daughter cells involves both chromosome-to-pole movement (anaphase A) and spindle pole-to-pole elongation (anaphase B).

An important issue in the study of chromosome segregation is defining the mechanism of anaphase A chromosome-to-pole movement. The most popular model for anaphase A is the "Pacman" kinetochore model, which postulates that the kinetochore pulls the chromosome poleward on relatively stationary kMTs and this movement is coupled to depolymerization of the kMTs at the kinetochore (Fig. 1A; reviewed in Rieder and Salmon, 1994; Rieder and Salmon, 1998; Yen and Schaar, 1996). The popularity of this model is derived in large part from the identification of the kinetochore as the primary site of kMT disassembly during chromosome-to-pole movement in vertebrate somatic cells (Mitchison et al., 1986; Wadsworth and Salmon, 1986; Gorbsky et al., 1987; Gorbsky et al., 1988; Mitchison and Salmon, 1992; Zhai et al., 1995; Waters et al., 1996).

Another model for anaphase A chromosome movement postulates that kinetochores are pulled poleward by the poleward movement or "flux" of kMTs coupled to depolymerization of kMT minus ends near the poles (Fig.

1B). According to this model, kMTs flux poleward (or treadmill, see Margolis and Wilson, 1981) during metaphase concurrent with plus end assembly at the kinetochores and minus end disassembly near the poles. In anaphase, assembly stops at the kinetochore and the poleward movement of the kMTs coupled to their minus end disassembly pulls the kinetochore and its associated chromosome poleward (Fig. 1B). Related "traction fiber" models have been proposed by Inoué and Sato (1967), Forer (1965, 1966), Margolis and Wilson (1981) and others (reviewed in Salmon, 1989; Fuge, 1989), primarily on the basis of indirect evidence for poleward MT transport, including observations that various types of organelles, "particles or states" and UV ablation zones in spindle fibers move poleward during both metaphase and anaphase.

Mitchison (1989) provided direct evidence for poleward MT flux by using fluorescence photoactivation to locally mark the lattice of kinetochore fiber MTs in mitotic PtK2 cells. Fluorescent marks on the kMTs moved poleward at an average rate of 0.5  $\mu\text{m}/\text{min}$  during metaphase with plus end assembly near the kinetochore being balanced by minus end disassembly near the poles. Subsequent fluorescence photoactivation analysis of the sites of kMT disassembly during anaphase in newt, PtK1 and porcine somatic cells has shown that the majority of kMT disassembly during chromosome-to-pole movement occurs at the kinetochore (Mitchison and Salmon, 1992; Zhai et al., 1995; Waters et al., 1996). In these cell types, chromosome-to-pole movement (1.5 - 2.5  $\mu\text{m}/\text{min}$ ) is much faster than anaphase poleward kMT flux (0.3- 0.5  $\mu\text{m}/\text{min}$ ). Thus, during anaphase, fluorescent marks made on kMTs near the kinetochore disappear because kinetochore poleward movement coupled to kMT disassembly at the kinetochore is 3 to 8 times faster than the rate of poleward flux coupled to kMT disassembly at the poles.

Waters et al. (1996) have shown in newt lung cells that, if MT assembly and disassembly at the kinetochore are blocked during anaphase by taxol concentrations that do not inhibit kMT poleward flux, then chromosomes are pulled poleward slowly at kMT flux rates. Taken together, these studies have led to the conclusion that, although poleward MT flux is capable of generating force to move chromosomes, it is only a minor contributor to anaphase A chromosome movement in vertebrate somatic cells.

The marking studies in somatic cells raise the question as to what is the function of poleward MT flux -- a concerted dynamic behavior of spindle MTs that reflects considerable structural complexity in the spindle. One possibility is that MT flux is the dominant mechanism for poleward chromosome movement in systems other than vertebrate somatic cells. Sawin and Mitchison (1991) found that the majority of MTs in spindles assembled in meiosis II metaphase-arrested *Xenopus* egg extracts flux poleward at  $2.9 \pm 0.4 \mu\text{m}/\text{min}$ , approximately 6 times faster than the rate of kMT poleward flux in somatic cells. Forer and co-workers found that in insect meiocytes both zones of reduced birefringence generated by UV ablation of spindle MTs (Forer, 1965; 1966) and acetylated tubulin distributions along kinetochore fibers (Wilson et al., 1994) move poleward at rates similar to chromosomes during anaphase A; however, interpretation of these two studies is complicated by the fact that the first involved cutting spindle MTs, and that the second involved extrapolating dynamic information from fixed samples. Nevertheless, these three observations suggest that poleward MT flux may play the predominant role in anaphase A chromosome movement in certain systems. Consistent with the flux hypothesis, direct observations of anaphase in *Xenopus* extract spindles showed that chromosomes move poleward at  $2.4 \pm 1 \mu\text{m}/\text{min}$  (Murray et al., 1996), within the range of values

observed for poleward MT flux during metaphase in this system (Sawin and Mitchison, 1991). However, Mitchison and Salmon (1992) showed in newt lung cells that the rate of kMT poleward flux during early anaphase is similar to that during metaphase, but slows down significantly in late anaphase. A subsequent study on porcine and marsupial somatic cells showed that kMT flux in these cell types was ~50% slower during anaphase than during metaphase (Zhai et al., 1995). Since these somatic cell studies demonstrated changes in the flux rate between metaphase and anaphase, determining whether poleward MT flux plays the predominant role during anaphase A in *Xenopus* extract spindles requires simultaneous observation of MT flux and anaphase chromosome movement.

In this paper we have used fluorescence photoactivation to mark the lattice of spindle MTs during anaphase in *Xenopus* extract spindles. We have directly compared the rate of poleward flux to the rate of poleward chromosome movement and find that both the spindle MT lattice and the disjoined chromosomes move poleward at about 2  $\mu\text{m}/\text{min}$  under our experimental conditions. We also show that anaphase A in the extract spindles exhibits a distinct pharmacological profile from anaphase A in somatic cell spindles, and that the extract spindle profile is consistent with a predominantly MT flux-driven mechanism for moving chromosomes poleward.

## **Materials and Methods**

### *In Vitro Spindle Assembly*

All experiments were performed using fresh cytostatic factor (CSF)-arrested *Xenopus* egg extracts prepared as described (Murray, 1991; Desai et al., 1998). Extracts were supplemented with 5-10  $\mu\text{g}/\text{ml}$  X-rhodamine tubulin,

200-400/ $\mu$ l permeabilized sperm nuclei and bipolar spindles were assembled as described (Shamu and Murray, 1992; Murray et al., 1996; Desai et al., 1998). Briefly, calcium was added to a final concentration of 0.4 mM (from a 10X (4 mM) stock in Sperm Dilution Buffer (SD); SD: 10 mM HEPES, pH 7.7, 100 mM KCl, 1 mM MgCl<sub>2</sub>, 150 mM sucrose, 10  $\mu$ g/ml cytochalasin D) to CSF extract containing sperm nuclei, incubated at room temperature (20-23°C) for 80' to allow the sperm DNA to decondense and replicate, after which 20  $\mu$ l of CSF extract (without any sperm nuclei but with X-rhodamine tubulin) was added to drive the reactions into metaphase. In order to maximize the time of use of an extract for real-time experiments, we stored CSF extracts on ice after preparation and started a new set of spindle assembly reactions every 3-3.5 hours. There is significant day-to-day variability in both the lifetime and anaphase competency of these extracts which considerably limits experimental manipulations.

X-rhodamine tubulin and bis-caged carboxyfluorescein tubulin (C2CF tubulin) were prepared using the high pH tubulin labeling protocol (Hyman et al., 1991; Desai and Mitchison, 1998). The C2CF tubulin used in these experiments was labeled to a stoichiometry of ~0.8 moles C2CF/mole tubulin. H1 kinase assays were performed as described (Murray, 1991).

#### *Sample Preparation for Real Time Analysis*

Slides and coverslips were cleaned using water, acetone and ethanol sequentially as described (Murray et al., 1996; Desai et al., 1998). For marking experiments, C2CF tubulin was added at least ten minutes prior to starting anaphase to a final concentration of 100-150  $\mu$ g/ml. All steps involving C2CF tubulin were performed under dim red illumination in a dark room. For simultaneous observation of poleward flux and chromosome-to-pole

movement, the 10X calcium stock in SD was supplemented with 5  $\mu\text{g}/\text{ml}$  DAPI (Ca/DAPI5). 1/9 vol of Ca/DAPI5 was added to a reaction supplemented with C2CF tubulin and 8  $\mu\text{l}$  of this mixture were pipeted onto a clean slide, covered using a clean 22 x 22 mm coverslip and sealed using Valap (1:1:1 vaseline:lanolin:paraffin). Sample preparations with large visible air bubbles were discarded. The sub-millimolar concentration of calcium added to the extract to initiate anaphase was sequestered within 1 minute to basal levels, as measured using Fluo-3 (Molecular Probes Inc., Eugene, OR) calcium fluorimetry (not shown). The calcium pulse did not appear to have a significant effect on assembled spindles since their morphology and MT density remained typical of metaphase until 5 to 10 minutes after calcium addition when anaphase chromosome segregation began.

For anaphase pharmacology studies, various 10X calcium stocks were prepared in SD containing 4 mM  $\text{CaCl}_2$ , 1  $\mu\text{g}/\text{ml}$  DAPI and 10X concentration of the desired dosage of a specific pharmacological agent. For flux pharmacology studies, DAPI was omitted from the stocks. Analysis of the effect of taxol on flux was performed on metaphase spindles. An analysis of the effect of AMPPNP on flux was done previously on metaphase *Xenopus* extract spindles (Sawin and Mitchison, 1991). Our analysis of the effect of AMPPNP on flux was done on anaphase spindles. Samples for pharmacology studies were prepared as described above, with a specific 10X stock being used to deliver a pharmacological agent.

### *Microscopy and Data Analysis*

Photoactivation experiments were performed on an upright Zeiss Photoscope III with a rotating stage and 60X, 1.4 NA Planapo objective. Spindles were located at low magnification and aligned with respect to the

photoactivation beam using phase contrast microscopy. Modifications of the microscope for photoactivation and for acquisition and storage of images at multiple wavelengths have been described (Sawin and Mitchison, 1991; Sawin and Mitchison, 1994; Mitchison et al., 1998). 100W mercury arcs were used for both illumination and photoactivation, and a SIT video camera (Dage-MTI, Wabash, WI) was used to acquire 8 frame averaged images in the fluorescein and X-rhodamine channels. Illumination intensity was controlled using a combination of an out-of-focus (epi-condenser) diaphragm and neutral density filters. To avoid activation of the C2CF tubulin, DAPI illumination was carefully limited by closing down the out-of-focus diaphragm, leaving the UV turning mirror used to guide the photoactivation beam (Mitchison, 1989; Mitchison et al., 1998) in the epi-illumination light path, and acquiring only 2 video frames per timepoint in the DAPI channel. Only the residual UV, not bounced out of the epifluorescence light path by the UV turning mirror, contributed to the DAPI excitation. The amount of DAPI, X-rhodamine tubulin and C2CF tubulin added to extracts was empirically optimized to allow image acquisition in all three channels at constant camera gain and black level. Images at each wavelength were acquired 5 seconds apart and sequential images at a specific wavelength were acquired 20-30 seconds apart. Images were stored on optical disks using a Panasonic TQ 3038F optical memory disc recorder and digitized for analysis using a Metamorph Imaging System (Universal Imaging Inc., West Chester, PA).

For each digitized sequence, the peak of fluorescence in the fluorescein channel (photoactivated C2CF-tubulin) and the leading edge of fluorescence in the DAPI channel (marking the leading edges of the chromosomes) were defined from fluorescence intensities measured using a 5 pixel-wide linescan



that was oriented along the trajectory of poleward chromosome movement and extended past the polar edge of the spindle. This linescan was also positioned such that distinct regions of photoactivated C2CF-tubulin and DAPI-labeled chromosomes could be monitored through most of the duration of anaphase A. At each time point, the intensity values in each fluorescence channel along this linescan were transferred to an Excel spreadsheet. The spindle pole was defined for each timepoint in the X-rhodamine channel by the position of the dropoff in fluorescence intensity at the polar edge of the spindle. The change in the distance at 30 sec - 1 minute intervals between the pole defined in the X-rhodamine channel and the peak of fluorescein fluorescence was used to measure flux rate and similarly the change in distance between the pole and the leading edge of DAPI fluorescence was used to measure chromosome movement rate. When feasible, rates were obtained from several linescans (2-4) through different regions of a spindle. These were generally similar to each other and their average value was used.

Given the considerable technical difficulty of simultaneous observations of poleward MT flux and anaphase chromosome movement in *Xenopus* extract spindles, analysis of the effects of pharmacological agents were performed independently for flux and chromosome movement. The photoactivation experiments were done as described above, except that the relatively tricky visualization of DAPI-labeled chromosomes was omitted. Analysis of anaphase chromosome movement was performed on a multiwavelength epifluorescence microscope described previously (Salmon et al., 1994; 1998). For these experiments, extracts were supplemented with X-rhodamine tubulin to 30-50  $\mu\text{g}/\text{ml}$  and images in the X-rhodamine and DAPI channels were acquired at 30 second intervals using a Nikon 20X, 0.7NA

Fluor objective (Murray et al., 1996). The movements of chromosomes at the metaphase plate were recorded at high magnification using a Nikon 60X, 1.4 NA objective. Using the Metamorph software, color overlays of the X-rhodamine and DAPI images were analyzed to determine chromosome-to-pole movement rates as described previously (Murray et al., 1996).

#### *Fixation and Immunofluorescence of Spindles During Anaphase*

To detect kinetochore antigens during anaphase chromosome movement *in vitro*, 20  $\mu$ l of a spindle assembly reaction were diluted into 2 ml of BRB80 + 30% (v/v) glycerol + 0.5% Triton X-100 at RT (BRB80: 80 mM K-PIPES, pH 6.8, 1mM MgCl<sub>2</sub>, 1 mM EGTA), mixed gently by inversion for 30 seconds - 1 minute, and then fixed by addition of 2 ml of BRB80 + 0.5% Triton X-100 + 30% (v/v) glycerol + 5% formaldehyde for ~10' at RT. The fixed reactions were layered onto a 4 ml cushion of 40% (v/v) glycerol in BRB80 and sedimented at 5500 rpm for 20' at 16 °C in an HS-4 rotor. After centrifugation, the sample was aspirated till just below the sample-cushion interface, rinsed with BRB80, and the rinse and the cushion aspirated prior to transferring the coverslips to a coverslip holder. The coverslips were briefly rinsed in TBSTx (20 mM Tris-Cl, pH 7.4, 150 mM NaCl, 0.1% Triton X-100) to remove residual glycerol, post-fixed using -20°C methanol, rehydrated in TBSTx, and processed for anti-CENP-E immunofluorescence using a cross-reactive anti-human CENP-E antibody as described (Desai et al., 1997).

## **Results**

### **Poleward Microtubule Flux and Chromosome Movement Occur at Similar Rates in *Xenopus* Egg Extract Spindles**

Metaphase-arrested *in vitro* spindles containing replicated chromosomes were induced into anaphase by addition of a pulse of calcium to inactivate the CSF metaphase arrest, as described by Murray and co-workers (Shamu and Murray, 1992; Murray et al., 1996). These previous studies showed that sister chromatids segregate under these conditions, but did not analyze the role of kinetochores in the observed segregation. To determine if poleward force on chromosomes during anaphase *in vitro* acts at their kinetochores, we examined the distribution of a known kinetochore protein. We found that CENP-E, a conserved kinetochore-localized MT motor in vertebrates (Yen et al., 1992; Wood et al., 1997; Desai et al., 1997), localizes to the leading edges of the poleward-moving chromosomes in anaphase (Fig. 2). Furthermore, during poleward movement the leading edges of chromosomes are often seen close to one end, consistent with the fact that many *Xenopus* chromosomes are "acrocentric", i. e., have their centromeres near one end of the chromosome (Graf and Kobel, 1991). Thus, kinetochores of *in vitro* spindles contain a conserved kinetochore MT motor protein and lead the chromosomes poleward in anaphase.

To directly compare the rate of chromosome poleward movement to that of spindle MT flux, we imaged both processes simultaneously using multiwavelength timelapse fluorescence microscopy. To visualize spindle structure, we added X rhodamine-labeled tubulin to the extract immediately after preparation. To visualize poleward MT flux, we added caged fluorescein tubulin to metaphase spindles 10 to 30 minutes prior to inducing anaphase. Both modified tubulins rapidly equilibrate into spindle MTs as a result of MT turnover (Sawin and Mitchison, 1991). Since UV illumination photolyzes caged fluorescein, activating its fluorescence, we initially avoided using UV-excited DNA binding dyes to visualize chromosome movement. Instead, we

attempted to use phase contrast microscopy, a method that was successful for similar studies in somatic cells. However, we found that chromosomes formed *in vitro* in *Xenopus* extracts lack sufficient phase density, relative to extract cytoplasm, to allow reliable tracking of their movement. Therefore, we developed conditions using minimal UV-excited DAPI fluorescence that allowed us to visualize chromosomes without causing significant uncaging of caged fluorescein. Using these conditions, we recorded spindles until they had just begun anaphase chromosome movement (approximately 8 - 12 minutes after calcium addition), then used a brief (1-3s duration) slit of UV illumination to fluorescently mark the MTs between the poleward-migrating chromosomes and a spindle pole. The subsequent movement of the fluorescent mark, the chromosomes and changes in spindle structure were recorded.

The result of an anaphase marking experiment performed using this procedure is shown in Figure 3A. In this experiment, the mark was made just to the left of the leading edges of the chromosomes as they started to move poleward. As shown in the middle column of Figure 3A, the fluorescent mark moved poleward during the next 5 minutes at a rate of about 2  $\mu\text{m}/\text{min}$ . Since the spindle pole-to-pole distance did not change significantly during this period, the movement of the mark must represent disassembly of the spindle MTs at their minus ends near the pole. During the same period the chromosomes moved poleward (Fig. 3A left and right columns). The striking correspondence between the poleward movement of the chromosomes and the fluorescent mark is evident in the right column of Figure 3A.

To analyze the data generated by such an experiment, we used fluorescence linescan intensity profiles along the same 5-pixel wide linescan

in all three channels to track chromosome leading edge-to-pole and peak of fluorescent mark intensity-to-pole distances as a function of time. As shown in Figure 3B, the movement of the fluorescent mark polewards closely parallels the movement of the leading edge of the chromosome mass (indicated by a dot in the linescan profile). The similarity of the average rates of anaphase poleward flux and anaphase chromosome movement from experiments performed on 11 spindles is shown in Figure 3C. After the onset of chromosome separation, chromosomes moved poleward at  $2.2 \pm 0.8$   $\mu\text{m}/\text{min}$  and MTs fluxed poleward at  $2.0 \pm 0.7$   $\mu\text{m}/\text{min}$  (mean  $\pm$  SD for 11 spindles). These average rates were not significantly different ( $P \leq 0.005$  in a *t*-test). As the mark moved poleward, it both lost intensity and broadened, indicating the existence of faster and slower fluxing MT populations within the mark. While the majority of segregating chromosomes did not move faster than the leading edge of the fluorescent mark, we occasionally observed short poleward movements by a few small chromosomes, well-separated from the chromosomal mass, that were faster than the average flux rate (not shown).

### **Pharmacological Comparison of Anaphase Chromosome Movement and Poleward Microtubule flux in *Xenopus* Extract Spindles**

The similarity between the rate of chromosome movement and the rate of poleward MT flux during anaphase suggests that MT flux may be the predominant mechanism for chromosome-to-pole movement in *Xenopus* extract spindles. If this were true, then agents that inhibit MT flux should also inhibit chromosome-to-pole movement. In a previous study testing the effect of a variety of agents on poleward MT flux in *Xenopus* extract metaphase spindles, only AMPPNP was found to inhibit flux, blocking flux at

a final concentration of 1.7 mM (Sawin and Mitchison, 1991). Therefore, to test the prediction that AMPPNP would also inhibit chromosome movement, we analyzed anaphase chromosome movement at three AMPPNP concentrations -- 0.5 mM, 1 mM and 1.5 mM. We found that AMPPNP inhibited the rate of chromosome-to-pole movement in a dose-dependent manner (Fig. 4A bottom row, Fig. 5C, Fig. 6A). We also confirmed that AMPPNP inhibited poleward MT flux by independently analyzing the effect of AMPPNP on MT flux in anaphase (Fig. 4B, Fig. 6B). Since the chromosome movement and flux measurements were performed in separate experiments on different extract preparations and under different experimental conditions, the rates of the two processes are not directly comparable.

To address the concern that AMPPNP inhibition of chromosome movement had little to do with flux but was an indirect result of inhibiting exit from metaphase, we measured cdc2-cyclin B kinase activity after calcium addition in the absence or presence of varying amounts of AMPPNP. cdc2-cyclin B kinase activity, as measured by histone H1 phosphorylation, decays to interphase levels about 10-12 minutes after calcium addition in untreated extracts (Shamu and Murray, 1992). We found that AMPPNP did not inhibit exit from metaphase but delayed the drop in H1 kinase activity by about 3 minutes at 0.5 mM, 6 minutes at 1 mM and 11 minutes at 1.5 mM (data not shown; n=2 experiments with kinase assays performed at 2 minute intervals for 30 minutes after calcium addition). This AMPPNP-induced delay in exit from metaphase is too short to account for the observed inhibition of chromosome-to-pole movement (see Fig. 4A, comparing top and bottom rows of panels). In addition, our analysis of chromosome movement in AMPPNP takes into consideration this delay, since chromosome position was

tracked until "karyomere-associated motility" was apparent on the filmed spindles. "Karyomere-associated motility" is the rapid motility of decondensing chromosomes with nuclear envelopes (karyomeres) towards centers of MT asters, that has been previously shown to occur after anaphase A and to require inactivation of cdc2-cyclin B kinase activity (Murray et al., 1996). Consistent with the results of the H1 kinase assays, karyomere-associated motility was also delayed in the AMPPNP-treated spindles.

AMPPNP also did not appear to inhibit sister chromatid separation, since separated sisters were visible on some of the analyzed spindles after being moved apart by spindle expansion (Fig. 4A bottom row). That the observed separation of sister chromatids in 1.5 mM AMPPNP is not due to chromosome-to-pole movement but due to spindle expansion is demonstrated by tracking the position of the spindle poles and of the chromosomes as a function of time (Fig. 5C).

In some of the spindles treated with 1.5 mM AMPPNP, we observed a small number of chromosomes (6 chromosomes from 5 spindles in 1.5 mM AMPPNP) that appeared to be well separated from the chromosomal mass and moved short poleward distances at rates significantly faster than those for the bulk chromosomal mass (average rate of 0.6  $\mu\text{m}/\text{min}$ ; maximum rate of 0.8  $\mu\text{m}/\text{min}$  versus average rate of 0.15  $\mu\text{m}/\text{min}$ ; maximum rate of 0.25  $\mu\text{m}/\text{min}$  for the bulk chromosomal mass). These faster chromosomes moved at one-third the control rates of chromosome movement ( $\sim 2$   $\mu\text{m}/\text{min}$ ), but significantly faster than expected from the independently measured average flux rate (0.25  $\mu\text{m}/\text{min}$ ). Each spindle contains at least 18 chromosomes, with many spindles containing more than 18 as a result of lateral fusion of single sperm nucleus spindles. The faster moving

chromosomes represent a small percentage (<5%) of the total number of observed chromosomes.

Taxol treatment of somatic newt lung cells during anaphase rapidly reduces the rate of chromosome-to-pole movement approximately 5-fold. This occurs because taxol rapidly blocks MT assembly/disassembly at the kinetochore, inhibiting the "Pacman" kinetochore mechanism for anaphase A that predominates in these cells. Chromosomes continue moving poleward at the slow kMT flux rates, because taxol does not initially block poleward MT flux (Waters et al., 1996). These results predict that, if poleward MT flux is the predominant mechanism for anaphase chromosome movement in *Xenopus* extract spindles, then taxol should have little effect on anaphase A velocity in this system. To test this hypothesis, we analyzed anaphase chromosome movement in *Xenopus* extract spindles in the presence of 0.1, 0.5, 1, and 2  $\mu\text{M}$  taxol. At 1 and 2  $\mu\text{M}$ , taxol did not affect the rate of chromosome-to-pole movement even though it greatly increased the MT density near the spindle poles (Fig 4A, middle row of panels; Fig. 5, Fig. 6A). The separated chromosomes migrated at control rates to the edge of this dense mass of MTs. Treatment with higher taxol concentrations (5  $\mu\text{M}$ ) was not possible because of the formation of taxol-tubulin aggregates throughout the extract. We also confirmed that 1  $\mu\text{M}$  taxol did not significantly affect the rate of poleward MT flux in metaphase *Xenopus* extract spindles (Fig. 4B, Fig. 6B). Analysis of the effect of taxol on MT flux was performed on metaphase spindles because the combination of the exit from metaphase and the taxol treatment greatly perturbed anaphase spindle structure, making marking experiments very difficult. The similar effects of taxol on MT flux during both metaphase and anaphase in somatic cells suggests that the sensitivity of the flux machinery to taxol does not change between metaphase and



anaphase (Waters et al., 1996). We found that at longer times after addition of taxol (>30') metaphase spindles possessed extremely dense MT asters near the spindle poles and very weak MT density in the spindle mid region. Marks made at the edge of the very dense zone moved poleward slowly at less than 1  $\mu\text{m}/\text{min}$  (not shown). Although the complex kinetic effects of taxol treatment remain to be explored, in the time and place that most anaphase chromosome movement occurs (between 5' and 15' after the addition of taxol and from the middle of the spindle to the edge of the dense MT asters), chromosome-to-pole movement and poleward MT flux were unaffected.

In addition to poleward MT flux, a different type of minus end-directed poleward transport has been described recently in *Xenopus* extract spindles (Heald et al., 1996; Heald et al., 1997). When added to extracts, short fluorescently labeled MTs were found to move poleward with their minus end leading at average rates of about 6  $\mu\text{m}/\text{min}$ , 3 times faster than anaphase chromosome movement. This poleward transport of short MTs was unaffected by addition of 2.5 mM AMPPNP but was inhibited by addition of either vanadate, which is known to inhibit cytoplasmic dynein motor activity, or an anti-cytoplasmic dynein intermediate chain monoclonal antibody (Heald et al., 1996; Heald et al., 1997). These results suggest that cytoplasmic dynein is responsible for the observed transport. To test if this dynein-dependent poleward transport plays any role in anaphase chromosome movement, we monitored anaphase in the presence of 25  $\mu\text{M}$  or 50  $\mu\text{M}$  vanadate. Although vanadate often accelerated spindle dissolution during anaphase (not shown), we did not find a significant effect of vanadate addition at these concentrations on the rate of chromosome-to-pole movement (Fig 6A). Rapid spindle dissolution during anaphase in the presence of vanadate prevented us from determining the effect of vanadate

on anaphase poleward MT flux. However, cytoplasmic dynein does not appear to play a major role in poleward MT flux since neither treatment with 50 - 150  $\mu$ M vanadate (Sawin and Mitchison, 1991) nor addition of p50<sup>dynamitin</sup>, a specific inhibitor of cytoplasmic dynein function (Echeverri et al., 1996), has a significant effect on flux in metaphase *Xenopus* extract spindles (M. Shirasu and T. Wittman, unpublished results).

### **Poleward Forces Act on Kinetochores During Metaphase in *Xenopus* Extract Spindles**

Since poleward MT flux occurs during both metaphase and anaphase in *Xenopus* extract spindles, we looked for evidence of a poleward force acting on kinetochores during metaphase. In the *in vitro* spindles, chromosome arms are normally confined to a narrow equatorial region at metaphase (Fig. 2 and Fig. 7A). However, unlike in somatic cells, the chromosomes on the *in vitro* spindles do not oscillate (not shown), indicating that the *in vitro* kinetochores do not exhibit directional instability. Thus, it was possible that poleward forces at kinetochores occur only after activation of anaphase in *Xenopus* extract spindles. Evidence that there is a poleward force on kinetochores during metaphase came from the morphology of chromosomes after spindles were held for 4-8 hours in CSF metaphase arrest. Over this period, chromosome arms became partially disjoined and acrocentric centromere regions were seen extended poleward (Fig. 7B). There was no detectable movement of the leading edges of the partially disjoined chromosomes over a 10 minute period indicating that poleward movement of the kinetochores was constrained by incomplete disjunction of the chromosome arms. Consistent with this hypothesis, small chromosomes were occasionally observed to move poleward at a rate similar to anaphase

when they were no longer constrained by attachments near the metaphase plate (not shown). The prolonged metaphase-arrested spindles exhibited normal metaphase spindle morphology and retained anaphase competency since addition of a calcium pulse to these spindles activated the completion of chromosome disjunction and normal poleward chromosome movement (not shown).

## **Discussion**

### **Anaphase A and Poleward Microtubule Flux Occur at Similar Rates in *Xenopus* Extract Spindles**

Our anaphase marking experiments demonstrate that in *Xenopus* extract spindles the leading edge of the chromosomal mass moves poleward at the same average rate as a mark made on the spindle MTs ( $\sim 2 \mu\text{m}/\text{min}$ ). In contrast, kinetochores in vertebrate somatic cells move poleward during most of anaphase A at about  $2 \mu\text{m}/\text{min}$  while fluorescent marks on the kMTs flux poleward much more slowly at  $0.3$  to  $0.5 \mu\text{m}/\text{min}$  (Mitchison and Salmon, 1992; Zhai et al., 1995). These results indicate that the "poleward flux/traction fiber" model (Fig. 1B) applies for anaphase A chromosome movement in spindles assembled in *Xenopus* extracts.

One caveat, when comparing MT marking experiments in *Xenopus* extract spindles to marking experiments in somatic cell spindles, is that MT populations detected by the marking procedure in the two systems are not the same. Marking experiments in somatic cell spindles detect primarily kMTs (Mitchison, 1989; Mitchison and Salmon, 1992; Zhai et al., 1995; Waters et al., 1996), whereas in *Xenopus* extract spindles they detect a large majority of the spindle MTs (Sawin and Mitchison, 1991). This difference most likely arises from the very different kMT/nonkMT ratios in embryonic/meiotic versus

somatic spindles and the much greater total number of MTs in the large embryonic spindles (Salmon and Segall, 1980; Sawin and Mitchison, 1991; Wise et al., 1991). Since *in vitro* spindle marking experiments are dominated by nonkMTs (Sawin and Mitchison, 1991; Sawin and Mitchison, 1994), the conclusion from marking studies that poleward MT flux is the predominant mechanism for anaphase A chromosome movement rests on the untested assumption that kMTs and nonkMTs flux at the same rate. One way to avoid this assumption would be to determine the nonkMT flux rate in somatic cells, where the kMT flux rate is already known. However, the rapid turnover of nonkMTs has prevented a determination of their flux rate in somatic cells. Given our inability to distinguish kMTs from nonkMTs in *Xenopus* extract spindles, we have attempted to strengthen the conclusion from the marking experiment by comparing the response of anaphase A chromosome movement and poleward MT flux to treatment with different pharmacological agents.

### **Anaphase A and Poleward Microtubule Flux Exhibit Similar Responses to Pharmacological Perturbations in *Xenopus* Extract Spindles**

If kinetochores and their associated chromosomes are pulled poleward primarily by MT flux, then inhibition of flux should inhibit anaphase A, whereas inhibition of MT disassembly at kinetochores should not inhibit anaphase A. An important finding in this study is that 1.5 mM AMPPNP, previously shown to inhibit flux (Sawin and Mitchison, 1991), inhibits anaphase A in the *in vitro* spindles. In contrast, microinjection of AMPPNP at final concentrations up to 5 mM in mitotic PtK1 cells does not substantially inhibit anaphase A, although it does strongly inhibit anaphase B (Lee, 1989). These results are consistent with an AMPPNP-insensitive "Pacman"

kinetochore mechanism (Fig. 1A) predominating during anaphase A in somatic cells versus an AMPPNP-sensitive poleward flux mechanism (Fig. 1B) predominating during anaphase A in *Xenopus* extracts.

Interpretation of AMPPNP effects in extracts is complicated by the relative non-specificity of this inhibitor. Several lines of evidence suggest that inhibition of poleward chromosome movement by AMPPNP is not due to inhibition of exit from metaphase or inhibition of chromosome disjunction. First, measurement of H1 kinase levels showed that AMPPNP did not inhibit exit from metaphase although it did delay the drop in H1 kinase activity in a dose-dependent manner. However, this delay was too short to account for the observed inhibition of chromosome-to-pole movement. Second, concentrations of AMPPNP higher than those used in our study did not inhibit either exit from metaphase or chromosome disjunction in PtK1 cells (Lee, 1989). Third, in the presence of AMPPNP, spindle pole-to-pole elongation revealed the presence of separated sisters on the *in vitro* spindles (Fig. 4A, Fig. 5C).

The lack of an effect of taxol treatments on the rate of chromosome-to-pole movement is also consistent with poleward MT flux playing the predominant role during anaphase A in *Xenopus* extract spindles. This result was predicted from the effect of taxol on mitotic newt lung cells, where it does not immediately inhibit flux but does inhibit MT plus end assembly dynamics at the kinetochore and the component of anaphase A produced by kinetochores (Waters et al., 1996). Chromosome-to-pole movement at control rates in the presence of vanadate also excludes a significant role for dynein-dependent transport in anaphase chromosome movement in *Xenopus* extract spindles.

The combination of the marking studies and the pharmacology strongly suggest that MT flux plays a more dominant role in poleward chromosome movement in *Xenopus* extract spindles than in vertebrate somatic cells. However, in the AMPPNP treatments, as well as in control spindles, a small number of chromosomes moved significantly faster than the rest of the chromosomal mass and the independently measured average flux rate. These fast movements might represent either "Pacman" kinetochore activity or the latching of chromosomes onto a different type of poleward transport mechanism, such as the dynein-dependent transport of MT fragments (Heald et al., 1996; Heald et al., 1997). Alternatively, the faster movements may represent differentially fluxing MT subpopulations, the existence of which is indicated by spreading of the width of the fluorescent mark in both control (Fig. 3B) and AMPPNP-treated spindles (Sawin and Mitchison, 1991).

### **Implications of Two Distinct Mechanisms for Anaphase A Chromosome Movement**

It is tempting to speculate that anaphase A is produced primarily by "Pacman" kinetochore activity in cell types that have oscillating chromosomes, whereas a MT flux mechanism predominates in cell types that do not exhibit chromosome oscillations. In addition to *Xenopus* extract spindles, chromosome oscillations do not occur in spindles of insect spermatocytes (Forer 1965, 1966; Nicklas, 1989), higher plants (Hard and Allen, 1977; Khodjakov et al. 1996) and echinoderm embryos (Ito et al., 1994a,b). Nicklas (1989) severed spindle fibers between the chromosomes and the pole of anaphase grasshopper spermatocytes and found that chromosome poleward movement persisted toward the severed ends of the fibers. From

these results, Nicklas (1989) proposed that force generation for anaphase A is at or close to the kinetochore for this cell type. However, it is possible that the mechanisms which support/organize the poleward ends of the severed spindle fibers also produce poleward flux and minus end depolymerization. MT marking experiments using non-perturbing methods, like the fluorescence photoactivation method used in our study, are urgently needed in these different systems to determine the generality of a predominantly poleward flux-driven mechanism for anaphase A.

Although it is possible that different cell types use fundamentally different mechanisms for anaphase A, we favor the idea that both mechanisms exist in all higher eukaryotic mitotic and meiotic spindles with one of them predominating during anaphase A (see also Mitchison and Salmon, 1992). We think this because: 1) Poleward MT flux makes a small but significant contribution to anaphase A in vertebrate somatic cells, where "Pacman" kinetochore movement predominates. Furthermore, in the later stages of anaphase A in newt lung cells, the kinetochores "park" on the MT lattice and are pulled poleward exclusively by MT flux (Mitchison and Salmon, 1992), much like kinetochores throughout anaphase A in *Xenopus* extract spindles; 2) Kinetochores on *Xenopus* extract spindles, where poleward MT flux appears to predominate, recruit kinetochore components such as CENP-E, MCAK/XKCM1 and cytoplasmic dynein that are present at the kinetochores of somatic cells (Desai et al., 1997; Walczak et al., 1996; Wood et al., 1997). In addition, we saw limited evidence for occasional chromosome movement faster than the flux rate, possibly indicative of a "Pacman" contribution; 3) In insect meiosis, where poleward movement of MT ablation zones at anaphase A rates argues for a predominance of the flux mechanism, analysis of acetylated tubulin distributions indicates that at least

some depolymerization occurs at kinetochores during anaphase A (Wilson et al., 1994).

Why would many, perhaps all, cells have apparently redundant mechanisms for poleward chromosome movement? One possibility is that overlapping mechanisms provide a fail-safe system and increase the fidelity of segregation. Alternatively, both mechanisms play other roles in mitosis/meiosis, and may happen to overlap in moving chromosomes poleward. Specifically, we suspect that poleward MT flux, in addition to its role in moving chromosomes, is probably important in spindle assembly and may also help align chromosomes at the metaphase plate. MT dynamics at kinetochores, in addition to its role in moving chromosomes, may reflect the mechanisms used to attach MTs to kinetochores, and ensure bipolar orientation of chromosomes. In addition, motors at kinetochores may communicate with the checkpoint system (Nicklas, 1997; Rieder and Salmon, 1998) that proofreads this attachment using a tension sensor, which might be a motor itself.

### **Acknowledgments**

We would like to thank Andrew Murray for his role in starting this collaborative project and for his constant encouragement; Shinya Inoué and the Woods Hole Marine Biological Laboratory for providing laboratory space; the MBL Physiology course for access to equipment; Karen Oegema, Claire Walczak, Jason Swedlow, Clare Waterman-Storer and Mimi Shirasu for helpful comments on the manuscript. This work was supported by grants from the NIH to T. J. M. and to E. D. S. (NIH GM24364). A.D. is a Howard Hughes Medical Institute pre-doctoral fellow.



## Footnotes

1. *Abbreviations used in this paper:* MT, Microtubule; kMT, kinetochore microtubule; nonkMT, nonkinetochore microtubule; C2CF, bis-caged carboxyfluorescein; AMPPNP, 5'-adenylylimidodiphosphate; DAPI, 4',6'-diamidino-2-phenylindole; CSF, cytostatic factor.

## References

- Desai, A., H.W. Deacon, C.E. Walczak, and T.J. Mitchison. 1997. A method that allows the assembly of kinetochore components onto chromosomes condensed in clarified *Xenopus* egg extracts. *Proc. Nat. Acad. Sci. USA*. 94:12378-12383.
- Desai, A., and T.J. Mitchison. 1998. Preparation and characterization of caged fluorescein tubulin. *Methods Enzymol.* In Press.
- Desai, A., A.W. Murray, T.J. Mitchison, and C.E. Walczak. 1998. The use of *Xenopus* egg extracts to study mitotic spindle assembly and function *in vitro*. *Methods Cell Biol.* In press.
- Echeverri, C.J., B.M. Paschal, K.T. Vaughan, and R.B. Vallee. 1996. Molecular characterization of the 50-kD subunit of dynactin reveals function for the complex in chromosome alignment and spindle organization during mitosis. *J. Cell Biol.* 132:617-33.
- Forer, A. 1965. Local reduction of spindle birefringence in living *Nephrotoma suturalis* (Loew) spermatocytes induced by ultraviolet microbeam irradiation. *J. Cell Biol.* 25:95-117.
- Forer, A. 1966. Characterization of the mitotic traction system, and evidence that birefringent spindle fibers neither produce nor transmit force for chromosome movement. *Chromosoma (Berl.)*. 19:44-98.

- Fuge, H. 1989. Traction fibres in chromosome movement: the pros and cons. *Biol. Cell.* 66:209-13.
- Gorbsky, G.J., P.J. Sammak, and G.G. Borisy. 1987. Chromosomes move poleward in anaphase along stationary microtubules that coordinately disassemble from their kinetochore ends. *J. Cell Biol.* 104:9-18.
- Gorbsky, G.J., P.J. Sammak, and G.G. Borisy. 1988. Microtubule dynamics and chromosome motion visualized in living anaphase cells. *J. Cell Biol.* 106:1185-92.
- Graf, J.D., and H.R. Kobel. 1991. Genetics of *Xenopus laevis*. *Methods Cell Biol.* 36:19-34.
- Hard, R., and R.D. Allen. 1977. Behaviour of kinetochore fibres in *Haemanthus katherinae* during anaphase movements of chromosomes. *J. Cell Sci.* 27:47-56.
- Heald, R., R. Tournebize, T. Blank, R. Sandaltzopoulos, P. Becker, A. Hyman, and E. Karsenti. 1996. Self-organization of microtubules into bipolar spindles around artificial chromosomes in *Xenopus* egg extracts. *Nature.* 382:420-5.
- Heald, R., R. Tournebize, A. Habermann, E. Karsenti, and A. Hyman. 1997. Spindle assembly in *Xenopus* egg extracts: respective roles of centrosomes and microtubule self-organization. *J. Cell Biol.* 138:615-28.
- Hyman, A., D. Drechsel, D. Kellogg, S. Salsler, K. Sawin, P. Steffen, L. Wordeman, and T. Mitchison. 1991. Preparation of modified tubulins. *Methods Enzymol.* 196:478-85.
- Inoué, S., and H. Sato. 1967. Cell motility by labile association of molecules. The nature of mitotic spindle fibers and their role in chromosome movement. *J. Gen. Physiol.* 50:Suppl:259-92.

- Ito, K. M. Masuda, K. Fujiwara, H. Hayashi, and H. Sato. 1994a. Metaphase and anaphase in the artificially induced monopolar spindle. *Proc. Nat. Acad. Sci. USA*. 91:3921-3925.
- Ito, K. Masuda, K. Fujiwara, and H. Sato. 1994b. Do astral microtubules play a role in metaphase chromosome positioning? *Biol. Cell*. 82:95-102.
- Khodjakov, A., R.W. Cole, A.S. Bajer, and C.L. Rieder, 1996, The force for poleward chromosome motion in *Haemanthus* cells acts along the length of the chromosome during metaphase but only at the kinetochore during anaphase. *J. Cell Biol.* 132:1093-104.
- Lee, G.M. 1989. Characterization of mitotic motors by their relative sensitivity to AMP-PNP. *J. Cell Sci.* 94:425-41.
- Margolis, R.L., and L. Wilson. 1981. Microtubule treadmills--possible molecular machinery. *Nature*. 293:705-11.
- Mitchison, T., L. Evans, E. Schulze, and M. Kirschner. 1986. Sites of microtubule assembly and disassembly in the mitotic spindle. *Cell*. 45:515-27.
- Mitchison, T.J. 1989. Polewards microtubule flux in the mitotic spindle: evidence from photoactivation of fluorescence. *J. Cell Biol.* 109:637-52.
- Mitchison, T.J., K.E. Sawin, J.A. Theriot, K. Gee, and A. Mallavarapu. 1998. Caged Fluorescent Probes. *Methods Enzymol.* In Press.
- Mitchison, T.J., and E.D. Salmon. 1992. Poleward kinetochore fiber movement occurs during both metaphase and anaphase-A in newt lung cell mitosis. *J. Cell Biol.* 119:569-82.
- Murray, A.W. 1991. Cell cycle extracts. *Methods Cell Biol.* 36:581-605.
- Murray, A.W., A.B. Desai, and E.D. Salmon. 1996. Real time observation of anaphase *in vitro*. *Proc. Natl. Acad. Sci. USA*. 93:12327-32.
- Nicklas, R.B. 1989. The motor for poleward chromosome movement in anaphase is in or near the kinetochore. *J. Cell Biol.* 109:2245-55.

- Nicklas, R.B. 1997. How cells get the right chromosomes. *Science*. 275:632-7.
- Rieder, C.L., and E.D. Salmon. 1994. Motile kinetochores and polar ejection forces dictate chromosome position on the vertebrate mitotic spindle. *J. Cell Biol.* 124:223-33.
- Rieder, C.L., and E.D. Salmon. 1998. The vertebrate kinetochore: steward for chromosome attachment, positioning on the spindle and the metaphase/anaphase transition. *Trends Cell Biol.* In press.
- Salmon, E.D. 1989. Microtubule dynamics and chromosome movement. *In Mitosis: Molecules and Mechanisms*. J. Hyams and B. R. Brinkley, editors. Academic Press, N.Y. 119- 181.
- Salmon, E.D., and R.R. Segall. 1980. Calcium-labile mitotic spindles isolated from sea urchin eggs (*Lytechinus variegatus*). *J. Cell Biol.* 86:355-65.
- Salmon, E. D. , T. Inoué, A. Desai and A. W. Murray. 1994. High resolution multimode digital imaging system for mitosis studies *in vivo* and *in vitro*. *Biol. Bull.* 187: 231-232.
- Salmon, E. D. , S.L. Shaw, J. Waters, C. M. Waterman-Storer, P. S. Maddox, E. Yeh, and K. Bloom. 1998. A high resolution multimode digital microscope system. *Methods Cell Biol.* 56: 185-215. In press.
- Sawin, K.E., and T.J. Mitchison. 1991. Poleward microtubule flux in mitotic spindles assembled *in vitro*. *J. Cell Biol.* 112:941-54.
- Sawin, K.E., and T.J. Mitchison. 1994. Microtubule flux in mitosis is independent of chromosomes, centrosomes, and antiparallel microtubules. *Mol. Biol. Cell.* 5:217-26.
- Shamu, C.E., and A.W. Murray. 1992. Sister chromatid separation in frog egg extracts requires DNA topoisomerase II activity during anaphase. *J. Cell Biol.* 117:921-34.

- Wadsworth, P., and E.D. Salmon. 1986. Analysis of the treadmilling model during metaphase of mitosis using fluorescence redistribution after photobleaching. *J. Cell Biol.* 102:1032-8.
- Walczak, C.E., T.J. Mitchison, and A. Desai. 1996. XKCM1: a *Xenopus* kinesin-related protein that regulates microtubule dynamics during mitotic spindle assembly. *Cell.* 84:37-47.
- Waters, J.C., T.J. Mitchison, C.L. Rieder, and E.D. Salmon. 1996. The kinetochore microtubule minus-end disassembly associated with poleward flux produces a force that can do work. *Mol. Biol. Cell.* 7:1547-58.
- Wilson, P.J., A. Forer, and C. Leggiadro. 1994. Evidence that kinetochore microtubules in crane-fly spermatocytes disassemble during anaphase primarily at the poleward end. *J. Cell Sci.* 107:3015-27.
- Wise, D., L. Cassimeris, C.L. Rieder, P. Wadsworth, and E.D. Salmon. 1991. Chromosome fiber dynamics and congression oscillations in metaphase PtK2 cells at 23 degrees C. *Cell. Motil. Cytoskeleton.* 18:131-42.
- Wood, K.W., R. Sakowicz, L.S.B. Goldstein, and D.W. Cleveland. 1997. CENP-E Is a Plus End-Directed Kinetochore Motor Required for Metaphase Chromosome Alignment. *Cell.* 91, 357-366.
- Yen, T.J., G. Li, B.T. Schaar, I. Szilak, and D.W. Cleveland. 1992. CENP-E is a putative kinetochore motor that accumulates just before mitosis. *Nature.* 359:536-9.
- Yen, T.J., and B.T. Schaar. 1996. Kinetochore function: molecular motors, switches and gates. *Curr. Opin. Cell Biol.* 8:381-8.
- Zhai, Y., P.J. Kronebusch, and G.G. Borisy. 1995. Kinetochore microtubule dynamics and the metaphase-anaphase transition. *J Cell Biol.* 131:721-34.

## Figure Legends

Figure 1. Two models for anaphase A chromosome-to-pole movement. For simplicity, only one half of the bipolar spindle and one kMT connecting the kinetochore to the spindle pole are shown. (A) "Pacman" kinetochore: Kinetochores pull the chromosome poleward on relatively stationary kMTs coupled to kMT disassembly at the kinetochore. (B) Poleward MT Flux ("traction fiber"): Poleward flux of kMTs pulls chromosomes poleward coupled to kMT disassembly near the pole. The two models can be distinguished by making a fluorescent mark on the kMTs (indicated by the lighter subunits) between the kinetochore and the spindle pole and monitoring the behavior of the mark as the chromosomes move poleward.

Figure 2. Immunofluorescence micrographs of fixed spindles showing that kinetochores lead chromosome-to-pole movement during anaphase in *Xenopus* extract spindles. Spindle MTs are stained red using rhodamine tubulin, chromosome are stained blue by DAPI and CENP-E is stained green using an anti-CENP-E primary and fluorescein-labeled secondary antibodies. Metaphase-arrested bipolar spindles with replicated chromosomes contained tight metaphase plates with sister kinetochores of bivalent chromosomes localized to the equatorial region of the spindle (top panel). Addition of a pulse of calcium to the extract inactivated the metaphase arrest and 8 minutes after calcium addition separated sister chromatids were seen moving poleward (bottom panel). Discrete foci of CENP-E are clearly visible at the leading edges of the poleward-migrating chromosomes. Bar, 10  $\mu\text{m}$ .

Figure 3. Simultaneous observation of chromosome movement and poleward MT flux in *Xenopus* extract spindles. (A) Panels from a sequence showing the similarity of poleward MT flux and chromosome movement during anaphase in *Xenopus* extract spindles. X-rhodamine tubulin-labeled spindle MTs are red, the photoactivated C2CF tubulin-containing MTs on the spindle MT lattice are green and the DAPI-labeled chromosomes are blue. The left column shows three-color overlays of the spindle, the mark and the chromosomes; the middle column shows two-color overlays of the fluorescent mark on the spindle MTs; and the right column shows two-color overlays of the chromosomes and the fluorescent mark. Time elapsed after the mark was made is indicated in seconds on the top left corner of the three-color overlay panels. For this particular sequence the mark was made 11 minutes after addition of calcium to trigger anaphase. Bar, 20  $\mu\text{m}$ . (B) Fluorescence intensity linescan analysis of chromosome-to-pole movement and poleward MT flux during anaphase in *Xenopus* extract spindles. Fluorescence intensity along the spindle axis in the fluorescein channel is plotted for four different time points for the sequence in Fig. 3A. The position of the leading edge of the chromosomes, obtained from linescans in the DAPI channel, is indicated by dots on the fluorescence intensity profiles of the mark. The left spindle pole is located at the X-axis origin. The fluorescent mark, which was made close to the leading edges of the chromosomes, moved poleward and decayed in intensity, presumably as a result of spindle MT turnover. The mark also broadened as it moved, indicating the existence of differentially fluxing spindle MT subpopulations. (C) Summary of the analysis of rates of poleward MT flux (F) and chromosome-to-pole movement (C) during anaphase in *Xenopus* extract spindles. The plotted values represent the mean  $\pm$  SD for rates measured on 11 spindles.

Figure 4. Pharmacological analysis of anaphase chromosome movement and poleward MT flux in *Xenopus* extract spindles. (A) Effect of taxol and AMPPNP treatments on chromosome movement and spindle structure during anaphase *in vitro*. Top row of panels represent a control anaphase, the middle row of panels represents anaphase in 1  $\mu$ M taxol and the bottom row of panels represents anaphase in 1.5 mM AMPPNP. Taxol and AMPPNP were added along with the calcium used to initiate anaphase (t=0 min). Each timepoint in the sequence is represented by paired DAPI-labeled chromosome (left) and X-rhodamine tubulin (right) images and the time after calcium addition is stamped in minutes on the lower right corner of the X-rhodamine tubulin image. Note both the much later times after calcium addition and the 5-fold larger intervals (10 minutes versus 2 minutes) between consecutive timepoints for the 1.5 mM AMPPNP sequence. The observed separation of sister chromatids in 1.5 mM AMPPNP is not due to chromosome-to-pole movement but primarily due to spindle elongation (see Fig. 5). Bar, 20  $\mu$ M.

(B) Effect of taxol and AMPPNP treatments on poleward MT flux. Paired X-rhodamine tubulin and fluorescein tubulin images are shown 1 minute (for control and 1  $\mu$ M taxol-treated spindles) and 3 minutes (for 1.5 mM AMPPNP-treated spindles) after the fluorescent mark was made on the spindle MTs. The initial position of the mark on the spindle is indicated by a white arrowhead. The 1  $\mu$ M taxol spindle was marked 8 minutes after taxol addition. The 1.5 mM AMPPNP spindle was marked approximately 10 minutes after addition of calcium and AMPPNP. Bar-splitting occurs as a result of poleward flux of MTs emanating from opposite spindle poles (Sawin and Mitchison, 1991). The similar extent of splitting of the initially central fluorescent mark is evident in both the control and taxol-treated spindles.



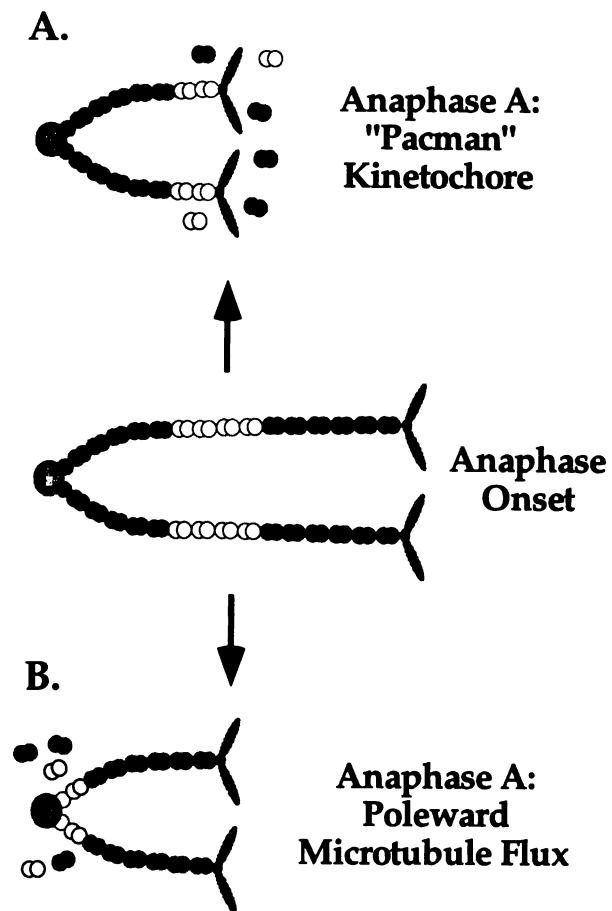
Significant bar-splitting is not evident in the presence of 1.5 mM AMPPNP. Even at much later times (up to 10' after marking the spindle), there is no significant bar-splitting at this AMPPNP concentration (see also Sawin and Mitchison, 1991). Bar, 10  $\mu\text{m}$ .

Figure 5. Anaphase kinetics of chromosome separation and spindle elongation in (A) control, (B) 1  $\mu\text{M}$  taxol and (C) 1.5 mM AMPPNP. Chromosome separation was measured as the distance (in  $\mu\text{m}$ ) between the leading edges of separating sister chromatids as described (Murray et al., 1996). The arrows mark the region used to calculate the chromosome-to-pole movement rates after subtracting out the contribution from spindle elongation. Time 0 is when calcium was added to initiate anaphase. The rapid spindle elongation after chromosome separation in 1  $\mu\text{M}$  taxol and the reduction in pole-to-pole distance after chromosome separation in the control sequence occur as a consequence of cytoplasmic flows in the extract moving the separated half spindles. There is no significant chromosome-to-pole movement in 1.5 mM AMPPNP for this particular spindle. These traces are for the sequences shown in Figure 4A.

Figure 6. Summary of the analysis of the rates of chromosome-to-pole movement (A) and poleward MT flux (B) for the indicated treatments. The anaphase poleward MT flux values are replotted from Figure 3C. The experiments summarized here were performed on 13 different extract preparations. For the analysis of chromosome-to-pole movement a total of 65 sequences were acquired of which 35 were analyzed to generate the data shown in (A). Each condition represents analysis of chromosome movement on 3-5 spindles, with the exception of 25  $\mu\text{M}$  vanadate (2 spindles) and 2  $\mu\text{M}$

taxol (2 spindles). Multiple measurements were often performed on single spindles and the observed effects were qualitatively confirmed in both sequences that were not analyzed due to extensive flow-driven movements and fixed images acquired throughout the sample preparation at the end of each sequence. The flux measurements were made for 6 spindles in 1 mM AMPPNP, 4 spindles in 1.5 mM AMPPNP and 6 spindles in 1  $\mu$ M taxol. The analysis of the effect of AMPPNP on flux was done on anaphase (A) spindles whereas that of taxol on flux was done on metaphase (M) spindles.

Figure 7. Morphology of chromosomes on *Xenopus* extract spindles in early metaphase arrest (A) and after a prolonged metaphase arrest (B). Arrowheads in (B) indicate the acrocentric centromere regions at the poleward edges of the partially disjoined chromosomes. This morphology was observed in experiments on several different extracts after a prolonged metaphase arrest. Bar, 10  $\mu$ m.

**Figure 1**

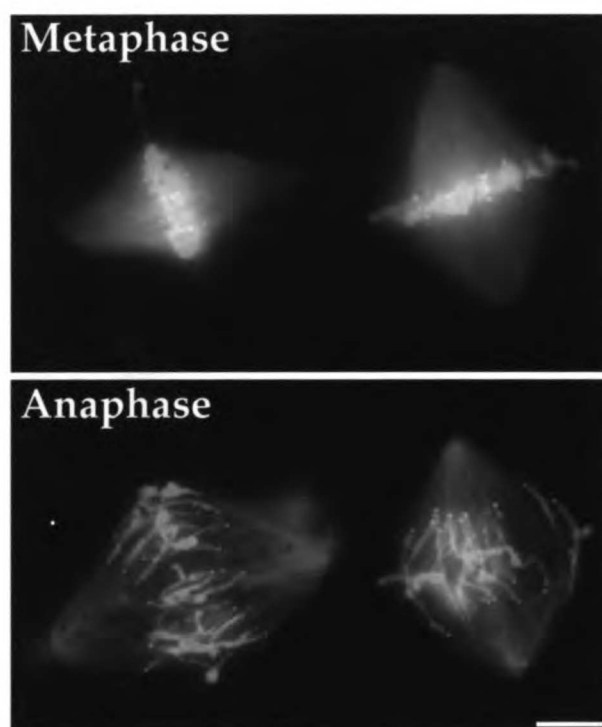
**Figure 2**

Figure 3

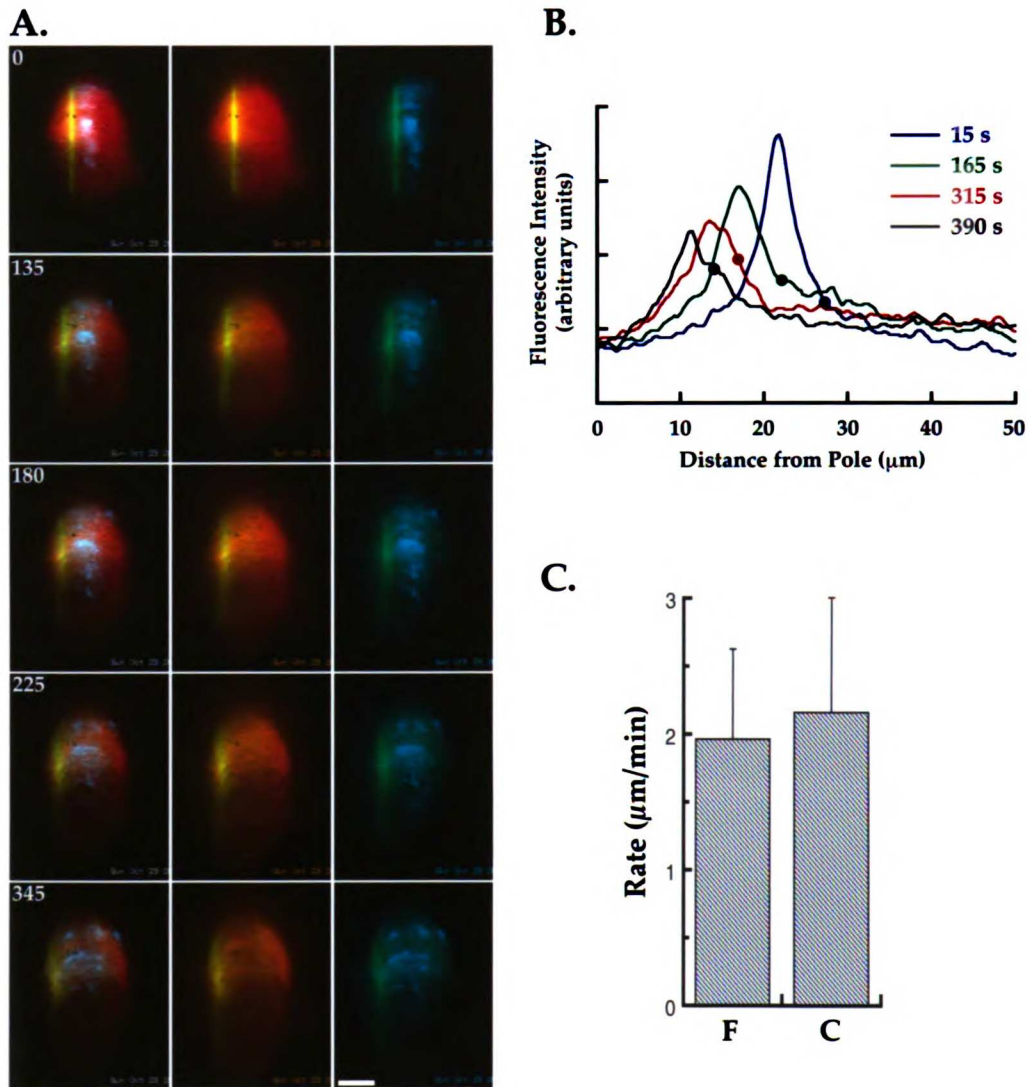


Figure 4

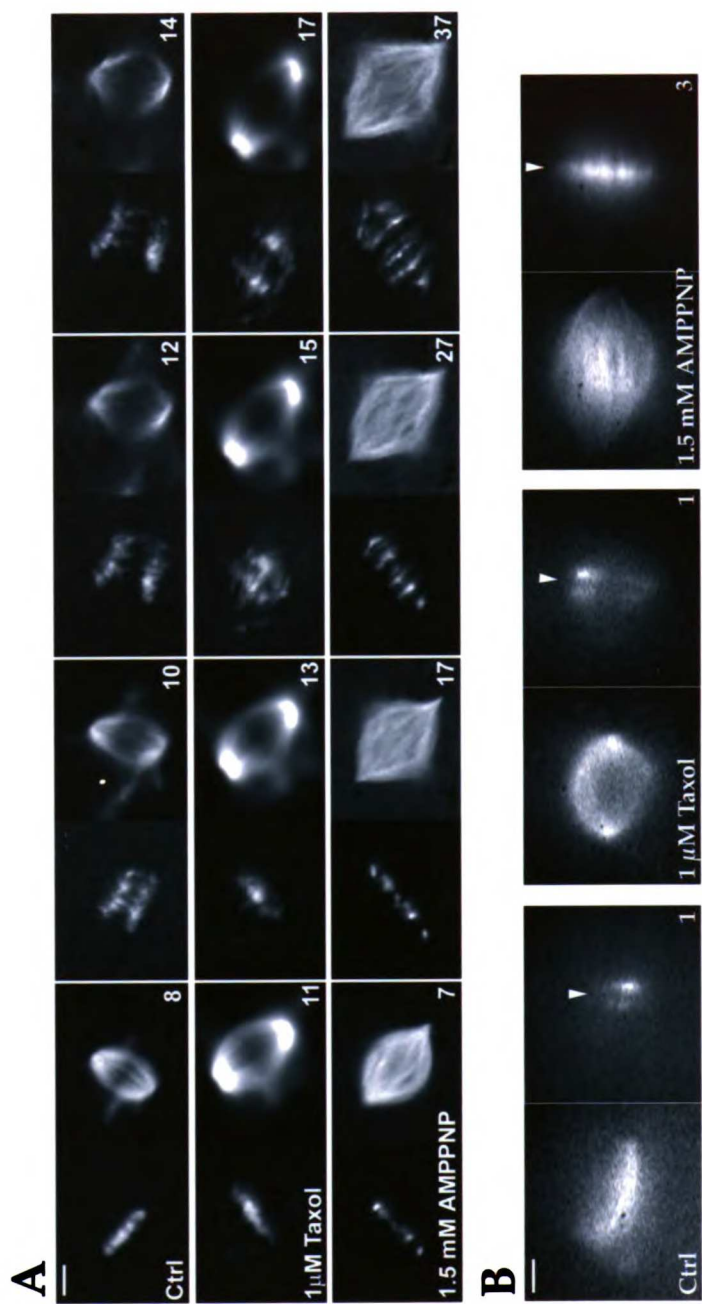


Figure 5

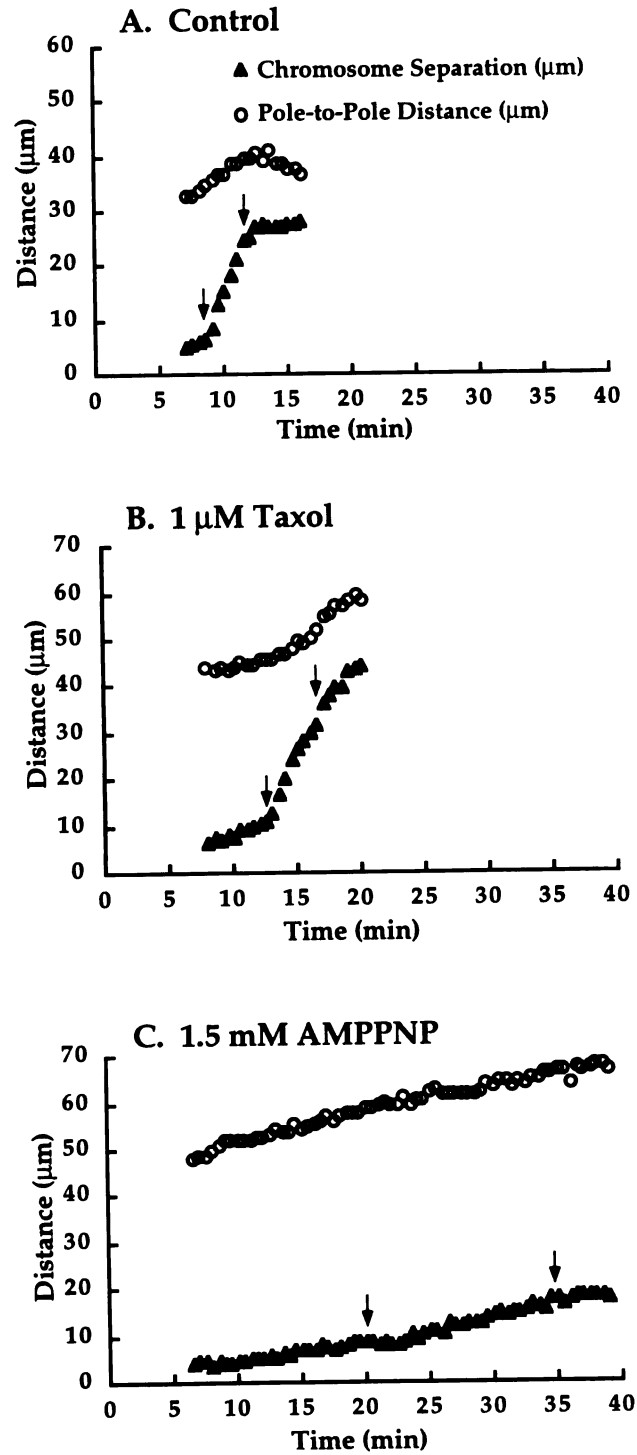
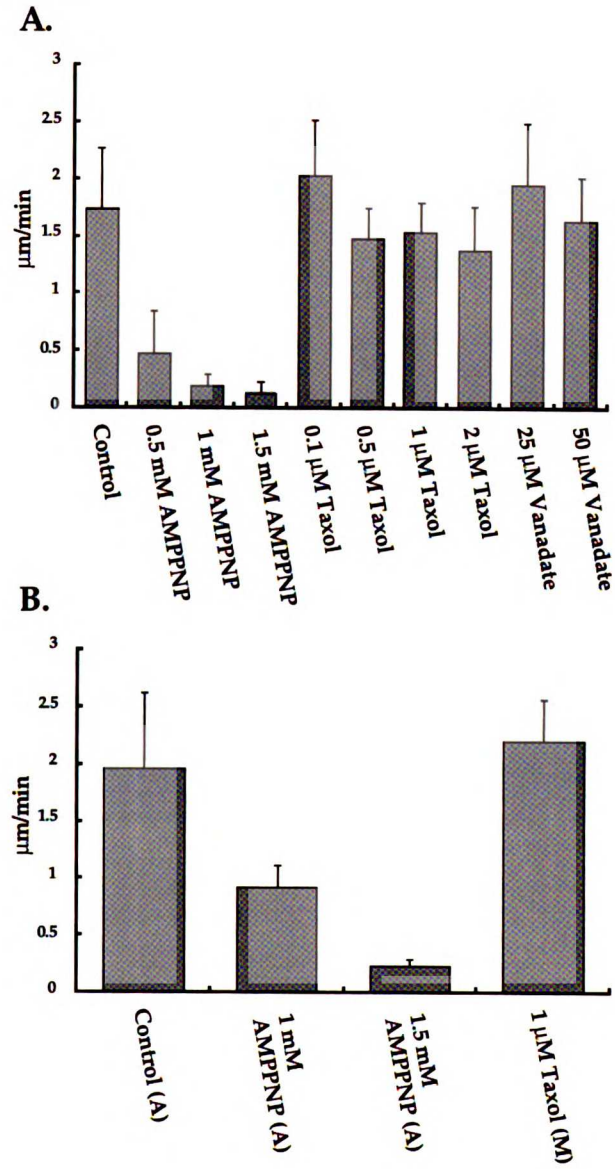
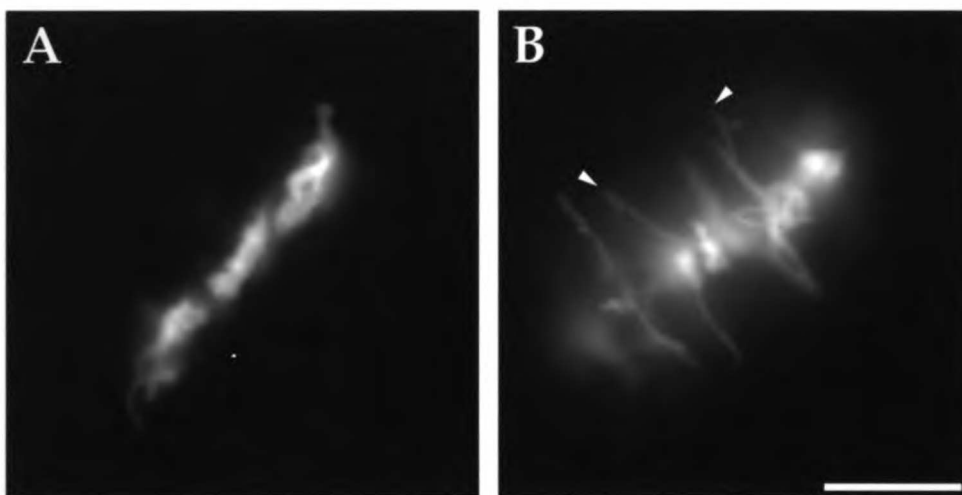


Figure 6





**Figure 7**

## Chapter 4

### **XKCM1: A Microtubule-Destabilizing Kinesin**

The text of this chapter has been reproduced from *Cell* (1996), Volume 84 pages 37-47. Copyright Cell Press.

This work was done in collaboration with Dr. C. E. Walczak, a post-doctoral fellow in the Mitchison lab. I performed the analysis of microtubule dynamics, and helped Dr. Walczak with the functional analysis of XKCM1 in *Xenopus* extracts. I also helped Dr. Walczak write the paper with the aid of comments from Dr. Mitchison.

# XKCM1: A *Xenopus* Kinesin-Related Protein That Regulates Microtubule Dynamics during Mitotic Spindle Assembly

Claire E. Walczak,\* Timothy J. Mitchison,\* and Arshad Desai†

\*Department of Cellular and Molecular Pharmacology  
University of California, San Francisco  
San Francisco, California 94143-0450

†Department of Biochemistry and Biophysics  
University of California, San Francisco  
San Francisco, California 94143-0448

## Summary

We isolated a cDNA clone encoding a kinesin-related protein, which we named XKCM1. Antibodies to XKCM1 stain mitotic centromeres and spindle poles. Immunodepletion and antibody addition experiments in an *in vitro* spindle assembly assay show that XKCM1 is required for both establishment and maintenance of mitotic spindles. The structures that form in the absence of XKCM1 contain abnormally long microtubules. This long microtubule defect can be rescued by the addition of purified XKCM1 protein. Analysis of microtubule dynamics in a clarified mitotic extract reveals that loss of XKCM1 function causes a 4-fold suppression in the catastrophe frequency. XKCM1 thus exhibits a novel activity for a kinesin-related protein by promoting microtubule depolymerization during mitotic spindle assembly.

## Introduction

The faithful segregation of genetic material to daughter cells is essential for the survival of an organism. This process is carried out by the mitotic spindle, which consists of a dynamic array of microtubules responsible for distributing replicated sister chromatids to each daughter cell.

Microtubules are polar polymers that exhibit nonequilibrium polymerization dynamics termed dynamic instability (Mitchison and Kirschner, 1984). Microtubules can coexist in both growing and shrinking states; these states interconvert frequently and stochastically both *in vitro* and *in vivo*. Dynamic instability is thought to provide microtubules with the ability to search three-dimensional space more effectively than would be possible for a simple equilibrium polymer (Holy and Leibler, 1994). Perhaps this ability evolved to allow the rapid capture of chromosomes by microtubules during the early stages of spindle assembly (reviewed by Kirschner and Mitchison, 1986). Consistent with this idea is the observation that microtubule turnover increases dramatically during mitosis relative to interphase (Salmon et al., 1984; Saxton et al., 1984). This increase in microtubule turnover probably plays a crucial role in the assembly of the mitotic spindle (reviewed by Inoué and Salmon, 1995).

Detailed analysis of the cell cycle regulation of microtubule behavior has been performed in *Xenopus* egg extracts (Belmont et al., 1990; Verde et al., 1990, 1992).

These studies showed, first, that the polymerization dynamics of microtubules *in vivo* is significantly different from that of pure tubulin, suggesting the presence of cellular factors that regulate dynamics, and, second, that microtubules in mitosis are much more dynamic than those in interphase, primarily as a result of an increase in the frequency of transitions from the growth state to the shrinkage state (catastrophes), suggesting that there exist one or more cell cycle-regulated factors that affect microtubule dynamics. These phenomenological observations have yet to be extended to molecular mechanisms.

In addition to cell cycle-dependent regulation of bulk spindle microtubule dynamics, real-time analysis of the behavior of chromosomes in spindles suggests that chromosomes possess the ability to modulate the polymerization dynamics of a subset of spindle microtubules attached at their kinetochores. Extensive live analysis of cells undergoing mitosis has shown that chromosomes constantly oscillate on the mitotic spindle (Bajer, 1982; Skibbens et al., 1993). For a chromosome to change direction, the kinetochore must catalyze a coordinate switch in the polymerization state of its kinetochore microtubules.

In addition to regulating dynamics, kinetochores may couple the movement of chromosomes to the polymerization/depolymerization cycles of spindle microtubules to power chromosome movement (reviewed by Rieder and Salmon, 1994; Inoué and Salmon, 1995). Alternatively, mechanochemical motor proteins targeted to kinetochores may move chromosomes by translocating along spindle microtubules. Support for the latter hypothesis came from the localization of three motor proteins, cytoplasmic dynein and the kinesin-related proteins (KRPs) centromere protein E (CENP-E) and mitotic centromere-associated kinesin (MCAK), to mammalian kinetochores (Pfarr et al., 1990; Steuer et al., 1990; Yen et al., 1991; Wordeman and Mitchison, 1995). A recent *in vitro* study on CENP-E and kinesin has led to a unifying view of these two hypotheses by showing that motor molecules can couple their attached cargo to depolymerizing microtubules (Lombillo et al., 1995a, 1995b). These studies suggest that, in addition to moving along spindle microtubules, motor proteins at the kinetochore may be able to couple the movement of chromosomes directly to depolymerizing spindle microtubules (reviewed by Desai and Mitchison, 1995). Although these findings hint at how a chromosome can move along a depolymerizing microtubule, they leave open the question of how chromosomes switch their direction of movement on the spindle as they oscillate.

To explore further the mechanisms of mitotic spindle assembly and chromosome dynamics, we isolated KRPs from *Xenopus* that might be important in these processes. *Xenopus* egg extracts provide both a manipulable *in vitro* system to examine motor function during spindle assembly and a biochemically enriched source of material required for mitosis. We used an antibody to a conserved region of the kinesin motor domain

(Sawin et al., 1992b) to isolate clones encoding KRPs from a *Xenopus* ovary cDNA library. One of the identified KRPs, which we named XKCM1 (for *Xenopus* kinesin central motor 1), is essential for mitotic spindle assembly *in vitro*, localizes to centromeres, and appears to regulate the polymerization dynamics of microtubules, a novel activity for a KRP.

## Results

### Identification and Characterization of XKCM1

To identify KRPs important for mitotic spindle assembly and function, we screened a *Xenopus* ovary cDNA library with the anti-HIPYR peptide antibody, which was raised against a conserved sequence in kinesin motor domains (Sawin et al., 1992b). The most abundant clone isolated (56 of 75) encoded the protein XKCM1. Other clones isolated in this screen will be described elsewhere.

The cDNA for XKCM1 is 2402 nt in length and encodes a 730 amino acid protein with a predicted molecular mass of 83 kDa (Figure 1A). Based on high sequence homology, XKCM1 belongs to the KIF2 family of kinesins, originally identified in a screen for KRPs important in neuronal vesicular transport (Aizawa et al., 1992). The closest homolog of XKCM1 is MCAK, which was isolated from CHO cells in a screen similar to the one described here (Wordeman and Mitchison, 1995).

Structural analysis of the XKCM1 sequence predicts a protein with a 250 amino acid amino-terminal globular domain, a centrally located 350 amino acid motor domain, and a 130 amino acid  $\alpha$ -helical tail, portions of which are predicted to form an  $\alpha$ -helical coiled coil (Lupas et al., 1991) (Figure 1B). To generate reagents to probe the function of XKCM1, we raised polyclonal antibodies to a glutathione S-transferase fusion protein containing the amino-terminal globular domain of XKCM1. These affinity-purified antibodies recognized a doublet in *Xenopus* egg extracts with a molecular mass of 85 kDa, close to the predicted size of the XKCM1 protein (Figure 1C, lanes 1 and 2). We estimate that XKCM1 is present at approximately 10  $\mu$ g/ml in these extracts. In addition, these antibodies were able to immunoprecipitate an 85 kDa doublet from *Xenopus* egg extracts (Figure 3A).

To show that XKCM1 has properties consistent with it being a KRP, we performed microtubule binding experiments (Figure 1C). *Xenopus* egg high speed supernatants were incubated in the presence of AMP-PNP, taxol, and an ATP depletion system. The assembled microtubules were sedimented along with bound proteins, and the release of XKCM1 from microtubules was analyzed using different extraction conditions. XKCM1 quantitatively sedimented with microtubules under ATP depletion conditions (Figure 1C, lanes 1 and 2). In addition, XKCM1 was released from microtubules with a combination of ATP and 0.5 M NaCl (Figure 1C, lanes 9 and 10), but was not released from microtubules with either ATP or 0.5 M NaCl (lanes 3–6).

### XKCM1 Is Found on Centromeres and Centrosomes during Mitosis

We determined the localization of XKCM1 in both tissue culture cells and mitotic spindles assembled *in vitro*. In

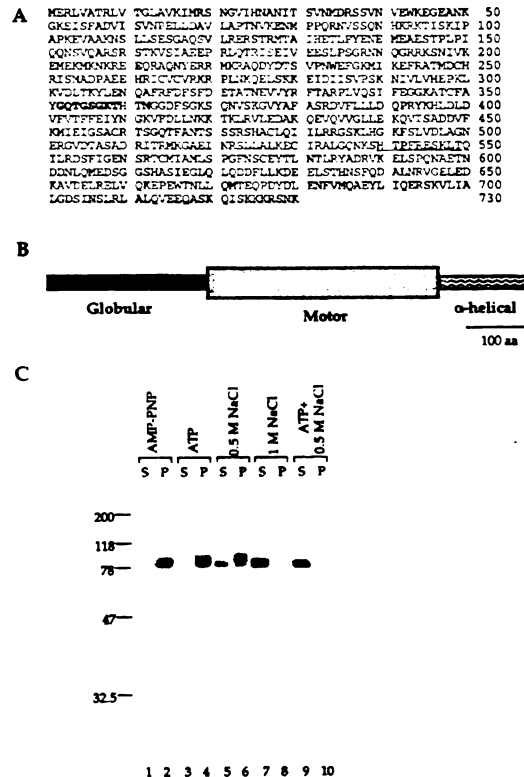


Figure 1. XKCM1 is a KRP

(A) The deduced amino acid sequence of XKCM1. The putative P loop is indicated in bold, and the conserved peptide sequence recognized by the anti-HIPYR peptide antibody used to isolate the clone is underlined.

(B) A schematic representation of XKCM1 structure. XKCM1 contains an amino-terminal globular domain, a central motor domain, and a carboxy-terminal  $\alpha$ -helical tail.

(C) Immunoblots of microtubule pelleting assays in *Xenopus* egg extracts. Microtubules were polymerized in mitotic high speed supernatants of *Xenopus* egg extracts and pelleted in the absence of ATP and the presence of AMP-PNP (lanes 1 and 2). The microtubule pellet, with associated proteins, was resuspended and extracted with 2 mM Mg-ATP (lanes 3 and 4), 0.5 M NaCl (lanes 5 and 6), 1 M NaCl (lanes 7 and 8), or 2 mM Mg-ATP plus 0.5 M NaCl (lanes 9 and 10). The blots were probed with anti-XKCM1.

the *Xenopus* tissue culture cell line, XL177, the immunolocalization of XKCM1 was quite complex. During interphase, the protein was found as a soluble pool present in both the nucleus and the cytoplasm (Figure 2A, I); this soluble pool persisted throughout mitosis, but was most apparent during prometaphase to telophase, when the cells are most rounded. In addition, a portion of XKCM1 localized during mitosis to the centromeric region of the mitotic chromosomes and to the centrosomal region of the spindle (Figure 2A, PM to T). Centromeric localization persisted throughout mitosis and decreased in intensity by anaphase, but could still be detected at telophase (Figure 2A, A and T). Localization to the centrosomal region of the spindle was evident from prometaphase to anaphase (Figure 2A, PM to A).

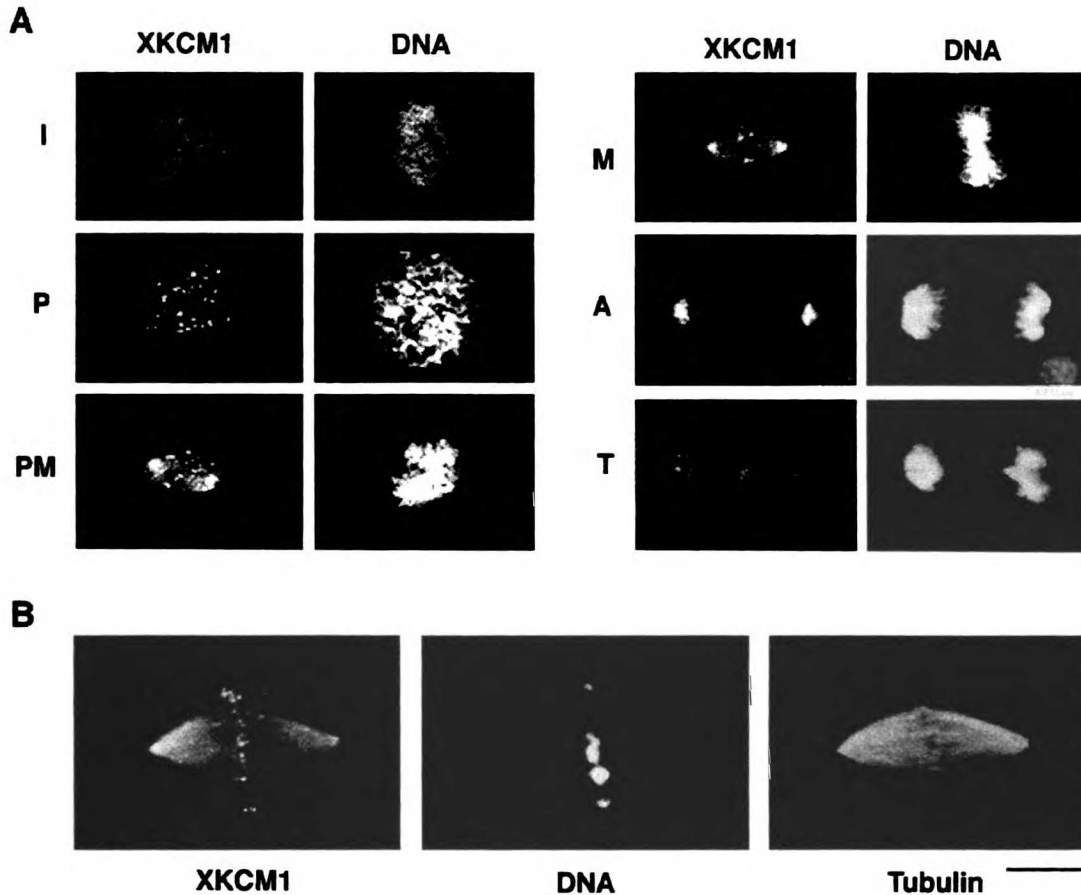


Figure 2. Immunolocalization of XKCM1

(A) Immunolocalization of XKCM1 in *Xenopus* tissue culture cells. The cells were stained with 1  $\mu\text{g/ml}$  anti-XKCM1 followed by fluorescein isothiocyanate (FITC)-conjugated goat anti-rabbit secondary antibody. DNA was visualized by staining with 0.05  $\mu\text{g/ml}$  propidium iodide. Images were recorded on a Bio-Rad MRC-600 laser scanning confocal microscope. Interphase (I), prophase (P), prometaphase (PM), metaphase (M), anaphase (A), and telophase (T) are shown. Scale bar is 20  $\mu\text{m}$ .

(B) Immunolocalization of XKCM1 on *in vitro* assembled spindles. Mitotic spindles assembled *in vitro* were isolated onto coverslips, fixed, and stained with anti-XKCM1, followed by FITC-conjugated goat anti-rabbit secondary antibody. DNA was visualized by staining with Hoechst 33528, and microtubules were visualized by adding rhodamine tubulin to extracts. Images were recorded with a Zeiss Photomicroscope III. Scale bar is 20  $\mu\text{m}$ .

This localization is consistent with the immunolocalization and biochemical analysis of MCAK, the CHO cell homolog of XKCM1 (Wordeman and Mitchison, 1995). The observed localization was competed by inclusion of the amino-terminal fusion protein in the primary antibody solution and was not observed with a nonimmune immunoglobulin G (IgG) antibody or with antibodies to two other *Xenopus* KRPs, indicating that the staining is specific for the XKCM1 antibodies (data not shown). If cells were permeabilized before antibody staining, XKCM1 was found all along microtubules in both mitotic and interphase cells. This staining was eliminated by inclusion of ATP in the permeabilization buffer, suggesting that it is the result of ATP depletion during permeabilization and subsequent rigor binding of the motor to microtubules (data not shown).

On spindles assembled *in vitro*, XKCM1 was found at

the centromeric regions as well as at the centrosomes, but there was also a diffuse staining of the entire spindle (Figure 2B). This more diffuse staining along the length of spindle microtubules could not be reduced by increasing the ATP concentration during the isolation procedure, suggesting that it may represent a true difference in XKCM1 distribution between *in vitro* assembled spindles and those in tissue culture cells. Another possibility is that there are more microtubules in *in vitro* assembled spindles, and we thus see a higher intensity of staining.

#### XKCM1 Is Required for Assembly and Maintenance of the Mitotic Spindle

To probe the function of XKCM1, we took advantage of the ability to form mitotic spindles *in vitro* in *Xenopus* egg extracts. Upon addition of sperm chromatin to a

mitotically arrested *Xenopus* egg extract, there is a time-dependent formation of a mitotic spindle (Lohka and Maller, 1985; Sawin and Mitchison, 1991; Shamu and Murray, 1992). We investigated the effect of XKCM1 removal on this process. We estimate that greater than 99% of XKCM1 could be removed from the extract by immunodepletion, with a quantitative recovery of the protein in the immunoprecipitated pellet (Figures 3A and 3B, lanes 1 and 2). In mock-depleted extracts (using generic rabbit IgG as a control), there was a time-dependent formation of a bipolar spindle (Figures 4A and 4B). Over 70% of the nuclei formed a classic spindle-like structure (Figure 5A). When XKCM1 was removed from the extract, there was a gross morphological disruption of mitotic spindle assembly. At early timepoints, abnormally large microtubule asters formed, which had centrally located chromatin with microtubules emanating in a sunburst pattern from the center of the structure (Figure 4C). With time, the XKCM1-depleted extracts formed huge aggregated structures with long microtubules radiating from the outer portion of the structure (Figure 4D). Over 90% of added nuclei participated in forming distorted structures in the XKCM1-depleted extracts (Figure 5A). The same results were obtained if antibodies to XKCM1 were added to extracts prior to spindle assembly (data not shown). A final concentration of antibody in the extract as low as 10  $\mu$ g/ml resulted in the same aberrant structures as in the immunodepleted extracts. Although the long microtubules seen in the XKCM1-immunodepleted extract are reminiscent of interphase-length microtubules, the extract remained mitotic, as indicated by the condensed chromatin and high levels of histone H1 kinase activity (data not shown). When antibodies to XKCM1 were added to extracts that had already formed spindles, there was a rapid perturbation of spindle structure (< 2 min) beginning with growth of long microtubules from the outer parts of the spindle and eventually resulting in huge, distorted structures that were indistinguishable from those induced by antibody addition prior to spindle assembly or by immunodepletion (data not shown). Taken together, these results show that XKCM1 is required both for assembly and maintenance of normal spindle structure *in vitro*.

The endogenous level of XKCM1 is important for spindle assembly. We found that removing as little as 25% of the XKCM1 from extracts resulted in aberrant structures with morphology similar to those in the fully depleted extract. This suggests that the concentration of XKCM1 present in the extract is important for proper spindle assembly (data not shown).

#### Isolated XKCM1 Rescues the Defect in Depleted Extracts

To prove that the observed disruption of spindle assembly is specifically due to XKCM1 removal, we purified the native protein from *Xenopus* egg extracts to add back to depleted extracts. We synthesized a peptide to the carboxy-terminal ten amino acids of XKCM1 (XKCM1-CTP) and used this peptide for the production of polyclonal antibodies. These antibodies were able to immunodeplete XKCM1 from extracts and caused the same spindle assembly defects seen using the anti-XKCM1 antibodies raised to the entire amino-terminal domain of XKCM1 (data not shown). We used these peptide antibodies to purify XKCM1 by immunoaffinity chromatography. Ammonium sulfate cuts of *Xenopus* egg high speed supernatants were passed over a column of XKCM1-CTP antibodies immobilized on protein A resin. The flowthrough fraction of the column contained the majority of the total extract protein (Figure 3C, lanes L and F). The bound protein on the column was eluted with XKCM1-CTP peptide (Figure 3C, lanes 1–10). Fractions 2–6 of the XKCM1 eluted from the affinity column were pooled, concentrated, and used for reconstitution of spindle assembly. We estimate that the protein is on average 90% pure using this procedure.

We immunodepleted XKCM1 from *Xenopus* egg extracts and then added back purified XKCM1 prior to spindle assembly to determine whether the pure protein could rescue the defect in the depleted extracts. The amount of XKCM1 added back to the immunodepleted extract was equivalent to the amount present endogenously in extracts as judged by quantitative blotting (Figure 3B, lane 3). Addition of purified XKCM1 suppressed the long microtubule phenotype, proving that

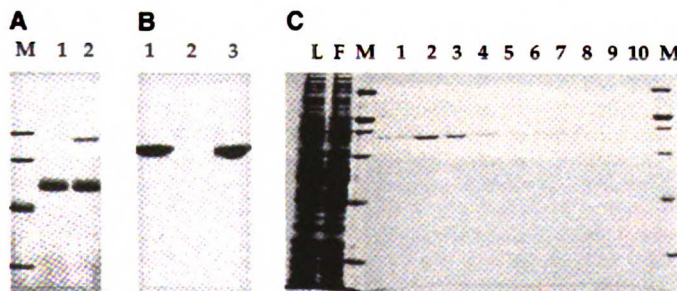


Figure 3. Biochemical Analysis of XKCM1 Protein

(A) Immunoprecipitation of XKCM1 from egg extracts. Immunoprecipitation was performed using control rabbit IgG (lane 1) or affinity-purified anti-XKCM1 (lane 2). The protein A complexes were washed, separated by 10% SDS-PAGE, and visualized by staining with Coomassie blue. Molecular mass markers (M) are 97, 66, 45, and 31 kDa.

(B) Immunodepletion and addback of XKCM1 to extracts. CSF extracts were immunodepleted with control IgG (lane 1), anti-XKCM1 (lane 2), or anti-XKCM1, followed by the addition of purified XKCM1 protein (lane 3). The

extracts were separated by 10% SDS-PAGE, transferred to nitrocellulose, and then probed with anti-XKCM1.  
(C) Affinity purification of XKCM1. XKCM1 was purified on an affinity column of anti-peptide antibodies that recognize the carboxyl terminus of XKCM1. Fractions were eluted with XKCM1 carboxy-terminal peptide, precipitated with trichloroacetic acid, separated by 10% SDS-PAGE, and visualized by staining with Coomassie. The column load (L) was a 25%–40% ammonium sulfate cut of a *Xenopus* egg extract. Also shown are the flowthrough of column (F) and fractions 1–10 (1 column volume each). Molecular mass markers (M) are 200, 116, 97, 66, 45, and 31 kDa. Fractions 2–6 were pooled, concentrated, and used in the functional reconstitution.

the observed defect is mediated by loss of XKCM1 (Figure 4E). We did not observe a high percentage of bipolar mitotic spindles in the rescued extracts, but this was also true for a mock-depleted extract with control buffer added back. Thus, the reconstituted structures (Figure 4E) resembled those in a control extract that had undergone the same series of manipulations (data not shown). The reconstituted spindles were often less fusiform shaped and smaller and had a less organized microtubular array compared with spindles that assembled in an unperturbed extract. Pure XKCM1 must be added back to extracts at a concentration similar to that found endogenously in extracts in order for it to rescue the depleted extracts. If too little XKCM1 was added back to the immunodepleted extract, we were unable to suppress the long microtubule phenotype. In combination with partial immunodepletion experiments (see above), this strongly suggests that the concentration of XKCM1 in extracts is critical for proper spindle assembly. To quantitate the reconstitution, we measured the area of

control spindles, XKCM1-depleted structures, and reconstituted structures (Figure 5B). XKCM1-immunodepleted structures were approximately ten times larger than mock-depleted structures. This means that the longest microtubules were increased in length an average of 10-fold, although their high density precluded accurate length measurements. Addition of purified XKCM1 to the immunodepleted extract resulted in structures that were the same size as controls. These results strongly suggest that loss of XKCM1 function by removal of the protein from extracts is responsible for the observed long microtubules.

#### Loss of XKCM1 Function Alters Microtubule Dynamics

The extremely long microtubules seen in the XKCM1-depleted structures suggested that some aspect of microtubule dynamics might be altered in the absence of XKCM1 function. To test this possibility, we measured the parameters of microtubule dynamic instability in high

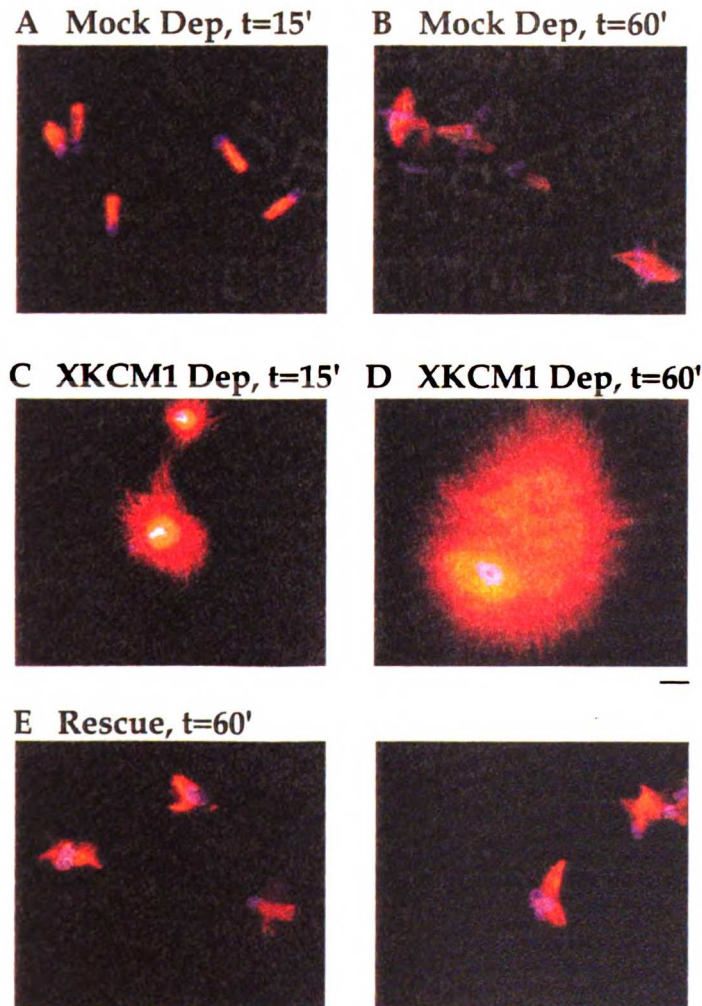
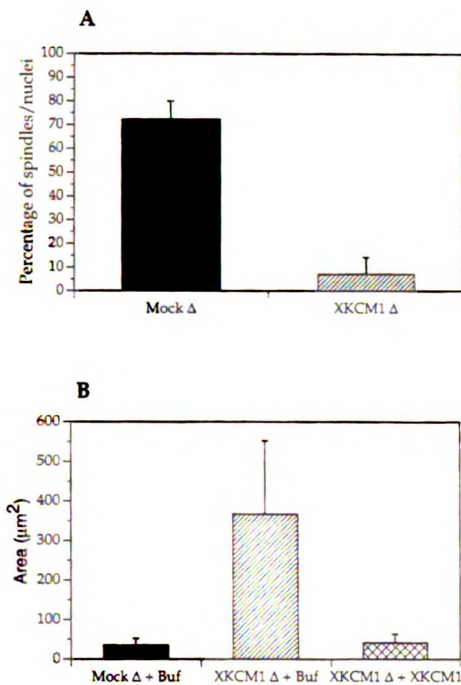


Figure 4. XKCM1 Is Required for Mitotic Spindle Assembly

Mitotic spindles were assembled in a mock-depleted extract (A and B) or an XKCM1-depleted extract (C and D). Two timepoints are shown for each assembly condition. In the absence of XKCM1, huge microtubule asters form. The bright white spot in the center of the aster is where the DNA (blue) and tubulin (red) are overlaid and have saturated the film. Scale bar for (A)–(D) is 20  $\mu\text{m}$ .

(E) Mitotic spindles were assembled in XKCM1-immunodepleted extracts that were reconstituted by the addition of purified XKCM1 prior to spindle assembly. The long microtubules seen in the immunodepleted extracts are no longer present; instead, structures resembling mitotic spindles are formed. Two representative fields of view are shown. Rhodamine-labeled microtubules are shown in red, and DNA is in blue. Scale bar is 20  $\mu\text{m}$ .

Cell  
42

**Figure 5. Quantitation of XKCM1 Immunodepletion and Rescue with Pure XKCM1**

(A) Effect of XKCM1 immunodepletion on spindle assembly. Mitotic spindles were assembled in either mock-depleted extracts (Mock Δ) or in XKCM1-depleted extracts (XKCM1 Δ). Structures that assembled were sedimented onto coverslips, and the percentage of spindle-like structures that formed per nuclei was quantitated. The bars represent mean  $\pm$  95% confidence interval of ten independent experiments ( $n = 2927$  nuclei for mock-depleted samples;  $n = 2961$  nuclei for XKCM1-depleted samples).

(B) Reconstitution of spindle assembly with purified XKCM1. Mitotic spindles were assembled in mock-depleted extracts with control buffer added (Mock Δ plus Buf), in XKCM1-depleted extracts with control buffer added (XKCM1 Δ plus Buf), or in XKCM1-depleted extracts that were reconstituted by the addition of purified XKCM1 (XKCM1 Δ plus XKCM1). Structures were sedimented onto coverslips, and the area was measured as described in Experimental Procedures. The bars represent the mean area  $\pm$  1 SD for the area of 100 structures measured in each condition in a single experiment, but are representative of data from three separate experiments.

speed supernatants of mitotic egg extracts in the presence of either control IgG or anti-XKCM1. We compared the growth rates and shrinkage rates, as well as the frequency of transitions from growth to shrinkage (catastrophe frequency) and the frequency of transitions from shrinkage to growth (rescue frequency). We found no significant difference in the growth rates or the shrinkage rates (Figure 6A). However, we found a 4-fold suppression in the catastrophe frequency in extracts that had anti-XKCM1 added relative to extracts that had control IgG added (Figure 6B). The rescue frequency did not differ significantly between the two conditions, although it was difficult to measure rescue accurately in the antibody-treated extracts owing to the limited number of observed catastrophes. We repeated our analysis of dynamics parameters on extracts that had

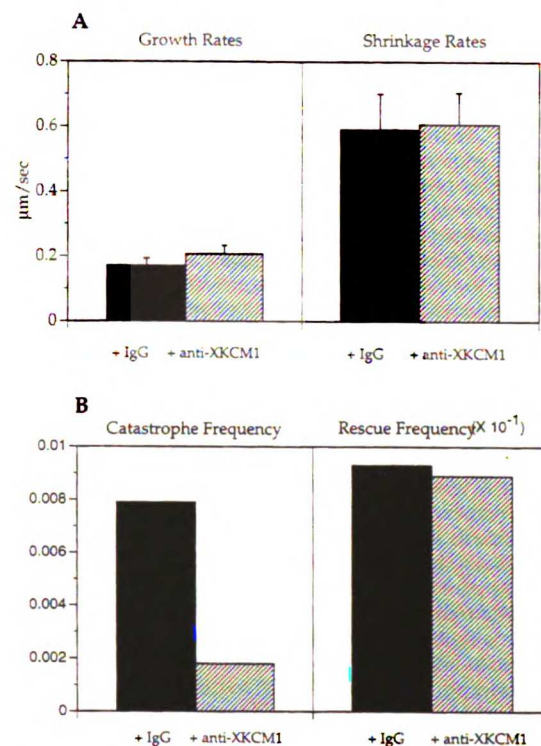


**Figure 6. Removal of XKCM1 Suppresses Catastrophes in Mitotic High Speed Supernatants**

We measured the parameters of microtubule dynamics in extracts that had either control IgG or XKCM1 antibodies added. There was no significant difference in the growth or shrinkage rates (A) with either antibody addition ( $n = 34$  microtubules for IgG addition;  $n = 60$  microtubules for anti-XKCM1 addition). There was, however, a 4-fold suppression of the catastrophe frequency (B) in the presence of XKCM1 antibodies ( $t_{\text{growth}} = 2922$  s for IgG addition;  $t_{\text{growth}} = 6167$  s for anti-XKCM1 addition). There was no significant difference in the rescue frequency (B) with either antibody addition ( $t_{\text{rescue}} = 215$  s for IgG addition;  $t_{\text{rescue}} = 112$  s for anti-XKCM1 addition), although it is difficult to measure accurately the rescue frequency in the absence of many catastrophes. The parameters were essentially identical for immunodepleted extracts.

been immunodepleted of XKCM1 and found that the measured parameters were essentially identical to those determined in the XKCM1 antibody addition experiments (data not shown). These results imply that XKCM1 acts as a catastrophe promoter in extracts. The loss of XKCM1 function causes a suppression of catastrophes, which results in the observed long microtubules.

## Discussion

### The KIF2 Family of Kinesins

XKCM1 belongs to a family of kinesins that contain centrally located motor domains. The parental member of this family, KIF2, was originally identified in mouse brain in a polymerase chain reaction (PCR) screen for motors important in neuronal vesicle transport (Aizawa et al., 1992). Subsequent reports have shown that mouse KIF2 is a fast ( $0.5 \mu\text{m/s}$ ), plus end-directed microtubule motor



that associates with a subclass of neuronal vesicles. XKCM1 is 76% identical to KIF2 within the motor domain (and 48% identical overall). XKCM1 is also highly homologous to MCAK (79% identical in the motor domain and 55% identical overall), which was identified in CHO cells in a screen similar to that described here (Wordeman and Mitchison, 1995).

There are at least two and possibly three functionally distinct classes of motors within the KIF2 family. Phylogenetic analysis generates three subgroupings within the KIF2 family. XKCM1 groups with MCAK and rKRP2, a kinesin-related protein isolated from rat testes (Sperry and Zhao, submitted). XKCM1 and MCAK exhibit a similar pattern of localization in tissue culture cells, and an anti-MCAK monoclonal antibody cross-reacts with a 90 kDa polypeptide in *Xenopus* egg extracts (Wordeman and Mitchison, 1995). rKRP2 is expressed highly in testes and may function as a meiotic motor; its localization in tissue culture cells has yet to be determined. The second subclass of the KIF2 family contains KIF2 itself as well as a second *Xenopus* KIF2 homolog, which we isolated in our screen (C. E. W. and T. J. M., unpublished data). This partial clone, which we refer to as *XKIF2*, encodes a protein that is 96% identical to the motor domain of mouse KIF2 and 90% identical overall. The extent of sequence identity suggests that *XKIF2* is likely to be the true functional homolog of mouse KIF2. The fact that there are two KIF2 homologs in *Xenopus* suggests that there may be two KIF2 homologs in other organisms as well, but they have yet to be identified. A third subgrouping within the KIF2 family contains a sole member, DSK1, which localizes to diatom spindle midzones and is important for spindle elongation (Wein and Cande, personal communication). DSK1 is only 26% identical overall, and 44% identical within the motor domain, to XKCM1. It is unclear whether the lower homology and the functional differences between DSK1 and other KIF2 family members are a result of evolutionary divergence or if there is a third KIF2 subclass in all organisms.

#### Biochemical Properties of XKCM1

XKCM1 has properties consistent with it being a microtubule motor protein. In extracts, the protein binds and releases from microtubules in an ATP-dependent manner. Although we have not yet been able to demonstrate motor activity using either purified preparations of XKCM1 or a bacterially expressed version of XKCM1 in an *in vitro* microtubule gliding assay, we believe that XKCM1 will likely be a plus end-directed microtubule motor, given the high sequence identity with KIF2 within the motor domain.

Preliminary analysis of the behavior of XKCM1 on both gel filtration and sucrose gradients suggests that XKCM1 exists as a dimer in extracts (C. E. W. and T. J. M., unpublished data). Based on our immunoprecipitation data, which showed no coprecipitation of any other proteins with XKCM1, and the purification of XKCM1, which also showed no associated proteins, we propose that XKCM1 functions as a simple dimer with no light chains. This does not rule out the possibility

that XKCM1 interacts transiently with other proteins to carry out its function.

#### XKCM1 Regulates Microtubule Dynamics

XKCM1 appears to regulate the catastrophe frequency of microtubules in mitotic *Xenopus* egg extracts. It is unclear whether this is likely to be a general property of motor molecules or specific to this particular motor. For example, depletion of Eg5 or Xklp1, two mitotic KRPs, from *Xenopus* egg extracts does not distort the spindle as dramatically as XKCM1 immunodepletion (Sawin et al., 1992a; Vernos et al., 1995), suggesting that the control of microtubule dynamics by a motor protein is a specialized property of XKCM1. The minus end-directed kinesin Kar3 can depolymerize the minus ends of taxol-stabilized microtubules as it translocates along them, suggesting that this motor may also destabilize microtubules (Endow et al., 1994). However, it is unclear what relevance this has to the *in vivo* function of Kar3.

We have drawn a model (Figure 7A) depicting how XKCM1 might cause catastrophes of microtubules. XKCM1 is shown walking along microtubules toward the plus end. When it reaches the end of the microtubule, it causes a destabilization of the microtubule end, initiating catastrophic depolymerization of the microtubule. It has been shown that the end of a depolymerizing microtubule is frayed (Mandelkow et al., 1991; Chrétien et al., 1995). A motor at the end of a microtubule might tweak the protofilaments of the microtubule apart, thus triggering depolymerization. It has been shown more recently that KRPs cause a conformational change of tubulin upon binding (Hirose et al., 1995; Hoenger et al., 1995; Kikkawa et al., 1995). One could imagine that certain types of KRPs might cause different changes in the conformation of the end of the microtubule. Some KRPs, like XKCM1, could trigger a catastrophe, while other motors might have no effect or could even stabilize microtubule ends. In support of our model, we have preliminary evidence suggesting that purified XKCM1 destabilizes microtubules assembled *in vitro*. We are currently investigating in detail the mechanism by which pure XKCM1 affects the polymerization dynamics of pure tubulin.

#### XKCM1 Is Required for Spindle Assembly

Removal of XKCM1 function increases microtubule stability and thus blocks spindle assembly at an early stage. The fact that the XKCM1-depleted structures cannot reorganize and form an abnormally large spindle suggests that microtubule dynamics are indeed necessary for spindle formation.

One possible model of XKCM1 function is that it modulates the dynamics of microtubules between interphase and mitosis. It has been shown that during this cell cycle progression there is an increase in the microtubule catastrophe frequency in *Xenopus* egg extracts (Belmont et al., 1990). It is possible that XKCM1 is the catastrophe factor responsible for the difference between interphase and mitotic microtubule dynamics, but at the present time we have no evidence to support this model. Although a more careful analysis will be

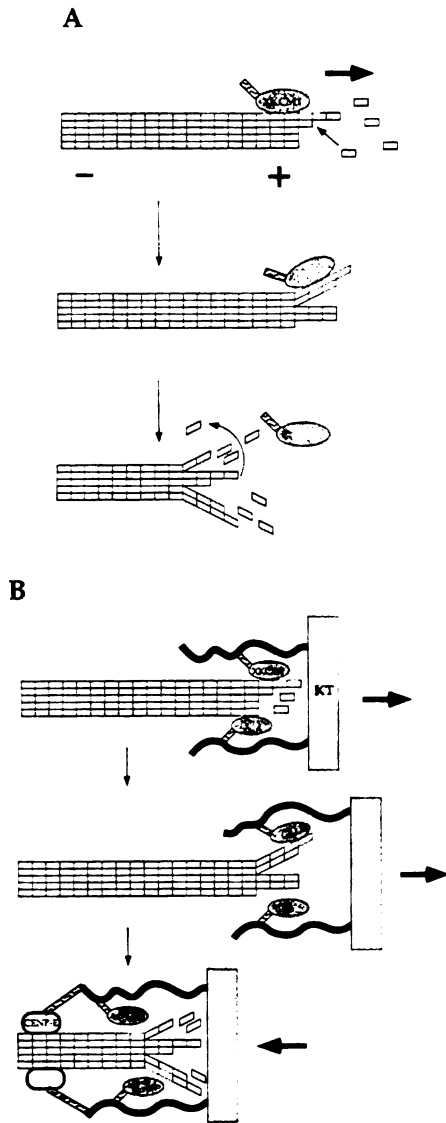


Figure 7. Model for XKCM1 Destabilization of Microtubules

(A) XKCM1 destabilizes microtubule ends. XKCM1 (stippled structure) walks along microtubules toward the plus end of a growing microtubule (indicated by subunit addition). As it approaches the end of the microtubule, it destabilizes the microtubule end, which results in microtubule depolymerization (indicated by subunit loss). XKCM1 is now free to bind to another microtubule and cause the same phenomenon.

(B) XKCM1 function at the kinetochore. XKCM1, bound to the kinetochore, walks along the microtubule, resulting in movement away from the pole. Upon reaching the end of the microtubule, it triggers a catastrophe resulting in depolymerization and movement back toward the pole. It is postulated that CENP-E acts to couple chromosome movement to the depolymerizing microtubule. (See text for further discussion).

necessary before making a judgment on this role, preliminary experiments looking at the effect of XKCM1 antibody addition to interphase extracts have also shown

an increase in the number of microtubules present, suggesting that XKCM1 depolymerizing activity is active during interphase. We plan to explore the regulation of XKCM1 more thoroughly.

#### XKCM1 Function on Kinetochores

We favor a model that implicates XKCM1 function in the regulation of microtubule dynamics at the kinetochore (Figure 7B) in addition to its role in spindle assembly. An elegant high resolution video analysis of chromosome movement in *Newt* lung cells has shown that kinetochores oscillate throughout mitosis (Skibbens et al., 1993). It is thought that these oscillations are the result of switching between phases of growth and shrinkage of kinetochore microtubules. Microtubule motor proteins are attractive candidates for forming the transient linkage between a kinetochore and a microtubule because they are able to stay connected to a microtubule as they translocate along it. XKCM1 might act to regulate the transitions at the end of kinetochore microtubules. By being bound to the kinetochore, as demonstrated in our immunofluorescent staining, XKCM1 would be positioned near the end of the microtubule. It could then walk along a microtubule toward the plus end, possibly representing the plus end-directed kinetochore motor detected *in vitro* (Hyman and Mitchison, 1991). Upon reaching the end of the microtubule, XKCM1 would trigger a catastrophe. The chromosome would then move back toward the pole concomitant with microtubule depolymerization. It has been proposed that CENP-E might act as a kinetochore coupler to depolymerizing microtubules (Lombillo et al., 1995b; reviewed by Desai and Mitchison, 1995).

Earlier work by Hyman and Mitchison (1990) showed that isolated chromosomes could modulate the dynamics of microtubules *in vitro*, specifically that kinetochores increase the catastrophe rate of their bound microtubules. This activity was inhibited in the presence of AMP-PNP, suggesting the need for a kinetochore ATPase to cause catastrophes. Perhaps XKCM1 represents the ATP-dependent kinetochore-bound catastrophe factor they saw in their assays. We plan to repeat the *in vitro* kinetochore depolymerization assays in the presence of our XKCM1-blocking antibody to address this putative role of XKCM1.

In summary, we have isolated a KRP that plays a unique role in mitotic spindle morphogenesis. XKCM1 appears to act by regulating microtubule dynamics. This activity is a novel activity for a KRP and, furthermore, represents the identification of a physiological regulator of catastrophes. Our experiments suggest that XKCM1 acts directly on microtubules, causing a destabilization and eventual depolymerization of the microtubule. To analyze the mechanism of this destabilization, it will be necessary to show definitively that purified XKCM1 increases the catastrophe frequency of pure microtubules in the absence of any other proteins that could also influence microtubule dynamics.

#### Experimental Procedures

##### Isolation of XKCM1 Clone

Affinity-purified anti-HIPYR peptide antibody (Sawin et al., 1992b) was used to screen a  $\lambda$ Uni-ZAP *Xenopus* ovary cDNA library (Stratagene) according to standard procedures (Sambrook et al., 1989).

In brief, after plaque lifts, the filters were washed in TBST (20 mM Tris [pH 7.4], 150 mM NaCl, 0.1% Tween 20) and then incubated in boiling water for 5 min to reduce background (Kellogg and Alberts, 1992). The filters were washed in TBST and blocked overnight in TBST plus 5% nonfat dry milk plus 0.1% Na<sub>2</sub>S<sub>2</sub>O<sub>5</sub>. The primary antibody was diluted to 1 µg/ml in blocking buffer and incubated for 1.5 hr, followed by alkaline phosphatase-labeled goat anti-rabbit secondary antibody (Promega). Positive clones were detected using colorimetric detection. We screened 900,000 plaques and isolated 75 positive clones. Plasmid DNA was obtained from each clone by *in vivo* excision according to the protocol of the manufacturer. HIPYR-positive clones were categorized by restriction mapping, PCR, Southern blotting, and sequencing. By these characterizations, we found that 56 of 75 clones encoded XKCM1. The other clones will be described elsewhere. A single cDNA clone, clone 11B, was fully sequenced on both strands using Sequenase Version 2.0 (United States Biochemicals). Gaps and ambiguities were resolved using an automated DNA sequencer (performed by the Biomolecular Resource Center DNA Sequencing Facility at the University of California, San Francisco).

#### Protein Expression and Antibody Production

The region corresponding to amino acids 2–264 was inserted using PCR into pGEX-2T (Smith et al., 1988) (clone pGEX-11BNT) and into pMAL-CRII (clone pMAL-11BNT). The glutathione S-transferase fusion protein was used for rabbit antibody production (Berkeley Antibody), and the antibodies were affinity purified on the MBP fusion protein. Antibodies were affinity purified according to published procedures (Harlow and Lane, 1988). Antibodies (anti-XKCM1) were eluted from the affinity column with 100 mM glycine (pH 2.5), 150 mM NaCl, neutralized, and then dialyzed against 10 mM HEPES, (pH 7.2), 100 mM KCl before being concentrated for use in the experiments described.

A carboxy-terminal peptide antibody (anti-XKCM1-CTP) was generated against the synthetic peptide (C)QISKKKRSNK (synthesized by the Biomolecular Resource Center), which corresponds to the last ten amino acids of XKCM1. An amino-terminal cysteine was added to the peptide for sulfhydryl coupling. All peptide conjugation procedures and antibody affinity purification were as described previously (Sawin et al., 1992b). Antibodies were dialyzed and concentrated as described above.

#### Microtubule Pelleting Assays and Immunoblotting

High speed supernatants of *Xenopus* egg extracts were prepared from crude cytosolic factor (CSF)-arrested extracts (Murray, 1991) as described previously (Hirano and Mitchison, 1993). Extracts were thawed, diluted 2-fold with CSF-XB (10 mM K-HEPES [pH 7.7], 50 mM sucrose, 2 mM MgCl<sub>2</sub>, 0.1 mM CaCl<sub>2</sub>, 100 mM KCl, 5 mM EGTA), and centrifuged at 50,000 rpm for 15 min in a TLA 100 rotor (Beckman). An ATP depletion system (15 U/ml hexokinase, 20 U/ml apyrase, 20 mM glucose) was added, as well as 10 µM taxol and 2 mM Mg-AMP-PNP. The extract was incubated for 30 min at 25°C and then layered onto a 1 ml cushion of 40% glycerol in Na-BRB80 (80 mM Na-PIPES [pH 6.8], 1 mM MgCl<sub>2</sub>, 1 mM EGTA) and centrifuged in a TLA 100.3 rotor for 20 min at 60,000 rpm and 25°C. An aliquot was removed from the top of the cushion and saved for gel and immunoblot analysis. The pellets were washed and resuspended in BRB80 plus 10 µM taxol plus one of the following additions: 2 mM Mg-ATP; 0.5 M NaCl; 1 M NaCl; or 2 mM Mg-ATP plus 0.5 M NaCl. The samples were incubated for 30 min at 25°C and then centrifuged in a TLA 100 rotor for 30 min at 50,000 rpm at 25°C. Supernatants and pellets were resuspended in equivalent volumes of sample buffer and used for gel and immunoblot analysis.

SDS-polyacrylamide gel electrophoresis (SDS-PAGE) and electrophoretic transfer were performed according to routine protocols (Harlow and Lane, 1988). Immunoblots were blocked for at least 2 hr in 5% NFDM in TBST plus 0.1% Na<sub>2</sub>S<sub>2</sub>O<sub>5</sub>, rinsed, and incubated in primary antibody (0.1 µg/ml affinity-purified antibody diluted in 2% BSA in TBST plus 0.1% Na<sub>2</sub>S<sub>2</sub>O<sub>5</sub>), followed by horseradish peroxidase-conjugated secondary antibody (1:2500). Blots were rinsed and developed with enhanced chemiluminescence (Amersham).

#### Immunofluorescence

XL177 cells were grown on polylysine-coated glass coverslips to near confluency. Coverslips were rinsed in TBS, and then cells were fixed with 4% formaldehyde in BRB80 containing 5 mM EGTA for 20 min. Coverslips were processed essentially as described previously (Sawin et al., 1992b). All micrographs were taken on a Bio-Rad MRC-600 laser scanning confocal microscope. Series of optical sections through the cell were collected and projected onto a single image plane. Images were transferred to Adobe Photoshop, digitally processed, and printed on a Fujix Pictography 3000 (Better Image Productions).

Extract-assembled spindles were prepared as described below. After methanol fixation, coverslips were washed in TBS-TX (TBS plus 0.1% Triton X-100), blocked, and stained with primary and secondary antibodies as above. DNA was visualized with 10 µg/ml Hoechst 33258, and the coverslips were mounted as above. Photomicrographs were taken on a Zeiss Photomicroscope III with Kodak Ektachrome Elite 200 film. Slides were printed and then scanned into a computer using a color scanner (UMAX Model PS-2400X). Images were collected in Adobe Photoshop and processed as above.

#### Spindle Assembly and Immunodepletion

CSF-arrested extracts were prepared essentially as described previously (Murray, 1991), except that the crushing spin was performed at 10,000 rpm for 15 min with full brake in an SW55 Ti rotor (Beckman). These extracts are technically meiosis II-arrested extracts, but are referred to as mitotic extracts or CSF extracts in this paper (see Sawin and Mitchison [1991] for a more detailed explanation). Mitotic spindle assembly was carried out as described previously (Sawin and Mitchison, 1991) using only freshly prepared extracts. The final concentration of sperm nuclei was 150 sperm per microliter. For immunodepletion experiments, we used CSF extract-assembled spindles because the process of immunodepletion often perturbed the extract sufficiently to inhibit cycled spindle assembly. For antibody addition experiments and for immunofluorescent staining of spindles, CSF extracts were cycled into interphase with the addition of Ca<sup>2+</sup> and then back into mitosis with fresh CSF extract as described previously (Sawin and Mitchison, 1991; Shamu and Murray, 1992). Results from the two different types of extract preparations were indistinguishable.

For immunodepletions, Affi-Prep protein A beads (Bio-Rad) were washed three times in TBS-TX and then coated with affinity-purified antibodies to XKCM1 or with control rabbit IgG (Accurate Chemical and Scientific) for 1 hr at 4°C. The beads were washed one time with TBS-TX and three times with CSF-XB containing 10 µg/ml protease inhibitors (leupeptin, pepstatin A, and chymostatin). After the last wash, we removed as much liquid as possible so as not to dilute the extract. Freshly made CSF extract was added, and the mixture was gently rotated for 1 hr at 4°C. It was important to be very gentle in the immunodepletions or the extract would activate and become an interphase extract. After incubation of extract with beads, the beads were removed by centrifugation for 20 s in a microfuge at top speed. The supernatant was saved and used as the immunodepleted extract. The beads were washed three times in CSF-XB, one time in TBS-TX, and one time in TBS and then boiled in sample buffer before gel analysis. We used the ratio of 25 µl of beads:4 µg of antibody:200 µl of extract. For all immunodepletions, an equivalent volume of mock-depleted extract or XKCM1-depleted extract was analyzed by immunoblot to determine the extent of depletion. For antibody addition experiments, antibodies were added as one-tenth final volume diluted in sperm dilution buffer (5 mM K-HEPES [pH 7.7], 1 mM MgCl<sub>2</sub>, 100 mM KCl, 150 mM sucrose).

For data quantitation, spindles were assembled as described above, and, at the indicated timepoint, 20 µl of the extract was removed and diluted into 2 ml of BRB80, 30% glycerol, 0.5% Triton X-100, 1 mM Mg-ATP. This was layered onto a cushion containing BRB80, 40% glycerol, 1 mM Mg-ATP and centrifuged onto coverslips at 6000 × g for 30 min at 16°C. Coverslips were postfixed in -20°C methanol, washed in TBS-TX, stained with Hoechst 33258,

and mounted as described above for immunofluorescence. Photographs were taken on a Zeiss Photomicroscope III. The results presented represent quantitated data from at least three individual experiments at three different timepoints with at least 250 nuclei counted for each datapoint. We observed qualitatively the same results with at least ten independent extracts.

#### Purification of XKCM1 from Extracts

XKCM1 was purified from high speed supernatants of *Xenopus* egg extracts by immunoaffinity chromatography. We prepared 25% ammonium sulfate supernatants as described elsewhere (Zheng et al., 1995) and froze them at  $-80^{\circ}\text{C}$  until use. All steps were carried out at  $4^{\circ}\text{C}$ . The 25% ammonium sulfate supernatants were thawed, brought to 40% saturation with solid ammonium sulfate, rotated for 1 hr, and then pelleted at  $27,000 \times g$  for 15 min. The pellet was resuspended in MB1 (10 mM K-HEPES [pH 7.2], 2 mM  $\text{MgCl}_2$ , 100 mM KCl, 50 mM sucrose, 1 mM EGTA, 50  $\mu\text{M}$  Mg-ATP, 0.1 mM DTT, 0.1  $\mu\text{g}/\text{ml}$  protease inhibitors) and dialyzed against the same overnight. The dialyzed 25%–40% ammonium sulfate cut was clarified by centrifugation for 10 min at full speed in a microfuge before use. Affinity columns were prepared by washing Affi-Prep protein A beads three times in TBS-TX and then coating with affinity-purified XKCM1-CTP antibodies for 1 hr. We used a ratio of 25  $\mu\text{g}$  of antibody:50  $\mu\text{l}$  of beads:1 ml of extract. After antibody binding, the beads were washed one time in TBS-TX and four times in MB1. The washed beads were added to the clarified ammonium sulfate cuts and rotated for 2 hr. The mixture was poured into a column and then washed with 20 vol of MB1. To elute the XKCM1, we added 1 column volume of MB1 plus 250  $\mu\text{g}/\text{ml}$  XKCM1 carboxy-terminal peptide to the resin, allowed it to flow in, and incubated it for 1 hr. The column was then eluted with 7 additional column volumes of MB1 plus 250  $\mu\text{g}/\text{ml}$  XKCM1 carboxy-terminal peptide. Fractions were analyzed by SDS-PAGE. Fractions that contained pure XKCM1 were pooled, casein was added to 100  $\mu\text{g}/\text{ml}$  as a carrier protein, and samples were concentrated 40-fold in Microcon-30 concentrators (Amicon). For the mock buffer control, we used MB1 plus 250  $\mu\text{g}/\text{ml}$  XKCM1 carboxy-terminal peptide plus 100  $\mu\text{g}/\text{ml}$  casein and concentrated it side by side with the purified XKCM1.

#### Reconstitution of Spindle Assembly with Purified XKCM1

Mitotic spindle assembly and immunodepletions were carried out as described above. For reconstitution of spindle assembly, extracts were immunodepleted and then one-tenth or one-fifth final volume of the pure XKCM1 or the mock buffer control was added to the extract. Spindles were allowed to assemble and then sedimented onto coverslips as described above. Images were recorded with an Olympus  $60 \times 1.4$  NA lens through a silicon-intensified target camera (COHU), which was controlled by Maxvision image processor (Datacube) driven by a 386 AT microcomputer. Images were recorded onto an optical memory disk recorder (Panasonic) and analyzed with Image-1 analysis software (Universal Imaging Corporation). We recorded area measurements for at least 50 nuclei in two independent experiments at two timepoints. Data were qualitatively observed with four independent preparations of XKCM1 protein on at least six different extracts.

#### Assaying Microtubule Dynamics

Mitotic extracts prepared as above were clarified as described (Hirano and Mitchison, 1993) and frozen in 50  $\mu\text{l}$  aliquots. In the case of immunodepletions, extracts were immunodepleted as described above using a ratio of 75  $\mu\text{l}$  of beads:12  $\mu\text{g}$  of antibody:450  $\mu\text{l}$  of extract before freezing in 50  $\mu\text{l}$  aliquots. For assaying dynamics, an aliquot was thawed, diluted 2-fold with XBE2 (CSF-XB containing 2 mM  $\text{MgCl}_2$  containing 1.5 $\times$  energy mix (150 mM creatine phosphate, 20 mM ATP, 20 mM  $\text{MgCl}_2$ ) and 37.5  $\mu\text{g}/\text{ml}$  creatine kinase, and centrifuged for 5 min in a microfuge. For antibody addition experiments, affinity-purified anti-XKCM1 or control IgG was diluted to 0.5 mg/ml in sperm dilution buffer and added to the supernatant at 25  $\mu\text{g}/\text{ml}$  on ice. Tetrahymena axonemes prepared as per Mitchison and Kirschner (1984) were washed by diluting 100-fold in XBE2 plus 0.1% Triton X-100, pelleted for 5 min in a microfuge, and resuspended to  $10^7$  per milliliter in XBE2. Axonemes were adhered to the

coverslip for 3 min in a 5–8  $\mu\text{l}$  flow cell prepared as described previously (Vale, 1991). Unadhered axonemes were washed out using 40  $\mu\text{l}$  of XBE2, and 25  $\mu\text{l}$  of clarified extract was flowed into the chamber. Assembly of axonemes was observed using VE-DIC microscopy for 20 min at  $23^{\circ}\text{C}$ – $24^{\circ}\text{C}$ , and the parameters describing microtubule dynamic instability were determined using home-written software according to the conventions of Walker et al. (1988). Under our experimental conditions, we were only able to calculate the rates of plus end microtubule dynamics. VE-DIC was performed using a Zeiss Axioplan microscope illuminated with a 50 W mercury lamp and equipped with a 1.4 NA condenser and a  $63 \times 1.4$  NA Planapochromatic objective. The image was projected using a  $4 \times$  tube onto the target of a Hamamatsu Newvicon camera, and the image was averaged for four frames and contrast-enhanced using a Hamamatsu Argus 20 image processor. The enhanced, four frame-averaged image was stored on S-VHS videotape, which was used for analysis using a home-written program (W. Marshall and R. D. Vale, personal communication). Antibody addition and immunodepletion experiments were performed on separate extract preparations.

#### Acknowledgments

Correspondence should be addressed to C. E. W. We thank all the members of the Mitchison laboratory (past and present) for helpful comments, criticism, and discussion throughout the course of this work, especially Tatsuya Hirano for never-ending suggestions and Linda Wordeman and Ken Sawin, whose earlier work provided the inspiration for this project. We are grateful to YiXian Zheng for her generous donation of ammonium sulfate supernatants and to Wayne Forrester and Scott Ballantyne for molecular biology instruction. We are also thankful to Matt Welch and Karen Oegema for invaluable comments on the manuscript. This work was supported by a National Institutes of Health (NIH) grant (GM39565-07) and a grant from the Human Frontier Science Program (RG350/94) to T. J. M.; C. E. W. is an NIH postdoctoral fellow; A. D. is a Howard Hughes Medical Institute predoctoral fellow.

Received September 21, 1995; revised November 8, 1995.

#### References

- Aizawa, H., Sekine, Y., Takemura, R., Zhang, Z., Nangaku, M., and Hirokawa, N. (1992). Kinesin family in murine central nervous system. *J. Cell Biol.* 119, 1287–1296.
- Bajer, A.S. (1982). Functional autonomy of monopolar spindle and evidence for oscillatory movement in mitosis. *J. Cell Biol.* 93, 33–48.
- Belmont, L.D., Hyman, A.A., Sawin, K.E., and Mitchison, T.J. (1990). Real-time visualization of cell cycle-dependent changes in microtubule dynamics in cytoplasmic extracts. *Cell* 62, 579–589.
- Chrétien, D., Fuller, S.D., and Karsenti, E. (1995). Structure of growing microtubule ends: two-dimensional sheets close into tubes at variable rates. *J. Cell Biol.* 129, 1311–1328.
- Desai, A., and Mitchison, T.J. (1995). A new role for motor proteins as couplers to depolymerizing microtubules. *J. Cell Biol.* 128, 1–4.
- Endow, S.A., Kang, S.J., Satterwhite, L.L., Rose, M.D., Skeen, V.P., and Salmon, E.D. (1994). Yeast Kar3 is a minus-end microtubule motor protein that destabilizes microtubules preferentially at the minus ends. *EMBO J.* 13, 2708–2713.
- Harlow, E., and Lane, D. (1988). *Antibodies: A Laboratory Manual* (Cold Spring Harbor, New York: Cold Spring Harbor Laboratory).
- Hirano, T., and Mitchison, T.J. (1993). Topoisomerase II does not play a scaffolding role in the organization of mitotic chromosomes assembled in *Xenopus* egg extracts. *J. Cell Biol.* 120, 601–612.
- Hirose, K., Lockhart, A., Cross, R.A., and Amos, L.A. (1995). Nucleotide-dependent angular change in kinesin motor domain bound to tubulin. *Nature* 376, 277–279.
- Hoenger, A., Sablin, E.P., Vale, R.D., Fletterick, R.J., and Milligan, R.A. (1995). Three-dimensional structure of a tubulin-motor-protein complex. *Nature* 376, 271–274.
- Holy, T.E., and Leibler, S. (1994). Dynamic instability of microtubules

- as an efficient way to search in space. *Proc. Natl. Acad. Sci. USA* **91**, 5682-5685.
- Hyman, A.A., and Mitchison, T.J. (1990). Modulation of microtubule stability by kinetochores *in vitro*. *J. Cell Biol.* **110**, 1607-1616.
- Hyman, A.A., and Mitchison, T.J. (1991). Two different microtubule-based motor activities with opposite polarities in kinetochores. *Nature* **351**, 206-211.
- Inoué, S., and Salmon, E.D. (1995). Force generation by microtubule assembly/disassembly in mitosis and related movements. *Mol. Biol. Cell*, 1619-1640.
- Kellogg, D.R., and Alberts, B.M. (1992). Purification of a multiprotein complex containing centrosomal proteins from the *Drosophila* embryo by chromatography with low-affinity polyclonal antibodies. *Mol. Biol. Cell* **3**, 1-11.
- Kikkawa, M., Ishikawa, T., Wakabayashi, T., and Hirokawa, N. (1995). Three-dimensional structure of the kinesin head-microtubule complex. *Nature* **376**, 274-277.
- Kirschner, M.W., and Mitchison, T.J. (1986). Beyond self assembly: from microtubules to morphogenesis. *Cell* **45**, 329-342.
- Lohka, M.J., and Maller, J.L. (1985). Induction of nuclear envelope breakdown, chromosome condensation, and spindle formation in cell-free extracts. *J. Cell Biol.* **101**, 518-523.
- Lombillo, V.A., Nislow, C., Yen, T.J., Gelfand, V.I., and McIntosh, J.R. (1995a). Antibodies to the kinesin motor domain and CENP-E inhibit microtubule depolymerization-dependent motion of chromosomes *in vitro*. *J. Cell Biol.* **128**, 107-115.
- Lombillo, V.A., Stewart, R.J., and McIntosh, J.R. (1995b). Minus-end-directed motion of kinesin-coated microspheres driven by microtubule depolymerization. *Nature* **373**, 161-164.
- Lupas, A., Van Dyke, M., and Stock, J. (1991). Predicting coiled coils from protein sequences. *Science* **252**, 1162-1164.
- Mandelkow, E.M., Mandelkow, E., and Milligan, R.A. (1991). Microtubule dynamics and microtubule caps-a time-resolved cryo-electron microscopy study. *J. Cell Biol.* **114**, 977-991.
- Mitchison, T.J., and Kirschner, M.W. (1984). Dynamic instability of microtubule growth. *Nature* **312**, 237-242.
- Murray, A.W. (1991). Cell cycle extracts. In *Methods in Cell Biology*, B.K. Kay and H.B. Peng, eds. (San Diego, California: Academic Press), pp. 581-605.
- Pfarr, C.M., Coue, M., Grisson, P.M., Hays, T.S., Porter, M.E., and McIntosh, J.R. (1990). Cytoplasmic dynein is localized to kinetochores during mitosis. *Nature* **345**, 263-265.
- Rieder, C.L., and Salmon, E.D. (1994). Motile kinetochores and polar ejection forces dictate chromosome position on the vertebrate mitotic spindle. *J. Cell Biol.* **124**, 223-233.
- Salmon, E.D., Leslie, R.J., Karow, W.M., McIntosh, J.R., and Saxton, R.J. (1984). Spindle microtubule dynamics in sea urchin embryos: analysis using fluorescence-labeled tubulin and measurements of fluorescence redistribution after laser photobleaching. *J. Cell Biol.* **99**, 2165-2174.
- Sambrook, J., Fritsch, E., and Maniatis, T. (1989). *Molecular Cloning: A Laboratory Manual* (Cold Spring Harbor, New York: Cold Spring Harbor Laboratory Press).
- Sawin, K.E., and Mitchison, T.J. (1991). Mitotic spindle assembly by two different pathways *in vitro*. *J. Cell Biol.* **112**, 925-940.
- Sawin, K.E., LeGuellec, K., Philippe, M., and Mitchison, T.J. (1992a). Mitotic spindle organization by a plus-end directed microtubule motor. *Nature* **359**, 540-543.
- Sawin, K.E., Mitchison, T.J., and Wordeman, L.G. (1992b). Evidence for kinesin-like proteins in the mitotic apparatus using peptide antibodies. *J. Cell Sci.* **102**, 303-313.
- Saxton, W.M., Stemple, D.L., Leslie, R.J., Salmon, E.D., Zavortink, M., and McIntosh, J.R. (1984). Tubulin dynamics in cultured mammalian cells. *J. Cell Biol.* **99**, 2175-2186.
- Shamu, C.E., and Murray, A.W. (1992). Sister chromatid separation in frog egg extracts requires DNA topoisomerase II activity during anaphase. *J. Cell Biol.* **117**, 921-934.
- Skibbens, R., Skeen, V.P., and Salmon, E.D. (1993). Directional instability of kinetochore motility during chromosome congression and segregation in mitotic newt lung cells: a push-pull mechanism. *J. Cell Biol.* **122**, 859-875.
- Smith, D.B., Rubira, M.R., Simpson, R.J., Davern, K.M., Tui, W.U., Board, P.G., and Mitchell, G.F. (1988). Expression of an enzymatically-active parasite molecule in *Escherichia coli*: *Schistosoma japonicum* glutathione S-transferase. *Mol. Biochem. Parasitol.* **27**, 249-256.
- Steuer, E.R., Wordeman, L., Schroer, T.A., and Sheetz, M.P. (1990). Localization of cytoplasmic dynein to mitotic spindles and kinetochores. *Nature* **345**, 266-268.
- Vale, R.D. (1991). Severing of stable microtubules by a mitotically activated protein in *Xenopus* egg extracts. *Cell* **64**, 827-839.
- Verde, F., Labbe, J.-c., Doree, M., and Karsenti, E. (1990). Regulation of microtubule dynamics by *cdc2* protein kinase in cell-free extracts of *Xenopus* eggs. *Nature* **343**, 233-238.
- Verde, F., Dogterom, M., Stelzer, E., Karsenti, E., and Leibler, S. (1992). Control of microtubule dynamics and length by cyclin A- and cyclin B-dependent kinases in *Xenopus* egg extracts. *J. Cell Biol.* **118**, 1097-1108.
- Vermos, I., Raats, J., Hirano, T., Heasman, J., Karsenti, E., and Wylie, C. (1995). Xklp1, a chromosomal *Xenopus* kinesin-like protein essential for spindle organization and chromosome positioning. *Cell* **81**, 117-127.
- Walker, R.A., O'Brien, E.T., Pryer, N.K., Sobeiro, M.F., Voter, W.A., Erickson, H.P., and Salmon, E.D. (1988). Dynamic instability of individual microtubules analysed by video light microscopy: rate constants and transition frequencies. *J. Cell Biol.* **107**, 1437-1448.
- Wordeman, L., and Mitchison, T. (1995). Identification and partial characterization of mitotic centromere-associated kinesin, a kinesin-related protein that associates with centromeres during mitosis. *J. Cell Biol.* **128**, 95-105.
- Yen, T.J., Compton, D.A., Wise, D., Zinkowski, R.P., Brinkley, B.R., Earnshaw, W.C., and Cleveland, D.W. (1991). CENP-E, a novel human centromere-associated protein required for progression from metaphase to anaphase. *EMBO J.* **10**, 1245-1254.
- Zheng, Y., Wong, M., Alberts, B., and Mitchison, T. (1995). Nucleation of microtubule assembly by a  $\gamma$ -tubulin containing ring complex. *Nature* **378**, 578-583.

#### GenBank Accession Numbers

The sequence of XKCM1 is available under accession number U36485; the sequence for XKIF2 described in this report is available under accession number U36486.

#### Note Added in Proof

The authors inadvertently left out the citation for the work describing mouse KIF2 localization and motility. The correct reference is: Noda, Y., Sato-Yoshitake, R., Kondo, S., Nangaku, M., and Hirokawa, N. KIF2 is a new microtubule-based anterograde motor that transports membranous organelles distinct from those carried by kinesin heavy chain or KIF3A/B. *J. Cell Biol.* **129**, 157-167, 1995.

## **Chapter 5**

# **Mechanism of Microtubule Destabilization by XKCM1 and XKIF2 -- Two Internal Catalytic Domain Subfamily Kinesins**

I performed all the experiments described in this chapter. This work was done in collaboration with Dr. C. E. Walczak, a post-doctoral fellow in the Mitchison lab who identified XKCM1 and XKIF2, and worked out their baculovirus expression with the help of Suzie Verma, a technician in the Mitchison lab.

**Microtubule Destabilization by XKCM1 and XKIF2 -- Two Internal Catalytic  
Domain Subfamily Kinesins**

Arshad Desai\*, Suzie Verma#, Timothy J. Mitchison\$ and Claire E. Walczak#

\*Department of Biochemistry and Biophysics,

#Department of Cellular and Molecular Pharmacology, University of  
California, San Francisco and

\$Department of Cell Biology, Harvard Medical School

## Introduction

Microtubules (MTs) are noncovalent polymers of the  $\alpha\beta$  tubulin heterodimer that are essential for cell division in all eukaryotes and serve many additional intracellular functions. Kinesins are mechanochemical enzymes discovered on the basis of their ability to transport organelles along MTs in an ATP-dependent manner (Vale et al., 1985; Hirokawa, 1998). Different members of the kinesin superfamily have been implicated in a variety of cellular processes. Distinct biological roles for kinesins are derived primarily from their association with different cellular cargoes via specialized targeting domains (Vale and Fletterick, 1997; Hirokawa, 1998; Vallee and Sheetz, 1996). In addition to being tracks for motor-dependent trafficking of cargoes, the intracellular functions of MTs also intimately involve their polymerization dynamics. MTs utilize polymerization-dependent GTP hydrolysis on  $\beta$ -tubulin to generate dynamic instability, a special polymerization behavior where both polymerizing and depolymerizing MTs coexist in the same population and infrequently interconvert between these two states (Mitchison and Kirschner, 1984; Desai and Mitchison, 1997). A popular hypothesis for the mechanism of dynamic instability postulates a heterogeneity in nucleotide content at MT ends combined with the difference in the lattice stability of GTP- versus GDP-tubulin (Mitchison and Kirschner, 1984; Desai and Mitchison, 1997). Polymerizing ends are thought to maintain a stabilizing "cap" of GTP/GDP.P<sub>i</sub>, the loss of which results in exposure of an unstable GDP-tubulin core and subsequent rapid depolymerization. Thus, the tubulin molecule has an intrinsic lattice destabilization mechanism that is powered by the GTP hydrolysis on  $\beta$ -tubulin that accompanies polymerization. Consistent with this notion, tubulin polymerized with GMPCPP, a slowly hydrolyzable GTP analog that is essentially non-



hydrolyzable in the time scale of most experiments, does not display lattice destabilization and is not dynamically unstable (Hyman et al., 1992).

*In vivo* analysis of MT dynamics has revealed the presence of extensive regulatory mechanisms for modulating the intrinsic dynamic instability of tubulin (Cassimeris, 1993; Desai and Mitchison, 1997; McNally, 1996). Particularly, the rapidity of MT turnover *in vivo*, relative to MTs assembled with pure tubulin *in vitro*, indicates the existence of intracellular mechanisms for destabilizing MTs. This is thought to be achieved in large part by increasing the frequency of transitions from the polymerization phase to the depolymerization phase (frequency of catastrophe; Belmont et al., 1990; Walker et al., 1988; Desai and Mitchison, 1997). The high frequency of catastrophe *in vivo* has long been suspected to be the result of the action of cellular proteins that specifically target and destabilize the specialized stabilizing sites ("caps") at polymerizing MT ends (Walker et al., 1988; Belmont et al., 1990; Verde et al., 1992; Cassimeris, 1993; Desai and Mitchison, 1997).

We have previously described analysis of XKCM1, an internal catalytic domain subfamily (Kin I subfamily; Vale and Fletterick, 1997) member of the kinesin superfamily, during *in vitro* spindle assembly in *Xenopus* egg extracts (Chapter 4; Walczak et al., 1996). XKCM1 depletion causes excessive microtubule polymerization, severely disrupting spindle assembly. Direct analysis of microtubule dynamics showed that inhibition of XKCM1 function caused a four-fold reduction in the catastrophe frequency. These results suggested that XKCM1 destabilized MTs by inducing MT catastrophes in frog egg extracts either by a direct or an indirect mechanism. Given that XKCM1 is a kinesin superfamily member, we expected it to directly interact with the MT lattice, although its perturbation of MT dynamics may have been either a

direct effect of XKCM1 at MT ends or may have involved XKCM1 delivering a catastrophe-inducing factor to MT ends.

Here we report the ability of pure XKCM1 and XKIF2, another Kin I subfamily kinesin implicated in neuronal development, to directly destabilize MT polymerization in an ATP-dependent manner. XKIF2 is the *Xenopus* homolog of mouse KIF2 (mKIF2; Noda et al., 1995). Although XKCM1 and X/mKIF2 share a high degree of homology in their catalytic domains, they are not very homologous in their N- and C-terminal domains and are implicated in very different biological processes. A fraction of XKCM1 localizes to the centromere/kinetochore region during mitosis in vertebrates and is implicated in chromosome movement/spindle function whereas mKIF2 is highly expressed in the embryonic nervous system where it is implicated in neuronal development as a fast plus end-directed axonal transport motor (Noda et al., 1995). Given the similarities and the differences of XKCM1 and XKIF2 we have compared the activities of these two proteins using a variety of *in vitro* assays. Our findings indicate that both these proteins directly target to the ends of MTs and trigger a destabilizing conformational change. This unique activity requires these proteins to have ATP or an ATP-like analog bound to the active site but does not require ATP hydrolysis. ATP hydrolysis acts to make the action of these proteins catalytic. These results present the first detailed characterization of the mechanism of a physiological MT-destabilizing protein and also provide clear evidence for a non-motile function for the internal catalytic domain subfamily of kinesins.

## **Materials and Methods**

*Baculovirus expression and purification of XKCM1/XKIF2*

Full length, untagged XKCM1 and XKIF2 were expressed in baculovirus according to established procedures. Cells expressing the proteins were harvested using a rubber policeman and pelleted at 4°C. Cell pellets were frozen in liquid nitrogen and stored at -80°C. For purifying the recombinant proteins frozen cells were lysed by trituration (what vol) in lysis buffer (BRB80 + 125 mM KCl + 2 mM EGTA + 1 mM DTT + 0.5 mM MgATP + 1 mM PMSF + 10 µg/ml leupeptin/pepstatin/chymostatin; BRB80: 80 mM K-Pipes, 1mM MgCl<sub>2</sub>, 1 mM EGTA, pH 6.8 with KOH) and the lysate cleared by centrifugation. Cleared lysate was loaded onto a HiTrap SP Sepharose column (Pharmacia) and eluted with a salt gradient. The eluting peak of XKCM1/XIF2 (assayed by SDS-PAGE) was collected and loaded onto a Superose 6 gel filtration column (Pharmacia) equilibrated in BRB80 + 75 mM KCl + 1 mM DTT + 10 µM MgATP + 1 µg/ml leupeptin/pepstatin/chymostatin (LPC). The peak of full length XKCM1/XKIF2 (assayed by SDS-PAGE) was loaded onto a 1 ml Mono S column (Pharmacia) equilibrated in BRB80 + 75 mM KCl + 1 mM DTT + 10 µM MgATP + 1 µg/ml LPC and eluted with an increasing salt gradient. MonoS-purified XKCM1/XKIF2 peak fractions were supplemented with solid sucrose to 10% (w/v) and frozen in liquid nitrogen. Concentration of the purified proteins was determined by Bradford using BSA as a standard as well as by A<sub>280</sub> using extinction coefficients calculated from sequence.

#### *Microtubule substrates and depolymerization assays*

Long CPP microtubules were polymerized by diluting a frozen mix of 10 µM tubulin in BRB80 + 1 mM DTT + 0.5 - 1 mM GMPCPP to 2 µM tubulin with warm BRB80 + 1 mM DTT and incubating at 37°C for 20'-30'. Segmented CPP MTs were prepared by diluting bright CPP seeds (1:2

rhodamine labeled : unlabeled tubulin) into 1.5  $\mu$ M dim mix tubulin (1:11 rhodamine labeled : unlabeled tubulin; prepared by diluting 10  $\mu$ M dim tubulin mix in BRB80 + 1mM DTT + 0.5 mM GMPCPP to 1.5  $\mu$ M on ice with BRB80 + 1 mM DTT) and incubating at 37°C for 1-2 hours. Depolymerization assays involved mixing 1-2  $\mu$ M GMPCPP microtubules with XKCM1 and XKIF2 at 1/20-1/40 molar ratios to the tubulin in BRB80 + 50 mM KCl + 1 mM DTT + 1.5 mM MgATP and incubating at RT. Depolymerization was monitored by squashing 1  $\mu$ l of reaction mix under a coverslip. Quantitative analysis was performed by sedimenting MTs at 90K rpm for 5' in a TLA100 rotor. Fixed and real-time assays on dynamic MTs nucleated off axonemes were performed as described (Mitchison and Kirschner, 1984; Walker et al., 1988) except that in the latter double-stick tape flow cells (Vale, 1991) were used and the flow cell surface was blocked with 5 mg/ml BSA after adsorption of axonemes. Hydrolysis of GMPCPP during depolymerization was assayed using TLC as described (Hyman et al., 1992). All ATP reactions contained 1 -2 mM MgATP and all AMPPNP reactions contained 5 mM MgAMPPNP.

#### *Real Time Analysis of Depolymerization*

For real time analysis, double-stick flow cell surfaces were coated with a very dilute partially pure fraction of XKIF2 and blocked with BSA. Segmented CPP MTs were flowed in and allowed to adsorb to the flow cell surface and then rinsed extensively with BRB80 + 1 mM DTT + 1.5 mM MgATP + 1X Oxygen Scavenging Mix (Vale et al., 1996). 20 - 40 nM XKCM1 either untreated or preincubated for 10' on ice with 100  $\mu$ g/ml anti-XKCM1 antibody (>10-fold molar excess) was diluted into BRB80 + 1 mM DTT + 1.5 mM MgATP + 1 mg/ml BSA + 1X Oxygen Scavenging Mix and introduce into the flow cell and the reaction monitored using timelapse fluorescence

microscopy with a 60X, 1.4 NA Nikon objective and a Princeton Instruments cooled CCD camera. When the microtubule substrate was nearly depolymerized to the seed, bacterial kinesin (K560) diluted to 20  $\mu\text{g}/\text{ml}$  was introduced into the flow cell and the resultant motility recorded to unambiguously determine the polarity of the substrate MTs.

#### *Immunofluorescence analysis and negative stain electron microscopy*

Reactions of GMPCPP MTs and XKCM1/XKIF2 were fixed using 10 volumes of 1% glutaraldehyde in BRB80 and sedimented onto coverslips as described (Evans et al., 1985; Mitchison and Kirschner, 1984). Coverslips were post-fixed in methanol, rehydrated, blocked with BSA and processed for immunofluorescence using an affinity-purified anti-Cterm XKCM1 antibody. ATP reactions were fixed at the mid-point of depolymerization (gauged by visual analysis). AMPPNP reactions were fixed after incubating XKCM1 and GMPCPP MTs at RT for 15'.

Negative stain electron microscopy (EM) was performed by adsorbing 1-2  $\mu\text{l}$  of a reaction mix to a glow-discharged carbon-coated 200-mesh copper EM grid for  $\sim 10$  sec, and then applying 20  $\mu\text{l}$  of 0.5% aqueous uranyl acetate onto the specimen while simultaneously absorbing it using a Whatman #1 filter paper strip. The grid was thoroughly wicked with the filter paper and dried at RT for  $\sim 5'$  prior to viewing with a Philips EM400 electron microscope.

## **Results and Discussion**

### **XKCM1 and XKIF2 are ATP-Dependent Inhibitors of Microtubule Assembly that Induce Catastrophes**

Full length, untagged XKCM1 and XKIF2 were expressed in baculovirus and purified by conventional chromatography (Figure 1). Both purified proteins inhibited MT assembly off axonemes in an ATP-dependent manner at highly substoichiometric concentrations (Figure 2). A similar activity was detected on native XKCM1 purified by immunoaffinity from *Xenopus* egg extracts (not shown). To analyze this destabilizing effect at higher resolution, we used VEDIC analysis of single MTs to determine the effect of XKCM1 on prepolymerized MTs. MTs were polymerized off axonemes in a flow cell using 7  $\mu\text{M}$  purified *Xenopus* egg tubulin and monitored in real-time. After 15', a mixture of 7  $\mu\text{M}$  tubulin and a control buffer or 7  $\mu\text{M}$  tubulin and 0.1  $\mu\text{M}$  XKCM1 was introduced into the flow cell. In the reaction with control buffer, while some MTs were ripped off axonemes as a result of shear forces generated during the solution exchange, all residual MTs remained in the polymerizing phase (n= 20 MTs). In contrast, in the reaction with XKCM1 all MTs (n= 15 MTs) underwent catastrophes at both ends and began depolymerizing. Unfortunately, we could not find conditions that prevented the introduced XKCM1 from rapidly adsorbing to the flow cell surface, thereby becoming inactivated. This adsorption resulted in rapid binding of the MTs to the glass surface in reactions containing XKCM1 and significantly slowed the depolymerization rate relative to that observed on control MTs depolymerized by isothermal dilution. The depolymerization slowed further gradually, eventually stopping completely after which the residual MTs persisted without significant changes in length on the glass surface. After a variable period the surface adsorbed MTs started regrowth, presumably because all the introduced XKCM1 had been inactivated by adsorption to the flow cell surface. Significantly, the intrinsic catastrophe frequency of *Xenopus* egg tubulin is very low relative to bovine brain tubulin (no catastrophes

observed in >3 hr of observation of MTs in the polymerization phase; catastrophe frequency  $<0.0001 \text{ s}^{-1}$ ). Therefore, the striking induction of catastrophes by XKCM1 indicates it is a potent catastrophe factor that can target to and destabilize the stabilizing sites at MT ends.

### **Substoichiometric XKCM1 and XKIF2 Depolymerize Stabilized Microtubule Substrates**

In order to analyze what XKCM1/XKIF2 do at the stabilizing sites at MT ends, we tested their effect on MTs polymerized with GMPCPP, a slowly hydrolyzable GTP analog for tubulin that is essentially nonhydrolyzable in the time course of most experiments, as well as MTs stabilized with the drug taxol. Substoichiometric amounts of XKCM1 and XKIF2 depolymerized both taxol- (not shown) and GMPCPP-stabilized MTs in the presence of ATP (Figure 3). This activity required ATP, was inhibited by the nonhydrolyzable ATP analog, AMPPNP, and was also inhibited in the case of XKCM1 by an anti-XKCM1 antibody. The anti-XKCM1 antibody inhibited the activity of XKCM1 but not of XKIF2. Given that XKCM1 and XKIF2 are purified by the same sequence of chromatographic steps, this result rigorously eliminates the observed activity being due to a cofractionating contaminant. Sedimentation analysis quantitatively demonstrated total depolymerization of the substrate MTs (not shown). Gel filtration analysis indicated that the tubulin released into the supernatant by the action of XKCM1/XKIF2 is 6S tubulin dimer. In addition,  $85 \pm 5\%$  of this released tubulin was capable of repolymerizing into MTs, indicating that the action of XKCM1/XKIF2 was reversible (not shown). Given that GMPCPP and taxol eliminate the intrinsic destabilization mechanism built into tubulin polymerization, the depolymerization of subunits of GMPCPP- and taxol MTs requires stoichiometric action. The

ability of substoichiometric amounts of XKCM1 and XKIF2 to completely depolymerize these MTs indicates that the depolymerization activity of these ATPases is catalytic and presumably involves ATP hydrolysis by their catalytic domains.

### **Real Time Analysis of Depolymerization by XKCM1 and XKIF2**

A previously published report indicated that mouse KIF2 was a fast plus end directed motor protein (Noda et al., 1995). This result suggested that a possible mechanism by which XKCM1 and XKIF2 act is to use conventional motility to target themselves to MT plus ends and cause a destabilizing conformational change at the end (Walczak et al., 1996). In order to test the two predictions of this hypothesis -- depolymerization would be endwise and would occur preferentially from the plus end -- we analyzed the depolymerization of GMPCPP MTs in real time using a fluorescence microscopy assay designed to unambiguously assign polarity to the substrate MTs. Using this assay we found that XKCM1 depolymerized GMPCPP MTs equivalently from both ends (Figure 4; n=15 MTs). We also obtained similar results using taxol-stabilized MTs as substrates (not shown). In order to perform an experiment under conditions more similar to the earlier study (Noda et al., 1995), we used XKIF2 in a conventional motility assay with taxol-stabilized MTs. We observed the substrate taxol MTs adsorb to the coverslip surface and then undergo slow bipolar depolymerization but never observed any motility of the MTs on the glass surface (not shown). Parallel control assays with kinesin exhibited normal MT-motility without any MT depolymerization (not shown). In addition, ATPase analysis of XKCM1 and XKIF2 showed that both proteins have very weak MT-stimulated ATPase activity, providing indirect evidence inconsistent with XKIF2 being a fast plus



end-directed motor (not shown). A precedence in conventional kinesins of intramolecular inhibition resulting in much weaker ATPase activity relative to that expected from their velocity, does not make this analysis definitive but, in combination with the "motility" assays and the depolymerization analysis of segmented MTs, strongly suggests that XKIF2 is not a fast plus end-directed MT motor.

### **Determining the Mechanism of Microtubule End Destabilization by XKCM1 and XKIF2**

In order to determine what XKCM1/XKIF2 did at MT ends to cause destabilization, we used GMPCPP MTs to distinguish between two possibilities: 1) XKCM1 induced GMPCPP(GTP) hydrolysis release leading to destabilization of the MT lattice by the intrinsic destabilization mechanism of tubulin and 2) XKCM1 extrinsically disrupted interprotofilament interactions at MT ends independent of the nucleotide state of the tubulin. Previous studies established that treatment of GMPCPP MTs with glycerol in the presence of sodium, but not potassium, ions induced hydrolysis of the normal  $\beta$ - $\gamma$  phosphate bond of this analog, destabilizing the MT (Caplow et al., 1994; Fig. 5C). In order to determine if XKCM1 was a physiological regulator whose mechanism of action was phenocopied by these *in vitro* solution conditions, we analyzed whether depolymerization of GMPCPP MTs by XKCM1 was accompanied by hydrolysis of the GMPCPP. Using MTs polymerized with [ $\gamma^{32}$ P]GMPCPP we found that XKCM1 depolymerized GMPCPP MTs (Fig. 5A) without causing hydrolysis of the lattice-bound GMPCPP (Fig. 5B). In order to determine whether XKCM1 affected interprotofilament contact at MT ends, we analyzed the GMPCPP MTs as they were being depolymerized by negative stain EM. We found that, during

depolymerization by XKCM1 (and XKIF2), peeling protofilaments were present at the ends of the MTs (Figure 6). Such peeled protofilaments were found on most of the residual MTs in the process of being depolymerized and larger protofilament aggregates were also observed on the grids. No such peeled protofilaments were ever observed on the ends of control GMPCPP MTs ( $n > 200$  MTs). A careful quantitative analysis was hindered by the tendency of the protofilament peels to detach from the MT, the very small number of MTs left as a result of depolymerization by XKCM1/XKIF2 and the tendency of the protofilament peels from different MTs to aggregate. Where clearly visible, we observed protofilament peels at both MT ends, as expected from our polarity analysis (Fig. 4; see also Fig. 8). This combination of analysis of hydrolysis and of end ultrastructure clearly indicates the ability of XKCM1 to depolymerize GMPCPP MTs by peeling apart protofilaments at their ends without utilizing hydrolysis of the nucleotide bound to the tubulin subunits in the MT lattice. Thus, these kinesins can extrinsically destabilize tubulin conformation in the MT lattice at the MT end, independent of the intrinsic mechanism built into tubulin polymerization by hydrolysis of the tubulin-bound nucleotide. By extension from studies with this GTP analog, these results suggest that XKCM1 and XKIF2 can induce catastrophes on dynamic MTs without inducing GTP hydrolysis on the postulated stabilizing GTP-tubulin subunits at the polymerizing MT end.

### **Role of ATP Hydrolysis by the Catalytic Domain in the Destabilization Reaction Cycle**

The catalytic action of XKCM1 and XKIF2 resulting in depolymerization of taxol-GMPCPP- and taxol-stabilized MTs requires ATP. No significant tubulin dimer release is observed in AMPPNP. ATPase assays

indicated that ATP hydrolysis was occurring during the depolymerization reaction (not shown). In order to characterize the role of ATP hydrolysis by the catalytic domain of these kinesin superfamily members in this non-motor activity, we attempted to distinguish which of the following three steps of the destabilization reaction cycle required ATP hydrolysis: 1) targeting to MT ends, 2) inducing the destabilizing conformational change (protofilament peeling) at MT ends, 3) recycling for multiple depolymerization cycles.

In order to distinguish between these three possible roles for ATP hydrolysis, we developed a direct assay to analyze the targeting and accumulation of XKCM1 at MT ends. Using this assay we found that XKCM1 accumulated at both MT ends in the presence of AMPPNP (Fig. 7). The observed localization is not an AMPPNP artifact but represents a true catalytic intermediate in the destabilization reaction since it was also observed in GMPCPP MTs undergoing depolymerization in the presence of ATP (not shown). In addition with the polarity analysis, this result conclusively rules out a role for ATP hydrolysis by the catalytic domain in targeting XKCM1 to MT ends, i.e., end-targeting via a conventional motility mechanism. Furthermore, these results clearly reveal that XKCM1 in the ATP-like state (mimicked here by binding of AMPPNP) has an intrinsic affinity for MT ends, where it targets and accumulates preferentially over the MT lattice. GFP-kinesin used in a similar assay did not show end targeting but localized all along the lengths of the MTs (not shown), confirming that this property of XKCM1 and XKIF2 is distinct from conventional kinesins. The relative affinity for XKCM1 and XKIF2 for MT ends versus MT sides is difficult to estimate, because the nature and concentration of end sites is not clear. However, end sites must necessarily be far fewer than wall sites, probably by 4 or more orders of magnitude at these MT lengths, further highlighting the

uniqueness of the ability of these two kinesin superfamily members to target MT ends.

To determine if ATP hydrolysis was necessary to induce the conformational change seen at GMPCPP MT ends, we analyzed GMPCPP MTs by negative stain EM in the presence of AMPPNP. We found clear evidence for protofilament peeling resulting in large protofilament bulbs at both MT ends in the presence of AMPPNP; control MTs had completely flush ends (Figure 8). This result indicates that ATP hydrolysis is not necessary to induce the conformational change at MT ends by XKCM1. Notably, ADP did not cause end accumulation and formation of protofilament bulbs (not shown). These results indicate that the binding energy of the ATP-like state of XKCM1 and XKIF2 at MT ends causes a destabilizing conformational change at the end. By elimination, these two results indicate that ATP hydrolysis makes the action of XKCM1 catalytic, allowing substoichiometric amounts of XKCM1 to completely depolymerize the stabilized GMPCPP and taxol MT substrates.

### **Model for the Induction of Catastrophes by XKCM1 and XKIF2**

Given the results described above we propose the model drawn in Figure 9 for how the internal catalytic domain subfamily kinesins XKIF2 and XKCM1 target to MT ends and induce catastrophes. These proteins have a higher affinity for structures at MT ends rather than MT walls. We propose these end structures to be exposed protofilaments that are known to exist at polymerizing MT ends (Chretien et al., 1995; Desai and Mitchison, 1997). The binding energy of these proteins induces a destabilizing conformational change at the end that results in a catastrophe. The strength of coupling of the interaction of these proteins with a MT end to the induction of

**c**atastrophe remains to be elucidated in further studies. ATP hydrolysis **r**eleases XKCM1/XKIF2 off the released tubulin dimer/oligomer for **s**ubsequent action at another MT end. This model does not address the **r**elative affinity of these proteins for MT walls versus MT ends. We do not **e**xpect a complete absence of interaction with MT walls, but do predict **s**ignificant differences in this interaction from motile kinesins. The ability of **b**oth XKCM1, a protein implicated in mitosis, and XKIF2, a protein implicated **i**n neuronal development, to execute this unique non-motile activity **i**ndicates the potential for this entire subclass of kinesins as being regulators **o**f MT dynamics rather than motor proteins. A major future direction will be **a**nalysis of the biological roles of these proteins in light of their remarkable *in vitro* activity.

## **References**

- B**elmont, L.D., A.A. Hyman, K.E. Sawin, and T.J. Mitchison. 1990. Real-time **v**isualization of cell cycle-dependent changes in microtubule dynamics in **c**ytoplasmic extracts. *Cell*. 62:579-89.
- C**aplow, M., R.L. Ruhlen, and J. Shanks. 1994. The free energy for hydrolysis **o**f a microtubule-bound nucleotide triphosphate is near zero: all of the free **e**nergy for hydrolysis is stored in the microtubule lattice. *J Cell Biol*. 127:779-88.
- C**assimeris, L. 1993. Regulation of microtubule dynamic instability. *Cell Motil Cytoskeleton*. 26:275-81.
- C**hretien, D., S.D. Fuller, and E. Karsenti. 1995. Structure of growing **m**icrotubule ends: two-dimensional sheets close into tubes at variable rates. *J Cell Biol*. 129:1311-28.

- Desai, A., and T.J. Mitchison.** 1997. Microtubule polymerization dynamics. *Annu. Rev. Cell Dev. Biol.* 13:83-117.
- Evans, L., T. Mitchison, and M. Kirschner.** 1985. Influence of the centrosome on the structure of nucleated microtubules. *J Cell Biol.* 100:1185-91.
- Hirokawa, N.** 1998. Kinesin and dynein superfamily proteins and the mechanism of organelle transport. *Science.* 279:519-26.
- Hyman, A.A., S. Salser, D.N. Drechsel, N. Unwin, and T.J. Mitchison.** 1992. Role of GTP hydrolysis in microtubule dynamics: information from a slowly hydrolyzable analogue, GMPCPP. *Mol Biol Cell.* 3:1155-67.
- McNally, F.J.** 1996. Modulation of microtubule dynamics during the cell cycle. *Curr Opin Cell Biol.* 8:23-9.
- Mitchison, T., and M. Kirschner.** 1984. Dynamic instability of microtubule growth. *Nature.* 312:237-42.
- Noda, Y., R. Sato-Yoshitake, S. Kondo, M. Nangaku, and N. Hirokawa.** 1995. KIF2 is a new microtubule-based anterograde motor that transports membranous organelles distinct from those carried by kinesin heavy chain or KIF3A/B. *J Cell Biol.* 129:157-67.
- Vale, R.D.** 1991. Severing of stable microtubules by a mitotically activated protein in *Xenopus* egg extracts. *Cell.* 64:827-39.
- Vale, R.D., and R.J. Fletterick.** 1997. The design plan of kinesin motors. *Ann Rev Cell Dev Biol.* 13:745-77.
- Vale, R.D., T. Funatsu, D.W. Pierce, L. Romberg, Y. Harada, and T. Yanagida.** 1996. Direct observation of single kinesin molecules moving along microtubules. *Nature.* 380:451-3.
- Vale, R.D., T.S. Reese, and M.P. Sheetz.** 1985. Identification of a novel force-generating protein, kinesin, involved in microtubule-based motility. *Cell.* 42:39-50.

Vallee, R.B., and M.P. Sheetz. 1996. Targeting of motor proteins. *Science*. 271:1539-44.

Verde, F., M. Dogterom, E. Stelzer, E. Karsenti, and S. Leibler. 1992. Control of microtubule dynamics and length by cyclin A- and cyclin B-dependent kinases in *Xenopus* egg extracts. *J Cell Biol.* 118:1097-108.

Walczak, C.E., T.J. Mitchison, and A. Desai. 1996. XKCM1: a *Xenopus* kinesin-related protein that regulates microtubule dynamics during mitotic spindle assembly. *Cell.* 84:37-47.

Walker, R.A., E.T. O'Brien, N.K. Pryer, M.F. Soboeiro, W.A. Voter, H.P. Erickson, and E.D. Salmon. 1988. Dynamic instability of individual microtubules analyzed by video light microscopy: rate constants and transition frequencies. *J Cell Biol.* 107:1437-48.】

## Figure Legends

**Figure 1.** Baculovirus expression and purification of XKCM1 and XKIF2. Clarified lysate (1), SP Sepharose flowthrough (2), SP Sepharose elution (3), Superose 6 peak (4) and Mono S peak (5) from an XKIF2 prep. The final pool is ~12  $\mu$ M XKIF2<sub>dimer</sub>. Lane 6 shows XKCM1 prepared by a similar protocol.

**Figure 2.** Effect of XKCM1 on MT polymerization off axonemes. Note that MT polymerization is performed in 1 mM GTP indicating that GTP does not substitute effectively for ATP in the MT-polymerization inhibition assay of XKCM1. There is ~1 XKCM1 for every 100 tubulin subunits in this reaction.

**Figure 3.** Depolymerization of 2  $\mu$ M GMPCPP MTs by 50 nM XKCM1 (1:40 XKCM1:tubulin ratio). Panels show microscope fields after 15' of incubation

at RT. ATP reaction contains 1.5 mM MgATP and AMPPNP reaction contains 5 mM MgAMPPNP. Kinesin was added to 30-70 nM in the presence of 1.5 mM MgATP. The same result is obtained with XKIF2.

**Figure 4.** Real time analysis of GMPCPP MT depolymerization by XKCM1. Plus and minus signs indicate polarity of the MT substrate. Times indicated are in minutes. Similar results are obtained with XKIF2.

**Figure 5.** XKCM1 depolymerizes GMPCPP MTs without stimulating GMPCPP hydrolysis. (A) Visual assay of depolymerization of GMPCPP MTs containing [ $\gamma^{32}\text{P}$ ]GMPCPP. (B) TLC analysis of CPP hydrolysis. There is no significant hydrolysis over the buffer control in the XKCM1 depolymerized CPP microtubules, as indicated by phosphorimager analysis. (C) Control demonstrating that the substrate MTs contain [ $\gamma^{32}\text{P}$ ]GMPCPP. Hydrolysis occurs in sodium-glycerol but not in potassium-glycerol (Caplow et al., 1994).

**Figure 6.** Presence of protofilament peeling at GMPCPP MT ends undergoing XKCM1-induced depolymerization. The same result is obtained with XKIF2.

**Figure 7.** XKCM1 targets to both MT ends in AMPPNP.

**Figure 8.** XKCM1 induces protofilament peeling at both MT ends in AMPPNP. The same result is obtained with XKIF2.

**Figure 9.** A model for induction of catastrophes on dynamic MTs by XKCM1 and XKIF2.



**Figure 1**

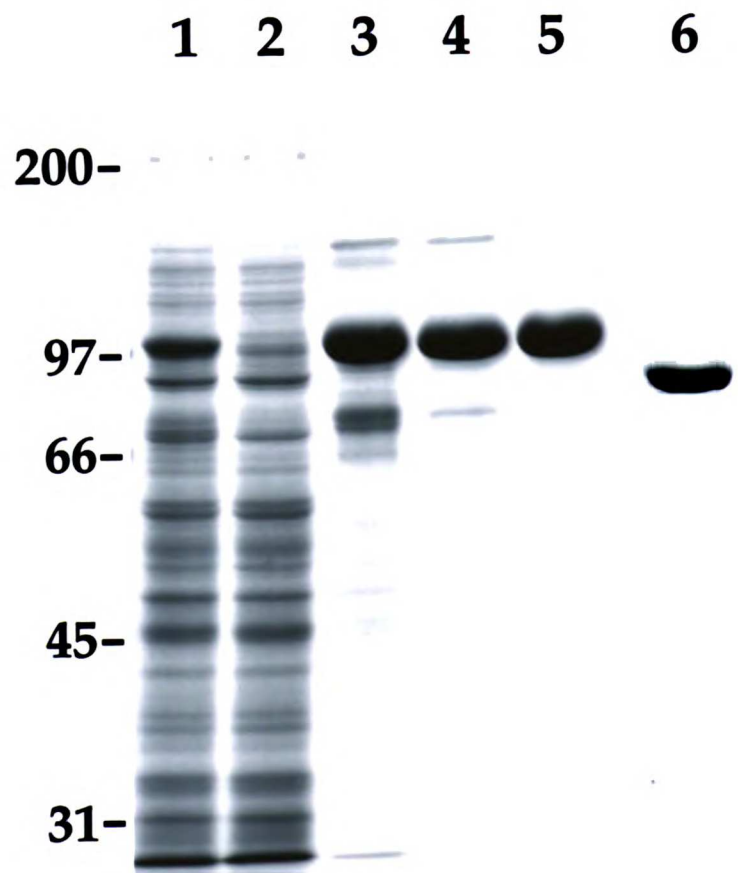
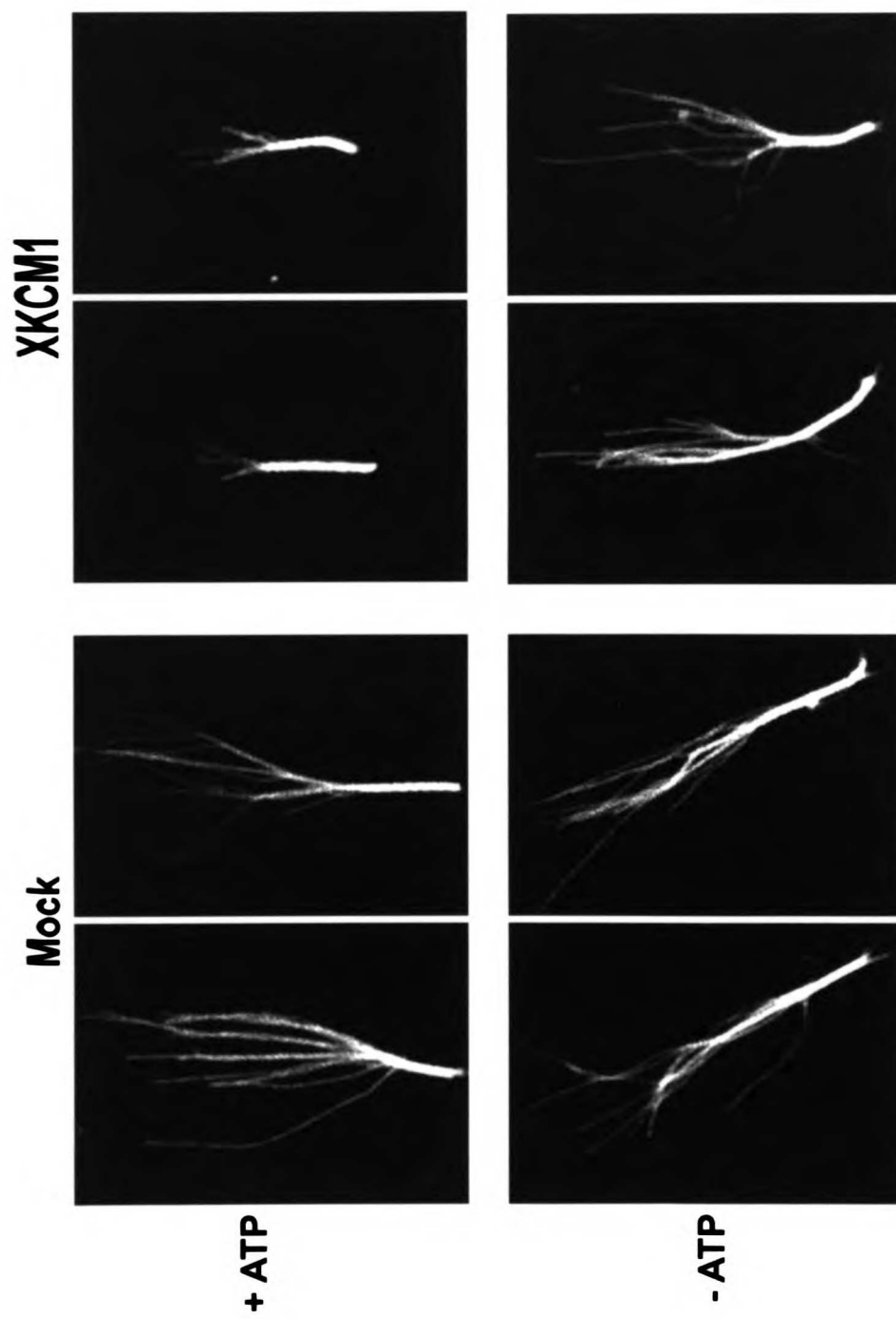
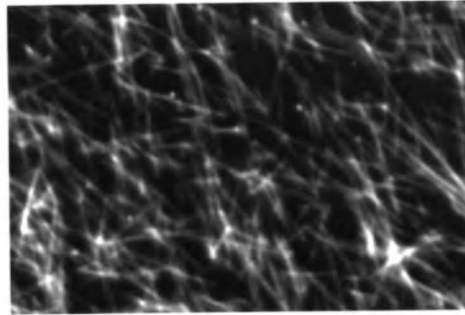
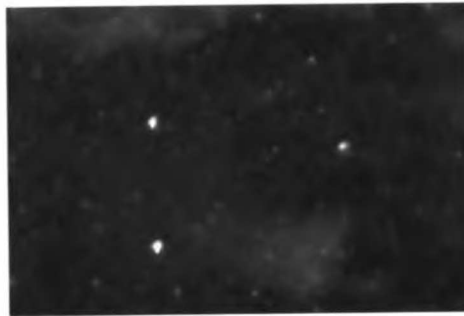
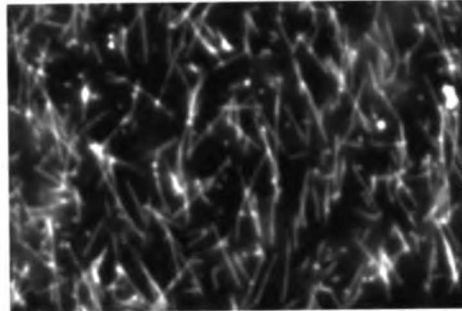
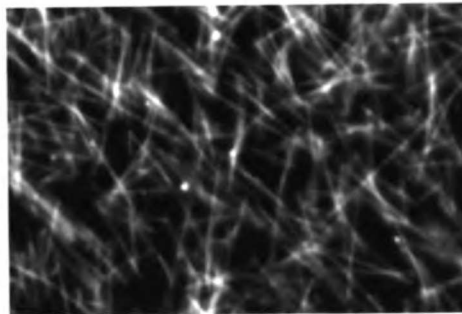
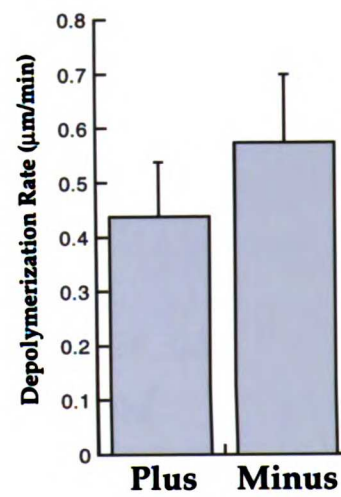
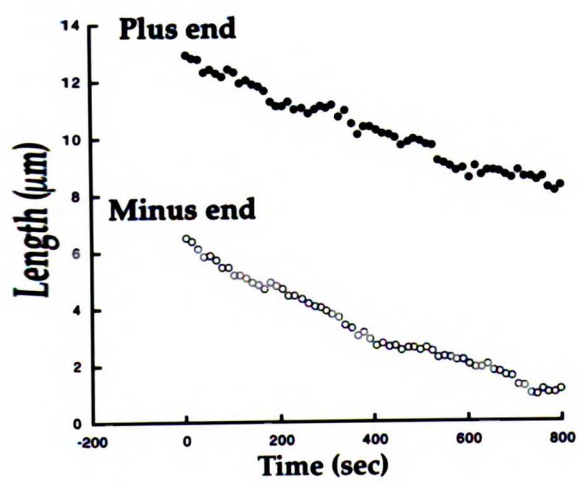
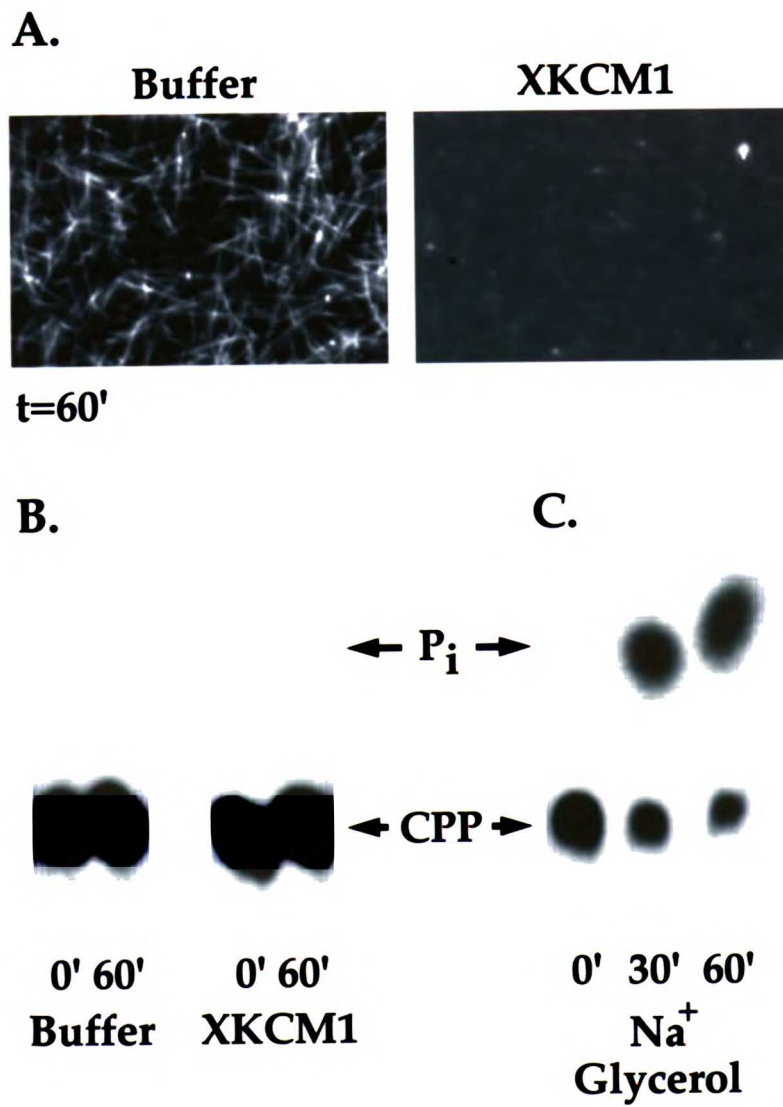


Figure 2

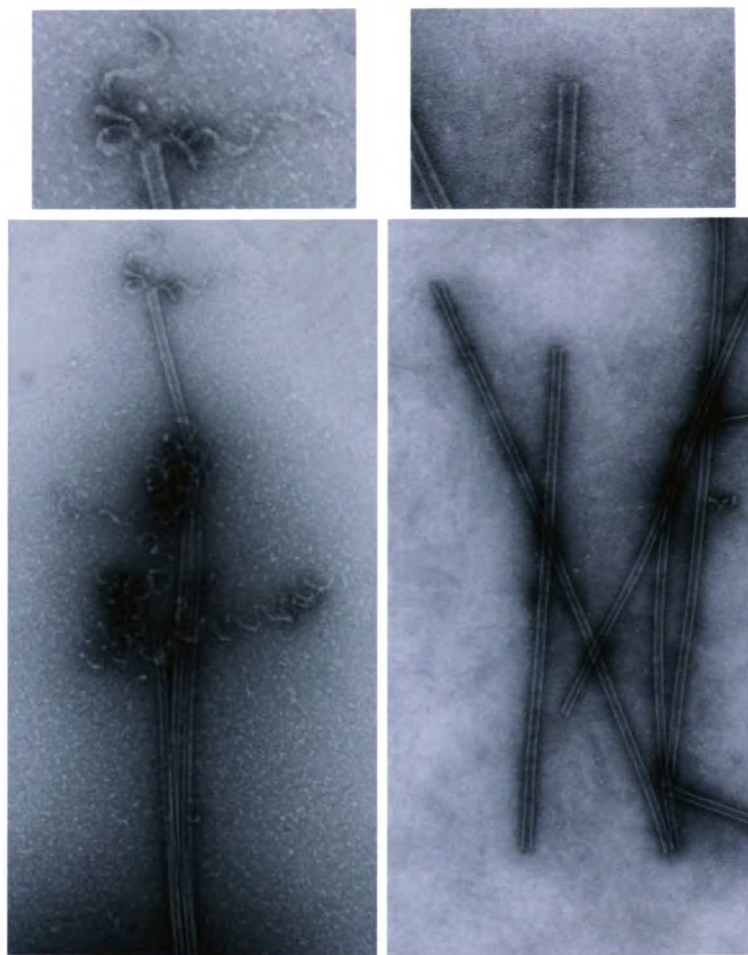


**Figure 3****Control  
Buffer  
(ATP)****XKCM1  
(ATP)****XKCM1  
(AMPPNP)****Kinesin  
(ATP)****t = 15' at RT**

**Figure 4**

**Figure 5**

**Figure 6**



**XKCM1**

**Control  
Buffer**

**Figure 7**

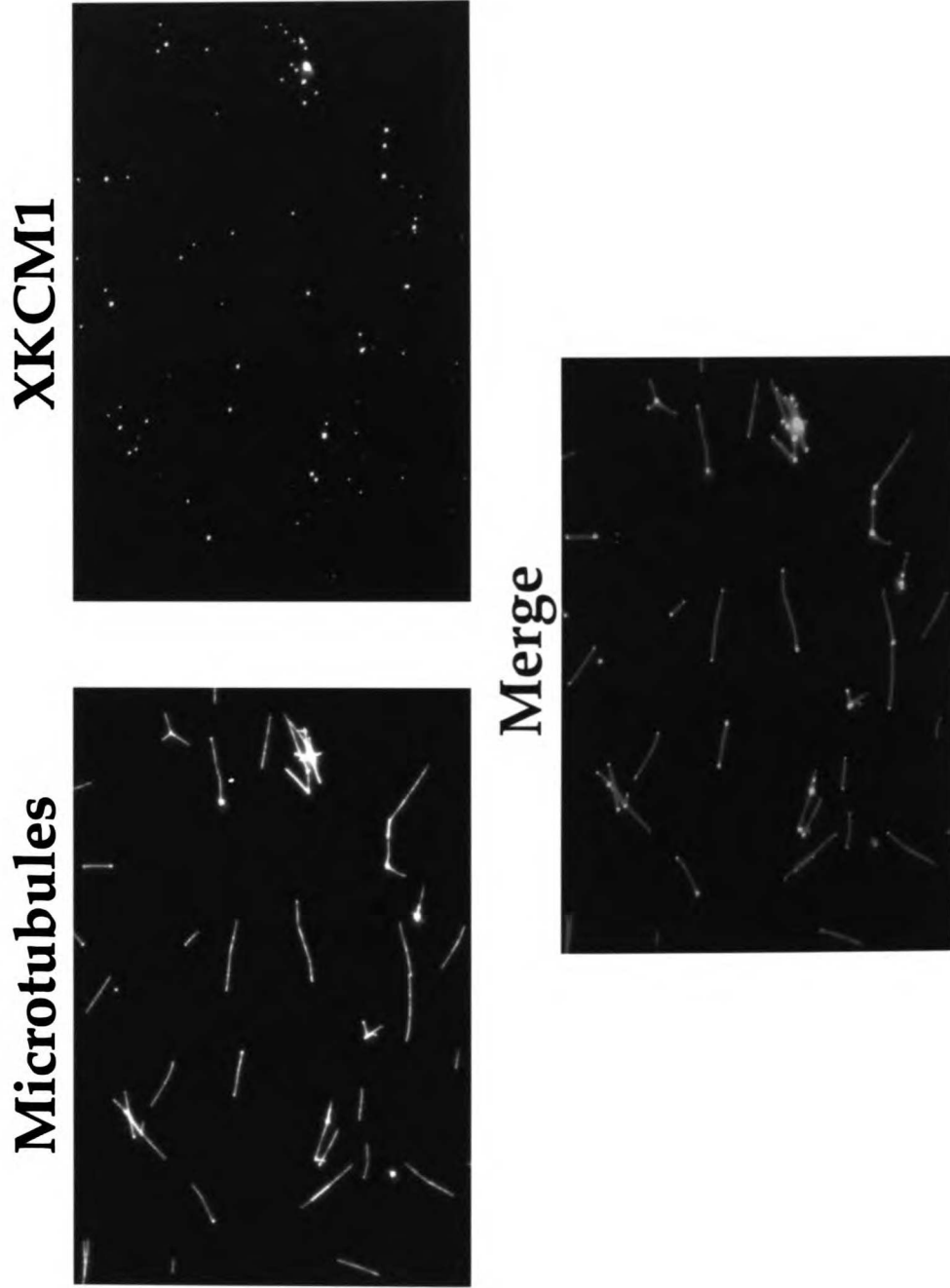
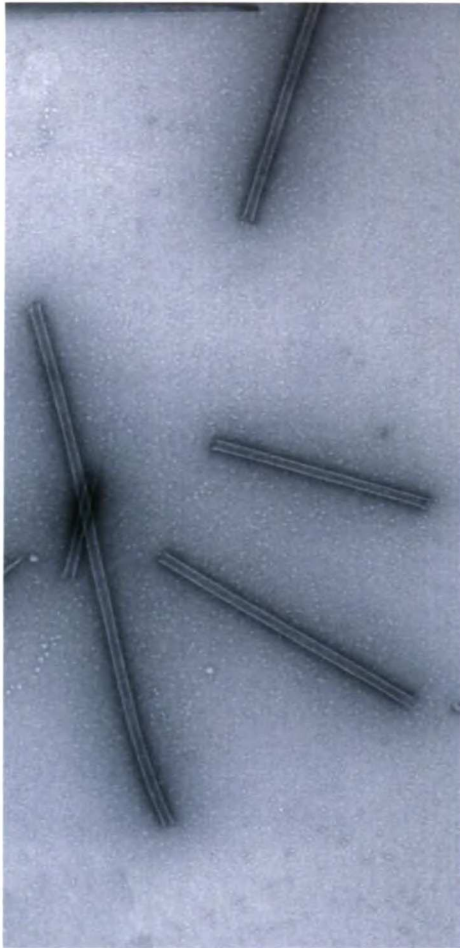


**Figure 8**

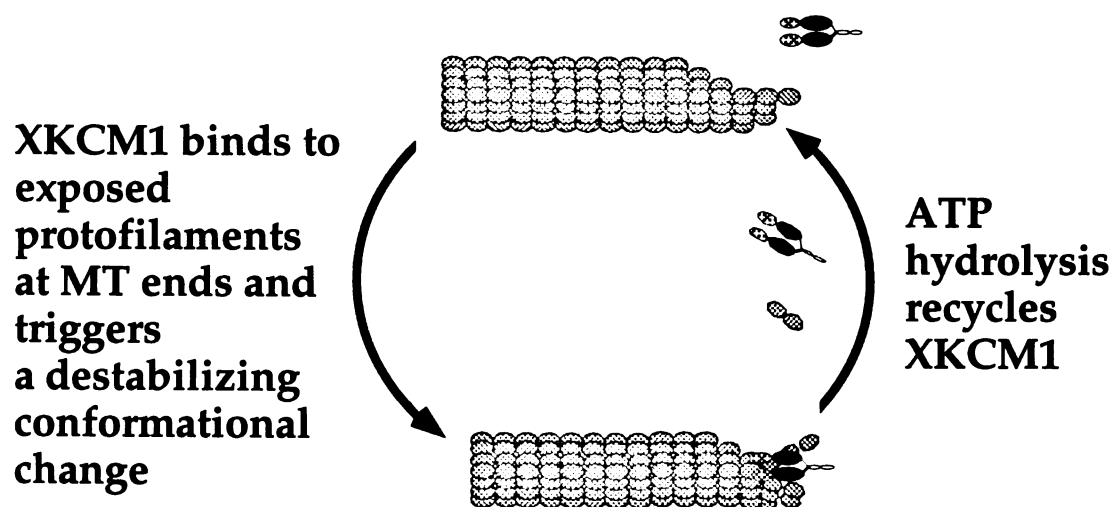


**XKCM1**



**Control**



**Figure 9**

## Appendix I

### Real Time Observation of Anaphase *in vitro*

This appendix has been reproduced from the Proceedings of the National Academy of Sciences, 1996, Volume 93 pages 12327-32. Copyright (1996) National Academy of Sciences, U.S.A.

I performed the real-time experiments described in this appendix together with Dr. A. Murray and Dr. E. D. Salmon. The analysis of the experiments was performed by Dr. Salmon and the paper was written by Dr. Murray, with comments from Dr. Salmon and myself.

Proc. Natl. Acad. Sci. USA  
Vol. 93, pp. 12327–12332, October 1996  
Cell Biology

## Real time observation of anaphase *in vitro*

ANDREW W. MURRAY\*<sup>†‡§</sup>, ARSHAD B. DESAI\*<sup>‡</sup>, AND E. D. SALMON\*<sup>†</sup>

\*Marine Biological Laboratory, Woods Hole, MA 02543; Departments of <sup>†</sup>Physiology and <sup>‡</sup>Biochemistry, University of California, San Francisco, CA 94143; and <sup>§</sup>Department of Biology, University of North Carolina, Chapel Hill, NC 27596

Communicated by Shinya Inoué, Marine Biological Laboratory, Woods Hole, MA, June 18, 1996 (received for review April 15, 1996)

**ABSTRACT** We used digital fluorescence microscopy to make real-time observations of anaphase chromosome movement and changes in microtubule organization in spindles assembled in *Xenopus* egg extracts. Anaphase chromosome movement in these extracts resembled that seen in living vertebrate cells. During anaphase chromosomes moved toward the spindle poles (anaphase A) and the majority reached positions very close to the spindle poles. The average rate of chromosome to pole movement (2.4  $\mu\text{m}/\text{min}$ ) was similar to earlier measurements of poleward microtubule flux during metaphase. An increase in pole-to-pole distance (anaphase B) occurred in some spindles. The ploidy of the spindles we examined allowed us to observe two novel features of mitosis. First, during anaphase, multiple microtubule organizing centers migrated 40  $\mu\text{m}$  or more away from the spindle poles. Second, in telophase, decondensing chromosomes often moved rapidly (7–23  $\mu\text{m}/\text{min}$ ) away from the spindle poles toward the centers of these asters. This telophase chromosome movement suggests that the surface of decondensing chromosomes, and by extension those of intact nuclei, bear minus-end-directed microtubule motors. Preventing the inactivation of Cdc2/cyclin B complexes by adding nondegradable cyclin B allowed anaphase A to occur at normal velocities, but reduced the ejection of asters from the spindles, blocked chromosome decondensation, and inhibited telophase chromosome movement. In the presence of nondegradable cyclin B, chromosome movement to the poles converted bipolar spindles into pairs of independent monopolar spindles, demonstrating the role of sister chromatid linkage in maintaining spindle bipolarity.

The orderly segregation of chromosomes at mitosis has fascinated cell biologists for more than 100 years (1). What are the components of the spindle, how do they interact with each other to produce a reproducible yet highly dynamic structure, and how do the activities that regulate the cell cycle sequentially induce formation of the spindle and chromosome segregation? The ultimate answer to these questions will require assembling functional spindles from purified components and studying how defined molecules regulate spindle behavior. This paper presents a step toward this goal: real-time observations of anaphase in spindles assembled in a test tube.

Analyzing mitosis in tissue culture cells and early embryos has revealed the dynamic behavior of the microtubules that comprise the spindle and their interactions with the kinetochores, the specialized regions that attach chromosomes to the spindle (reviewed in ref. 2). Studies on frog eggs identified maturation promoting factor (MPF) as the activity that induced mitosis and meiosis, and showed that MPF was an active protein kinase composed of Cdc2 complexed to cyclin B (reviewed in ref. 3). The proteolysis of cyclin B inactivates MPF, inducing chromosome decondensation, nuclear envelope formation, and changes in microtubule dynamics that convert the short dynamic microtubules of the metaphase spindle into the long, relatively stable microtubules of inter-

phase cells (2, 4–7). Inactivating MPF destroys interactions between microtubules and chromatin (8) and this change is believed to contribute to the disassembly of the spindle and the formation of interphase asters, circularly symmetric arrays of microtubules that are nucleated at the center of the array.

Extracts of frog eggs can recapitulate the cell cycle *in vitro* (9–11) and assemble functional spindles. Experiments on spindle behavior (4, 10, 12, 13) exploit the natural cell cycle arrest of unfertilized frog eggs, which are held in metaphase of meiosis II by the activity cytostatic factor (CSF), the product of the *c-mos* protooncogene (14). At fertilization, an increase in the cytoplasmic calcium concentration overcomes the action of CSF, triggering the destruction of cyclin B and the onset of anaphase (15). In extracts, the addition of exogenous calcium mimics fertilization, and analyzing fixed samples has shown that sister chromatid separation requires the activity of topoisomerase II (4) and depends on the ubiquitin-mediated proteolysis of proteins other than cyclin B (5).

We present real-time observations of changes in microtubule organization and chromosome movements as extracts are induced to proceed from metaphase, through anaphase, and into interphase. The rate and extent of anaphase A movement in these preparations is independent of the destruction of cyclin B and the inactivation of MPF. The polyploid spindles we have observed expel multiple asters during the metaphase to anaphase transition without compromising the orderly movement of the condensed chromosomes to their spindle poles. In telophase, the decondensing chromosomes move rapidly, often over many micrometers, toward the centers of the expelled asters. Preventing MPF inactivation suppresses both aster expulsion and telophase chromosome movement.

### MATERIALS AND METHODS

**Slide and Extract Preparation.** Slides and coverslips were successively washed with distilled water, ethanol, and acetone. Slides were coated with latex beads: 30  $\mu\text{l}$  of a 100-fold dilution of 12  $\mu\text{m}$  diameter latex beads (Sigma) in ethanol were spread on the surface of a slide and allowed to air dry. This procedure yields a density of beads that maintains separation between slide and coverslip without interfering with spindle observation.

Spindles were prepared using CSF-arrested extracts from *Xenopus* eggs (4) and induced to enter anaphase by adding  $\text{CaCl}_2$  to 0.3 mM. Immediately after calcium addition, 4  $\mu\text{l}$  of the extract was placed on a glass slide that had been coated with 12- $\mu\text{m}$ -diameter latex beads, and an 18  $\times$  18 mm coverslip was gently placed on top of the drop. The preparation was sealed by flowing a 2:1 mixture of trichlorotrifluoroethane (Aldrich)/halocarbon oil (Halocarbon Products, Hackensack, NJ), around the perimeter of the extract. The induction of anaphase in the presence of nondegradable cyclin B (cyclin

Abbreviations: MPF, maturation promoting factor; CSF, cytostatic factor; DAPI, 4',6'-diamidino-2-phenylindole.

<sup>§</sup>To whom reprint requests should be addressed at: Physiology Box 0444, University of California, San Francisco, CA 94143-0444. e-mail: amurray@cgl.ucsf.edu.

The publication costs of this article were defrayed in part by page charge payment. This article must therefore be hereby marked "advertisement" in accordance with 18 U.S.C. §1734 solely to indicate this fact.

B- $\Delta$ 90) has been described (5). Cyclin B- $\Delta$ 90 was added at least 40 min after the addition of CSF and 20–30 min before calcium was added to induce anaphase.

**Microscopy and Data Analysis.** A digital epifluorescence microscope was constructed for these experiments (16). We visualized DNA by including 4',6'-diamidino-2-phenylindole (DAPI) at 0.05  $\mu$ g/ml, and the microtubules were visualized by supplementing the extracts with 50–100  $\mu$ g/ml of tetramethylrhodamine-labeled tubulin (13). Fluorescent images of chromosomes and spindles were recorded in time-lapse by epifluorescence microscopy using a Nikon FX-A microscope, with a  $\times 20$ , NA = 0.75 lens and a Hamamatsu C4880 cooled charge-coupled device camera (Hamamatsu Photonics, Middlesex, NJ) operated in the super high gain mode for a  $300 \times 300$  pixel, 12-bit deep central region of the detector. At 30- or 60-sec intervals, DAPI, rhodamine, and sometimes phase contrast digital images, exposed for 600 msec, were recorded into separate image stacks within a Metamorph digital imaging computer (Universal Image, West Chester, PA). A multiple bandpass dichromatic epifluorescent filter and multiple excitation and neutral density filter wheels were used to control illumination wavelength and intensity. The camera, shutters for epi- and transillumination, and the filter wheels were all controlled by Metamorph. Changes in spindle fluorescence intensity, chromosome movements, and aster dynamics were quantified by using morphometric analysis algorithms in Metamorph in combination with spreadsheet analysis (Microsoft EXCEL). Photographs were prepared using Adobe PHOTOSHOP, labeled in CLARIS DRAW, and printed on a Tektronics Phaser dye sublimation printer.

## RESULTS

We examined the transition from metaphase to anaphase in frog egg extracts by real time digital fluorescence microscopy. The extracts were supplemented with rhodamine-labeled tubulin and the DNA-binding dye DAPI to visualize microtubules and chromosomes. Metaphase spindles were prepared by a two step procedure. Sperm nuclei were added to a CSF-arrested extract, and calcium was added to induce the inactivation of MPF and formation of interphase nuclei. The extracts were incubated for 80 min to allow DNA replication, centrosome duplication, and the sequestration of the added calcium into membrane-bound compartments (17). More CSF-

arrested extract was then added to induce nuclear envelope breakdown and spindle assembly (4). The spindles were induced to enter anaphase by adding exogenous calcium to induce the ubiquitin-dependent proteolysis of cyclin B and unknown proteins that are required to maintain the linkage between sister chromatids (4, 5). Immediately after calcium addition, a portion of the extract was transferred to a microscope slide, sealed with a layer of halocarbon oil, and observed by epifluorescent microscopy with a cooled charge-coupled device camera. We collected paired images of the rhodamine-labeled microtubules and the DAPI-stained DNA at 30-sec intervals for a period of about 30 min.

**Anaphase Chromosome Movement.** Fig. 1A shows a series of images from a typical spindle proceeding through anaphase and into interphase (times are indicated in minutes after the onset of anaphase). This spindle, like the majority of those in the extracts, had more chromosomes than an individual sperm, was probably formed from the contents of several sperm nuclei and thus contained multiple centrosomes (13). The pulse of calcium initiated the following changes: the ejection of asters from the spindle, the separation of sister chromatids, anaphase A and anaphase B, splaying outward of the half-spindles, decreasing microtubule density in the spindle, and in telophase, the rapid movement of decondensing chromosomes toward the centers of expelled asters. These changes are described in more detail below.

Shortly before anaphase chromosome movement started, asters began to migrate away from several different sites near and along the ends of the barrel-shaped spindles, and these microtubule-organizing centers continued to move away from the spindle throughout anaphase (Figs. 1A and 2A). We also observed asters near, but clearly separated from, the poles of anaphase spindles in samples fixed from reactions in test tubes. This strongly suggests that astral expulsion is not restricted to spindles between a slide and coverslip. The number of asters expelled was roughly correlated with the width of the spindle and reached a maximum of about 16 per spindle. The average rate of astral movement away from their exit site in the spindle was 4.3  $\mu$ m/min over an average distance of 43  $\mu$ m (Table 1). The speed of expulsion remained roughly constant as the asters moved away from the spindle, suggesting that the forces acting on the asters do not change as the separation between the asters and the remainder of the spindle increases (data not shown).

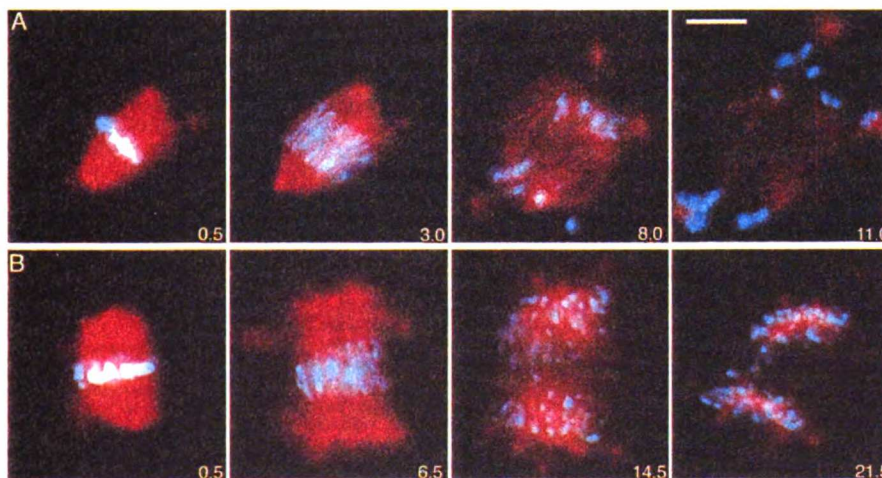


FIG. 1. Anaphase chromosome movements and spindle dynamics *in vitro*. Rhodamine-labeled microtubules are shown in red while DAPI labeled chromosomes are shown in blue green. Time is given in minutes after the onset of anaphase. (A) Anaphase in a control extract. (B) Anaphase in an extract with added cyclin B- $\Delta$ 90. (Bar = 20  $\mu$ m.)

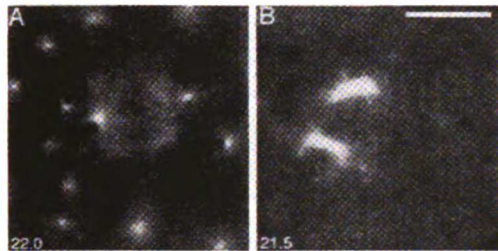


FIG. 2. Astral ejection (*A*, control) and cyclin B- $\Delta$ 90-treated spindles (*B*). In *A*, the large dark regions are the latex beads and the small dark regions are telophase chromosomes. In the control spindle, the asters grew large by late anaphase; many have already moved beyond the field of view. With cyclin B- $\Delta$ 90, ejection of tiny dim asters occurs over short distances. Time is given in min after onset of anaphase. (Bar = 20  $\mu$ m.)

During anaphase, chromosomes moved directly toward the ends of the spindle along paths parallel to the long axis of the spindle and were not attracted by any of the asters that had left the spindle (Figs. 1*A* and 3*A*). During this movement, a specific part of the chromosome, which we presume to be the kinetochore, led the movement toward the spindle pole. The observation that the paths of the chromosomes do not converge to a point as they approach the end of the spindle suggests that the functional spindle poles are distributed structures that lie along the two ends of the barrel-shaped spindles. Within a given spindle the rate of anaphase A showed little variation among chromosomes, and the variation among a population of spindles was small (average rate =  $2.4 \pm 1.0$   $\mu$ m/min; Table 1). The extent of anaphase B was extremely variable, with some spindles showing no increase in pole to pole separation and others showing a 50% increase in the length of the spindle (Fig. 3*A* and Table 1).

In telophase of mitosis in early embryos, individual chromosomes acquire an intact nuclear envelope as they decondense (18). We monitored this process by the conversion of elongated chromosomes into roughly spherical structures that excluded the background fluorescence of unpolymerized rhodamine tubulin. As they formed, telophase chromosomes became capable of moving rapidly ( $15 \pm 6$   $\mu$ m/min; Table 1) and over long distances (as much as 23  $\mu$ m) toward the centers of expelled asters and in some cases could be seen to alternate between moving toward two different aster centers (see three marked telophase chromosomes on Fig. 4). As the individual telophase chromosomes approached an aster they fused with each other to form an interphase nucleus.

**Anaphase in the Presence of Nondegradable Cyclin B.** Since MPF has been reported to control the dynamic behavior of microtubules (6, 7), we studied spindles undergoing anaphase

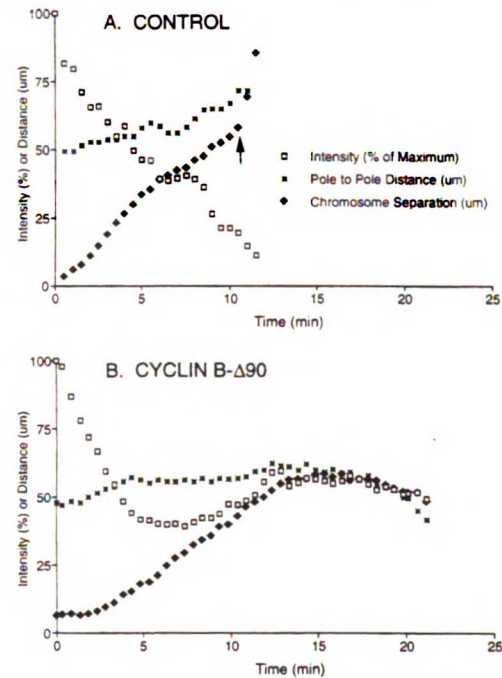


FIG. 3. Anaphase kinetics of chromosome separation, spindle pole elongation and spindle assembly without (*A*) and with (*B*) added cyclin-B  $\Delta$ 90. Chromosome separation was measured as the distance (in  $\mu$ m) between the leading edges of separating sister chromatids. Microtubule density was measured as the percentage of initial intensity in the rhodamine channel at a location midway between the metaphase position of the chromosomes and the poles. Time is given in minutes after the onset of anaphase. The arrow in *A* marks the onset of telophase chromosome movement. In *B*, the interpolar distance shortened in late anaphase because the two half-spindles were pushed closer together by flow in the cytoplasmic extract.

in the presence of cyclin B- $\Delta$ 90, which cannot be degraded and thus prevents the inactivation of MPF (19). The addition of calcium to these spindles induced anaphase chromosome movement, whose rate and extent was not significantly different from that of control spindles (Figs. 1*B* and 3*B* and Table 1). When the chromosomes reached the spindle poles, however, they did not decondense or show movements toward any of the asters that had been expelled from the spindles. These

Table 1. The effect of cyclin-B  $\Delta$ 90 on anaphase movements

Movement	Added cyclin	Velocity,* $\mu$ m/min	Distance,* $\mu$ m	Measurements
Anaphase A <sup>†</sup>	None	$2.4 \pm 1.0$	$21 \pm 9$	11
	Cyclin-B $\Delta$ 90	$1.9 \pm 0.7$	$22 \pm 7$	8
Anaphase B	None	$1.6 \pm 1.4$	$13 \pm 10$	5
	Cyclin-B $\Delta$ 90	$2.0 \pm 1.1$	$15 \pm 7$	4
Telophase chromosome Motility	None	$15 \pm 6$	$18 \pm 10$	14
	Cyclin-B $\Delta$ 90	0	0	
Aster ejection	None	$4.4 \pm 2.0$	$45 \pm 31$	15
	Cyclin-B $\Delta$ 90	$1.6 \pm 1.6$	$12 \pm 6$	13

\*Average  $\pm$  SD.

<sup>†</sup>Anaphase A velocities were obtained from measurements of either chromosome to pole movement directly or by subtracting the contribution of pole to pole elongation from the kinetics of measurements of sister chromatid separation (Fig. 3).

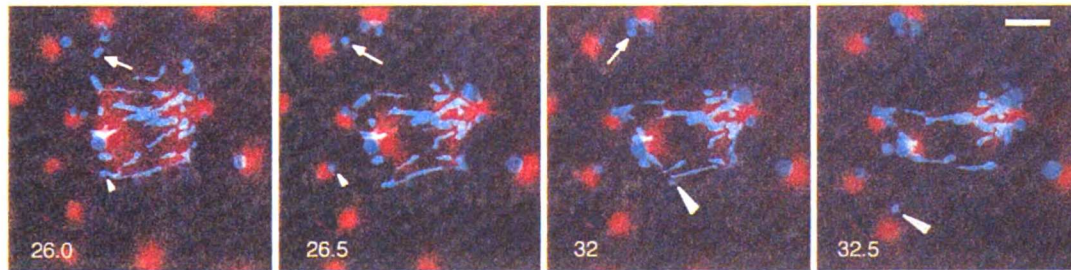


FIG. 4. Telophase chromosome movements toward aster centers in a control spindle preparation with multiple ejected asters as described in the legend to Fig. 24. Pseudocolor is as described for Fig. 1, except the intensity in the rhodamine image has been enhanced to show the weak fluorescence of the telophase asters. Time is given in minutes after the onset of anaphase. Note that the upper telophase chromosome marked by the arrow moves first to the center of the left aster then later to the right aster. The middle telophase chromosome marked by the small arrowhead moves to the left center. The lower telophase chromosome marked by a large arrowhead moves toward a lower aster center. (Bar = 20  $\mu\text{m}$ .)

results extend earlier studies (5, 20) which showed that MPF inactivation is not required for chromosome segregation, although it is essential for chromosome decondensation and nuclear envelope reformation.

The behavior of the spindle microtubules in the presence of cyclin B- $\Delta$ 90 differed in three other respects from that seen in control extracts. (i) Although aster ejection still occurred in the presence of cyclin B- $\Delta$ 90, the rate of aster ejection was only one-third of that seen in control spindles and the average ejection distance was much shorter (Table 1). Both of these differences are statistically significant ( $P \leq 0.001$  in the paired  $t$  test). (ii) The asters in extracts containing cyclin B- $\Delta$ 90 remained tiny in comparison to the asters expelled in control extracts (compare Fig. 2A and B). (iii) In the regions between the spindle poles and the chromosomes moving toward them, the microtubule density fell more slowly in extracts containing cyclin B- $\Delta$ 90 (compare Fig. 3A and B).

In cyclin B- $\Delta$ 90-treated extracts, the decline in microtubule density differed greatly between two types of spindles. In most spindles, the great majority of chromosomes segregated successfully and the microtubule density at the site of the former metaphase plate dropped to undetectable levels (see Fig. 1B). Even in those spindles that lacked anaphase B, this loss converted the spindles into two apparently independent half spindles, each of whose length was less than half that of the original metaphase spindle. In a minority of spindles a significant fraction of the chromosomes failed to segregate from each other. When this happened, the density of microtubules near the metaphase plate stayed high, and the spindle remained a single bipolar structure, even though about half the chromosomes segregated normally to the poles (Fig. 5). This observation implies that chromosomes stabilize the interactions between antiparallel microtubules that occur near the metaphase plate. We do not know why some spindles, with or without cyclin B- $\Delta$ 90, fail to segregate all their chromosomes. Possibilities include failures in chromosome replication or condensation, or physical interactions between the nonsegregating chromosomes and the glass of the slide or coverslip.

## DISCUSSION

We used digital fluorescence microscopy to follow the progress of anaphase in frog egg extracts. Most aspects of spindle behavior in these extracts closely parallel those seen in real cells, but we have also observed two novel phenomena: the expulsion of microtubule asters from the spindle during anaphase, and a novel form of microtubule-mediated motility shown by telophase chromosomes. Preventing the inactivation of MPF has no effect on anaphase A, reduces aster ejection and the fall in microtubule density seen between the spindle

pole and the advancing chromosomes, and completely blocks the fast telophase chromosome movement.

**Anaphase Aster Ejection.** Aster expulsion during anaphase helps to clarify the relationship between spindle poles and other microtubule-organizing centers. The spindles we observed probably arose by side-to-side fusion of multiple spindles, each containing a pair of centrosomes (13). Thus the expelled asters are likely centrosomes, although we cannot exclude the possibility that they are centriole-free microtubule organizing centers like those assembled in taxol-treated frog egg extracts (21).

Whatever their source, these extra asters are clearly functionally different from the spindle poles in anaphase: the departing asters do not grossly affect the organization of microtubules within the spindle, and as long as chromosomes stay condensed they are not attracted to the migrating asters. This observation is consistent with other demonstrations that spindle poles are specialized structures that can function in the absence of centrosomes (22, 23), although we do not know whether the spindle poles we observed retain any functional centrosomes. Examining diploid spindles in lysed eggs shows that microtubule asters (which presumably contain the centrosome) can be detached from mitotic spindles without

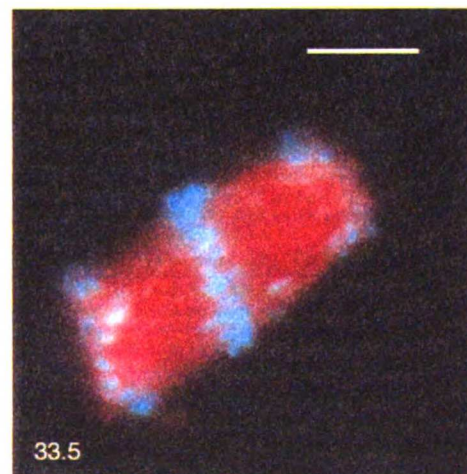


FIG. 5. The role of chromosomes in maintaining spindle integrity demonstrated by a cyclin B- $\Delta$ 90-treated spindle with stuck chromosomes in late anaphase. Pseudocolor is the same as described in the legend for Fig. 1. Time is given in minutes after onset of anaphase. (Bar = 20  $\mu\text{m}$ .)

affecting anaphase spindle organization or chromosome segregation (unpublished results). Perhaps the primary role of the centrosomes is to nucleate the array of microtubules that captures the kinetochores early in mitosis. As mitosis progresses, the interaction of these kinetochore microtubules with each other and with other components of the spindle may create a spindle pole that can function after removal of the centrosome.

**Telophase Chromosome Movement.** At the end of anaphase, we saw chromosomes decondense and make rapid movements toward any nearby aster, often moving first toward one and then toward another. This movement is hard to see in telophase tissue culture cells whose chromosomes decondense collectively to form an interphase nucleus associated with a single aster. In early embryonic cells, the decondensing chromosomes form telophase chromosomes by acquiring a nuclear envelope before they fuse with each other to form a single nucleus (18). In our experiments, the presence of extra asters revealed the differences between the movements of telophase chromosomes and condensed mitotic chromosomes. Two observations suggest that aster-directed movement requires a nuclear envelope: movement does not start until the telophase chromosomes exclude the fluorescence of unpolymerized tubulin, and chromosomes in extracts containing nondegradable cyclin do not decondense or exhibit this movement. Perhaps aster directed-movement is due to association between the nuclear envelope and a minus-end directed microtubule motor, such as cytoplasmic dynein (24) or Kar3 (25). In a daughter cell with a single aster, a nuclear envelope-associated motor would move the telophase chromosomes to the center of the aster, inducing them to fuse into a single interphase nucleus. Minus-end-directed motors on the nuclear envelope could also explain the migration of the female pronucleus toward the center of the sperm aster in fertilized eggs (26).

**MPF and Anaphase.** We used nondegradable cyclin B to ask what aspects of anaphase required the inactivation of MPF. Sister chromatid separation, anaphase A, and anaphase B, all occurred normally, confirming that these events are independent of MPF inactivation (5, 20). In contrast, three other events were affected by adding nondegradable cyclin: chromosomes did not decondense, the expelled asters were smaller and moved away from the spindle more slowly, and there was a smaller fall in the microtubule density between the advancing chromosomes and the spindle poles. These events are normally induced by the effects of MPF on microtubule dynamics (6, 7), the activity and localization of microtubule motors (27, 28), and the ability of chromatin to stabilize microtubules (29). Inactivating MPF increases the average length of microtubules but decreases the number of microtubules generated by a centrosome (30). For free asters, this increase in length would allow microtubule-dependent forces (generated by microtubule motors or polymerization) to move the asters more rapidly. At the spindle poles, less microtubule nucleation and less stabilization of microtubules by chromatin may explain why the density of microtubules between the chromosomes and the spindle poles falls.

Anaphase in the presence of nondegradable cyclin converts a spindle into two half spindles (Fig. 1B and ref. 5), suggesting that the linkage between sister chromatids maintains spindle bipolarity. Several mechanisms may stabilize the metaphase spindle. In each half of the spindle, the kinetochores stabilize bundles of microtubules running from the pole to the kinetochore. Because the two sister chromatids face in opposite directions, the linkage between them links the poles to each other via the kinetochore microtubules (reviewed in ref. 2). Microtubules that do not terminate at the kinetochore can be stabilized by poorly defined interactions with chromatin (reviewed in refs. 31 and 32). Finally, analyzing spindles with unreplacated chromosomes suggests that antiparallel interactions between microtubules nucleated at opposite poles of the

spindle plays an important role in establishing and stabilizing bipolarity (13). Once sister chromatids separate and move apart, these stabilizing influences decline, microtubules ending in the center of the spindle depolymerize, and the spindle breaks in two. If the different microtubule-stabilizing mechanisms act synergistically, the metaphase spindle would be quite stable but would rapidly break down as sisters separate. Anaphase B still occurs in cells whose spindles lack chromosomes (D. Zhang and B. Nicklas, personal communication) suggesting that there are chromosome-independent mechanisms that allow the spindle to respond to changes in MPF activity.

**Anaphase A and Poleward Microtubule Flux.** During both metaphase and anaphase, marks made on microtubules move toward the spindle pole [polewards flux (23, 33)]. In kinetochore microtubules, flux occurs because microtubule depolymerization at the spindle pole is balanced by polymerization at the kinetochore making the individual subunits of the microtubule (the microtubule lattice) move to the pole. What is the relationship between flux and anaphase chromosome movement? During the initial stages of anaphase in tissue culture cells, chromosomes move toward the poles three to six times faster than marks made on kinetochore microtubules (23, 34). We have not measured flux and chromosome movement simultaneously for the spindles in *Xenopus* extracts, but chromosome movement in anaphase A (2.4  $\mu\text{m}/\text{min}$ ) occurs at about the rate of poleward microtubule flux in metaphase *Xenopus* spindles (12). This similarity suggests that anaphase A in early embryos may be driven entirely by poleward flux. However, since flux measurements in *Xenopus* spindles are dominated by nonkinetochore microtubules, this conclusion rests on the untested assumption that flux occurs at the same rate in kinetochore and nonkinetochore microtubules.

Following anaphase in individual spindles in cell extracts has revealed phenomena that were not easily seen in intact cells. This approach will greatly increase the range of experiments on spindle behavior that are accessible to real-time observation and should ultimately enable us to reconstitute functional spindles from purified components.

We thank the Marine Biological Laboratory, Nikon Inc., Universal Imaging Inc., the Program in Architectural Dynamics, and Shinya and Ted Inoue for their support for this collaborative project. Liz Blanton and Paul Maddox provided expert assistance for data analysis and digital photography. We are grateful to Cori Bargmann, Tim Mitchison, David Morgan, and Claire Waterman-Storer for their insightful comments on the manuscript. This work was supported by a Marine Biological Laboratory Nikon Fellowship to A.W.M., a Marine Biological Laboratory Rand Fellowship to E.D.S., and grants from the National Institutes of Health (to A.W.M. and E.D.S.) and the Packard Foundation (to A.W.M.). A.B.D. is a predoctoral fellow of the Howard Hughes Medical Institute.

1. Wilson, E. B. (1928) *The Cell in Development and Heredity* (Macmillan, New York), 3rd Ed.
2. Inoue, S. & Salmon, E. D. (1995) *Mol. Biol. Cell* **6**, 1619-1640.
3. Murray, A. & Hunt, T. (1993) *The Cell Cycle: An Introduction* (Oxford Univ. Press, New York).
4. Shamu, C. E. & Murray, A. W. (1992) *J. Cell Biol.* **117**, 921-934.
5. Holloway, S. L., Glotzer, M., King, R. W. & Murray, A. W. (1993) *Cell* **73**, 1393-1402.
6. Belmont, L. D., Hyman, A. A., Sawin, K. E. & Mitchison, T. J. (1990) *Cell* **62**, 579-589.
7. Verde, F., Dogterom, M., Stelzer, E., Karsenti, E. & Leibler, S. (1992) *J. Cell Biol.* **118**, 1097-1108.
8. Karsenti, E., Kobayashi, S., Mitchison, T. & Kirschner, M. (1984) *J. Cell Biol.* **98**, 1763-1776.
9. Lohka, M. J. & Masui, Y. (1983) *Science* **220**, 719-721.
10. Lohka, M. & Maller, J. (1985) *J. Cell Biol.* **101**, 518-523.
11. Murray, A. W. & Kirschner, M. W. (1989) *Nature (London)* **339**, 275-280.
12. Sawin, K. E. & Mitchison, T. J. (1991) *J. Cell Biol.* **112**, 941-954.
13. Sawin, K. E. & Mitchison, T. J. (1991) *J. Cell Biol.* **112**, 925-940.

12332 Cell Biology: Murray *et al.**Proc. Natl. Acad. Sci. USA* 93 (1996)

14. Sagata, N., Watanabe, N., Vande Woude, G. F. & Ikawa, Y. (1989) *Nature (London)* **342**, 512-518.
15. Watanabe, N., Hunt, T., Ikawa, Y. & Sagata, N. (1991) *Nature (London)* **352**, 247-248.
16. Salmon, E. D., Inoue, T., Desai, A. & Murray, A. W. (1994) *Biol. Bull.* **187**, 231-232.
17. Sullivan, K. M., Busa, W. B. & Wilson, K. L. (1993) *Cell* **73**, 1411-1422.
18. Ito, S., Dan, K. & Goodenough, D. (1981) *Chromosoma* **83**, 441-453.
19. Murray, A. W., Solomon, M. J. & Kirschner, M. W. (1989) *Nature (London)* **339**, 280-286.
20. Surana, U., Amon, A., Dowzer, C., McGrew, J., Byers, B. & Nasmyth, K. (1993) *EMBO J.* **12**, 1969-1978.
21. Verde, F., Berrez, J. M., Antony, C. & Karsenti, E. (1991) *J. Cell Biol.* **112**, 1177-1187.
22. Hiramoto, Y. & Nakano, Y. (1988) *Cell Motil. Cytoskeleton* **10**, 172-184.
23. Mitchison, T. J. & Salmon, E. D. (1992) *J. Cell Biol.* **119**, 569-582.
24. Paschal, B. M., Shpetner, H. S. & Vallee, R. B. (1987) *J. Cell Biol.* **105**, 1273-1282.
25. Endow, S. A., Kang, S. J., Satterwhite, L. L., Rose, M. D., Skeen, V. P. & Salmon, E. D. (1994) *EMBO J.* **13**, 2708-2713.
26. Aronson, J. F. (1971) *J. Cell Biol.* **51**, 579-583.
27. Blangy, A., Lane, H. A., d'Herin, P., Harper, M., Kress, M. & Nigg, E. A. (1995) *Cell* **83**, 1159-1169.
28. Sawin, K. E. & Mitchison, T. J. (1995) *Proc. Natl. Acad. Sci. USA* **92**, 4289-4293.
29. Karsenti, E., Newport, J., Hubble, R. & Kirschner, M. (1984) *J. Cell Biol.* **98**, 1730-1745.
30. Kuriyama, R. & Borisy, G. G. (1981) *J. Cell Biol.* **91**, 822-826.
31. Vernos, I. & Karsenti, E. (1996) *Curr. Opin. Cell Biol.* **8**, 4-9.
32. Waters, J. C. & Salmon, E. D. (1995) *BioEssays* **17**, 911-914.
33. Mitchison, T. J. (1989) *J. Cell Biol.* **109**, 637-652.
34. Zhai, Y., Kronebusch, P. J. & Borisy, G. G. (1995) *J. Cell Biol.* **131**, 721-734.



## **Appendix II**

### ***Xenopus* Extract Methodology**

This appendix has been submitted for publication in a volume of *Methods in Cell Biology*

**THE USE OF *XENOPUS* EGG EXTRACTS TO STUDY MITOTIC SPINDLE  
ASSEMBLY AND FUNCTION *IN VITRO***

Arshad Desai\*, Andrew Murray#, Timothy J. Mitchison+, and Claire E.  
Walczak+

\*Department of Biochemistry and Biophysics, # Department of Physiology,  
and +Department of Cellular and Molecular Pharmacology, University of  
California- San Francisco, San Francisco, CA 94143

## Table of Contents

- I. Introduction
- II. Preparation of CSF Extracts for Spindle Assembly
  - A. Requirements for Extract Preparation
  - B. Protocol for Extract Preparation
  - C. General Considerations for Preparing Spindle Assembly Extracts
  - D. Procedure for Extract Preparation
  - E. Preparation and Use of Sperm Nuclei and Fluorescent Tubulin
- III. Spindle Assembly Reactions
  - A. General Considerations for Spindle Assembly Reactions
  - B. Reagents Required for Spindle Assembly
  - C. CSF Spindle Assembly
  - D. Cycled Spindle Assembly
- IV. Monitoring Spindle Assembly Reactions
  - A. Methods for Pelleting Spindles onto Coverslips
  - B. Time Course Experiments
- V. Manipulation of Extracts
  - A. Immunodepletion of Extracts
  - B. Reagent Addition to Extracts
- VI. Data Analysis and Interpretation
- VII. Anaphase *in vitro*
  - A. Preparation of Anaphase-Competent Extracts
  - B. Setting up and Monitoring Anaphase Reactions
  - C. Real Time Analysis of Anaphase *in vitro*
  - D. Manipulation of Anaphase *in vitro*
- VIII. Conclusions
  - Acknowledgments

## References

### I. Introduction

Since Flemming first described mitosis more than a century ago, understanding the mechanisms underlying cell division has been a major focus in cell biology (Flemming, 1965). Over the years, the study of cell division has evolved from a detailed description of mitosis by the early cytologists to a modern molecular investigation. Essential for this evolution has been the development of experimental systems where molecular and observational studies can be linked. Extracts from unfertilized *Xenopus* eggs provide one such system. These extracts are capable of maintaining specific cell cycle states and carrying out many of the events associated with cell division *in vitro* (Lohka and Masui, 1983; Blow and Laskey, 1986; Hutchison et al., 1988; Murray and Kirschner, 1989). In addition to providing fundamental insights into the nature of the cell cycle, these extracts have been very useful for dissecting downstream mitotic processes such as regulation of microtubule dynamics, chromosome condensation, mitotic spindle assembly, sister chromatid separation, anaphase chromosome movement, and kinetochore assembly (Lohka and Maller, 1985; Belmont et al., 1990; Verde et al., 1990; Hirano and Mitchison, 1991; Sawin and Mitchison, 1991; Shamu and Murray, 1992; Murray et al., 1996; Desai et al., in press). A hallmark of studies in *Xenopus* extracts has been the combination of detailed structural and functional analysis of complex macromolecular assemblies such as the mitotic spindle with the manipulation of selected components. Similar feats have been difficult to accomplish in genetic systems such as budding yeast, because the cytology is limiting and the biochemistry is difficult.

Furthermore, *Xenopus* extracts also provide insight into the mechanisms of vertebrate mitosis, the details of which may not be revealed from studies in lower eukaryotes.

The two most useful attributes of *Xenopus* extracts are their ability to maintain specific cell cycle states and to recapitulate many of the detailed morphological changes associated with mitosis. Both of these features depend on the natural cell cycle arrest of the frog egg and on the ability to make concentrated extracts that retain many of the properties of intact cytoplasm. Mature *Xenopus* eggs are arrested in metaphase of meiosis II by an activity termed cytostatic factor (CSF), which is thought to be the product of the *c-mos* protooncogene (Sagata et al., 1989). Sperm entry triggers a calcium spike that initiates a series of events leading to the destruction of CSF and exit from the meiosis II metaphase arrest. This calcium-sensitivity of the CSF arrest is exploited in the preparation of extracts by use of the calcium chelator EGTA. The presence of EGTA in buffers results in extracts that maintain the CSF arrest (referred to as CSF extracts) but can be induced to exit the CSF arrest by addition of calcium (Lohka and Maller, 1985). This convenient control of cell cycle state allows one to easily obtain *in vitro* spindles with replicated chromosomes as described below in detail. It should be noted that CSF extracts are meiotic (meiosis II) and not mitotic cytoplasm, a distinction that has not generally been made in the literature. However, given the mechanistic similarity of meiosis II and mitosis, studies using CSF extracts should be generally relevant to the study of mitosis, and several phenotypes of depletion of spindle assembly components in CSF extracts have also been observed in antibody injection experiments in somatic cells (Sawin et al., 1992; Blangy et al., 1995; Gaglio et al., 1995; Gaglio et al., 1996; Merdes et al., 1996; Gaglio et al., 1997; Heald et al., 1997) as well as with genetic analysis of

mitotic mutants (Enos and Morris, 1990; Hagan and Yanagida, 1990; Hoyt et al., 1992; Roof et al., 1992).

In this chapter, we will present detailed methods for the preparation of CSF extracts and for performing spindle assembly reactions. We will also describe methods for depleting specific components from extracts, an approach that has been used successfully to determine the contributions of both motor and non-motor components to spindle assembly (Sawin et al., 1992; Merdes et al., 1996; Walczak et al., 1996; Walczak et al., 1997). Finally, we will describe methods for analyzing anaphase *in vitro* (Murray et al., 1996). We recommend that anyone interested in using *Xenopus* egg extracts as an experimental system should first consult the chapter by Murray (1991) that provides an introduction to the early stages of the *Xenopus* life cycle, documents the history of cell cycle extracts, provides detailed technical descriptions on the preparation of different types of extracts, gives advice on troubleshooting problems with extracts, and serves as the basis for several of the procedures described here.

## II. Preparation of CSF Extracts for Spindle Assembly

### A. Requirements for Extract Preparation

#### 1. BUFFER AND REAGENT STOCKS

10X MMR:

50 mM Na-HEPES, pH to 7.8 with NaOH; 1 mM EDTA; 1 M NaCl; 20 mM KCl;  
10 mM MgCl<sub>2</sub>; 20 mM CaCl<sub>2</sub>

Autoclave and store at RT; if desired, MMR can also be prepared as a 25X stock

20X XB Salts:

2 M KCl; 20 mM MgCl<sub>2</sub>; 2 mM CaCl<sub>2</sub>

sterile filter and store at 4°C

*2M Sucrose:*

sterile filter or autoclave and store at 4°C or in aliquots at -20 °C

*1M K-HEPES:*

pH to 7.7 with KOH, sterile filter and store at 4 °C or in aliquots at -20°C

*0.5M K-EGTA:*

pH to 7.7 with KOH, sterile filter and store at RT

*1M MgCl<sub>2</sub>:*

sterile filter and store at RT

*20X Energy Mix:*

150 mM creatine phosphate

20 mM ATP

20 mM MgCl<sub>2</sub>;

store in 100 µl aliquots at -20°C

*Protease Inhibitors (LPC):*

10 mg/ml each of leupeptin, pepstatin A, and chymostatin dissolved in DMSO; store in 100 µl aliquots at -20°C

*Cytochalasin B or D:*

10 mg/ml in DMSO; store in 10 or 50 µl aliquots at -20°C

(Note: Both protease inhibitors and cytochalasin stocks can be frozen and thawed multiple times without detriment)

*5% Gelatin (w/v):*

dissolved in water; autoclave and store in aliquots at -20°C

*Cysteine, free base:*

Sigma #C-7755

*Versilube F-50 :*

ANDPAK- EMA

*Hormone stocks for priming frogs and inducing ovulation:*

Pregnant Mare Serum Gonadotropin (PMSG): 100 U/ml (Calbiochem # 367222) made up in water and stored at -20°C

Human Chorionic Gonadotropin (HCG): 1000 U/ml (Sigma # CG-10) made up in water and stored at 4°C

(Hormones are injected into the dorsal lymph sac using a 27 gauge needle)

## 2. EQUIPMENT

*Glass petri dishes :*

60, 100, 150 mm diameter regular and 150 mm diameter high-sided, i.e., 150 mm diameter, 75 mm height

*13 X 51 mm UltraClear tubes*

(Beckman # 344057)



## *Ultracentrifuge and SW50.1/ SW55.1 rotor*

### *Clinical centrifuge*

### 3. PRIMED FROGS

Frogs for extract preparation are primed using progesterone (present in PMSG) which induces maturation of oocytes. Priming is performed in two steps by injection with 50 U of PMSG (0.5 ml of 100 U/ml stock) on day 1 and 25 U of PMSG (0.25 ml) on day 3. Primed frogs are stored in dechlorinated water containing 2 gram/liter rock salt in a cool room (ambient temperature of 16°C - 20°C), and can be induced to lay eggs for up to two weeks after the second priming.

### B. Protocol for Extract Preparation

#### 1. DAY BEFORE EXTRACT PREP

16-18 hours before extract preparation, 4-6 primed frogs are induced to ovulate by injection with 500 U (0.5 ml) of HCG. After injection, frogs are rinsed well in distilled water, put individually into plastic buckets (Fisher #03-484-21) containing 2 l MMR and stored overnight in a 16°C incubator.

#### 2. SETUP FOR EXTRACT PREPARATION

For a 4-6 frog prep, you will need the following prior to beginning the prep:

##### *a. Buffers:*

(prepare just before use unless indicated otherwise; all graduated cylinders and glassware should be rinsed well with double distilled water (dd H<sub>2</sub>O) prior to use)

2-3 l 1X MMR (the MMR can be made the night before and stored in a plastic carboy in the 16 °C incubator)

200 ml Dejellying Solution: 2% (w/v) cysteine in 1X XB Salts; pH to 7.8 by adding 0.9 ml of 10 N NaOH

750 ml XB: 10 mM K-HEPES, pH 7.7, 100 mM KCl, 1 mM MgCl<sub>2</sub>, 0.1 mM CaCl<sub>2</sub>, 50 mM sucrose; prepare using 20X XB salts, 2M sucrose and 1M K-HEPES, pH 7.7 stocks; to maintain a pH of 7.7 at 10 mM HEPES, add 11 µl 10 N KOH per 100 ml XB

250 ml CSF-XB: XB + 1 mM MgCl<sub>2</sub> + 5 mM EGTA; to prepare, transfer 250 ml of XB (from the 750 ml prepared above) to a separate graduated cylinder and add EGTA to 5 mM and MgCl<sub>2</sub> to 1 mM final

100 ml CSF-XB + PIs: CSF-XB + 10 µg/ml LPC; to prepare, transfer 100 ml of CSF-XB (from the 250 ml prepared above) to a separate graduated cylinder and add LPC to 10 µg/ml (mix immediately after adding LPC)

*b. Equipment, etc.:*

SW55.1 or SW50.1 rotor at 16 °C in ultracentrifuge

2 Pasteur pipettes with tips broken and fire-polished to ~3-4 mm diameter

4-6 13x51 mm Ultraclear tubes

2 150 mm regular petri dishes, 1 high-sided 150 mm petri dish; rinse well with ddH<sub>2</sub>O and coat with 100 µg/ml gelatin (thaw gelatin at 37°C, pour ~30 ml MMR into petri dish, pipet in 60 µl of gelatin and swirl well for ~30s, pour out MMR and replace with XB); if making a squeezed egg extract in parallel (see Section VII A) gelatin coat 4 60 mm petri dishes (15 ml MMR and 30 µl gelatin) and fill with MMR for squeezing frogs into, and coat 1 100 mm petri dish for processing the squeezed eggs after dejelling

600 ml glass beaker (rinsed well with dd H<sub>2</sub>O)

### C. General Considerations for Preparing Spindle Assembly Extracts

Spindle assembly is best performed using freshly prepared extracts because freezing extracts considerably decreases their ability to form bipolar spindles. For spindle assembly extracts, egg quality must take precedence over egg quantity. Because 1-2 ml of extract is more than sufficient for most experiments, it is best not to use any batches of eggs containing significant numbers (>10%) of lysed eggs, activated eggs (detected by contraction of dark pigment at the animal pole), or "puffballs" (eggs which are swollen and often white and puffy). Strings of eggs which do not have fully separated jelly coats can be used as a last resort unless they contain a high percentage of deformed or activated eggs. Any batches of eggs which are distinguishable in quality should be processed separately. Although the best spindle assembly extracts are often made from freshly squeezed eggs, we have had good success with laid eggs and will focus here on their use. Further discussion of squeezed egg extracts is presented in the section on anaphase *in vitro* (Section VII A).

For laid eggs, extract preparation should begin 16-18 hrs after HCG injection. We recommend that the temperature of the buffers and the room where eggs will be manipulated to not exceed 23°C (ideally 18°C-20°C). Warmer temperatures will almost certainly result in lower quality extracts. Rinsing of eggs after dejellying is best performed in gelatin-coated petri dishes by swirling the dishes a couple of times and pouring out the buffer. Never pour solutions directly onto the dejellied eggs as they are quite fragile. Pour the solutions down the side of the wash vessel, and then gently swirl the eggs. Maximal buffer exchange in petri dishes can be achieved by turning the dish away from you and quickly removing buffer at the edge of the egg mass using a wide bore pasteur pipet prior to pouring in the next wash buffer. During the washes, the eggs should be 'gardened', i.e., visibly deformed eggs, activated eggs, puffballs and large pieces of debris should be removed using the wide bore pasteur pipets. However, one should not get so caught up in removing bad eggs and debris that they slow the preparation of the extract down. Time is another important variable. Generally it should be possible to go from collecting of eggs to the crushing spin in 45' to 1 hr.

#### D. Procedure for Extract Preparation

- 1) Combine batches of good laid eggs and remove as much MMR as possible.
- 2) Wash eggs in 2-3L of MMR until all of the debris is removed. Combine good egg batches in a frog bucket, rinse a couple of times with MMR and pour the eggs into a 600 ml beaker for the rest of the MMR washes. Since eggs settle quickly, pouring out the MMR immediately after the eggs have settled allows easy removal of debris. Eggs should be gardened during this step and during washes after dejellying.

- 3) Remove as much MMR as possible and rinse eggs into dejelling solution.
- 4) Swirl gently and intermittently in the dejelling solution. While the eggs are dejelling, pipet 1 ml of CSF-XB + PIs to each 13 x 51 mm Ultraclear centrifuge tube and add 10  $\mu$ l of 10 mg/ml cytochalasin B/D per tube (flick the tube well immediately after pipeting in the cytochalasin, or it will precipitate).
- 5) After eggs are dejellied ( this will take 7-10' and the volume will decrease approximately 5-fold; eggs will pack tightly and orient with their vegetal poles down), remove as much dejelling solution as possible, rinse eggs with residual dejelling solution and once with XB, then transfer eggs to gelatin-coated petri dishes. Wash dejellied eggs 3-4X with XB in the petri dish as described above (Section II C). For larger batches of eggs, we recommend using the high-sided 150 mm petri dishes.
- 6) Wash eggs 2-3X in CSF-XB. Remove as much buffer as possible.
- 7) Wash eggs 2X in CSF-XB + PIs. Leave eggs in a small volume of CSF-XB + PIs after the second wash.
- 8) Draw eggs up into the wide bore pasteur pipet and slowly drop them into the 1 ml CSF-XB + PIs + 100  $\mu$ g/ml cytochalasin solution in the ultraclear tube. Insert the pipet below the meniscus to break the surface tension and gently release eggs into the solution. Minimize transfer of buffer along with the eggs.
- 9) Aspirate excess buffer from the top of the eggs.
- 10) Put the ultraclear tubes into 14 ml polypropylene roundbottom culture tubes (Falcon #2059) and spin for 10s at setting #4 (approx. 1500 rpm) in a clinical centrifuge.
- 11) Gently aspirate buffer from top of the eggs and layer on 0.75-1 ml of Versilube F-50. Use of versilube minimizes dilution during extract preparation. The density of versilube is intermediate between that of buffer

and cytoplasm, thus versilube displaces buffer between the eggs during the packing spin but floats to the top of the cytoplasmic layer during the crushing spin.

12) Pack the eggs by spinning at setting #5 for 30s (2000 rpm) and full speed (#7) for 15 sec (2500- 3000 rpm) in the clinical centrifuge.

13) Aspirate all buffer and versilube from the top of the packed eggs.

14) Transfer the tubes containing the packed eggs to the SW55.1 rotor in the ultracentrifuge. Crush the eggs by centrifugation at 10,000 rpm for 15' at 16°C (full brake).

15) Store tubes with crushed eggs on ice. The light yellow layer on top represents the lipid droplets and the dark layer on the bottom contains the yolk and nuclei. The cytoplasmic layer is the muddy or straw colored layer in the middle of the tube. Prior to collecting the cytoplasmic layer, wipe the sides of the tubes with 95% ethanol. Puncture the tube near the bottom of the cytoplasmic layer with an 18 gauge needle (on a 1 cc syringe), and gently draw out the extract. (See Figure 3 of Murray chapter for a picture of an extract (Murray, 1991). We find it best to use a new needle for each centrifuge tube. Transfer the collected extract to a 5 ml snap cap tube and estimate its volume.

16) Add 1/1000 volume of protease inhibitor (LPC) and cytochalasin stocks, 1/20 volume of 20X Energy Mix and 1/40 volume of 2M sucrose. Note that some people do not add additional sucrose to the extract after preparation, but we find that it often helps stabilize the extract during immunodepletions (Section V A).

## E. Preparation and Use of Sperm Nuclei and Fluorescent Tubulin

Sperm nuclei are prepared exactly as described by Murray (Murray, 1991) and stored in small aliquots at -80°C at a density of  $1-5 \times 10^7$ /ml. Sperm

nuclei can be frozen and thawed multiple times without apparent loss of activity, but we prefer to store them in small aliquots and only freeze-thaw once for spindle assembly reactions. Sperm nuclei are added to extracts at a 1/100-1/200 dilution yielding a final concentration of 100-300 nuclei/ $\mu$ l.

Fluorescent tubulin is used to monitor microtubule distributions during spindle assembly and is prepared by the high pH labeling protocol described by Hyman et al. (1991). Either fluorescein, tetramethyl rhodamine or X-rhodamine labeled tubulin can be used to monitor spindle assembly. We generally use X-rhodamine labeled tubulin because it has better spectral separation from fluorescein than does tetramethyl rhodamine, allowing double label immunofluorescence studies with fluorescein-conjugated secondary antibodies (Section IV). Our X-rhodamine labeled tubulin preps have final concentrations varying between 15 to 25 mg/ml with labeling stoichiometries between 0.5 and 1. For monitoring spindle assembly, we add X-rhodamine tubulin to the extract at a final concentration of 20-50  $\mu$ g/ml (generally a 1/400 dilution). Although tubulin by itself is highly unstable, it appears to be very stable in the extract and can be added immediately after extract preparation.

### III. Spindle Assembly Reactions

Three types of spindle assembly reactions have been described in the literature (Sawin and Mitchison, 1991; Heald et al., 1996). In the first type of reaction, termed CSF spindle assembly, each sperm nucleus added to the extract drives the formation of a half spindle. Two such half spindles then fuse to form a bipolar mitotic spindle (Fig. 1 top pathway) (Sawin and Mitchison, 1991). Thus two haploid sperm nuclei drive the formation of a single bipolar spindle. In the second type of reaction, termed cycled spindle

assembly or interphase-to-mitosis spindle assembly, calcium is added to a CSF extract containing sperm nuclei, inactivating the CSF arrest and driving the extract into interphase. As the nuclei in the extract cycle through interphase their DNA is replicated once (Sawin and Mitchison, 1991). Fresh CSF extract without any sperm nuclei is then added to drive the extract containing replicated sperm nuclei into metaphase. In this type of spindle assembly reaction, each sperm nucleus undergoes one round of replication and drives the formation of a bipolar mitotic spindle (Fig. 1, bottom pathway). Cycled spindles containing bivalent chromosomes are arrested in metaphase by CSF -- addition of calcium for a second time results in inactivation of CSF and anaphase chromosome segregation (Shamu and Murray, 1992). Recently, Heald and coworkers (1996) have described the assembly of spindles around DNA-coated beads in extracts. These studies demonstrated that chromatin-coated beads are sufficient to generate a bipolar mitotic spindle in the absence of centrosomes and kinetochores. A chapter describing the use of DNA-coated beads for studying spindle assembly has been presented recently (Heald et al., in press).

### A. General Considerations for Spindle Assembly Reactions

*Xenopus* extracts are a powerful tool for studying mitosis but their use can be very frustrating because of high variability. These extracts are very sensitive to physical perturbations and must be treated gently to ensure the best results. Avoid pipeting up and down vigorously with narrow bore pipet tips or dropping tubes containing extract reactions since either of these can sufficiently perturb the extract to disrupt the spindle assembly process. We recommend pipeting with either commercially available wide bore P-200 tips (Rainin HR-250W) or regular P-200 tips that have been cut off to an opening



of ~2 mm diameter, and mixing by either gently tapping the bottom of the tube or inverting the tube 2 or 3 times. Use a fresh pipet tip for each aliquot, especially for experiments requiring quantitation as these extracts are very viscous. Never vortex a tube containing extract as this will surely destroy the extract. Finally, avoid diluting the extract with buffer or other reagents as this can also inhibit spindle assembly (see Section V B for more discussion of dilution).

To set up spindle assembly reactions, add sperm nuclei and labeled tubulin to a large volume of extract and then aliquot it into individual reactions. The extract is very viscous and difficult to pipet accurately. Use a fresh pipet tip for each aliquot to ensure reproducibility and allow for a 20% volume loss upon aliquoting. Do not exceed a reaction volume of greater than 50  $\mu$ l/1.5 ml eppendorf tube since larger reaction volumes tend to inhibit spindle assembly. We recommend incubating reactions at 20 °C in a cooled water bath (a home made one can be a plastic tray containing water with a little bit of ice to maintain 20 °C). However, if the room temperature is stable from day to day and does not exceed 24-25°C, then the reactions can be incubated on the bench top.

## B. Reagents Required for Spindle Assembly

Sperm nuclei at  $1-5 \times 10^7$ /ml

Fluorescently-labeled tubulin

Extract Fix: 60% (v/v) glycerol, 1X MMR, 1  $\mu$ g/ml Hoechst 33342/33258, 10% formaldehyde (from 37% (w/v) stock)

Sperm Dilution Buffer (1X): 10 mM HEPES, pH 7.7, 1 mM MgCl<sub>2</sub>, 100 mM KCl, 150 mM sucrose, 10 µg/ml cytochalasin B/D; can be prepared as a 5X stock; both 1X buffer and 5X stock should be stored at -20°C

10X Calcium: 4 mM CaCl<sub>2</sub> in 1X sperm dilution buffer

### C. CSF Spindle Assembly

To CSF extract containing labeled tubulin add sperm nuclei to a final concentration of 100-300/µl. Mix gently, aliquot 25 µl/tube and incubate at 20 °C. At 15', 30', 45' and 60' take samples to test the progress of the reaction as follows: pipet 1 µl aliquot of the reaction on a microscope slide, overlay with 3 µl of extract fix, cover gently with an 18 X 18 mm coverslip and view by fluorescence microscopy. At the 15' time point, small microtubule asters emanate from the sperm centrosome (Fig. 2 top); these often have a very dense core of microtubules. By 30' the chromatin has migrated away from the centrosome, and the microtubules are polarized toward the chromatin- these structures are termed half spindles (Fig. 2 middle). Between 30' and 60', half spindles begin to fuse to form bipolar spindles (Fig. 2 bottom). During CSF spindle assembly, the percentage of total structures that are bipolar spindles varies considerably from extract to extract. In a typical extract, 40 to 60 % of the total structures are bipolar spindles by the 60' time point. This number can range from less than 10 % in really poor extracts to greater than 90 % in the best extracts.

### D. Cycled Spindle Assembly

For cycled spindle assembly the extract is divided into two tubes after the addition of labeled tubulin. One tube is supplemented with sperm nuclei

and cycled into interphase by the addition of calcium while the second tube is held on ice until it is needed to drive the extract with replicated sperm nuclei back into metaphase. Specifically, to one half of the extract containing labeled tubulin add sperm nuclei. Withdraw a small amount as a negative control (~20  $\mu$ l), and to the rest add 1/10 volume of 10X Calcium solution. Mix the calcium into the extract gently but thoroughly, aliquot 20  $\mu$ l/tube, and incubate both the aliquot withdrawn prior to calcium addition and the reaction tubes supplemented with calcium at 20°C for 80'. During this incubation the extract is monitored by taking samples at 30', 45', and 60' time points as described above (Section IIIC). Reactions to which calcium was added should exit the CSF arrest and cycle through interphase; negative control sample (withdrawn before calcium addition) should remain in CSF (mitotic) arrest. Morphology of the mitotic arrest is described above (Section IIIC). The reactions with calcium should look as follows: after 30', the sperm nucleus should be swollen and many free microtubules should be present in the extract; after 45', the sperm nucleus should be large and round and resemble a typical mammalian cell interphase nucleus; after 60', the sperm nucleus should appear large and reticular much like an early prophase nucleus suggesting that the extract may be starting to cycle back into metaphase. In our experience, extracts that have irregularly-shaped interphase nuclei at the 45' time point tend to be less robust in generating mitotic spindles. After 80' at RT, 20  $\mu$ l of CSF extract containing labeled tubulin but not sperm nuclei is added to each reaction (this represents an equal volume of extract added to the initial reaction), mixed in gently and incubated at 20°C for 60' to allow establishment of the metaphase CSF arrest and formation of bipolar spindles. The reactions containing bipolar spindles can be held at room temperature for many hours without detriment,

although with increased time the number of single bipolar spindles drops significantly because the spindles tend to aggregate laterally, forming large multipolar structures.

In general, cycled spindle assembly results in a more uniform distribution of structures than CSF spindle assembly and yields a higher proportion of bipolar spindles (80 to 90% of total structures at 60'). Cycled spindles have chromosomes aligned in an equatorial plane, highly reminiscent of a metaphase plate in somatic cells (Fig. 3 top). However, the tightness of the metaphase plate in cycled spindles can vary significantly between extracts. In good extracts, the chromosomes are tightly focused at the spindle equator, while in less robust extracts, the chromosomes tend to be both at the spindle equator and scattered on either side of the equator. These less robust extracts generally do not work well for anaphase chromosome segregation (Section VII).

The morphological pathway by which cycled spindles assemble remains to be clarified. Sawin and Mitchison first described the pathway as being chromatin driven, i.e., microtubules assembled in the region of the chromatin and with time organized into a bipolar structure with morphologically distinguishable poles (Sawin and Mitchison, 1991). This pathway is similar to that described more recently using chromatin coated magnetic beads, with the exception that spindles assembled from sperm nuclei contain centrosomes. However, Boleti and coworkers have reported the observation of two distinct centrosomal arrays of microtubules being separated to opposite sides of the nucleus in a more classical somatic cell-type spindle assembly pathway (Boleti et al., 1996). A clear picture of the cycled spindle assembly pathway awaits a thorough real-time study of this reaction using fluorescence video microscopy.

## IV. Monitoring Spindle Assembly Reactions

### A. Methods for Pelleting Spindles onto Coverslips

Spindle assembly reactions are routinely monitored using fixed squashes as described above (Section III C). However, for quantitative analysis we prefer to sediment the spindles from a large volume (20  $\mu$ l) of extract onto a coverslip. The advantages of sedimenting spindles onto coverslips are three-fold. First, spindles from 20  $\mu$ l of reaction are concentrated onto a 12 mm coverslip, providing a dense, relatively homogenous sample for quantitative analysis. Second, having the spindles fixed on coverslips allows one to perform immunofluorescence to analyze the localization of specific antigens on the *in vitro* spindles. Third, unlike squashes the pelleted samples are very stable when stored at -20°C. This allows one to prepare many samples at once but analyze them when convenient and store them for any future reanalysis. We use two procedures for pelleting spindles onto coverslips. In the first (method 1), reactions are diluted extensively into a microtubule-stabilizing buffer, pelleted unfixed onto coverslips and fixed onto the coverslips using methanol. Two limitations of this method are an extreme disruption of chromosome structure and day-to-day variability. More recently, we have developed an alternative method (method 2) that involves first diluting the spindles into a microtubule-stabilizing buffer, then fixing the spindles in solution using formaldehyde, pelleting the spindles onto coverslips and post-fixing using methanol. Using method 2 we have satisfied the demanding requirement of retaining the fine structure of chromosomes as they are undergoing anaphase without causing significant disruption of spindle structure (Figure 3 bottom).

## 1. REQUIREMENTS FOR PELLETING SPINDLES ONTO COVERSLEIPS

*BRB80:*

80 mM K-PIPES, pH 6.8 WITH KOH

1 mM MgCl<sub>2</sub>

1 mM EGTA

make as 5X stock, sterile filter and store at 4°C

*5 ml snap cap tubes :*

(Sarstedt # 55.526.006)

*Dilution buffer:*

BRB80 + 30% (v/v) glycerol + 0.5% Triton X-100

*Fixation buffer:* (for Method 2 only)

BRB80 + 30% (v/v) glycerol + 0.5% Triton X-100 + 4 % formaldehyde (added just before use from 37% stock)

*Cushion:*

BRB80 + 40% (v/v) glycerol

*Spindown tubes:*

(Evans et al., 1985) with 12 mm coverslips and 4 ml cushion at room temperature

*Coverslip holders :*

for 12 mm round coverslips; we use Thomas Scientific # 8542-E40

*-20°C methanol*

*TBS-TX:*

1X TBS (10 mM Tris, pH 7.4, 150 mM NaCl)

0.1% Triton X-100

*Mounting Medium:*

0.5% p-phenylenediamine (free base) in 90% glycerol, 20 mM Tris-Cl, pH 9.0

## 2. METHOD 1

1. Prior to beginning the spindown procedure, prepare spindown tubes with coverslips and cushion, and 5 ml snapcap tubes with 2 ml of dilution buffer. All buffers should be at RT.
2. Pipet 20  $\mu$ l of spindle assembly reaction into the dilution buffer. Prior to transferring the extract into the dilution buffer, we often pipet up and down 2-3X with a regular yellow tip to break any large aggregates.
3. Immediately cap the tube and mix by gently inverting 4-5X.
4. Using a disposable plastic transfer pipet, layer the diluted sample onto the cushion in the spindown tube. After dilution, the spindles are stable, so if a large number of samples are being pelleted, first do the dilution and mixing for all samples and then layer them sequentially onto cushions.
5. Centrifuge the tubes in an HS-4 rotor at 18°C for 20' at 5500 rpm (6000g). We use the HS-4 because it can hold 16 tubes; an HB-4, HB-6 or equivalent rotor can be used for smaller numbers of tubes.

6. Aspirate till just below the sample-cushion interface, rinse with BRB80, aspirate off the rinse and the cushion, and transfer the coverslips to a coverslip holder.
7. After all coverslips are in the holder, fix by immersion in -20°C methanol for 3'.
8. Rehydrate using two sequential 5' incubations in TBS-TX.
9. Label DNA by rinsing coverslips with 1 µg/ml Hoechst in TBS-TX for 30 seconds, mount in mounting medium and seal with nail polish. Rinse top surface of coverslip with water prior to observation.

### 3. METHOD 2

Method 2 is different from Method 1 as follows:

1. Dilute 20 µl of sample into 1 ml of dilution buffer as in step 2 of Method 1.
2. Dilute all samples first, then add 1 ml of fixation buffer and mix well by inversion.
3. Fix for 5' at RT prior to layering onto cushion.
4. After pelleting fixed spindles onto coverslips and aspirating the cushion after rinsing (step 6 above), post-fix the coverslips in -20°C methanol.

Using this method we have successfully preserved the fine structure of chromosomes (see Figure 3) without significantly compromising spindle structure.

Spindles pelleted onto coverslips using either method can be processed for immunofluorescence using antibodies to specific spindle components (Walczak et al., 1996). After rehydrating in TBS-TX, coverslips are blocked in TBS-TX + 2% BSA (Antibody Dilution Buffer or AbDil) for 15-30', incubated sequentially with primary and secondary antibodies diluted in AbDil, rinsed in TBS-TX containing 1 µg/ml Hoechst and mounted as described above. For



localizing antibodies added to inhibit function of a particular component, only incubation with the appropriate secondary is necessary (Walczak et al., 1997).

## B. Time Course Experiments

While characterizing the functions of spindle components using the CSF spindle assembly reaction, it is often desirable to monitor the intermediates in the pathway. In order to set up time course experiments for this purpose, it is important that samples for all time points are derived from a single pool of reaction mix and that they are sedimented onto coverslips at the same time. Specifically, to a volume of extract sufficient for all time points, add sperm nuclei and any other reagents such as antibodies or dominant negative fusion proteins, and store on ice. At various intervals beginning with  $t=0'$ , remove 25  $\mu\text{l}$  and transfer to a tube at 20°C. At the end of the timecourse, pellet all samples onto coverslips using either of the methods described above (Section IVA).

## V. Manipulation of Extracts

The ability to manipulate specific components in the extract by either immunodepletion or reagent addition and to assay the effects of these manipulations on spindle assembly is one of the main advantages of *Xenopus* egg extracts. A recent flurry of publications applying this strategy to dissect the role of both motor and non-motor components during spindle assembly demonstrates the value of this approach (Sawin et al., 1992; Vernos et al., 1995; Boleti et al., 1996; Heald et al., 1996; Merdes et al., 1996; Walczak et al., 1996; Heald et al., 1997; Walczak et al., 1997).

## A. Immunodepletion of Extracts

The main difficulty with immunodepletion of CSF extracts is that they lose the CSF arrest during or soon after immunodepletion. In our experience, the following actions seem to aid in immunodepleting proteins without losing the CSF arrest:

- a) During the CSF extract prep, after washing with XB, the eggs are washed thoroughly with CSF-XB without protease inhibitors (step 6 Section II D). This CSF-XB wash ensures that there is sufficient EGTA in the final extract to maintain a tight CSF arrest.
- b) Eggs are crushed at 10,000 rpm (full brake) in a SW55 rotor at 16 °C. Even a slightly faster spin (12,500 rpm) does not work well -- one does not get robust spindle assembly after immunodepletion.
- c) Antibodies are coated on BioRad Affi-Prep Protein A beads (BR# 156-0006). Unlike regular Protein A agarose beads, these high density beads sediment readily through the viscous extract at speeds gentle enough to not perturb the extract.
- d) Remove as much buffer as possible after coating the beads with antibody to avoid diluting the extract which will inhibit spindle assembly.
- e) Extracts are handled extremely gently during manipulations such as resuspending beads or sedimenting beads.

The ability to deplete a specific protein from the extract is dependent on both the quality of the antibody used for depletion and on the abundance of the protein being depleted. As far as antibody quality is concerned, for reasons we do not understand, we have had much better success with antibodies prepared by immunizing with native proteins as opposed to antibodies

generated against denatured proteins, e.g., proteins excised from acrylamide gels.

The protocol below is for depleting a protein present at ~10-20  $\mu\text{g}/\text{ml}$  in the extract using high affinity polyclonal antibodies. While this presents a good starting point, exact conditions must be optimized for each new antibody, particularly the amount of antibody needed for maximal depletion. As a control, we use an equivalent amount of random IgG from the same species -- given the extreme perturbation of the extract by the immunodepletion procedure all interpretations of depletion phenotypes must be restricted to comparison with random IgG depletion done at the same time and processed identically. The procedure for depletion is as follows:

1. Pipet 25  $\mu\text{l}$  of Affi-Prep Protein A beads (50  $\mu\text{l}$  of slurry) into a 0.5 ml eppendorf tube.
2. Wash beads 3X with 0.5 ml TBS-TX (20 mM Tris, pH 7.4, 150 mM NaCl, 0.1% Triton-X 100).
3. Add 4  $\mu\text{g}$  of antibody and bring total volume to 200  $\mu\text{l}$  total using TBS-TX.
4. Bind antibody to beads at 4  $^{\circ}\text{C}$  for 1 hr on rotator. Make sure beads are rolling around during the incubation.
5. Pellet beads in a microfuge for 20 sec, wash 1X TBS-TX, and 3X CSFXB + PIs using 200  $\mu\text{l}$ /wash. Remove as much buffer as possible to avoid diluting the extract.
6. Add 200  $\mu\text{l}$  of extract to each tube, resuspend beads in extract very gently using a wide-bore P-200 tip -- do not pipet up and down more than 3X and avoid tapping the tube or any other type of vigorous agitation.

7. Before the beads settle, rapidly place the tube on the rotator and rotate for 1 hr at 4°C. Make sure that the beads are mixing well with the extract during this period.
8. Pellet the beads for 20 sec in a microfuge and transfer the supernatant to a fresh tube -- this is the depleted extract. It is difficult to recover more than 175  $\mu$ l from a 200  $\mu$ l depletion without contaminating the extract with the beads. Save a small amount of depleted extract to test the extent of depletion by immunoblotting.
9. To analyze what is bound to the beads, wash the beads 2X with CSF-XB +PIs, 3X with TBS-TX and 1X with TBS. Resuspend the beads in 50  $\mu$ l SDS-PAGE sample buffer and boil to release the IgG-antigen complexes from the beads. Analyze the sample by SDS-PAGE and Coomassie brilliant blue staining.

Extracts that have been immunodepleted are far less robust than non-depleted extracts. A good CSF extract will remain mitotic for at least 6-10 hrs on ice whereas a depleted extract will remain mitotic for a few hours at most. We find that with depleted extracts CSF spindle assembly proceeds normally although the extent of bipolar spindle formation is reduced by 2-fold compared to the undepleted extract (Walczak et al., 1997). At a frequency lower than for CSF spindle assembly, we have successfully used immunodepleted extracts for cycled spindle assembly. We have yet to attempt anaphase chromosome segregation in depleted extracts.

We have tried to optimize the immunodepletion procedure to minimize perturbation of the extract but have yet to find the perfect conditions. We believe that the primary problem with immunodepletions is the physical perturbation of the extract by the beads as they are sloshing through the extract. Our most successful manipulation to minimize extract

perturbation has been to reduce the time of depletion to 30'-45' instead of 1 hour. However, with lowered times we also see a reduced efficiency of depletion; we have yet to systematically investigate this issue. We have also wondered whether doing the depletions at RT might be better since calcium uptake machinery would sequester released calcium more efficiently at RT than at 4°C and also whether adding antibody directly to extracts and collecting the antibody-antigen complexes later might be faster and less disruptive than using antibody coated beads. Addition of excess EGTA to sequester released calcium never gave reproducible improvements. Given the logical importance of immunodepletion experiments, technical improvements to immunodepletion procedures are eagerly awaited by many researchers.

## B. Reagent Addition to Extracts

A complementary approach to immunodepletions is to assay the effect of adding either inhibitory antibodies or dominant negative proteins on spindle assembly. This approach is useful because it is less perturbing to the extract than immunodepletion. In addition, it allows one to perturb protein function both before and after spindle assembly, thus allowing one to address the requirement of protein function in both the establishment and maintenance of spindle structure.

One concern with respect to addition of reagents to extracts is dilution of the extract. We recommend not adding reagents to greater than 10 % of extract volume since greater dilution results in poor extract performance. For antibodies, we recommend dialyzing into a buffer that is compatible with extracts such as 10 mM HEPES, pH 7.2, 100 mM KCl. In this buffer, several antibodies that we have generated are stable at -80°C and working stocks are

stable for several months at 4°C. 50 mM K-glutamate, pH 7.0, 0.5 mM MgCl<sub>2</sub> is also compatible with extracts and can be used for storage of antibodies. We avoid the use of CSF-XB or sperm dilution buffer for storing antibodies since both these buffers contain sucrose making them highly susceptible to bacterial contamination at 4°C. We also avoid adding azide to our antibody stocks. Dominant negative fusion proteins can be dialyzed into CSF-XB and stored at -80°C prior to addition to extracts.

The amount of antibody that must be added to perturb function depends on the quality of the antibody being used and on the abundance of the target protein in the extract. We have found that as little as 25-50 µg/ml of a very potent antibody, such as the polyclonal anti-XKCM1 antibody, completely inhibits XKCM1 function whereas 1 mg/ml of a monoclonal antibody to the intermediate chain of dynein is required to inhibit dynein function. We suggest that each new antibody be titrated to determine the amount necessary for full inhibition. Since the mode of action of dominant negative proteins is presumably to compete with the endogenous protein, the amount of fusion protein that must be added to perturb function depends on the endogenous concentration of the target protein. We recommend a 10-fold molar excess of fusion protein as a starting point but the concentration for optimal inhibition must be empirically determined for each protein.

## VI. Data Analysis and Interpretation

*Xenopus* extracts are very powerful for analyzing protein function in spindle assembly, but all extract workers admit that their use is plagued by variability. It is not uncommon to go through periods where several extracts in a row will not assemble nice spindles or where immunodepletions consistently lead to extract activation. This is perfectly normal and can only

be overcome by persistence. However, the extreme variability does necessitate care in performing and interpreting experiments, and we would like to discuss how we approach the analysis of protein function in spindle assembly.

To analyze spindle assembly defects, we recommend starting with technically simpler antibody addition experiments, varying the concentration of added antibody and analyzing the effect using spindowns to facilitate detailed analysis. We quantitatively characterize the phenotype in at least three different experiments on three different extracts, often preparing duplicate samples on a single extract to increase the sample size. Once the effect of antibody addition is clear, the next step is to determine the effect of protein depletion. The immunodepletion procedure itself perturbs the extract significantly making it difficult to discern subtle phenotypes. Furthermore, immunodepletion is technically much more difficult to execute than antibody addition. However, the results of antibody addition experiments must be interpreted cautiously in the absence of a confirmation of the observed effects by immunodepletion. In the absence of immunodepletions, combining antibody inhibition with a dominant negative approach might help strengthen conclusions with respect to the role of a specific protein in spindle assembly. In addition, determining the effect of manipulating a particular protein on all three types of spindle assembly reactions -- CSF spindle assembly, cycled spindle assembly and DNA bead spindle assembly -- can also provide greater insight into its role in spindle assembly (Heald et al., 1997). Performing identical manipulations on different types of spindle assembly reactions can also provide new insights into the process of spindle assembly itself, as demonstrated by recent work characterizing the role of centrosomes during spindle assembly (Heald et al.,

1997). Finally, the most desirable extension of the manipulation of specific components during spindle assembly is to reconstitute of spindle assembly by adding back purified protein to immunodepleted extract - the logical equivalent of a genetic complementation. However, as might be expected, this has proven to be quite difficult and has only been partially achieved (Merdes et al., 1996; Walczak et al., 1996). Future technical improvements in immunodepletion procedures will be necessary to achieve this goal.

The extreme variability between extracts makes identifying the effect of manipulating specific components heavily dependent upon the strength of the observed phenotype. Certain phenotypes, such as the one induced by inhibition of XKCM1, are extremely dramatic and can be easily defined in the first extract analyzed (Walczak et al., 1996). Others, such as the one induced by inhibition of the spindle motor XCTK2, are much more subtle and difficult to detect without careful inspection of many extracts (Walczak et al., 1997). Reproducibility and quantitative analysis become critical in determining the nature of subtler phenotypes.

## VII. Anaphase *in vitro*

Cycled spindles assembled in *Xenopus* egg extracts are capable of undergoing anaphase chromosome segregation (Shamu and Murray, 1992). This *in vitro* anaphase reaction has proven valuable both for dissecting the mechanism of sister chromatid separation and the mechanism of chromosome movement (Murray et al., 1996). However, successful anaphase *in vitro* requires considerably higher quality extracts than those used for spindle assembly and this has significantly limited the use of this reaction. Below we provide some hints to facilitate successful preparation of anaphase-competent extracts. We also describe methods to set up and monitor an



anaphase reaction using either fixed time points or timelapse fluorescence microscopy.

### A. Preparation of Anaphase-Competent Extracts

Extracts for monitoring anaphase are prepared exactly as described earlier for CSF extracts (Section II). Anaphase extracts require high quality eggs, and frogs which lay even small amounts of 'puffballs' or stringy eggs should not be used. Note that the absolute volume of extract required for these experiments is very small and quality should always take precedence over quantity. One factor, which should be minimized in the preparation of anaphase-competent extracts, is the time between egg-laying and extract preparation. Often the best extracts are prepared from freshly squeezed eggs since they have not been floating for several hours in "frog-conditioned" MMR. However, laid egg extracts, which are easier to prepare, can also be fully competent for anaphase. We routinely collect laid eggs from 4-6 frogs about 12-14 hours after injection with HCG (frogs are stored at 16 °C in 1X MMR as described before; generally 2-4 of the frogs lay eggs of sufficient quality for extract preparation), and prepare extracts from the laid eggs and freshly squeezed eggs in parallel. While squeezing the frogs, it is extremely important to avoid getting any frog skin secretions ('frog slime') into the squeezed eggs or the eggs will activate. Frog slime can be avoided by frequently dipping the frog into a bucket of clean distilled water during the squeezing process. Squeezed eggs from different frogs should be kept separate initially, but can be pooled after dejellying if they do not exhibit signs of activation. It is difficult to obtain large quantities of squeezed eggs, but from 4 frogs we generally get enough to fill 1/2-3/4 of a 13 X 51 mm ultraclear tube. The laid eggs and squeezed eggs are separately processed as described above for

the CSF extract prep. It is important to thoroughly wash out residual jelly coat after the dejellying step and to crush the eggs at 10,000 rpm for 15' at 16 °C (full brake). This speed spin results in highly turbid muddy-colored extracts. Faster spins result in clearer extracts that often suffer from extensive and rapid spindle aggregation, resulting in very limited time of manipulation and precluding any significant analysis. We would also like to note that newer frogs that have not been through multiple rounds of ovulation tend to be better for anaphase experiments, although, as with many other aspects of frog egg extracts, this is by no means definitive. Using frogs that have been through less than 2 cycles of ovulation (with at least a 3 month rest between ovulations) after being obtained from a distributor and taking great care in preparing the extracts, we have been able to successfully obtain anaphase extracts on a routine basis (70 % of the time).

## B. Setting up and Monitoring Anaphase Reactions

Anaphase reactions require spindles obtained by cycled spindle assembly as described above (Section III D). It is essential that the cycled spindles have tight metaphase plates; often, chromosomes on the spindles are not confined to a tight metaphase plate but stray over the entire spindle, and these extracts are not useful for anaphase. To perform an anaphase reaction, 9  $\mu$ l of a cycled spindle assembly reaction is mixed with 1  $\mu$ l of the 10X Calcium stock, and monitored by taking fixed time points every 5' for 30'. The added calcium should be mixed well with the extract, either by gently flicking the bottom of the tube or by gently pipeting up and down. The addition of calcium results in the destruction of CSF and exit from the metaphase arrest. Between 5' and 15' after calcium addition, clear evidence for anaphase should be evident in the chromosome morphology as depicted in Figure 3. In

addition to anaphase chromosome movement, changes in spindle structure, particularly thinning out of spindle MT density and expulsion of asters should be evident (Murray et al., 1996). By 25'-30', rounded interphase nuclei should be visible in the reaction. In a good anaphase extract, 40-80% of the spindles show clear evidence of anaphase. However, it is not unusual to have an extract whose spindles have tight metaphase plates but do not exhibit anaphase. In addition, the percentage of spindles that exhibit anaphase often decreases dramatically with aging of the extract.

### C. Real Time Analysis of Anaphase *in vitro*

#### 1. LENGTHENING EXTRACT LIFE SPAN

Although technically challenging, it is possible to observe anaphase *in vitro* in real time allowing detailed analysis of chromosome movement and spindle dynamics. Since there is no reliable procedure for freezing extracts while maintaining anaphase-competency, and since each anaphase reaction takes approximately 30 minutes during which only one spindle can be observed per field-of-view (of which less than 50% will provide analyzable data), it is essential to maximize the life span of the extract to perform real time analysis. We have found it best to stagger the entire spindle assembly reaction by 3.5-4 hours, storing the original extract on ice during the interim, to maximize the amount of time that observational studies can be performed. We find this to be better than storing the extract on ice after cycling through interphase, and have been able to use extracts routinely for 12-16 hours after preparation. We have also had some success with storing the cycled spindles at 10-12 °C and warming them up to room temperature for 10'-15' prior to their use. We note, however, that with increased time spindles will be

present in larger aggregates and the percentage of spindles capable of undergoing anaphase will decline.

## 2. SLIDE AND COVERSLIP CLEANING

*a. Requirements:* water, acetone, ethanol, slides and coverslips (22 x 22 mm; no. 1), hotplate, slide storage box, 100 mm tissue culture dish, coverslip spinner (optional).

It is essential to obtain homogenous sample films to avoid problems derived from air bubbles - we have often watched a spindle just beginning or in the middle of anaphase, only to have a bubble roll into view and wipe it out of existence. The key to good sample films is clean particulate-free slide and coverslip surfaces.

*b. cleaning slides:*

1. Set up three 50 ml conical tubes filled with water, acetone and ethanol and have a hotplate with a clean surface set such that the top feels hot to the touch (50-60 °C).
2. Holding the frosted end, dip the slide several times in water, then in acetone and finally in ethanol. Transfer to the hotplate surface to rapidly dry off the ethanol and store in a covered slide box. It is best to use a reasonably new box of slides to minimize particulates on the slides. If problems with bubbles persist, clean slides in a cup sonicator filled with warm water containing a small amount of detergent and rinse off the detergent prior to cleaning with acetone and ethanol.

*c. cleaning coverslips:*

Coverslips are cleaned exactly as slides, except that coverslip holders are used for rinsing 12 coverslips at a time and that the coverslips are dried using a homemade coverslip spinner. If no spinner is available, the coverslips can be dried by gently wiping both surfaces using lens paper (wear gloves while doing this). Clean coverslips can be stored in a plastic 100 mm tissue culture dish for several weeks.

### 3. SAMPLE PREPARATION

*a. Requirements:* Valap, hotplate (for melting Valap), clean slides and coverslips, 10X Calcium/DAPI stock (4 mM calcium chloride, 750 ng/ml DAPI in 1X Sperm Dilution buffer), extract reactions with cycled spindles

Spindle microtubules are visualized using X-rhodamine tubulin added to the extract just after preparation. Chromosomes are visualized using DAPI and it is most convenient (and least perturbing) to add the DAPI to the calcium stock used for triggering anaphase. The 10X calcium/DAPI stock can be stored indefinitely at -20°C and is not sensitive to freezing and thawing. Prior to sample preparation, make sure that melted Valap is available to seal the sample. Valap is a 1:1:1 mixture of vaseline:lanolin:paraffin prepared by weighing equal amounts of the three components into a beaker, melting and mixing them on a hotplate.

*b. Preparation of sample:*

1. Transfer 9  $\mu$ l of the cycled spindle assembly reaction to an eppendorf tube.
2. Add 1  $\mu$ l of the 10X Calcium/DAPI stock. Mix gently but thoroughly by flicking and pipeting up and down.
3. Pipet 8  $\mu$ l onto a clean slide. Cover gently with a clean 22 x 22 mm coverslip. It is essential not to squash the sample film too vigorously. If there

are a lot of bubbles in the film, the sample should be discarded and a new sample should be prepared; however, it is often impossible to avoid one or two small bubbles near the center of the coverslip.

4. Seal the edges with Valap and start observation (a Q-tip works well as a Valap applicator).

We have experimented with more elaborate schemes to prevent distortion of spindles during sample preparation, such as coating of the slide surface with spacer latex beads, and also with alternative means of sealing the sample that avoid any local heating problems associated with the use of Valap (Murray et al., 1996). However, we find that the simple procedure outlined above is sufficient for observing anaphase and considerably reduces the complexity of sample preparation.

#### 4. SAMPLE OBSERVATION

Given the variable composition of products in a spindle assembly reaction, it is essential to pick the correct type of spindle for observation. We find it best to scan the sample in the DAPI channel using a 20X dry objective lens (with a 25% transmission neutral density filter in the light path) and to select medium-sized spindles with tight metaphase plates for timelapsing. Often, small spindles are too sensitive to flows under the coverslip (which are highly variable from extract to extract) that cause them to either spin around or float out of the field-of-view (both of which make analysis nearly impossible). Larger aggregates, while they do exhibit nice anaphase, tend to be very messy and difficult to analyze. With a little practice, one can begin to pick spindles good for timelapsing anaphase with a frequency of 60-80%.

For acquiring images, we like to use low power dry objectives (20X, 0.5 or 0.75 NA) and a cooled charged-coupled device camera. The minimal

additional requirements for the real time observation are the ability to acquire images at two different wavelengths (X-rhodamine and DAPI), to store the acquired images, and to shutter the illuminating light to minimize photodamage. A detailed description of the microscope setup used to acquire the images shown in Figure 4 has been published (Salmon et al., 1994). Analysis of chromosome movement and spindle microtubule density can be performed on the collected images using one of several commercially available image analysis software packages.

#### D. Manipulation of Anaphase *in vitro*

Manipulation of anaphase reactions has been restricted to addition of either non-degradable cyclin (cyclin  $\Delta 90$ ) or pharmacological agents. For addition of cyclin  $\Delta 90$ , titrate the cyclin concentration such that physiological levels of H1 kinase are attained (Murray et al., 1989). For optimal results, the cyclin  $\Delta 90$  must be added to the extract for 20'-30' prior to triggering anaphase by addition of calcium. In the presence of cyclin  $\Delta 90$  sister separation appears normal although spindle microtubule density near the spindle poles does not decline and chromosome decondensation and formation of nuclei does not occur. For addition of pharmacological agents, trigger anaphase by adding 1/10 vol of a 10X Calcium/Agent stock and monitor as described above. If anaphase is being monitored in real-time, then add the agent from a 10X Calcium/DAPI/Agent stock. We have successfully used real-time analysis to monitor the effects of cyclin  $\Delta 90$ , AMPPNP, taxol, and vanadate on anaphase.

The more ambitious manipulation of depleting specific components and assaying the effect on chromosome segregation remains a technical challenge for the future. However, addition of reagents to anaphase reactions has been very useful, leading to the important discoveries that activation of

the cyclin destruction machinery is sufficient to promote sister chromatid separation and that topoisomerase II activity is required for sister separation (Shamu and Murray, 1992; Holloway et al., 1993).

## VIII. Conclusions

In this chapter we have described detailed procedures for the preparation of spindle assembly extracts, for manipulation of extracts to define the function of specific proteins in spindle assembly, and for the analysis of anaphase chromosome movement *in vitro*. The importance of *Xenopus* extracts for analyzing spindle assembly and function is evident from their increasing use in recent years. However, many technical advances remain to be made to allow a realization of the full potential of *Xenopus* extracts, particularly with respect to the manipulation and storage of extracts. We hope that the methods we have described will serve as a starting point for future studies on spindle assembly and function and will stimulate technical innovations that will expand the types of analyses possible using *Xenopus* egg extracts.

## ACKNOWLEDGMENTS

We thank Manfred Lohka and Yoshio Masui whose pioneering work led to the use of *Xenopus* egg extracts for studying spindle assembly and function; Manfred Lohka and James Maller, whose early observations on *in vitro* spindles led to the development of the spindle assembly reactions described here; Ken Sawin, who characterized the pathways of spindle assembly and performed the first immunodepletions and Caroline Shamu, who developed the *in vitro* anaphase reaction. We also thank Ted Salmon for his contributions to the analysis of anaphase *in vitro* and for many



stimulating discussions on spindle assembly and chromosome movement. Finally, we thank our colleagues in the *Xenopus* extract field and members of our laboratories for many technical discussions on performing extract experiments. This work was supported by an HHMI pre-doctoral fellowship to A.D, grants from the NIH and Packard Foundation to A.M, grants from the NIH and HFSP to T.J.M, and post-doctoral fellowships from the NIH and the DOD Breast Cancer Research Program to C.E.W.

#### REFERENCES

- Belmont, L. D., A. A. Hyman, K. E. Sawin and T. J. Mitchison (1990). "Real-time visualization of cell cycle dependent changes in microtubule dynamics in cytoplasmic extracts." Cell 62, 579-589.
- Blangy, A., H. A. Lane, P. d'Hérin, M. Harper, M. Kress and E. A. Nigg (1995). "Phosphorylation by p34cdc2 regulates spindle association of human Eg5, a kinesin-related motor essential for bipolar spindle formation *in vivo*." Cell 83, 1159-1169.
- Blow, J. J. and R. A. Laskey (1986). "Initiation of DNA replication in nuclei and purified DNA by a cell-free extract of *Xenopus* eggs." Cell 47, 577-587.
- Boleti, H., E. Karsenti and I. Vernos (1996). "Xklp2, a novel *Xenopus* centrosomal kinesin-like protein required for centrosome separation during mitosis." Cell 84, 49-59.
- Desai, A., H. W. Deacon, C. E. Walczak and T. J. Mitchison (in press). "A method that allows the assembly of kinetochore components onto chromosomes condensed in clarified *Xenopus* egg extracts." Proc. Natl. Acad. Sci.

Enos, A. P. and N. R. Morris (1990). "Mutation of a gene that encodes a kinesin-like protein blocks nuclear division in *A. nidulans*." Cell 60, 1019-1027.

Evans, L., T. J. Mitchison and M. W. Kirschner (1985). "Influence of the centrosome on the structure of nucleated microtubules." J Cell Biol 100, 1185-1191.

Flemming, W. (1965). "Contributions to the knowledge of the cell and its vital processes. Part II." J. Cell Biol. 25, 3-69.

Gaglio, T., M. A. Dionne and D. A. Compton (1997). "Mitotic spindle poles are organized by structural and motor proteins in addition to centrosomes." J. Cell Biol.

Gaglio, T., A. Saredi, J. Bingham, J. Hasbani, S. R. Gill, T. A. Schroer and D. A. Compton (1996). "Opposing motor activities are required for the organization of the mammalian mitotic spindle pole." J. Cell Biol. 135, 399-414.

Gaglio, T., A. Saredi and D. A. Compton (1995). "NuMA is required for the organization of microtubules into aster-like mitotic arrays." J. Cell Biol. 131, 693-708.

Hagan, I. and M. Yanagida (1990). "Novel potential mitotic motor protein encoded by the fission yeast *cut7+* gene." Nature 347, 563-6.

Heald, R., R. Tournebize, T. Blank, R. Sandaltzopoulos, P. Becker, A. Hyman and W. Karsenti (1996). "Self-organization of microtubules into bipolar spindles around artificial chromosomes in *Xenopus* egg extracts." 382, 420-425.

Heald, R., R. Tournebize, A. Habermann, E. Karsenti and A. Hyman (1997). "Spindle assembly in *Xenopus* egg extracts: respective roles of centrosomes and microtubule self-organization." J. Cell Biol. 138, 615-628.

Heald, R., R. Tournebise, I. Vernos, A. Murray, A. Hyman and E. Karsenti (in press). *In vitro* assays for mitotic spindle assembly and function. Cell Biology: A Laboratory Handbook. J. Celis.

Hirano, T. and T. J. Mitchison (1991). "Cell cycle control of higher-order chromatin assembly around naked DNA *in vitro*." J Cell Biol 115, 1479-89.

Holloway, S. L., M. Glotzer, R. W. King and A. W. Murray (1993). "Anaphase is initiated by proteolysis rather than by the inactivation of MPF." Cell 73, 1393-1402.

Hoyt, M. A., L. He, K. K. Loo and W. S. Saunders (1992). "Two *Saccharomyces cerevisiae* kinesin-related gene products required for mitotic spindle assembly." J. Cell Biol. 118, 109-120.

Hutchison, C. J., R. Cox and C. C. Ford (1988). "Periodic DNA synthesis in cell-free extracts of *Xenopus* eggs." EMBO 6, 2003-2010.

Hyman, A., D. Drechsel, D. Kellogg, S. Salser, K. Sawin, P. Steffen, L. Wordeman and T. Mitchison (1991). "Preparation of modified tubulins." Meth. Enzymol. 196, 478-485.

Lohka, M. J. and J. L. Maller (1985). "Induction of nuclear envelope breakdown, chromosome condensation, and spindle formation in cell-free extracts." J. Cell Biol. 101, 518-523.

Lohka, M. J. and Y. Masui (1983). "Formation *in vitro* of sperm pronuclei and mitotic chromosomes induced by amphibian ooplasmic components." Science 220, 719-721.

Merdes, A., K. Ramyar, J. D. Vechio and D. W. Cleveland (1996). "A complex of NuMA and cytoplasmic dynein is essential for mitotic spindle assembly." Cell 87, 447-458.

Murray, A. W. (1991). Cell cycle extracts. Methods in Cell Biology. B. K. Kay and H. B. Peng. San Diego, Academic Press. 36, 581-605.

- Murray, A. W., A. B. Desai and E. D. Salmon (1996). "Real time observation of anaphase *in vitro*." Proc. Natl. Acad. Sci. 93, 12327-32.
- Murray, A. W. and M. W. Kirschner (1989). "Cyclin Synthesis Drives the Early Embryonic Cell Cycle." Nature 339, 275-280.
- Murray, A. W., M. Solomon and M. W. Kirschner (1989). "The role of cyclin synthesis in the control of maturation promoting factor activity." Nature (Lond.) 339, 280-286.
- Roof, D. M., P. B. Meluh and M. D. Rose (1992). "Kinesin-related proteins required for assembly of the mitotic spindle." J. Cell Biol. 118, 95-108.
- Sagata, N., N. Watanabe, G. F. Vande Woude and Y. Ikawa (1989). "The c-mos proto-oncogene is a cytostatic factor responsible for meiotic arrest in vertebrate eggs." Nature 342, 512-518.
- Salmon, E. D., T. Inoue, A. Desai and A. W. Murray (1994). "High resolution multimode digital imaging system for mitosis studies *in vivo* and *in vitro*." Biological Bulletin 187, 231-232.
- Sawin, K. E., K. LeGuellec, M. Philippe and T. J. Mitchison (1992). "Mitotic spindle organization by a plus-end directed microtubule motor." Nature 359, 540-543.
- Sawin, K. E. and T. J. Mitchison (1991). "Mitotic spindle assembly by two different pathways *in vitro*." J. Cell Biol. 112, 925-940.
- Shamu, C. E. and A. W. Murray (1992). "Sister chromatid separation in frog egg extracts requires DNA topoisomerase II activity during anaphase." J. Cell Biol. 117, 921-934.
- Verde, F., J.-c. Labbe, M. Doree and E. Karsenti (1990). "Regulation of microtubule dynamics by cdc2 protein kinase in cell-free extracts of *Xenopus* eggs." Nature 343, 233-238.

Vernos, I., J. Raats, T. Hirano, J. Heasman, E. Karsenti and C. Wylie (1995). "Xklp1, a chromosomal *Xenopus* kinesin-like protein essential for spindle organization and chromosome positioning." Cell 81, 117-127.

Walczak, C. E., T. J. Mitchison and A. Desai (1996). "XKCM1: A *Xenopus* kinesin-related protein that regulates microtubule dynamics during mitotic spindle assembly." Cell 84, 37-47.

Walczak, C. E., S. Verma and T. J. Mitchison (1997). "XCTK2: A Kinesin-related protein that promotes mitotic spindle assembly in *Xenopus laevis* egg extracts." J. Cell Biol. 136, 859-870.

#### FIGURE LEGENDS

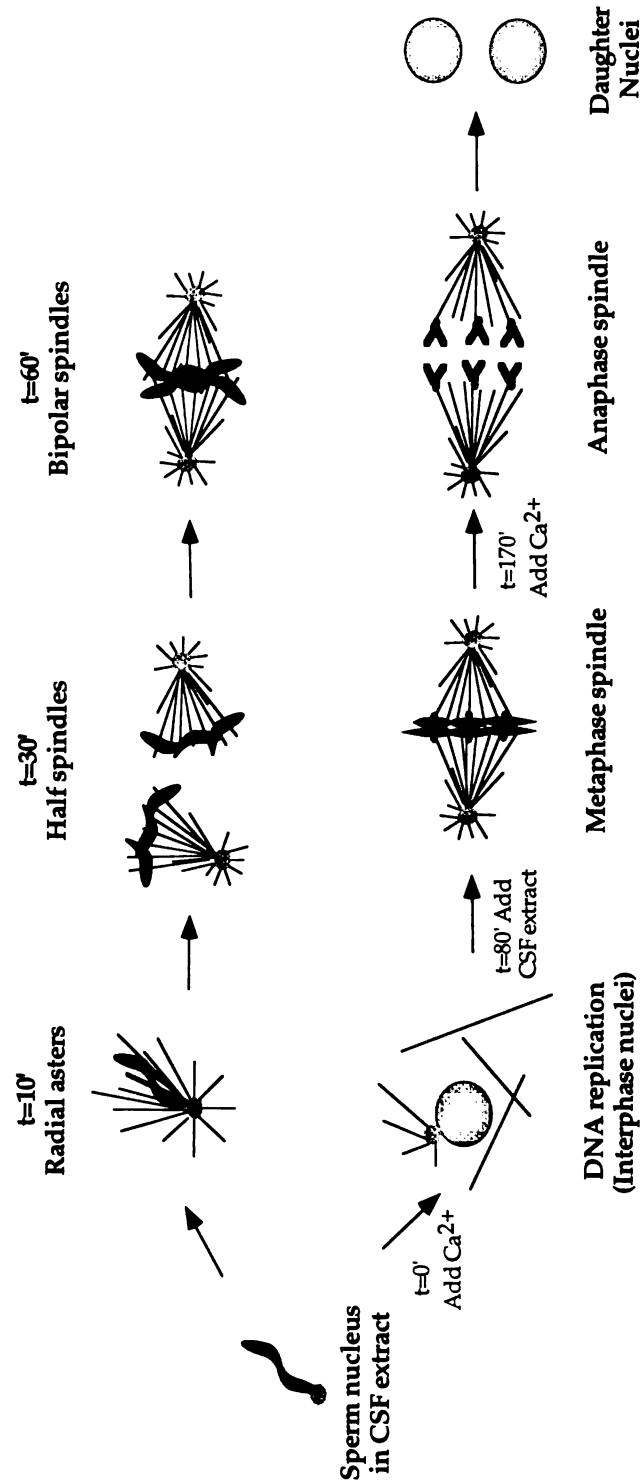
Figure 1. Cartoon diagramming the *in vitro* spindle assembly pathways. (Top) CSF spindle assembly. (Bottom) Cycled spindle assembly.

Figure 2. Reaction intermediates of CSF Spindle Assembly Reaction. Samples were removed from the reaction and sedimented onto coverslips as described in the text. The microtubules and chromatin structures formed during the reaction are shown for 15', 30', and 60' time points.

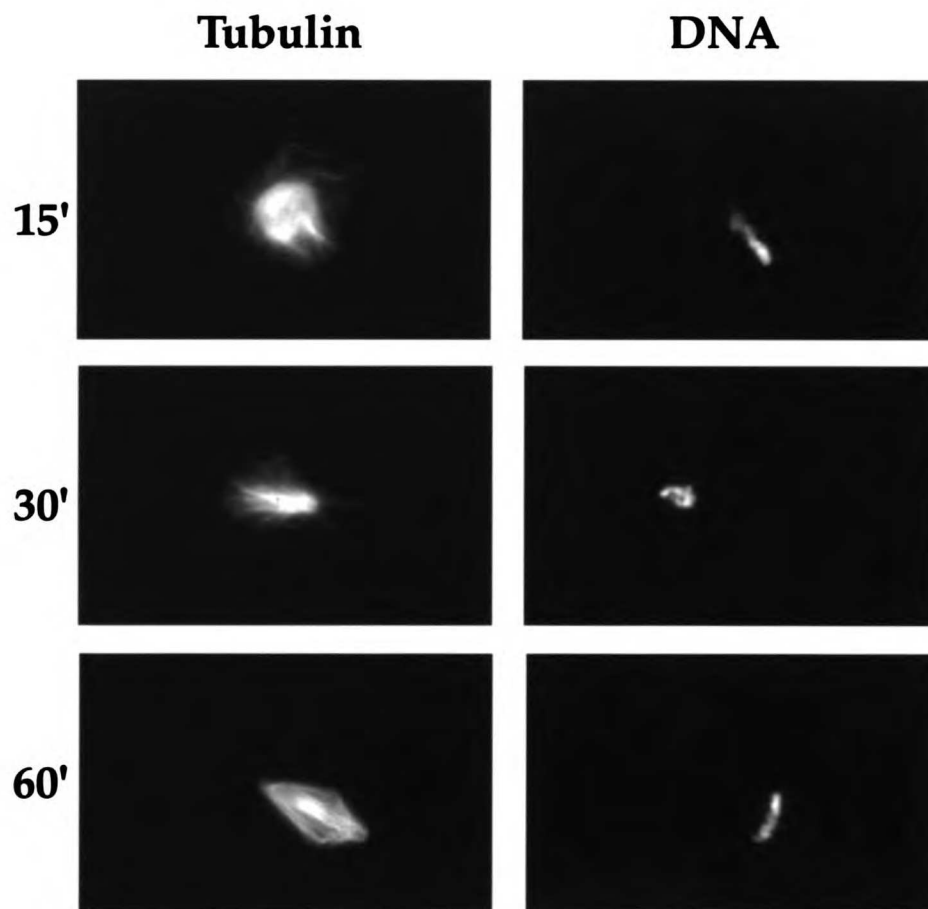
Figure 3. Optimal Fixation of Spindle Structures. Using the optimized fixation conditions it is possible to preserve chromosome structure and microtubule structure. Top panels are metaphase spindles assembled by the cycled spindle pathway. Bottom panels are spindles that have been induced to enter anaphase following calcium addition.

Figure 4. Time Course of Anaphase Chromosome Movement. Individual frames are presented from a time-lapse recording of anaphase *in vitro*.

Figure 1



U U U I L L W A I I

**Figure 2**

**Figure 3**

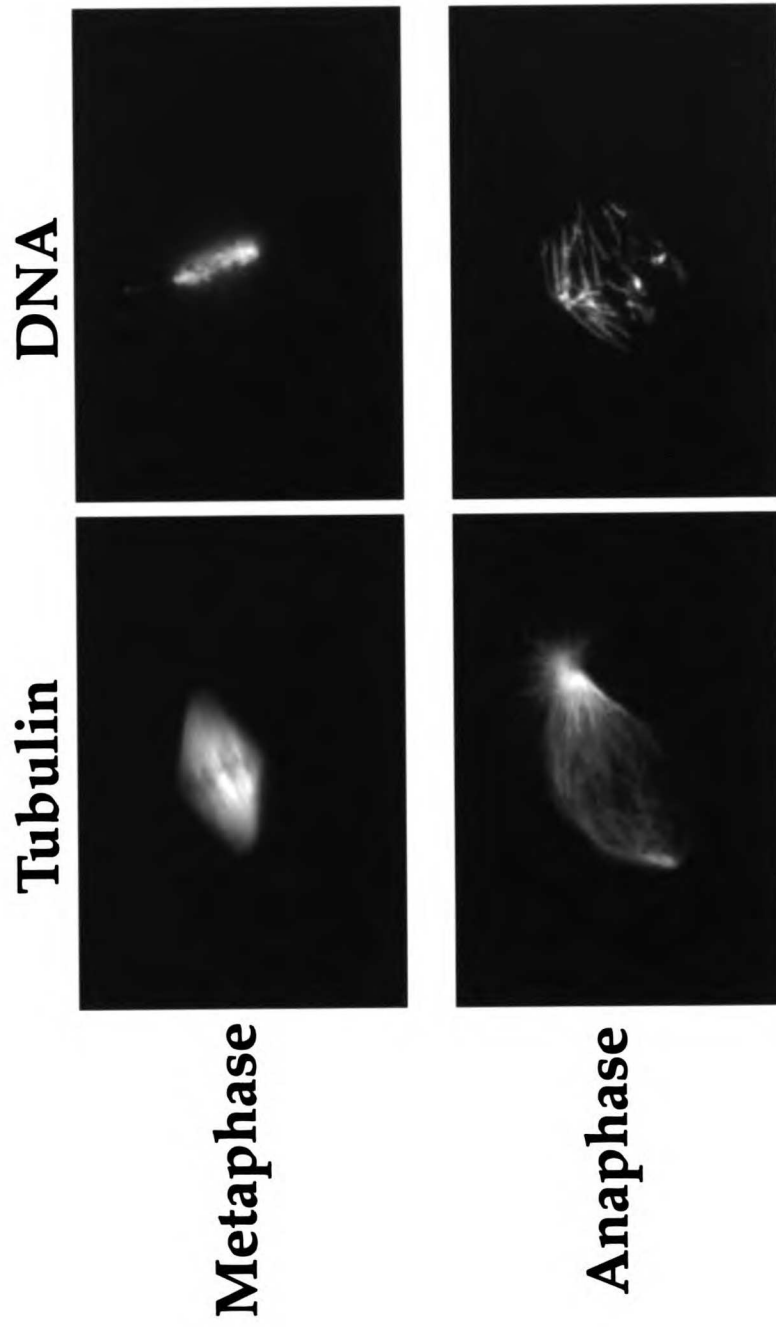
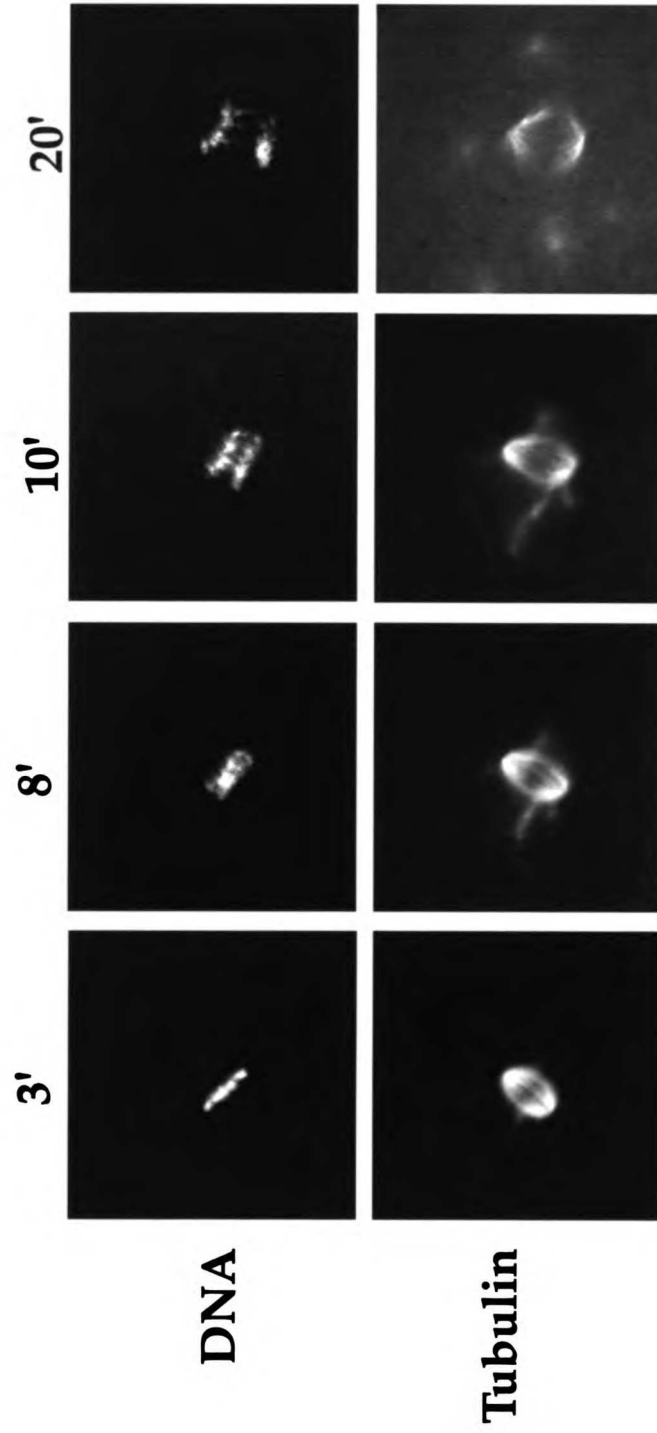




**Figure 4**



## Appendix III

### A Compendium of Microtubule Methodology

U  
S  
N  
A  
L  
A  
R  
C  
H  
I  
V  
E

## A Compendium of Microtubule Methodology

<b>1. Tubulin Basics.....</b>	<b>161</b>
<b>2. Large Scale Tubulin Preparation.....</b>	<b>163</b>
<b>3. Recycling Tubulin.....</b>	<b>171</b>
<b>4. Labeling Tubulin and Quantifying Labeling Stoichiometry.....</b>	<b>173</b>
<b>5. Tubulin Polymerization with GTP/GMPCPP/Taxol.....</b>	<b>180</b>
<b>6. Preparation of Segmented and Polarity Marked Microtubules.....</b>	<b>185</b>
<b>7. Microtubule Spindowns for Visual Analysis.....</b>	<b>189</b>
<b>8. Flow Cell Assays with Microtubules: Motility / Dynamics in Fluorescence and VE-DIC.....</b>	<b>191</b>
<b>9. Negative Stain Electron Microscopy of Microtubules.....</b>	<b>199</b>

(The protocols described here have evolved over many years through the collective efforts of members of the Mitchison, Kirschner, Alberts and Vale labs)

## 1. Tubulin Basics

### I. Useful Values

1 mg/ml tubulin = 10  $\mu$ M (assuming MW of heterodimer is 100,000; in reality it is ~110,000 but almost all tubulin labs use this convenient conversion relationship)

1  $\mu$ m of a microtubule has ~1700 tubulin heterodimers

Extinction coefficient of tubulin at 280 nm = 115,000  $M^{-1}cm^{-1}$  or 1.15  $(mg/ml)^{-1} cm^{-1}$ ; assuming that the MW of an  $\alpha\beta$  heterodimer is 100,000 daltons. This extinction coefficient was calculated from tubulin sequences and includes the contribution of the two bound guanine nucleotides to the absorbance at 280 nm

### II. Handling Tubulin

Tubulin is a labile molecule that converts to a non-polymerizing state within hours on ice. This lability demands a certain amount of care and discipline when handling tubulin. The following is what we recommend for general use of tubulin:

1. Tubulin is very stable at  $-80^{\circ}C$  and is best stored in small aliquots at this temperature. We generally prepare tubulin in large scale (see page 163) and store large aliquots of phosphocellulose column fractions at  $-80^{\circ}C$ . We recycle 3-4 of these large aliquots (see page 171) and store small aliquots of the recycled tubulin at  $-80^{\circ}C$  for daily use. One or more recycled aliquots is thawed for an experiment, and any leftover material discarded. Refreezing thawed aliquots of recycled tubulin is not recommended.

2. To use recycled tubulin, rapidly thaw the aliquot by placing it in a 37°C bath straight from the -80°C freezer (or from a liquid nitrogen dewar -- we often use liquid nitrogen to bring tubulin aliquots from the freezer to the 37°C bath/benchttop). When the tubulin is nearly thawed (i.e. when there is a very small amount of ice left in the tube) transfer the tube to an ice bucket; mix it by gentle flicking ~20s later and store on ice. Use the thawed tubulin for polymerization preferably within 30' of thawing. When quantitative analysis of tubulin polymerization is necessary, careful and consistent handling of tubulin aliquots is essential for reproducible results.

## 2. Large Scale Tubulin Preparation

Tubulin is purified from bovine/porcine brain by two cycles of polymerization/depolymerization followed by removal of copurifying proteins on a phosphocellulose (PC) column. The procedure described here is for a large scale prep (10 cow brains) that yields 1-4 grams of tubulin. The protocol can be scaled down if such a large prep is either not necessary or not doable. For ease of organization, all the pre-prep and day-of-prep activities are listed in outline form before details about the prep itself.

### I. Tubulin Prep Outline

#### Pre-Prep:

1. Call slaughterhouse and request fresh brains to be picked up the morning of prep
2. Pour and equilibrate phosphocellulose column
3. Make buffers
4. Ensure that reagents, such as ATP and GTP, are present in sufficient amount for the prep
5. Sign up for centrifuges and rotors and gather centrifuge tubes, blenders and motorized homogenizer/dounce
6. Prepare cooler for transporting brains night before prep and organize coldroom for morning mayhem

#### Prep Day:

7. Remove meninges, brain stems and blood clots, weigh and homogenize brains in blenders
8. Clarify homogenate and use supernatant for 1st polymerization cycle
9. Collect 1st cycle polymer fraction by centrifugation

10. Depolymerize 1st cycle polymer by homogenization at 0-4°C
11. Clarify depolymerization mix and use supernatant for 2nd polymerization cycle
12. Collect 2nd cycle polymer fraction by centrifugation
13. Depolymerize 2nd cycle polymer by homogenization at 0-4°C
14. Clarify depolymerization mix and load supernatant onto PC column
15. Collect flowthrough from PC column, aliquot and freeze at -80°C

## II. Buffers & Nucleotides

PB (Pipes/Polymerization Buffer): 0.1 M Pipes, pH 6.8, 0.5 mM MgCl<sub>2</sub>, 2 mM EGTA, 0.1 mM EDTA, 0.1 % β-mercaptoethanol, 1 mM ATP. Need 8 liters in coldroom

(Add ATP and BME just prior to beginning the prep)

CB (Column Buffer): 50 mM K-Pipes, pH 6.8; 1 mM EGTA; 0.2 mM MgCl<sub>2</sub>.

Need ~25 liters for equilibration, running and storage of PC column

CB + 1 M KCl: Need ~10 liters for prewashing and eluting the PC column

To make 1L of 10X CB:

151.2 grams PIPES, free acid

3.8 grams EGTA

2 ml of 1 M MgCl<sub>2</sub>

pH with KOH to pH 6.75, and bring up to 1 liter. Check pH at 1X is 6.7

Make 3.5 liters of 10X CB for 10-12 brain prep.

GTP- Sigma Type IIS- # G-8752

ATP- Sigma Grade 1- # A-2383

Glycerol -- 2-3L prewarmed to 37°C (store overnight in 37°C incubator)

### III. Preparing a 1L Phosphocellulose (PC) Column (begin 4-5 days before prep)

Resin: Whatman P11 Cellulose Phosphate -- fibrous cation exchanger

(1 gram of PC swells to about 4 ml packed resin)

Summary: To pour a 1L column, start with 220 grams dry resin divided into 5 aliquots of 44 grams. Treat each aliquot with acid/base in a 2L beaker as described below. Older procedures described the use of large Buchner funnels to rapidly remove the acid/base. However, gentle stirring of the resin with a plastic/glass rod to suspend it in a 2L beaker, followed by settling of the resin for 5' by gravity has worked well for us. This method also incorporates defining of the resin into the acid/base cycling protocol. After acid/base treatment the resin is washed well, packed, treated with BSA to block irreversible binding sites and equilibrated for use.

#### Solutions & Supplies:

5L 0.5N NaOH	220 grams Phosphocellulose
5L 0.5N HCl	5 2L beakers
13L 0.5M K-Phosphate, pH 6.8	1-1.5L cleaned column housing
5L ddH <sub>2</sub> O	2 stirring rods
12L CB + 1M KCl (see page 164)	Peristaltic pump
20L CB (see page 164)	2 aspirators with large traps and
300 ml 30 mg/ml BSA in CB (filtered)	10 ml plastic pipets as inlets

#### Column Preparation Procedure:

1. Pour 1L 0.5N NaOH into 5 x 2L beakers. Add 44 grams PC to each beaker stirring gently with a rod until the PC is wetted and an even slurry is present. Let stand at room temperature for 5'.
2. Aspirate off supernatant, including fines, and quickly add 1L 0.5M K-phosphate to neutralize, gently mixing with a rod. Check that pH is ~7 and let stand 5'.



3. Aspirate off supernatant, add 1L ddH<sub>2</sub>O and gently stir to resuspend settled resin. Allow the resin to settle.
5. Aspirate off supernatant, add 1L 0.5N HCl, gently stir to resuspend and wait 5'.
6. Aspirate off supernatant, add 1L 0.5M K-phosphate, stir and check pH is 7.
7. After resin has settled, aspirate supernatant and combine all the resin in a 4L beaker. Use the remaining 0.5M K-phosphate to wash the resin by resuspending, letting settle and aspirating the supernatant.
8. Wash 3 x 1L CB + 1M KCl as done in 7.
9. In the cold room, pour the resuspended resin into the column housing (with a mark approx. 50 cm high in a 5 cm ID housing) and pack by pumping from the bottom (i.e. the peristaltic pump is "sucking" buffer from the bottom of the column and depositing it into a waste jug). Pack at 45 ml/hour/cm cross-sectional area. For a 5 cm diameter column this is ~880 ml/hour or ~14.5 ml/min. After resin is packed, switch to pumping from the top. Run 7L of CB + 1M KCl through the column at 5-10 ml/min.
10. Wash with 10L CB. Check conductivity to ensure that all the KCl is gone. The resin may expand as the salt is washed out so make sure there is a large buffer head on the resin bed.
11. Load 300 ml of 30 mg/ml BSA (Fraction V; filtered) in CB, follow with 700 ml CB and stop the column. Leave the column sitting for 2 hr during which the BSA blocks irreversible binding sites on the resin -- this is very important the first time a column is used to prevent loss of the tubulin.
12. Wash the column with 2L CB + 1M KCl to elute BSA that is not irreversibly bound.
13. Wash column with 10L of CB. The column is now ready for use.

#### **IV. Brains**

It is essential to get fresh brains (they should be warm when handed to you at the slaughterhouse) -- yields decline significantly if the brains have been stored for a while after removal. Frozen brains do not work for preparing tubulin. The best preps have been done with freshly removed brains transported in an ice-filled cooler to the lab within 1-2 hours of removal. For transporting 10-12 brains from the slaughterhouse, we use 2 size 16 Coleman coolers containing 3 liters of cooled 1.5% (w/v) NaCl to which one large bag of party ice is added on the way to the slaughterhouse.

#### **V. Centrifuges and Rotors**

6 Sorvall RC-5C or equivalent lowspeed centrifuges

6 GSA or equivalent rotors (cold)

4 Beckman ultracentrifuges

4 Type 19 rotors (warm)

2 Type 35 rotors (warm)

2 Type 45Ti rotors (cold; need to warm up one after 1st cold use)

1 Type 50.2Ti rotor (cold)

cold = 4°C (put overnight in cold room)

warm = 37°C (put the rotors overnight in a large bacterial shaker set to 37°C)

#### **VI. Protocol:**

1. In the cold room, remove meninges (membrane surrounding the brain; best done by using paper towels to "blot" the brain surface), blood clots, and brain stems; weigh the brains and homogenize with equal volume of PB for 3 x 15s in a Waring blender.

2. Collect homogenate (~8-9 liters), transfer into 36 GSA bottles and spin 90' at 12K in a GSA rotor at 4°C.
3. Collect supernatant and transfer 1 liter to a 1.8L glass Fernbach flask that has 500 ml of 37°C glycerol. Add 0.1 mM GTP, 0.5 mM ATP, and 3.5 mM MgCl<sub>2</sub> (this gives 0.1 mM GTP, 1.5 mM ATP and 4 mM MgCl<sub>2</sub> final). The ATP and GTP are added as solids. Hold the flask in a warm water-filled sink and swirl constantly to dissolve the solids and to mix in the glycerol. Transfer to a 37°C bath, monitor temperature of mixture using a clean thermometer and polymerize for 60' after the temperature of the sample has reached 32°C. The approach to 37°C can be accelerated by swirling the flask in a large hot water (~50°C temperature) reservoir -- constant swirling is essential in this case to disperse the heat evenly and care must be taken to avoid overheating the mixture.
4. Transfer the polymerization mixture to Type 19 bottles, and spin for 2.5 hrs at 19K in 4 Type 19 rotors at 35°C. Use an additional Type 35 at 17.5K for 2.5 hrs if necessary. At the end of the spin set centrifuges to 4°C.
5. Decant and discard supernatant. In the cold room, resuspend the gelatinous pellets aiming for a final volume of ~700-800 ml. We use ~40-50 ml for 3 tubes, sequentially removing the pellets from each tube using a plastic scraper and making sure that all tubes get rinsed once or twice after the majority of the large gelatinous pellet has been removed. To homogenize the chunky pellet resuspension, we use a Yamato "pour-through" continuous flow homogenizer -- this is a device that drives a motorized teflon pestle in a funnel shaped glass barrel. Mixtures poured on top get homogenized by the pestle as they travel through the middle of the barrel and come out the bottom. We Yamato the chunky pellets till the resuspension is a smooth yellow liquid of ~700-800 ml total volume. After all the pellets are

homogenized, we depolymerize on ice for ~30' during which we continue Yamatoing the mixture once every 3'-5'. A large motorized teflon dounce or large tip sonicator can be used as alternatives to the Yamato for resuspending the chunky pellets. Check protein concentration by Bradford using BSA as a standard. If >20 mg/ml (which is unlikely), dilute to 20 mg/ml.

6. Spin the depolymerization mixture 30' at 35K in 2 Type 45 rotors at 4°C. At the end of the spin set the centrifuges to 35°C.

7. Decant supernatant into a 1L graduated cylinder in coldroom and measure volume. Pour into a 1.8L Fernbach flask, add half volume of 37°C glycerol, solid GTP to 0.5 mM final and MgCl<sub>2</sub> to 4 mM final (additional 3.5 mM). Set up polymerization as described in 3. above. Polymerize for 40' after temperature of mixture has reached 32°C.

8. Spin the polymerization mixture at 35 K at 35 °C for 1 hr in 2 Type 35s + 1 Type 45. Make sure one chilled centrifuge is available for the next spin.

9. Discard supernatant and resuspend pellets in a final volume of ~100-150 ml of CB, as described above in 5. Protein concentration by Bradford should not be more than 25 mg/ml. Depolymerize on ice for 40' and then spin the depolymerization mix 30' at 40K in a 50.2Ti rotor at 4°C.

10. Collect supernatant, measure concentration by Bradford and load onto the PC column (approx. 50 cm high X 5 cm ID = ~ 1L; Flow rate = 6 ml/min).

After the sample is loaded and ~150 ml buffer has flowed through start collecting fractions. The eluted tubulin will be apparent by its slight yellowish tinge. Measure concentration by Bradford using BSA as a standard and pool such that the final concentration is between 5-10 mg/ml. Mix pool on ice, make 3 ml aliquots in 5 ml snapcap polypropylene tubes and freeze in liquid nitrogen. Store frozen aliquots at -80°C.

The entire procedure, from time of arrival of brains till freezing of the tubulin will take ~17-18 hours. The next day, run 3 volumes of CB + 1M KCl to elute MAPs from the PC column (these can be collected if desired), and then equilibrate column into CB + 0.1% azide for storage. Phosphocellulose will lose capacity when stored wet -- this can be reduced by storage in a phosphate buffer (50 mM phosphate, pH 7 with 1 mM EGTA and 0.2 mM  $MgCl_2$ ) containing 0.1% azide.

### 3. Recycling Tubulin

We "recycle" tubulin fractions stored at  $-80^{\circ}\text{C}$  after the PC column and store the recycled tubulin in small aliquots for day-to-day use. We generally store recycled tubulin in Injection Buffer (IB) without free GTP. We do this because depolymerization appears to be much better in IB, IB is ideal for microinjections/adding tubulin to extracts, and the absence of free GTP makes polymerization with GMPCPP, a very useful GTP analog that has  $\sim 5\text{-}10\text{X}$  lower affinity than GTP for tubulin, relatively straightforward.

#### I. Solutions & Supplies

5X BRB80: (1X = 80 mM K-Pipes, 1 mM  $\text{MgCl}_2$ , 1 mM EGTA, pH 6.8 with KOH; store 5X BRB80 stock at  $4^{\circ}\text{C}$ )

10X IB: 500 mM K-glutamate; 0.5 mM  $\text{MgCl}_2$ , (pH of 1X  $\sim 7.0$ ; store 10X stock at  $-20^{\circ}\text{C}$ ; see pg 173-174 for details on making up IB)

Cushion: 60% glycerol in 1X BRB80 (warm =  $37^{\circ}\text{C}$ )

100 mM GTP

Glycerol

Small Dounce (2 ml)

50.2Ti rotor (warm =  $37^{\circ}\text{C}$ )

TLA100.2 or 100.3 rotor (cold =  $2\text{-}4^{\circ}\text{C}$ )

#### II. Recycling Protocol:

1. Thaw 3-4 3 ml PC column fractions at  $37^{\circ}\text{C}$ . Transfer to ice and mix in a 50 ml conical.
2. Add BRB80 to 0.5X, 4 mM  $\text{MgCl}_2$  and 1 mM GTP. This is assuming that the tubulin aliquots are in CB (50 mM K-Pipes, pH 6.8; 1 mM EGTA; 0.2 mM

MgCl<sub>2</sub>). Thus, the final buffer composition is 90 mM K-Pipes, pH 6.7, 1.5 mM EGTA, 4.2 mM MgCl<sub>2</sub>, 1 mM GTP. Mix by swirling and store on ice for 5'.

3. Transfer to 37°C. After 2' add half volume of glycerol (I find it convenient to pour in the glycerol on a balance, using density for glycerol = 1.26 g/ml).

Mix the glycerol in by gentle vortexing. Incubate at 37°C for 40'.

4. Layer on a warm 60% glycerol in BRB80 cushion (10-14 ml) in two 50.2Ti (or equivalent) tubes. Spin for 45' at 40K at 35°C in a 50.2 rotor.

5. Aspirate sample, rinse sample cushion interface with warm IX IB 2-3 times. Aspirate completely and rinse the tubulin pellet 2X with warm 1X IB to remove any residual glycerol. Do this while the pellet is held in a 37°C bath -- fill tube ~half-way with warm IB (rinsing sides and pellet well), then aspirate and repeat. This greatly reduces glycerol and GTP contamination in the final tubulin stock.

6. Resuspend pellet in 1-2 ml of ice cold IB (the exact volume will depend on the concentration and polymerizability of the tubulin in the column fractions). Transfer the chunky pellet in IB to an ice-cold 2 ml dounce. Gently dounce on ice to break up the chunks. Incubate at 0°C for 30'. During this cold depolymerization, keep douncing gently every 2'-3'. Gentle sonication can also be used to break up the pellets.

7. Spin 90K in TLA100.2 or TLA100.3 rotor at 2°C for 10'-15' to clarify the depolymerization mix.

8. Collect supernatant on ice and measure A<sub>280</sub> of a 1/100 dilution in IB. Calculate concentration of tubulin using an extinction coefficient of 115,000 M<sup>-1</sup>cm<sup>-1</sup>. Freeze in 10-50 µl aliquots in liquid nitrogen and store at -80°C.

(Note: 1 mg/ml tubulin = 10 µM)

#### 4. Labeling Tubulin and Quantifying Labeling Stoichiometry

This is a general procedure for coupling moieties with reactive succinimidyl esters to tubulin and we have used it successfully to derivatize tubulin with succinimidyl esters of biotin, digoxigenin, and a wide range of fluorochromes such as tetramethylrhodamine, X-rhodamine, fluorescein, Oregon Green, Cy3, Cy5 and C2CF (bis-caged carboxyfluorescein). The procedure involves labeling polymeric tubulin, thereby protecting residues important for microtubule assembly. The labeling is performed at high pH to optimize the reaction with the succinimidyl esters and functional tubulin is selected after the labeling reaction by one or more cycles of polymerization and depolymerization.

##### I. Solutions and Supplies:

bovine brain tubulin (5-10 mg/ml; 2-4 3 ml aliquots of PC fractions)

Dye stock in anhydrous DMSO (20-100 mM)

BRB80 (1X): 80 mM PIPES, 1 mM MgCl<sub>2</sub>, 1 mM EGTA, pH 6.8 with KOH

(generally made as a 5X stock and stored at 4 °C)

High pH Cushion: 0.1 M NaHEPES, pH 8.6, 1 mM MgCl<sub>2</sub>, 1 mM EGTA, 60%

(v/v) glycerol

Labeling Buffer: 0.1M NaHEPES, pH 8.6, 1 mM MgCl<sub>2</sub>, 1 mM EGTA, 40%

(v/v) glycerol

Quench: 2X BRB80, 100 mM K-Glutamate, 40% (v/v) glycerol

Low pH cushion: 60% (v/v) glycerol in 1X BRB80

10X IB (Injection Buffer): 500 mM K-Glutamate, 5 mM MgCl<sub>2</sub> (pH of 1X ~ 7.0)

50.2Ti rotor (warm = 37°C)

TLA100.4 or TLA100.3 and TLA100.2 rotors

Small Dounce (2 ml)



*Note:* 1M HEPES, pH to 8.6 with NaOH and store at -20 °C

2M K-Glutamate - dissolve glutamic acid to 2M, carefully pH with KOH such that 50 mM has a pH ~7.0 and store at -20°C

(All buffers for labeling can be stored indefinitely at -20°C; dye stocks are best prepared fresh from powder that has been stored anhydrously at -20°C; residual dye solution can be stored at -20°C or -80°C under anhydrous conditions)

## **II. Labeling Protocol**

The procedure described below can be scaled down if desired. It is essential to perform all steps involving caged dyes under a safelight in a room well-shielded from light. A piece of red acetate sheet taped over a dimly lit lamp is adequate as a safelight. Other dye labelings can be done under room light, minimizing exposure during incubations by using foil.

1. Thaw 2-4 PC column fractions (30-60 mg tubulin) and add BRB80 to 0.5X, MgCl<sub>2</sub> to 3.5 mM, GTP to 1 mM and store on ice for 5'. Transfer to 37°C and add DMSO to 10% final in two steps, mixing gently but thoroughly and incubate at 37 °C for 30 min. Alternatively, add half volume of glycerol to promote polymerization. In a side-by-side comparison, for reasons that are not clear, using DMSO instead of glycerol for the first polymerization step appears to increase the labeling stoichiometry by ~25% for C2CF-SNHS ester. For labeling with rhodamine (tetramethylrhodamine NHS ester) and X-rhodamine, we generally use glycerol polymerization.
2. Layer polymerized tubulin onto 20 ml warm High pH Cushion in two 50.2 Ti tubes. Pellet microtubules in a Beckman ultracentrifuge in a 50.2 Ti rotor at 40K for 45' at 35°C.

3. Aspirate the supernatant above the cushion and rinse the supernatant-cushion interface twice with warm (37 °C) Labeling Buffer. Aspirate the cushion and resuspend the pellet using a cutoff large pipet tip in 1 - 2 ml of warm labeling buffer. Take care to keep the tubulin warm during the resuspension and continue resuspending till no chunks of tubulin are visible. This is the most painful part of the labeling procedure.
4. Add 10- to 20-fold molar excess of the dye to tubulin. Estimate the tubulin concentration assuming ~70% recovery of the starting tubulin. For dyes such as Cy5 and Cy3, use a 5-pack for labeling ~25 mg. For most dyes we label for 30'-40' at 37°C. For C2CF-SNHS (caged fluorescein), we have found it best to add the dye in two steps (20' apart) and label for 60' at 37°C. After adding the dye stock, gently vortex the mixture every 2'-3' during the course of the labeling.
5. At end of labeling incubation add an equal volume of Quench to the labeling reaction and mix well. Incubate for 5'.
6. Layer the quenched labeling reaction onto two TLA100.3 (or TLA100.4) tubes containing 1.5 ml of Low pH Cushion. Spin at 80K for 20 min at 35 °C in a TLA100.3 or TLA100.4 rotor in a Beckman TLA100 ultracentrifuge.
7. Aspirate the supernatant above the cushion and rinse the supernatant-cushion interface twice with warm 1XBRB80. Aspirate the cushion and resuspend the pellet using a cutoff pipet tip in 1 ml of ice-cold 1X IB. Transfer resuspended chunks of the pellet to a small ice-cold dounce (1 or 2 ml volume) in an ice-water bath. Resuspend the pellet by gentle douncing till the suspension is uniform. Continue douncing intermittently for a total time of 30 min at 0°C.

Cold IB seems to promote more rapid depolymerization than BRB80; therefore, we use IB in the depolymerization step for all labeling procedures.

For small scale labelings the pellet can be resuspended directly in the centrifuge tube and sonicated gently using a microtip sonicator to speed depolymerization.

8. Spin the depolymerized tubulin in a TLA100.2 (or TLA100.3) rotor at 80K for 10' at 2°C.

9. Recover the supernatant from the cold spin, add BRB80 to 1X (from a 5X stock), MgCl<sub>2</sub> to 4 mM, GTP to 1 mM and incubate on ice for 3'. Warm to 37°C for 2', add 1/2 volume of glycerol (33% v/v final), mix well and polymerize at 37°C for 30 min.

10. Layer the polymerization reaction on a 1 ml Low pH Cushion in a TLA100.3 tube and pellet the microtubules at 80K in a TLA100.3 rotor for 20' at 37 °C.

11. Aspirate the supernatant above the cushion and rinse the supernatant-cushion interface twice with warm IB. Aspirate the cushion and rinse the pellet twice with 1 ml warm IB to remove any residual glycerol. Resuspend the pellet using a cutoff pipet tip in 0.2-0.3 ml of ice cold IB. This pellet should resuspend easily. Incubate at 0°C for 20 to 30 min.

12. Spin the depolymerized tubulin in a TLA100 or TLA100.2 rotor at 80K for 10' at 2°C. Recover the supernatant, quickly estimate the tubulin concentration, adjust with IB if desired and freeze in 3 - 5 µl aliquots in liquid nitrogen. We generally aim for a final tubulin concentration of 5 - 15 mg/ml (50 - 150 µM). Careful determination of tubulin concentration and labeling stoichiometry can be performed as described below, after the tubulin has been aliquoted and frozen. C2CF-tubulin should be stored at -80 °C in a foil-wrapped box.

### III. Quantifying Tubulin Concentration and Labeling Stoichiometry

To determine the tubulin concentration and stoichiometry of labeling, dilute the labeled tubulin 1/50 - 1/100 in IB and obtain a wavelength spectrum. Calculate the molar concentration of dye by using the absorbance at the peak wavelength and the extinction coefficient provided by the manufacturer. Determine the tubulin concentration by first subtracting out the contribution of the dye to the  $A_{280}$  and then using an extinction coefficient of  $115,000 \text{ M}^{-1}\text{cm}^{-1}$ . Table I provides a list of extinction coefficients and  $A_{280}$  absorbance (relative to absorbance at peak wavelength) for commonly used dyes. Note that the absorbance of fluorescein is pH-dependent and conjugates with fluorescein should either be diluted into a high pH buffer (~8.8-9.0) or the value measured at pH 7.0 multiplied by 1.2.

An example of calculating concentration and stoichiometry for labeling tubulin with tetramethylrhodamine (TMR) NHS ester:

$$\text{Tubulin concentration} = [(A_{280} - \text{Contribution of dye to } A_{280}) \times \text{Dilution Factor}] / \text{Extinction Coefficient of tubulin}$$

$$\text{TMR concentration} = (A_{555} \times \text{Dilution Factor}) / \text{Extinction Coefficient of TMR}$$

$$\text{Labeling Stoichiometry} = \text{TMR concentration} / \text{Tubulin concentration}$$

A wavelength spectrum of 1/100 dilution of the final labeled tubulin product gives the following absorbance values:

$$A_{280} = 0.23; A_{555} = 0.20$$

$$\text{Therefore, Tubulin concentration} = [(0.23 - (0.2 \times 0.2)) \times 100] / 115000 = 165 \mu\text{M}$$

$$\text{TMR concentration} = [0.20 \times 100] / 95000 = 210 \mu\text{M}$$

$$\text{Labeling Stoichiometry} = 210 / 165 = 1.3$$

To determine the concentration and labeling stoichiometry of C2CF-tubulin, the C2CF must be first uncaged to fluorescein. To do this, dilute the labeled tubulin 1/50 to 1/100 in IB + 2 mM DTT in an eppendorf tube. Put the

ependorf tube on a hand held UV lamp, cover with foil (shiny side down) and expose to long wavelength UV for 30'. Obtain a wavelength spectrum from 200 to 600 nm after the 30' activation, using IB + 2 mM DTT exposed to UV in parallel as a blank. An example of such a spectrum is shown in Figure 1A. Assuming a 100% efficiency for the uncaging reaction, the concentration of C2CF can be calculated from the spectrum after activation as follows:

$$\text{Concentration of C2CF} = (A_{495} \times \text{Dilution Factor} \times 1.2) / 80000$$

(The factor of 1.2 corrects for the pH dependence of the absorption spectrum of fluorescein)

#### **IV. Using Labeled Tubulins**

- a) Microinjection into cells/addition to extracts: For microinjections, we dilute the tubulin in IB to 2-5 mg/ml, clarify by centrifugation and inject ~1/10 of cell volume. For extract studies, we add the labeled tubulin to the extract (see Chapter 3, Chapter 4, Appendix I and Appendix II).
- b) Preparation of fluorescent microtubule substrates or for monitoring polymerization and dynamics of pure tubulin: We use a mixture of labeled and unlabeled tubulin for polymerization (see page 180). The ratio of labeled to unlabeled will depend on the particular application and on the brightness of the labeled tubulin. Labeled tubulins, especially those labeled to high stoichiometry, exhibit very different properties from unlabeled tubulin. Therefore, use the highest ratio of unlabeled to labeled tubulin that provides signal intensity sufficient for a particular experiment.

**Table 1. Properties of Fluorescent Dyes Used for Tubulin Labeling**

Dye	Excitation (nm)	Emission (nm)	$\epsilon\lambda_{\max}$ ( $M^{-1}cm^{-1}$ )	$\epsilon_{280}/\epsilon\lambda_{\max}$
Fluorescein	495	519	74,000	0.19
Oregon Green 488	495	521	76,000	0.19
Cy3	550	570	150,000	0.08
Tetramethylrhodamine	546	576	95,000	0.21
X-Rhodamine	574	602	78,000	0.20
Texas Red	583	603	116,000	0.15
Cy5	649	670	250,000	0.05

$\epsilon\lambda_{\max}$  = Extinction coefficient of dye at its peak wavelength

$\epsilon_{280}/\epsilon\lambda_{\max}$  = Absorbance of dye at 280 nm as a fraction of its absorbance at its peak wavelength

5 (and-6) carboxyfluorescein succinimidyl ester (Molecular Probes C-1311)

Oregon Green 488 carboxylic acid, succinimidyl ester 5-isomer (Molecular Probes O-6147)

5 (and-6) carboxytetramethylrhodamine succinimidyl ester (Molecular Probes C-1171)

5 (and-6) carboxy-X-rhodamine succinimidyl ester (Molecular Probes C-1309)

Texas Red-X succinimidyl ester, mixed isomers (Molecular Probes T-6134)

Cy3-OSu monofunctional reactive fluorophore (Amersham PA13100)

Cy5-OSu monofunctional reactive fluorophore (Amersham PA13600)

## **5. Tubulin Polymerization with GTP/GMPCPP/Taxol:**

### **I. Solutions:**

BRB80 (1X): 80 mM PIPES, 1 mM MgCl<sub>2</sub>, 1 mM EGTA, pH 6.8 with KOH

(generally made as a 5X stock and stored at 4 °C)

100 mM GTP

100 mM GMPCPP

Taxol: 10 mM stock; 100 μM, 10 μM and 1 μM dilutions (and/or 200 μM, 20 μM and 2 μM dilutions) all in anhydrous DMSO; Taxol is sold under the tradename "Paclitaxel" by Sigma

### **II. Prepolymerization Clarification:**

Although not absolutely necessary, we recommend mixing tubulin and nucleotides in 1X BRB80 for 5' on ice and then clarifying this mix using a TLA100 rotor for 5' at 90K at 2°C. We especially recommend this clarification when polymerization includes GMPCPP and/or highly labeled fluorescent tubulins. We also recommend a clarification spin on thawed labeled tubulins prior to microinjection.

### **III. GTP Polymerization**

1. On ice mix unlabeled tubulin and labeled tubulin at an appropriate ratio in 1X BRB80 with 1 mM DTT and 1 mM GTP. Incubate at 0°C for 5'.
2. Clarify mix in TLA100 rotor at 90K for 5' at 2°C.
3. Collect supernatant and incubate at 37°C. If the tubulin concentration is 2 mg/ml or higher, assembly will proceed rapidly to steady state (~30'). If the concentration is lower, nucleation can be limiting and the precise kinetics of approach to steady state is difficult to predict and will depend on the amount of active tubulin in your mix. For many experiments, we add seeds to

surmount the nucleation barrier, thereby specifically assaying elongation -- for this we routinely make GMPCPP seeds, wash out any free GMPCPP and add a small volume of the seeds (~1/50 vol) after the polymerization mix has been at 37°C for 1'. Axonemes or centrosomes can also be used as nucleating structures. If the purpose is labeling or recycling the tubulin, polymerization is promoted by addition of DMSO or glycerol as described above (see page 171 and 173).

#### IV. Taxol Polymerization

1. On ice mix unlabeled tubulin and labeled tubulin at an appropriate ratio in 1X BRB80 with 1 mM DTT and 1 mM GTP. Incubate at 0°C for 5'.
2. Clarify mix in TLA100 rotor at 90K for 5' at 2°C. Incubate supernatant at 37°C for 1'-2'.

Now there are two options :

I. Add taxol stepwise to equimolar as follows (for 1 mg/ml tubulin):

(Pipet in the taxol and immediately flick the tube to mix it in)

Add 1/10 vol 1  $\mu$ M taxol; Incubate at 37°C for 5'-10'

Add 1/10 vol 10  $\mu$ M taxol; Incubate at 37°C for 5'-10'

Add 1/10 vol 100  $\mu$ M taxol; Incubate at 37°C for 15'

Pellet microtubules over a warm 40% glycerol in BRB80 cushion in a TLA100, 100.2 or 100.3 rotor, aspirate and wash sample/cushion interface, rinse pellet and resuspend in warm BRB80 + 1 mM DTT + 10-20  $\mu$ M taxol (taxol should be at least equimolar and preferably in excess to the tubulin)

*Note:* If taxol is added all at once it will cause tubulin precipitation! If polymerizing 2 mg/ml tubulin, use 2  $\mu$ M, 20  $\mu$ M and 200  $\mu$ M steps



**OR** II. Add 10%(v/v) DMSO and incubate at 37°C for 20'-30'

Pellet and resuspend microtubules as described above

For DMSO polymerization it is best to have high tubulin concentrations (5-10 mg/ml) in the original mix before adding DMSO.

However, MTs must be resuspended after pelleting with equimolar taxol.

A "quick-and-dirty" taxol polymerization method (popular in motor labs where taxol microtubules are used as substrates for motility assays):

1. Thaw recycled tubulin stored in IB (generally 5-20 mg/ml)
2. Add equal volume 2X BRB80 + 2 mM DTT + 2 mM GTP + 20%  
DMSO
3. Incubate at 37°C for 20'-30'
4. Pellet microtubules and resuspend as described above

If there is labeled tubulin in the mix, dilute the microtubules to 1-10  $\mu\text{g/ml}$  and check under a fluorescent microscope. Taxol-stabilized microtubules can be sheared by diluting them to  $\sim 100 \mu\text{g/ml}$  and then passing them through a 27g needle  $\sim 5-6$  times. All dilutions of taxol stabilized microtubule should be done into buffers containing 10-20  $\mu\text{M}$  taxol.

## **V. GMPCPP Polymerization**

GMPCPP is the best current GTP analog for tubulin polymerization. Its major limitation is lack of commercial availability. In the presence of potassium as counterion, GMPCPP is very slowly hydrolyzed within the microtubule lattice, and is essentially non-hydrolyzable within the time course of most experiments. In the presence of sodium as counterion, GMPCPP is hydrolyzed slightly faster in the lattice -- this hydrolysis is accelerated tremendously by treatment with glycerol. Given this information on the

effect of buffer counterions on GMPCPP stability within microtubule lattices, we always use potassium counterion buffers for all our microtubule work. GMPCPP is a potent nucleator of microtubules. Therefore, at tubulin concentrations of 1 mg/ml or higher, very short numerous microtubules are formed in the presence of GMPCPP. If longer GMPCPP microtubules are desired, nucleation can be limited by diluting the tubulin to  $\sim 2\text{-}3\ \mu\text{M}$  (0.2 - 0.3 mg/ml). We generally make a 1-3 mg/ml CPP tubulin mix and store it at  $-80^\circ\text{C}$  in small aliquots. Directly polymerizing this mix results in short GMPCPP seeds. Diluting the mix while thawing it results in formation of longer CPP microtubules.

1. On ice mix unlabeled tubulin and labeled tubulin (1-3 mg/ml final) at an appropriate ratio in 1X BRB80 with 1 mM DTT and 0.5-1 mM GMPCPP. Incubate at  $0^\circ\text{C}$  for 5'-10'.
2. Clarify mix in TLA100 rotor at 90K for 5' at  $2^\circ\text{C}$ . Freeze supernatant in 5-10  $\mu\text{l}$  aliquots in liquid nitrogen and store at  $-80^\circ\text{C}$ .
- 3A. To form short GMPCPP seeds, transfer a tube from the freezer to a  $37^\circ\text{C}$  bath. Incubate 15'-20' at  $37^\circ\text{C}$ . Dilute to 150-200  $\mu\text{l}$  with warm BRB80 + 1 mM DTT, pellet the seeds in a TLA100 rotor (90K 5' at  $25\text{-}30^\circ\text{C}$ ), discard supernatant and resuspend pellet in 1-2X the starting volume of BRB80 + 1 mM DTT. This process removes free CPP and any unpolymerized tubulin. Seeds are generally added at 1/50-1/100 vol to a polymerization mix containing 1 mM GTP. Given the  $\sim 10\text{X}$  higher affinity of tubulin for GTP versus GMPCPP, the amount of GMPCPP added from a seed mix at these dilutions is insignificant. Therefore, we often add seeds directly into a polymerization mix without dilution/sedimentation.

**3B.** To form long GMPCPP microtubules, thaw a CPP mix tube by adding in enough warm BRB80 + 1 mM DTT such that the final tubulin concentration is 2-3  $\mu$ M (pipet in 37°C BRB80 + 1 mM DTT, mix by gently pipeting up and down until the frozen seed mix pellet is thawed, then place in 37°C bath). Incubate at 37°C for 30' or longer. Free CPP can be removed as described in 3A or the CPP microtubules can be used directly for assays.

## 6. Preparation of Segmented and Polarity Marked Microtubules

Segmented and polarity-marked microtubules are very useful for many different types of *in vitro* assays. Segmented microtubules are microtubules with a bright seed with a dim elongated segment on both ends. Polarity marked microtubules are microtubules with a bright seed and a dim elongated segment only on one end -- the plus end. Selective elongation of one end is achieved by inclusion of NEM-treated tubulin, a competitive inhibitor of minus end polymerization. More complex microtubule substrates such as GDP microtubule lattices capped with segments of GMPCPP tubulin can also be prepared by playing around with *in vitro* polymerization conditions. Also, segmented and polarity marked microtubules can be made from different color tubulins instead of different intensity of a single color tubulin as described here.

Note that the precise ratios of labeled to unlabeled tubulin described here may need to be adjusted depending on the labeled tubulin prep. Described here is what has worked well for us using tetramethylrhodamine NHS ester-labeled tubulin (stoichiometry of labeling ~1.5).

### I. Solutions:

BRB80 (1X): 80 mM PIPES, 1 mM MgCl<sub>2</sub>, 1 mM EGTA, pH 6.8 with KOH

(generally made as a 5X stock and stored at 4 °C)

100 mM GTP

100 mM GMPCPP

Taxol: 10 mM stock; 200 μM, 20 μM and 2 μM dilution all in anhydrous DMSO; sold under tradename "Paclitaxel" by Sigma

Bright GMPCPP Seed Mix (2 mg/ml; 1 part rhodamine tubulin to 2 parts unlabeled tubulin; prepared and stored at -80°C as described on page 182 - 183)

NEM GTP-Tubulin (prepared by treating recycled tubulin (~5-15 mg/ml) in BRB80 + 0.5 mM GTP with 1 mM NEM (N-ethylmaleimide; make a fresh 50 mM stock in water just before use) for 10' at 0°C, quenching the NEM with 8 mM  $\beta$ -mercaptoethanol for 10' at 0°C, freezing aliquots in liquid nitrogen and storing at -80°C.

NEM CPP-Tubulin (prepared by treating recycled tubulin (~5-15 mg/ml) in BRB80 + 0.5 mM GMPCPP with 1 mM NEM (freshly prepared as a 50 mM stock in water) for 10' at 0°C, quenching NEM with 8 mM  $\beta$ -mercaptoethanol for 10' at 0°C, freezing aliquots in liquid nitrogen and storing at -80°C.

## **II. Segmented Taxol Microtubules:**

1. Polymerize bright GMPCPP seed mix at 37°C for 15'-30'.
2. On ice prepare the dim elongation mix consisting of 15  $\mu$ M tubulin (1 part rhodamine tubulin to 10 parts unlabeled tubulin) in 1X BRB80, 1 mM DTT, 1 mM GTP. Incubate at 0°C for 5' and (optionally) clarify at 90K for 5' at 2°C in a TLA100 rotor.
3. Incubate dim elongation mix at 37°C for 1'. Add 1/10-1/20 volume of GMPCPP seeds and mix gently. Incubate at 37°C for 20'. GMPCPP seeds are cold-labile and will depolymerize on ice. Therefore, only add the seeds after the elongation mix has warmed up.
4. Add taxol stepwise to 20  $\mu$ M as described on page 181
5. The segmented taxol-stabilized microtubules can be pelleted over a glycerol cushion and resuspended, or used directly after dilution. All dilutions of taxol-stabilized MTs should be done into buffers containing 10-20  $\mu$ M taxol.

### III. Polarity Marked Taxol Microtubules:

1. Polymerize bright GMPCPP seed mix at 37°C for 15'-30'.
2. On ice prepare the dim polar elongation mix consisting of 15  $\mu\text{M}$  tubulin (1 part rhodamine tubulin to 10 parts unlabeled tubulin) and 12  $\mu\text{M}$  NEM GTP-tubulin in 1X BRB80, 1 mM DTT, 1 mM GTP. Incubate at 0°C for 5' and (optionally) clarify at 90K for 5' at 2°C in a TLA100 rotor.
3. Incubate dim polar elongation mix at 37°C for 1'. Add 1/10-1/20 volume of GMPCPP seeds and mix gently. Incubate at 37°C for 20'.
4. Add taxol stepwise to 20  $\mu\text{M}$  as described on page 181.
5. The polarity-marked taxol-stabilized microtubules can be pelleted over a glycerol cushion and resuspended, or used directly after dilution. All dilutions of taxol-stabilized MTs should be done into buffers containing 10-20  $\mu\text{M}$  taxol.

### IV. Segmented GMPCPP Microtubules:

1. Prepare dim GMPCPP Elongation Mix: 10  $\mu\text{M}$  (1 mg/ml) 1:9 rhodamine labeled: unlabeled tubulin in 1X BRB80, 1 mM DTT, 0.5 mM GMPCPP. Incubate on ice for 5'-10', spin 90K 5' in TLA100 at 2°C, freeze in liquid nitrogen in 10  $\mu\text{l}$  aliquots (or use fresh).
2. Thaw GMPCPP bright seed mix by adding 9 vol of warm (37°C) BRB80 + 1 mM DTT (resulting in 2  $\mu\text{M}$  tubulin final) and incubate at 37°C for 30'-45'.
3. Thaw CPP elongation mix and store on ice. Dilute as follows on ice:
  - 17  $\mu\text{l}$  BRB80 + 1 mM DTT
  - 3  $\mu\text{l}$  CPP elongation mix
 (This results in elongation of  $\sim 1.5$   $\mu\text{M}$  CPP-tubulin)

4. Incubate diluted CPP elongation mix at 37°C for 20 sec before adding 2  $\mu$ l of polymerized bright CPP seeds.
5. Incubate at 37°C for 1-2 hours. Pellet and resuspend or use directly.

#### **V. Polarity Marked GMPCPP Microtubules**

1. Prepare dim GMPCPP polar elongation mix: 10  $\mu$ M (1 mg/ml) 1:9 rhodamine labeled: unlabeled tubulin and 8  $\mu$ M NEM CPP-Tubulin in 1X BRB80, 1 mM DTT, 0.5 mM GMPCPP. Incubate on ice for 5'-10', spin 90K 5' in TLA100 at 2°C, freeze in liquid nitrogen in 10  $\mu$ l aliquots (or use fresh).
2. Thaw GMPCPP bright seed mix by adding 9 vol of warm (37°C) BRB80 + 1 mM DTT (2  $\mu$ M tubulin final) and incubate at 37°C for 30'-45'.
3. Thaw CPP polar elongation mix and store on ice. Dilute as follows on ice:  
17  $\mu$ l BRB80 + 1 mM DTT  
3  $\mu$ l CPP Polar Elongation Mix  
(This results in elongation of  $\sim$ 1.5  $\mu$ M CPP-tubulin)
4. Incubate diluted CPP polar elongation mix at 37°C for 20 sec before adding 2  $\mu$ l of polymerized bright CPP seeds.
5. Incubate at 37°C for 1-2 hours. Pellet and resuspend or use directly.

## 7. Microtubule Spindowns for Visual Analysis

Microtubule spindowns for visual analysis can be performed on single microtubules or microtubules nucleated from axonemes/centrosomes. Although live DIC analysis has largely superseded the use of visual fixed time points for analyzing microtubule dynamics, spindowns can still be very useful (see chapter 5 for an example). Procedures for fixing and pelleting microtubules onto coverslips are described here.

### I. Solutions & Supplies:

BRB80 (1X): 80 mM PIPES, 1 mM MgCl<sub>2</sub>, 1 mM EGTA, pH 6.8 with KOH  
(generally made as a 5X stock and stored at 4 °C)

Fix: 1% glutaraldehyde in BRB80 (prepare from a 50% glutaraldehyde stock just prior to use)

Lower cushion: BRB80 + 10% (v/v) glycerol

Spindown tubes with 12 mm coverslips: (see Appendix II page 131)

HB-4/HB-6 or equivalent rotor

A common problem with spindowns is guessing the right volume to sediment onto a 12 mm diameter coverslip. This will require some amount of practice/troubleshooting. With stable microtubules (taxol- or GMPCPP-stabilized), use squashes to guess what volume to spindown. Most of the time, people err on the side of excess -- e.g., it only takes ~0.2 µl of 1 µM CPP microtubules to get a good density of single microtubules on a 12 mm diameter circle coverslip.



## **II. Spindown Protocol**

- 1. Setup spindown tubes with chocks (plexiglass inserts) and coverslips and add 5 ml BRB80. Then use a very cutoff blue tip to underlay the BRB80 with ~2 ml of Cushion (BRB80 + 10% glycerol). Make sure the tubes are balanced and store in an ice bucket.**
- 2. Fix the reaction containing microtubules by adding 10 volumes of Fix and mixing gently with a cutoff tip. Incubate at RT for 3'.**
- 3. Dilute fixed reaction with 20-30 volumes of BRB80, mix by inversion and store on ice until all samples have been processed.**
- 4. Pipet the appropriate amount of fixed and diluted reaction on top of the BRB80 in the spindown tubes. Spin at 12,500 rpm in an HB-4/6 rotor at 20°C for 1-1.5 hours (start with rotor and centrifuge at 4°C; the centrifuge will heat up to 20°C very rapidly and this will save some centrifuge wear & tear)**
- 5. Aspirate and postfix in -20°C methanol for 5'. Rehydrate and either mount (if microtubules are fluorescent) or perform indirect immunofluorescence (see Chapter 5 for an example).**

The same procedure can be used with microtubules nucleated off axonemes or centrosomes. For pelleting these larger structures, use a 5 ml 30% (v/v) glycerol cushion and spin at 10K for 15'-20' at 20°C. Wash the sample cushion interface well prior to aspirating and processing the coverslips.

## 8. Flow Cell Assays with Microtubules: Motility / Dynamics in Fluorescence and VE-DIC

Flow cell assays are very useful for studying microtubule motility, microtubule dynamics, kinetochore-microtubule interactions and action of severing/depolymerizing factors on microtubules (see Chapter 4 and 5 for examples). Described here are some general procedures for flow cell assays.

Flow cells can be constructed in many different ways. The most common way is to place two strips of double-stick tape on a glass slide ~7-10 mm apart and cover with a 18x18 or 22x22 mm coverslip. This results in a ~12-15  $\mu$ l flow cell. Solutions are pipeted on one side and sucked out the other side by capillary action using Whatman #1 filter paper or a Kimwipe. Washes in flow cells should be ~4-8 chamber volumes and it is important to work in the middle of the cell (i.e. to avoid working close to the tape edge, where flow is not laminar resulting in poor washes/solution transfers).

For VE-DIC (video-enhanced differential interference contrast microscopy) coverslips must be cleaned thoroughly before use. We find that treating coverslips with acetone for 15'-30', followed by ethanol for 15', and then spin drying them works well for VE-DIC. Other labs use far more extensive and excruciating cleaning procedures. For fluorescence assays coverslips can be used straight from a box. In both cases, the coverslip surface is generally treated in some way depending on the precise assay requirement, e.g., the surface is coated with 5 mg/ml casein for 3' prior to adsorbing motor proteins for motility assays. For fluorescence assays, oxygen scavenging is essential and a glucose oxidase/catalase/glucose system works very well for this purpose.

## **I. Solutions, etc.:**

BRB80 (1X): 80 mM PIPES, 1 mM MgCl<sub>2</sub>, 1 mM EGTA, pH 6.8 with KOH  
(generally made as a 5X stock and stored at 4 °C)

5 mg/ml casein (Sigma C-5890; dissolve at 10-20 mg/ml in 20 mM Tris, pH 8.0, on a rotator in coldroom for several hours; spin at 70K in TLA100.4 and collect clear middle layer. Measure protein concentration by Bradford using BSA as a standard and dilute to 5 mg/ml. This can be filtered if desired then aliquoted and stored at -20°C or -80°C)

10 mg/ml HSA or high purity BSA in 1XBRB80; store at -20°C or -80°C (HSA = Human Serum Albumin)

Oxygen Scavengers (see below)

Flow Cells (cleaned coverslips for DIC)

Axonemes (for dynamics assays)

## **I. DIC Assays**

### A. Motility Assays

Described here is a simple protocol for assaying kinesin motility by VE-DIC. Variations on this type of assay have been used to demonstrate motility of other MT motor proteins. This assay does not provide polarity information on the motility. Although there are methods for making polar microtubule substrates for DIC, we generally use fluorescent polarity marked taxol-stabilized microtubules to determine polarity, as described later.

1. Coat flow cell with 5 mg/ml casein for 3'.
2. Rinse out casein with 80 µl BRB80 + 1 mM DTT + 3 mM MgATP.

3. Flow in kinesin (diluted to ~10-50  $\mu\text{g}/\text{ml}$  in BRB80 + 1 mM DTT + 3 mM MgATP for high density assays) and allow adsorption of kinesin for 5'.
4. Wash out unbound kinesin with 80  $\mu\text{l}$  BRB80 + 1 mM DTT + 3 mM MgATP + 1 mg/ml HSA + 10  $\mu\text{M}$  taxol
5. Transfer flow cell to microscope and setup DIC imaging.
6. Flow in 30  $\mu\text{l}$  10  $\mu\text{g}/\text{ml}$  taxol-stabilized microtubules (unlabeled) sheared to ~5-10  $\mu\text{m}$  length. The taxol-stabilized microtubules are diluted from a 1-2 mg/ml stock (prepared as described on page 181) into BRB80 + 1 mM DTT + 3 mM MgATP + 1 mg/ml HSA + 10  $\mu\text{M}$  taxol. After a reasonable density of microtubules have attached to the surface and started translocation, wash out unbound microtubules using 30  $\mu\text{l}$  BRB80 + 1 mM DTT + 3 mM MgATP + 1 mg/ml HSA + 10  $\mu\text{M}$  taxol and record motility. Once the reaction conditions are well-established, incubation with microtubules and removal of unbound microtubules can be done prior to transferring the flow cell to the microscope.

### B. Dynamics Assays

VE-DIC revolutionized analysis of microtubule dynamics by allowing observation of single dynamic microtubules in real-time. We have used VE-DIC for measuring dynamics of both pure tubulin and microtubules in clarified *Xenopus* egg extracts (see Chapter 4). We use axonemes as nucleators of microtubule assembly. The axonemes are adsorbed to the flow cell surface prior to flowing in tubulin. Dynamics measurements are generally performed in regimes where spontaneous nucleation is minimal -- thus, one can assume that the amount of polymer formed in the assay is miniscule and the monomer concentration is not changing during the observation. Care must be taken to ensure that this assumption is valid since depletion of monomer will affect the measured parameters of dynamics.

1. Coat a clean coverslip flow cell with axonemes and allow adsorption for 5' (adjust concentration and time of adsorption such that density is ~1-3 per field-of-view on the monitor).
2. Wash out unbound axonemes with 80  $\mu$ l of BRB80 + 1 mM DTT + 1 mM GTP + 0.5 mg/ml HSA
3. Flow in at least 3-4 chamber volumes of tubulin mix (i.e. tubulin in BRB80 + 1 mM DTT + 1 mM GTP + 0.5 mg/ml HSA), seal edges with Valap (1:1:1 mix of vaseline:lanolin:paraffin) and begin observation. To avoid surface effects, dynamics are measured by following microtubule ends growing down into the flow cell away from the coverslip surface -- these ends exhibit brownian motion in a focal plane below the coverslips surface as they polymerize/depolymerize.

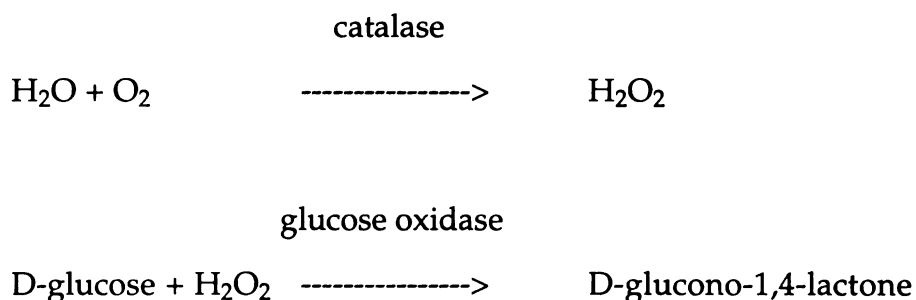
For mammalian tubulins, the temperature is raised to 35-37°C during observation. We have done this using warm air blowers or by wrapping the high NA condenser and objectives with thin silicone tubing through which hot water is circulated -- the temperature of the water is empirically adjusted such that the temperature of the immersion oil on the coverslip surface is 35-37°C (measured using a thermocouple probe). Many home-rigged schemes for controlling temperature on the microscope stage have been developed in different labs.

For assaying dynamics of microtubules in *Xenopus* egg extracts, we simply flow ~50  $\mu$ l of extract through a flow cell with adsorbed axonemes and then seal the cell with Valap. The high protein concentration of the extract eliminates need for blocking the coverslip surface.

## II. Fluorescence Assays:

### A. Oxygen Scavenging:

For live fluorescence microscopy it is essential to scavenge oxygen in order to limit photodamage. The most convenient method for doing this is using a glucose oxidase/glucose/catalase mix (OS mix). The component enzymes are stored as 100X stocks at  $-80^{\circ}\text{C}$  and thawed and used for ~2 hours after mixing. It is important to keep the OS mix in a sealed tube on ice. The principle by which the mix scavenges oxygen is as follows:



#### A1. 100X Stock Solutions:

<u>Glucose</u>	450 mg/ml in ddH <sub>2</sub> O ( $\approx 2.25$ M)
<u><math>\beta</math>-mercaptoethanol</u>	50% ( $\approx 7.15$ M; dilute from stock before use)
<u>Glucose Oxidase</u>	20 mg/ml (Sigma G-2133)
<u>Catalase</u>	3.5 mg/ml (Sigma C-40)

The glucose oxidase and catalase are made up in 12 mM K-PIPES, pH 6.8, 2 mM MgCl<sub>2</sub>, 1 mM EGTA, frozen in 20-50  $\mu\text{l}$  aliquots in liquid nitrogen and stored at  $-80^{\circ}\text{C}$ . We find it most convenient to prepare the glucose stock along with the glucose oxidase and catalase stocks, and store all three stock solutions in different colored tubes at  $-80^{\circ}\text{C}$ .

## A2. Using OS Mix:

1. Thaw 100X stocks of glucose, glucose oxidase and catalase and store on ice.

Prepare a 50%  $\beta$ -mercaptoethanol stock solution on ice.

2. Make a 10X OS Mix on ice: (recipe is for 50  $\mu$ l)

30  $\mu$ l BRB80 (0°C)

5  $\mu$ l of glucose oxidase, catalase,  $\beta$ -mercaptoethanol and glucose stocks

Add glucose last, after mixing the other components, and store the 10X OS

Mix in a sealed tube on ice (i.e. do not leave top open). Keep the tube on ice

and ensure that temperature of solution to which the OS Mix is added only

increases and does not decrease. Prepare a fresh 10X stock after ~2 hours for

optimal results. Add 1/9 vol of the 10X OS to the solutions used for washing

flow cells so that the sample is well equilibrated with 1X OS mix prior to

observation. Using this recipe, kinesin motility can be recorded with an

unshuttered/unattenuated mercury arc for >15'.

## B. Assays

Motility assays in fluorescence are generally performed with polarity marked taxol-stabilized microtubules (see page 187) to determine the polarity of the assayed motor protein. Kinetochore-microtubule interaction, microtubule severing and microtubule depolymerization assays (see Chapter 5) have also relied heavily on fluorescence microscopy combine with flow cell technology. It is important to be aware that fluorescence assays are subject to photodamage artifacts, especially if oxygen scavenging is not done properly, and also that the oxygen scavenging mix may affect the property being assayed (this is a real concern for measuring microtubule dynamics using fluorescence). Described below is a kinesin motility assay with polarity marked microtubules. A more complex assay for monitoring microtubule

depolymerization with unambiguous assignment of polarity to the substrate segmented MTs is described in Chapter 5.

1. Coat flow cell with 5 mg/ml casein for 3'.
2. Rinse out casein with 80  $\mu$ l BRB80 + 1 mM DTT + 3 mM MgATP.
3. Flow in kinesin (diluted to ~10-50  $\mu$ g/ml in BRB80 + 1 mM DTT + 3 mM MgATP for high density assays) and allow adsorption of kinesin for 3'-5'.
4. Wash out unbound kinesin with 80  $\mu$ l BRB80 + 1 mM DTT + 3 mM MgATP + 1 mg/ml HSA + 10  $\mu$ M taxol + 1X OS Mix
5. Flow in 30-50  $\mu$ l of 10  $\mu$ g/ml polarity marked taxol-stabilized microtubules (see page 187) diluted from a 1-2 mg/ml stock into BRB80 + 1 mM DTT + 3 mM MgATP + 10  $\mu$ M taxol + 1X OS Mix. Focus on the coverslip surface on an upright epifluorescence microscope.
6. After a reasonable density of microtubules have attached to the surface and started translocation, wash out unbound microtubules with 30  $\mu$ l BRB80 + 1 mM DTT + 3 mM MgATP + 10  $\mu$ M taxol + 1X OS Mix. Focus on a field-of view near the middle of the flow cell and record motility using shuttered attenuated illumination and a digital or video camera. Once the reaction conditions are well-established, incubation with microtubules and removal of unbound microtubules can be done prior to transferring the flow cell to the microscope. At low densities, MTs are not washed out since there is frequent release of the MTs from the coverslip surface and a reasonable MT density is necessary for rebinding of MTs.

Although good oxygen scavenging will allow observation with unshuttered illumination, it is a good idea for any live fluorescence studies to use shuttered and attenuated illumination (attenuation is generally done using neutral density filters). It is also essential to keep an eye open for a



decline in the performance of the OS Mix. If bleaching becomes apparent when focusing on the sample, prepare a fresh 10X OS Mix from stocks stored at -80°C.

## 9. Negative Stain Electron Microscopy of Microtubules

Negative staining is a rapid, qualitative method for analyzing microtubule structure at the EM level. Because negative staining involves deposition of heavy atom stains, structural artifacts such as flattening of the cylindrical microtubule and opening up of microtubules at the seam into flat sheets are common. Cryo-electron microscopy, where microtubules are flash frozen in a thin film of vitreous ice and imaged without staining, is currently regarded as the best method to view native microtubule structure at high resolution. Nevertheless, negative staining is very useful because of its ease, rapidity and lack of requirement for specialized equipment other than that found in a regular EM facility.

### I. Solutions and Supplies:

0.5% (w/v) Uranyl Acetate (prepare by dissolving 50 mg UA in 10 ml of ddH<sub>2</sub>O. Add water to tube containing UA, cover tube with foil and rotate in coldroom for several hours till fully dissolved. Filter through a 0.22 µm filter that has been prerinsed well with ddH<sub>2</sub>O. Filtered stain stored at 4°C in a foil-wrapped tube can be used for >1 year.)

Filter strips (prepared by cutting Whatman #1 filter paper into small slivers)

Grids (200 mesh copper grids that have been formvar coated, carbon coated)

Rinse (ddH<sub>2</sub>O with 5 mM EGTA or as appropriate)

### Negative Staining Protocol:

1. Glow discharge formvar and carbon coated grids just before use to increase their hydrophobicity.
2. Place sample on the grid (1-3 µl, sufficient to cover the grid surface).

3. ~10 sec later slowly pipet on 20  $\mu$ l of UA stain using a P-20. While pipeting onto the grid, gently absorb stain on the opposite side using a filter paper sliver. The staining procedure should take ~30s-1'.
4. Allow the grid to dry after absorbing as much stain as possible with the filter paper and examine the grid as soon as possible, preferably on the same day. If there are problems with stain precipitation, or with general stain background then rinses prior to staining may be necessary (see below).

We have found this straightforward negative staining procedure to work very well with stable microtubules such as taxol or CPP microtubules. We do not recommend using UA dissolved in 50% methanol, since we had highly irreproducible results with this stain. If there is a lot of salt or sucrose/glycerol in the buffer, then washing the sample prior to staining may be necessary. If dynamic microtubules undergoing polymerization at 37°C need to be examined, then a rinse with warm BRB80 may be necessary to remove the large amount of unpolymerized tubulin before applying stain.

Rinsing: There are several methods for rinsing the grid surface prior to applying stain. One method is to apply sample to the grid, allow adsorption for 10-30 sec, hold the grid tilted downward and drop 2-3 large drops of rinse (either ddH<sub>2</sub>O + 5 mM EGTA for removing interfering salts/buffer components/sucrose/glycerol or warm BRB80 for removing unpolymerized tubulin) over it and then apply the stain. Alternatively, rinsing can be done by placing a large drop of the rinse solution on parafilm and slowly drawing the grid, with the sample-coated surface facing the parafilm, over the surface of the rinse solution drop. The stain can then be applied as above.

Dilute samples can be concentrated on the grid by adsorption for longer times (1'-3'). Negative staining is relatively quick, so we recommend trying

both direct staining and rinsing prior to staining for the specific reaction conditions being analyzed.

## References

Allen, C., and G.G. Borisy. 1974. Structural polarity and directional growth of microtubules of *Chlamydomonas* flagella. *J Mol Biol.* 90:381-402.

Amos, L., and A. Klug. 1974. Arrangement of subunits in flagellar microtubules. *J Cell Sci.* 14:523-49.

Belmont, L.D., A.A. Hyman, K.E. Sawin, and T.J. Mitchison. 1990. Real-time visualization of cell cycle-dependent changes in microtubule dynamics in cytoplasmic extracts. *Cell.* 62:579-89.

Bloom, K. 1993. The centromere frontier: kinetochore components, microtubule-based motility, and the CEN-value paradox. *Cell.* 73:621-4.

Bre, M.H., R. Pepperkok, A.M. Hill, N. Levilliers, W. Ansorge, J. Smith, J. Doe, and N. Doe. 1990. Regulation of microtubule dynamics and nucleation during polarization in MDCK II cells. *J Cell Biol.* 111:3013-21.

Bulinski, J.C., and G.G. Gundersen. 1991. Stabilization of post-translational modification of microtubules during cellular morphogenesis. *Bioessays.* 13:285-93.

Burns, R.G. 1991. Alpha-, beta-, and gamma-tubulins: sequence comparisons and structural constraints. *Cell Motil Cytoskeleton.* 20:181-9.

Caplow, M., R.L. Ruhlen, and J. Shanks. 1994. The free energy for hydrolysis of a microtubule-bound nucleotide triphosphate is near zero: all of the free

energy for hydrolysis is stored in the microtubule lattice. *J Cell Biol.* 127:779-88.

Cassimeris, L. 1993. Regulation of microtubule dynamic instability. *Cell Motil Cytoskeleton.* 26:275-81.

David-Pfeuty, T., H.P. Erickson, and D. Pantaloni. 1977. Guanosinetriphosphatase activity of tubulin associated with microtubule assembly. *Proc Natl Acad Sci U S A.* 74:5372-6.

Desai, A., and T.J. Mitchison. 1997. Microtubule polymerization dynamics. *Annu. Rev. Cell Dev. Biol.* 13:83-117.

Erickson, H.P., and E.T. O'Brien. 1992. Microtubule dynamic instability and GTP hydrolysis. *Annu Rev Biophys Biomol Struct.* 21:145-66.

Gliksman, N.R., R.V. Skibbens, and E.D. Salmon. 1993. How the transition frequencies of microtubule dynamic instability (nucleation, catastrophe, and rescue) regulate microtubule dynamics in interphase and mitosis: analysis using a Monte Carlo computer simulation. *Mol Biol Cell.* 4:1035-50.

Gorbsky, G.J., P.J. Sammak, and G.G. Borisy. 1988. Microtubule dynamics and chromosome motion visualized in living anaphase cells. *J. Cell Biol.* 106:1185-92.

- Gundersen, G.G., and J.C. Bulinski. 1988. Selective stabilization of microtubules oriented toward the direction of cell migration. *Proc Natl Acad Sci U S A*. 85:5946-50.
- Hyams, J.S., and C.W. Lloyd. 1994. *Microtubules*. Wiley-Liss, Inc., New York.
- Hyman, A.A., and P.K. Sorger. 1995. Structure and function of kinetochores in budding yeast. *Ann Rev Cell Dev Biol*. 11:471-95.
- Inoué, S., and E.D. Salmon. 1995. Force generation by microtubule assembly/disassembly in mitosis and related movements. *Mol Biol Cell*. 6:1619-40.
- Kellogg, D.R., M. Moritz, and B.M. Alberts. 1994. The centrosome and cellular organization. *Annu Rev Biochem*. 63:639-74.
- MacNeal, R.K., and D.L. Purich. 1978. Stoichiometry and role of GTP hydrolysis in bovine neurotubule assembly. *J Biol Chem*. 253:4683-7.
- Mandelkow, E.M., E. Mandelkow, and R.A. Milligan. 1991. Microtubule dynamics and microtubule caps: a time-resolved cryo-electron microscopy study. *J Cell Biol*. 114:977-91.
- McNally, F.J. 1996. Modulation of microtubule dynamics during the cell cycle. *Curr Opin Cell Biol*. 8:23-9.



Melki, R., M.F. Carlier, D. Pantaloni, and S.N. Timasheff. 1989. Cold depolymerization of microtubules to double rings: geometric stabilization of assemblies. *Biochemistry*. 28:9143-52.

Mickey, B., and J. Howard. 1995. Rigidity of microtubules is increased by stabilizing agents. *J Cell Biol*. 130:909-17.

Mitchison, T., and M. Kirschner. 1984a. Dynamic instability of microtubule growth. *Nature*. 312:237-42.

Mitchison, T., and M. Kirschner. 1984b. Microtubule assembly nucleated by isolated centrosomes. *Nature*. 312:232-7.

Mitchison, T.J. 1988. Microtubule dynamics and kinetochore function in mitosis. *Annu Rev Cell Biol*. 4:527-49.

Mitchison, T.J. 1989. Polewards microtubule flux in the mitotic spindle: evidence from photoactivation of fluorescence. *J Cell Biol*. 109:637-52.

Mitchison, T.J., and E.D. Salmon. 1992. Poleward kinetochore fiber movement occurs during both metaphase and anaphase-A in newt lung cell mitosis. *J. Cell Biol*. 119:569-82.

Murray, A.W., and T. Hunt. 1993. The cell cycle: an introduction. W. H. Freeman, New York.

Oosawa, F., and S. Asakura. 1975. Thermodynamics of the polymerization of protein. Academic Press, New York.

Rieder, C.L., and E.D. Salmon. 1998. The vertebrate kinetochore: steward for chromosome attachment, positioning on the spindle and the metaphase/anaphase transition. *Trends Cell Biol.* In press.

Salmon, E.D. 1989. Microtubule dynamics and chromosome movement. *In* Mitosis: Molecules and Mechanisms. J. Hyams and B. R. Brinkley, editors. Academic Press, N.Y. 119- 181.

Salmon, E.D., R.J. Leslie, W.M. Saxton, M.L. Karow, and J.R. McIntosh. 1984. Spindle microtubule dynamics in sea urchin embryos: analysis using a fluorescein-labeled tubulin and measurements of fluorescence redistribution after laser photobleaching. *J Cell Biol.* 99:2165-74.

Spiegelman, B.M., S.M. Penningroth, and M.W. Kirschner. 1977. Turnover of tubulin and the N site GTP in Chinese hamster ovary cells. *Cell.* 12:587-600.

Tanaka, E., T. Ho, and M.W. Kirschner. 1995. The role of microtubule dynamics in growth cone motility and axonal growth. *J Cell Biol.* 128:139-55.

Vale, R.D., and R.J. Fletterick. 1997. The design plan of kinesin motors. *Ann Rev Cell Dev Biol.* 13:745-77.

Venier, P., A.C. Maggs, M.F. Carlier, and D. Pantaloni. 1994. Analysis of microtubule rigidity using hydrodynamic flow and thermal fluctuations. *J Biol Chem.* 269:13353-60.

Verde, F., M. Dogterom, E. Stelzer, E. Karsenti, and S. Leibler. 1992. Control of microtubule dynamics and length by cyclin A- and cyclin B-dependent kinases in *Xenopus* egg extracts. *J Cell Biol.* 118:1097-108.

Walker, R.A., E.T. O'Brien, N.K. Pryer, M.F. Soboeiro, W.A. Voter, H.P. Erickson, and E.D. Salmon. 1988. Dynamic instability of individual microtubules analyzed by video light microscopy: rate constants and transition frequencies. *J Cell Biol.* 107:1437-48.

Waterman-Storer, C.M., and E.D. Salmon. 1997. Actomyosin-based retrograde flow of microtubules in the lamella of migrating epithelial cells influences microtubule dynamic instability and turnover and is associated with microtubule breakage and treadmilling. *J Cell Biol.* 139:417-34.

Waters, J.C., T.J. Mitchison, C.L. Rieder, and E.D. Salmon. 1996. The kinetochore microtubule minus-end disassembly associated with poleward flux produces a force that can do work. *Mol. Biol. Cell.* 7:1547-58.

Weisenberg, R.C., G.G. Borisy, and E.W. Taylor. 1968. The colchicine-binding protein of mammalian brain and its relation to microtubules. *Biochemistry.* 7:4466-79.

Wilson, E.B. 1928. *The Cell in Development and Heredity*. MacMillan, New York.

Zhai, Y., P.J. Kronebusch, and G.G. Borisy. 1995. Kinetochore microtubule dynamics and the metaphase-anaphase transition. *J Cell Biol.* 131:721-34.

The first part of the document discusses the importance of maintaining accurate records of all transactions and activities. It emphasizes that proper record-keeping is essential for ensuring transparency and accountability in financial matters.

The second section outlines the various methods and tools used to collect and analyze data. This includes the use of spreadsheets, databases, and specialized software to manage large volumes of information efficiently.

The third part of the document focuses on the process of reporting and communication. It details how data is synthesized into clear and concise reports that provide valuable insights and recommendations to stakeholders.

Finally, the document concludes with a summary of the key findings and a call to action for continued improvement and innovation in data management practices.

# For reference

Not to be taken  
from the room.

